TRANSPORTATION RESEARCH
RECORD

No. 1275

Bridges and Structures

Bridge Research 1990

A peer-reviewed publication of the Transportation Research Board

TRANSPORTATION RESEARCH BOARD
NATIONAL RESEARCH COUNCIL
WASHINGTON, D.C. 1990

Transportation Research Record 1275
Price: $16.00

Subscriber Category
IIC bridges and structures

Modes
1 highway transportation
3 rail transportation

Subject Area
25 structures design and performance

TRB Publications Staff
Director of Publications: Nancy A. Ackerman
Senior Editor: Naomi C. Kassabian
Associate Editor: Alison G. Tobias
Assistant Editors: Luanne Crayton, Kathleen Solomon, Norman Solomon
Graphics Coordinator: Diane L. Ross
Office Manager: Phyllis D. Barber
Production Assistant: Betty L. Hawkins

Printed in the United States of America

Library of Congress Cataloging-in-Publication Data
National Research Council. Transportation Research Board.

Bridge research, 1990
p. cm.—(Transportation research record ISSN-0361-1981 ; no. 1275)
Papers presented at the 69th Annual Meeting of the Transportation Research Board, held Jan. 1990 in Washington, D.C.
"A peer-reviewed publication of the Transportation Research Board."
ISBN 0-309-05061-8
1. Bridges—Design and construction. 2. Bridges—Testing. I. National Research Council (U.S.). Transportation Research Board. Meeting (69th : 1990 : Washington, D.C.)
II. Series: Transportation research record ; 1275.
TE7.H5 no. 1275a
[TG300]
388 s624'.2—dc20 90-22562
CIP

Transportation Research Record 1275

Contents

Foreword

Lim et al. present the results of an experimental investigation of the seismic performance of bridge columns with moment-reducing details. Tests were conducted on reinforced concrete column specimens subjected to axial load and cycled inelastic lateral displacements. The main parameters investigated in the testing program were different moment-reducing hinge details, column aspect ratio, level of axial load, and low-cycle fatigue characteristics.

Schemmel and Zia conducted a study to determine the structural and economic benefits of using high-strength (6,000 to 12,000 psi) concrete in box beams for highway bridges. The goal was to establish a range of application of various beam designs in terms of span capacity. For shorter span lengths, 3-ft-wide spread box beams were found to be the most cost-effective. For longer spans, the 4-ft-wide adjacent box sections were less costly. Strand size does not appear to significantly influence the cost of a box beam.

Malier and Pliskin report on an experimental bridge constructed of high-strength concrete built at Joigny, France. The project is part of a national research program to verify the bridge's long-term behavior and durability in comparison with that of ordinary concrete bridges. The aim of the experiment was to demonstrate the feasibility of building a typical bridge using C 60 concrete and the unsophisticated means and materials that can be found everywhere in France.

Tallin and Petreshock modeled two bimodal distributions. The histogram of the gross vehicle weight (GVW) of trucks was obtained by weigh-in-motion for seven states.The lifetimes based on the two models were compared with each other and with the results obtained by assuming a single lognormal distribution. The results show that the lifetimes estimated using the bimodal distributions differ little from one another but are significantly shorter than the lifetimes estimated from the single lognormal distribution.

Zuraski conducted research demonstrating that ultrasonic testing procedures may be used to determine whether cracks have been initiated within a top flange surface that is embedded in concrete. Three Interstate highway bridges experiencing high volumes of truck traffic and containing AASHTO Category E cover plate details were examined during 1989. Application of the ultrasound technology is described and the results of this field investigation are presented.

Moore et al. evaluated the behavior of a 0.4-scale model of a two-span continuous plate-girder bridge with modular precast prestressed concrete deck panels. The bridge, designed according to Alternate Load Factor Design (ALFD), or Autostress Design, procedures, utilized noncompact plate girders with slender webs that fall beyond the present limits of the ALFD guide specification. A comprehensive plan was followed to subject the model to a series of tests to evaluate specific responses at simulated AASHTO service load, overload, and maximum load levels.

Campbell et al. conducted a laboratory study of the influences of four parameters—contact pressure, temperature, speed of travel, and roughness of the stainless steel surface—on the coefficient of friction at the interface between a tetrafuluorethylene (TFE) surface and stainless steel. It was concluded that the values of the coefficient of friction for TFE given in the Ontario Highway Bridge Design Code follow the proper trend and are conservative, but not unduly so, under the combination of low temperature, high speed of travel, and a rough mating surface.

Burke discusses the use of integrated bridge construction as a response to joint-related bridge damage caused by deicing chemicals and the restrained growth of rigid pavements. He sees an accelerated use of integrated conversion as an effective alternative to bridge joint rehabilitation.

Kane et al. detail the structure, site, and some factors that led to the choice of a double leaf concrete swing bridge for the Duwammish River in Seattle.

Dickson and GangaRao describe the tests performed and the results of their research to develop design guides for stressed-timber T-beam bridges. A bridge was built and a monitoring program initiated.

Shahawy and Garcia describe the current research program of the Florida Department of Transportation, available capabilities, and the necessary components required for successful laboratory and field testing. A brief description of research projects where both laboratory and field testing were utilized to develop new economical bridge systems is given.

Bein reviews relevant risk factors and presents a methodology for determining vessel impact energies and return periods for bridges located over navigable waters.

Suetoh et al. review all available data on unintended composite action in beam-and-slab bridges and investigate the factors influencing the existence of unintended composite action in noncompositely built beam-and-slab bridges. Test reports summarized in this paper have shown that the existence of natural or chemical bond is the single most important factor in determining whether a noncompositely built beam-and-slab system can be counted on to act compositely. However, the uncertainty surrounding the presence of composite behavior and the difficulty associated with verifying the existence of composite behavior make the assumption of composite behavior in a bridge designed noncompositely a questionable one.

Roschke and Aftab enhanced and converted five bridge analysis codes to the microcomputer environment. Bridge applications include linear elastic analysis of beam columns subjected to movable loads, linear and nonlinear frame analyses, and analysis of bent caps and continuous beams. Seamless integration of coded modules is performed so that existing mainframe programs become subroutines to the new microcomputer codes.

Moment-Reducing Hinge Details for the Bases of Bridge Columns

KUANG Y. LIM, DAVID I. MCLEAN, AND EDWARD H. HENLEY, JR.

Bridge foundations in seismic regions are designed to withstand the plastic hinge moments that develop at the bases of the bridge columns. In columns that are oversized for architectural or other reasons, this approach results in excessively large foundations. Various hinge details have been proposed to reduce the plastic moments transferred to the foundation and thereby reduce the size and cost of the foundation. The results of an experimental investigation of the seismic performance of bridge columns with moment-reducing details are presented. Tests were conducted on reinforced concrete column specimens subjected to axial load and cycled inelastic lateral displacements. The main parameters investigated in the testing program were different moment-reducing hinge details, the column aspect ratio, the level of axial load, and low-cycle fatigue characteristics. Columns with the moment-reducing details exhibited stable hinging behavior, even when subjected to repeated cycles at large displacement levels. The hinging behavior was similar to that for a conventional column with the same hinge dimensions and reinforcement. Flexure dominated the behavior of all the columns in this study, including those with an aspect ratio of 1.25. The level of axial load had only a limited effect on the behavior of the columns, with the moment-reducing details due to the confinement provided around the hinge region by the outer architectural column.

Bridge foundations in seismic regions are designed to withstand the plastic hinge moments that develop at the bases of the bridge columns. In columns that are oversized for architectural or other reasons, this approach results in excessively large foundations. Various hinge details for the bases of columns have been proposed, principally by bridge designers in the seismically active regions of the western United States, to reduce the plastic moments transferred to the foundations and thereby reduce the size and cost of the foundation.

The basic concept inherent in the modified hinge details is to provide a reduced moment capacity in the plastic hinging region at the bases of the columns. This is accomplished by placing a layer of easily compressed material at the base of the column, which provides partial discontinuity between the column and the footing. The discontinuity results in a smaller effective cross section at the column base and, thus, a reduced hinge capacity in the column. To a great extent, the modifications that have been suggested have been based on engineering judgment, and the behavior and safety of the moment-reducing details have not been fully established.

K. Y. Lim and D. I. McLean, Department of Civil and Environmental Engineering, Washington State University, Pullman, Wash. 99164–2910. E. H. Henley, Jr., Bridge and Structures Branch, Washington State Department of Transportation, Transportation Building KF-01, Olympia, Wash. 98504.

The results of an experimental investigation of the seismic performance of bridge columns with moment-reducing hinge details are presented. The hinge details investigated in this project are shown in Figure 1. Tests were conducted on reinforced concrete column specimens subjected to axial load and cycled inelastic lateral displacements. The main parameters investigated in the testing program were different moment-reducing hinge details, column aspect ratio, level of axial load, and low cycle fatigue characteristics.

EXPERIMENTAL PROGRAM

Reinforced concrete scale models of bridge columns were tested with different moment-reducing hinge details. The test specimens consisted of a single column member connected at the base to a rectangular footing. The specimens were subjected to increasing levels of cycled inelastic displacements under a constant axial load and were deflected in single curvature.

Experimental tests were performed on small-scale specimens of approximately 1/20 scale and moderate-scale specimens of approximately 1/6 scale. More than 50 small-scale specimens were tested. The small-scale tests provided a cost-efficient parametric study and also guided the selection of the parameters for the large-scale tests. Nine 1/6-scale specimens were tested. The larger, 1/6-scale tests resulted in a more realistic representation of the hinging behavior in actual bridge columns, and size effects were reduced when compared with the small-scale tests. Only the 1/6-scale test procedures and results are discussed in this paper. A detailed discussion of the test procedures and results for the small-scale study may be found elsewhere (*1*).

Test Specimens and Parameters

The test specimens were arranged in pairs: one specimen incorporated a hinge detail providing only horizontal discontinuity (CA detail) and the other specimen incorporated a hinge detail providing both vertical and horizontal discontinuity (WA detail). These details are shown in Figures 1a and 1b. The discontinuities between the column and the footing are provided by a layer of easily compressed material at the base of the column. Because only horizontal discontinuity is provided in the CA detail, the plastic hinging action in a column with this detail will be largely concentrated along a horizontal plane at the interface between the column and the footing. Both horizontal and vertical discontinuity are pro-

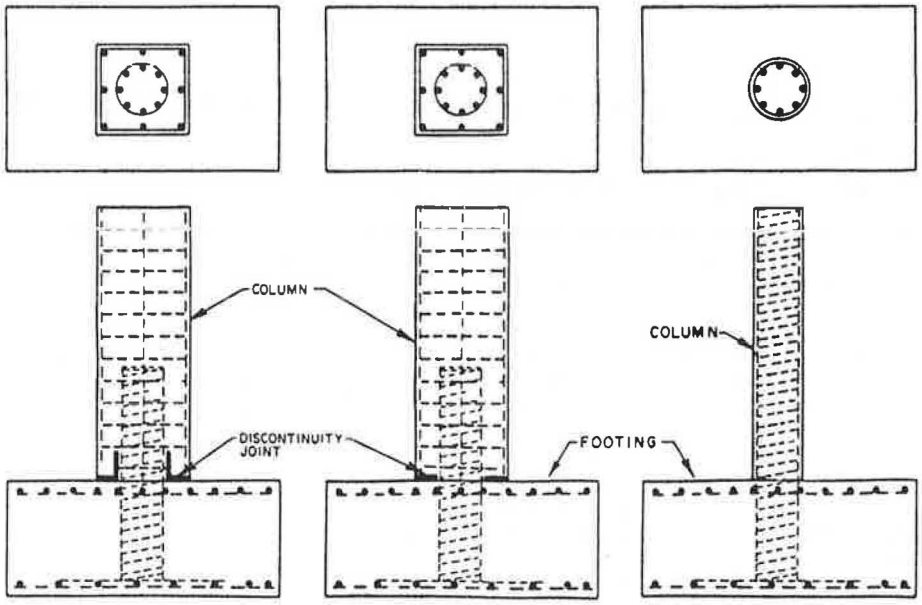

FIGURE 1 Hinge details investigated.

vided in the WA detail, with the objective of distributing the plastic stresses over a greater vertical length.

The testing program was carried out on four specimens incorporating the CA detail, four specimens incorporating the WA detail, and one reference or control column consisting of a column with the same dimensions and reinforcement as the hinge connection of the columns incorporating the moment-reducing hinge details (CON detail). Dimensions and reinforcement for a typical column specimen are shown in Figure 2.

Two column height-to-width ratios were investigated in the study: 1.25 and 2.5 measured with respect to the architectural column. The height of the architectural column, H, was varied while the cross-sectional dimensions of the column, D, were kept constant. Two levels of axial compression were studied: $P/(f'_c A_c) = 0.24$ and 0.35, where A_c is the cross-sectional area of the hinge connection measured out-to-out of the spiral. On the basis of actual designs of the moment-reducing hinge details and the results of the small-scale experimental study, a hinge longitudinal reinforcing ratio of 7.2 percent referenced to the area of the hinge connection and a hinge spiral reinforcing ratio of 1.5 percent were selected for use in all specimens.

The thickness of the horizontal discontinuity joint in the test specimens was 0.5 in. For the WA hinge detail, a vertical discontinuity joint with a height of 6 in. was also provided. On the basis of results from the small-scale tests, the horizontal joint thickness in both hinge details was increased to 1.0 in. at the outer edges of the column to allow the hinge to rotate without having the top of the footing contact the architectural column edge. The small-scale study indicated that hinge performance is independent of the shape of the architectural column if contact between the column edge and the footing is prevented. The discontinuity joints for columns with the CA and WA details are shown in Figure 3.

A summary of the details of the specimens of the testing program is given in Table 1.

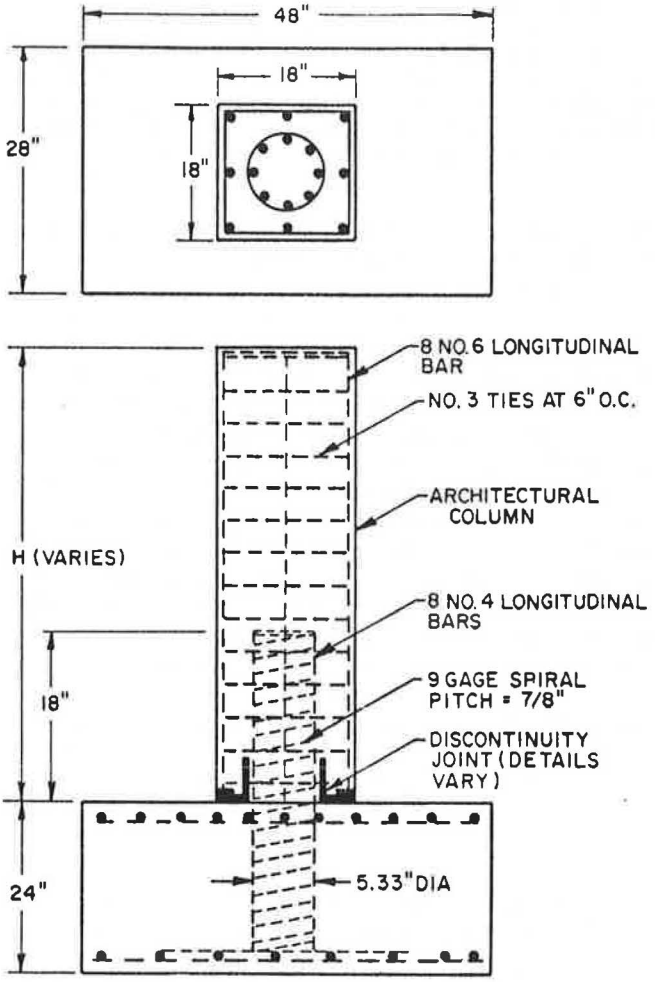

FIGURE 2 Typical dimensions and reinforcement of the column specimens.

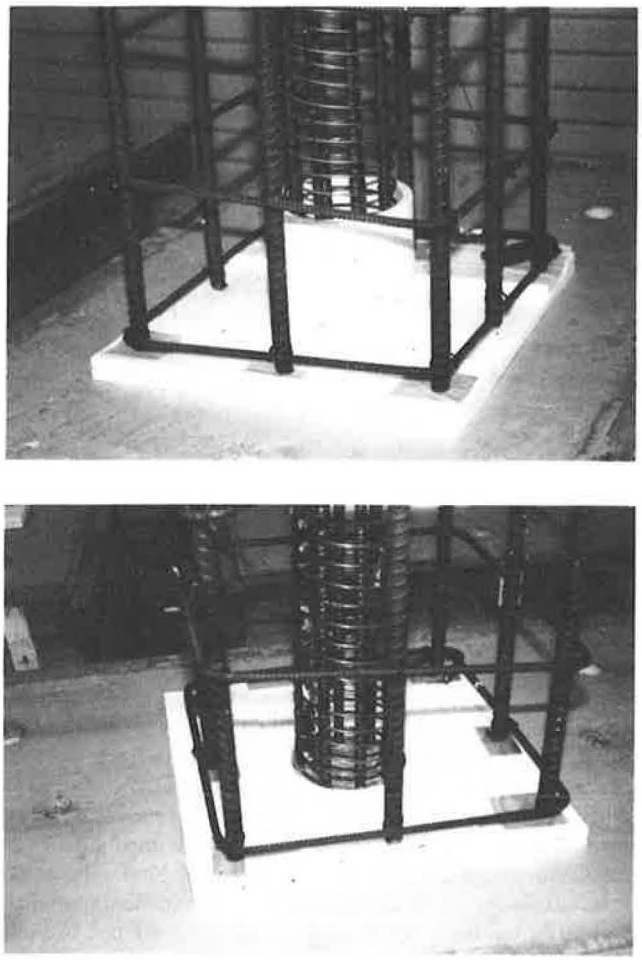

FIGURE 3 Hinge details before casting of the columns.

Materials

The concrete used in the specimens was a Washington State Department of Transportation Class AX mix (a typical mix used for bridge construction in Washington State). The concrete consisted of portland cement Type I/II, sand, river gravel coarse aggregate with a maximum size of ¾ in., water reducer, and an air-entraining agent. The mix resulted in an average compressive strength, measured at 28 days, of 5,000 psi.

Longitudinal reinforcement in the hinge region of the column specimens consisted of No. 4 ASTM Grade 60 reinforcing bars with a measured yield strength of approximately 65 ksi. Spiral reinforcement was provided in the hinge connection using 9 gauge (0.147-in.-diameter) ASTM A82 smooth bars with a measured yield strength of approximately 90 ksi.

The discontinuity joints were commercially manufactured preformed expanded polystyrene.

Test Apparatus, Instrumentation, and Procedures

After curing for approximately 28 days, the footing of a specimen to be tested was anchored to a laboratory strong floor. Axial force was first applied to the top of the column using a 55-kip actuator operated in force control. Axial forces were maintained at a constant level during a test. Lateral force was then applied slightly below the top of the column using a 22-kip actuator operated in displacement control. An analog signal of a prescribed ramp function was generated using a personal computer and sent to the servocontroller of the actuator. Figures 4 and 5 show the test setup.

Actuator loads and displacements were monitored during the tests. Linear variable displacement transformers (LVDTs) were mounted to the sides of the columns to measure the rotation of the column base. Strain gauges were used to monitor the strains in the longitudinal and spiral reinforcement within the hinging region. All data were recorded intermittently on the same personal computer used to generate control signals for the horizontal actuator.

The determination of the yield displacement, Δy, and the loading sequence was similar to the procedures used by Priestley and Park, Ang et al., and Park and Blakely (*2–4*). However, on the basis of preliminary tests, it was found that the ultimate moment capacities and stiffnesses, and hence the yield displacements, varied in columns with different details. In order to better compare the hinging behavior of columns with the CA and WA details, it was decided that parallel sets of columns would be subjected to the same displacement history. Thus, the same displacement value was defined as the yield displacement for columns incorporating different hinge

TABLE 1 SUMMARY OF THE TESTING PROGRAM

Specimen No.	Variable Studied	Aspect Ratio (H/D)	Axial Load (P/f'_cA_c)	Yield Displacement (in.)	Measured Yield Moment (in.-kips)	Measured Peak Moment (in.-kips)	Maximum Applied Shear Load (kips)
CA1	aspect ratio	2.50	0.24	0.30	181	270	6.0
WA1	"	2.50	0.24	0.30	133	212	4.7
CON2	hinge detail	*	0.24	0.15	93	209	9.3
CA2	"	1.25	0.24	0.15	162	279	12.4
WA2	"	1.25	0.24	0.15	142	250	11.1
CA3	axial load	1.25	0.35	0.15	166	277	12.3
WA3	"	1.25	0.35	0.15	135	240	10.7
CA4	low-cycle fatigue	1.25	0.24	0.15	138	271	12.0
WA4	"	1.25	0.24	0.15	130	236	10.5

* circular control column with the same height as Units CA2 and WA2

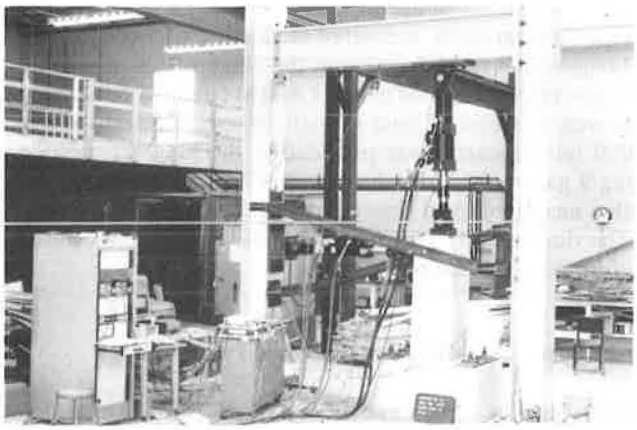

FIGURE 4 Test setup.

details but with the same aspect ratio. The typical loading sequence used for the tests was two cycles at displacement ductility factors (i.e., multiple values of Δy) of μ = 1, 2, 4, 6, 8, 10, and 12. Figure 6 shows the typical loading sequence.

RESULTS AND DISCUSSION

A summary of the test results for all specimens is presented in Table 1. Column performance was evaluated with respect to the moment capacity and displacement ductility attained, the overall hysteresis behavior, and degradation and energy dissipation characteristics. Rather than a discussion of the results for each specimen individually, results for groups of specimens are presented to facilitate correlation of the influence of various parameters with column performance and to obtain behavioral trends.

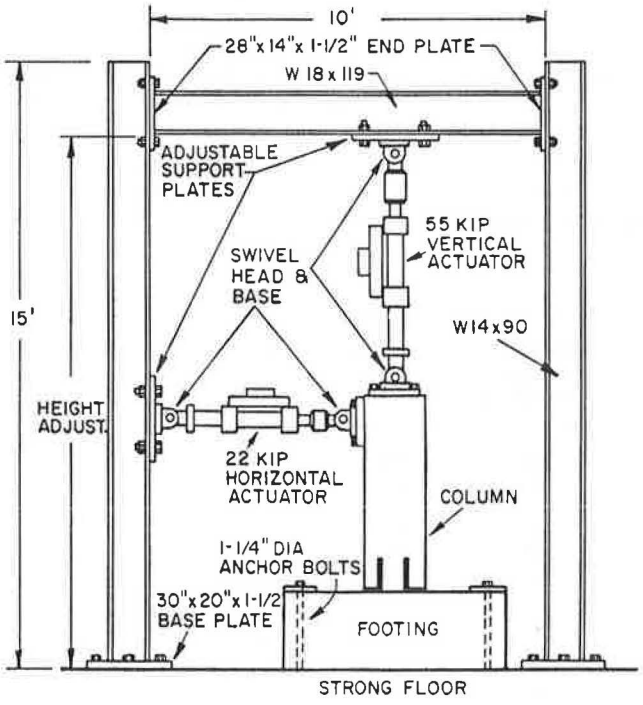

FIGURE 5 Schematic drawing of the test setup and reaction frame.

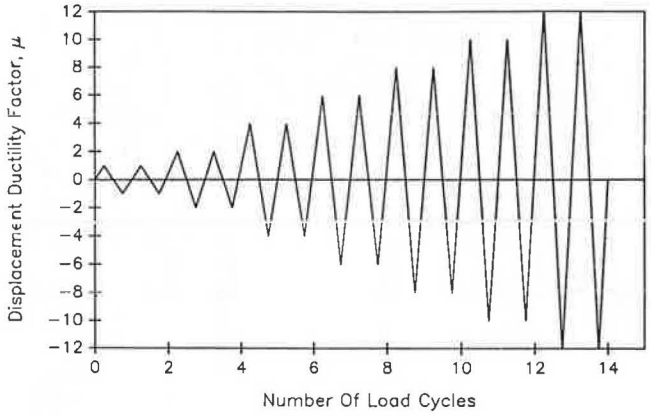

FIGURE 6 Typical loading sequence.

General Behavior

Tests were performed on columns incorporating a WA detail (Unit WA2), a CA detail (Unit CA2), and a circular control column (Unit CON2) with the same dimensions and reinforcement as the inner hinge of the modified columns. These columns were subjected to an axial load level of $0.24f'_cA_c$, and the columns had an aspect ratio of 1.25. The load-displacement hysteresis curves for Units WA2, CA2, and CON2 are shown in Figures 7, 8, and 9, respectively. The lateral loads presented are the true lateral loads on the specimens, including P-Δ effects and secondary effects from the axial load. The hysteresis curves for all three specimens show excellent stability even at displacement levels of μ = 12. No evidence of any sudden drop in load-carrying capability was observed, and the plastic hinges continued to absorb energy throughout the tests.

Figure 10 shows the plots of the shear strength envelope curves for these columns, which is obtained by plotting the maximum shear force attained at each peak displacement level with respect to that displacement. For Units WA2 and CA2, very little degradation in strength is observed. However, some degradation can be seen in Unit CON2 begining after μ = 4. Also from Figure 10, it can be seen that Unit CA2 exhibited the greatest stiffness and Unit CON2, the least stiffness. Two reasons can be cited for the difference in stiffness observed in these specimens. First, the elastic stiffness of the control column is less than that of the architectural columns with the moment-reducing details. Second, the moment-reducing details may have the effect of "pinching" the rebar crossing the interface between the column and the footing, particularly with the CA detail, thereby introducing larger strain values in the longitudinal reinforcement of the moment-reducing details. Readings from strain gauges mounted on the longitudinal bars at the bases of the columns indicated that the strains were consistently higher in Units CA2 and WA2 than in Unit CON2 for the same level of displacement. The largest strain values, for the same level of displacement, were recorded in UnitCA2.

Effects of Column Aspect Ratio

To evaluate the effects of column aspect ratio on the behavior of the modified hinges, test results for columns with aspect

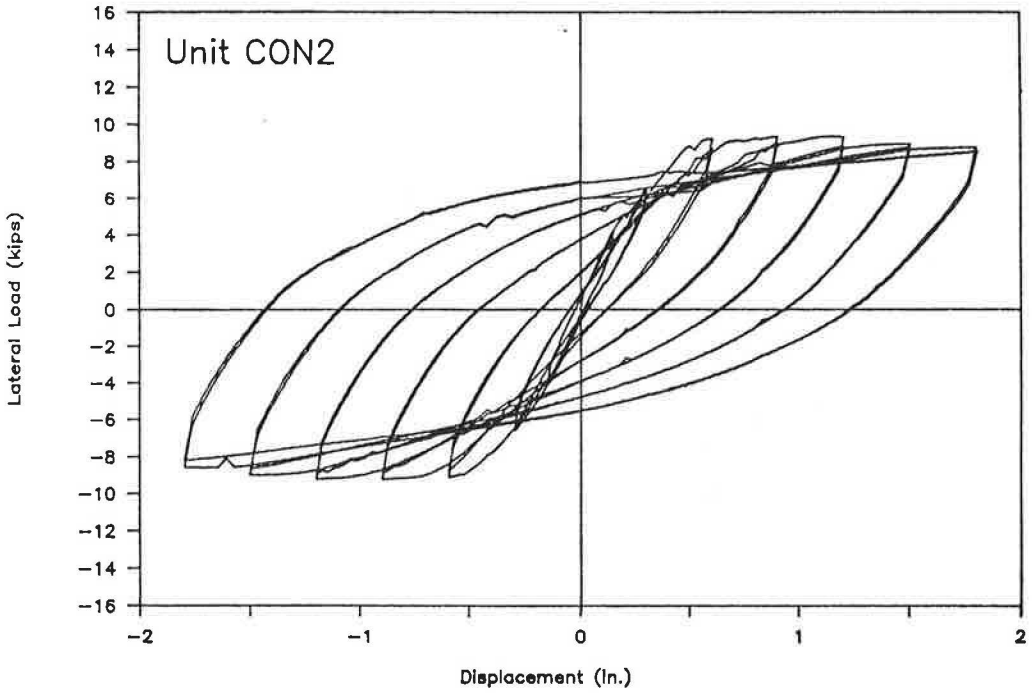

FIGURE 9 Lateral load-displacement hysteresis curves for Unit CON2.

in strength occurred in the columns with the higher aspect ratio, particularly for the column with the WA detail. It can also be seen that the drop in strength from the first to the second cycle of loading for the columns incorporating the CA detail was approximately constant for the two aspect ratios. However, the drop was greater in the shorter column incorporating the WA detail.

Effects of Axial Load Level

To examine the effect of the axial load levels on the modified column performance, Units WA2 and CA2 and Units WA3 and CA3 were tested with axial load levels of $0.24f'_cA_c$ and $0.35f'_cA_c$, respectively. The hysteresis curves for Units WA3 and CA3 are shown in Figures 15 and 16, respectively. Comparing these hysteresis curves with those for Units WA2 and CA2, it can be seen that there is only a small difference between the curves for the specimens with the WA details, and there is virtually no difference in the curves for the specimens with the CA details.

Figures 17 and 18 show the shear strength envelope curves for Units WA2 and WA3 and Units CA2 and CA3, respectively. In the columns with the WA detail, the larger axial load resulted in a greater drop in strength. In the columns with the CA detail, axial load seemed to have little effect on the strength. The reason that these columns are relatively unaffected by axial load level may be the considerable confining effect provided around the hinge region by the outer architectural column, particularly with the CA detail.

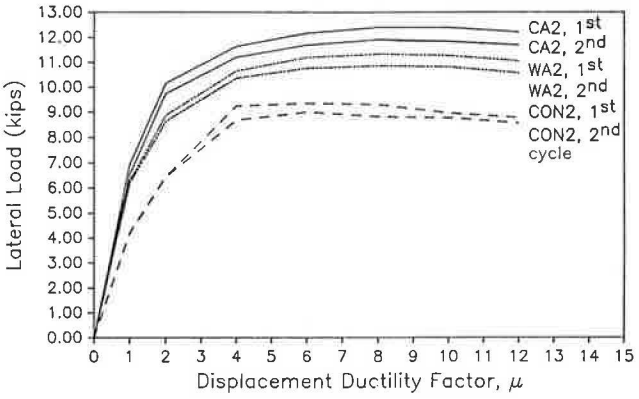

FIGURE 10 Shear strength envelope curves for Units CON2, WA2, and CA2.

Effects of Low-Cycle Fatigue

Tests were performed on Column Units WA4 and CA4 to evaluate the low-cycle fatigue characteristics of the moment-reducing hinge details. Both units were cycled to a displacement level of $\mu = 10$ and then subjected to multiple cycles at this displacement level. The hysteresis curves for Units WA4 and CA4 are shown in Figures 19 and 20, respectively. For both specimens, very little degradation occurred after the completion of the second cycle at $\mu = 10$. The hinges continued to exhibit stable plastic behavior even after being cycled up to 16 times at this displacement level.

Repeatability of Results

Units WA4 and CA4 were constructed identically to Units CA2 and WA2. The two sets of columns were also loaded identically through two cycles of loading to a displacement ductility level of $\mu = 10$. Hence, comparing the results from

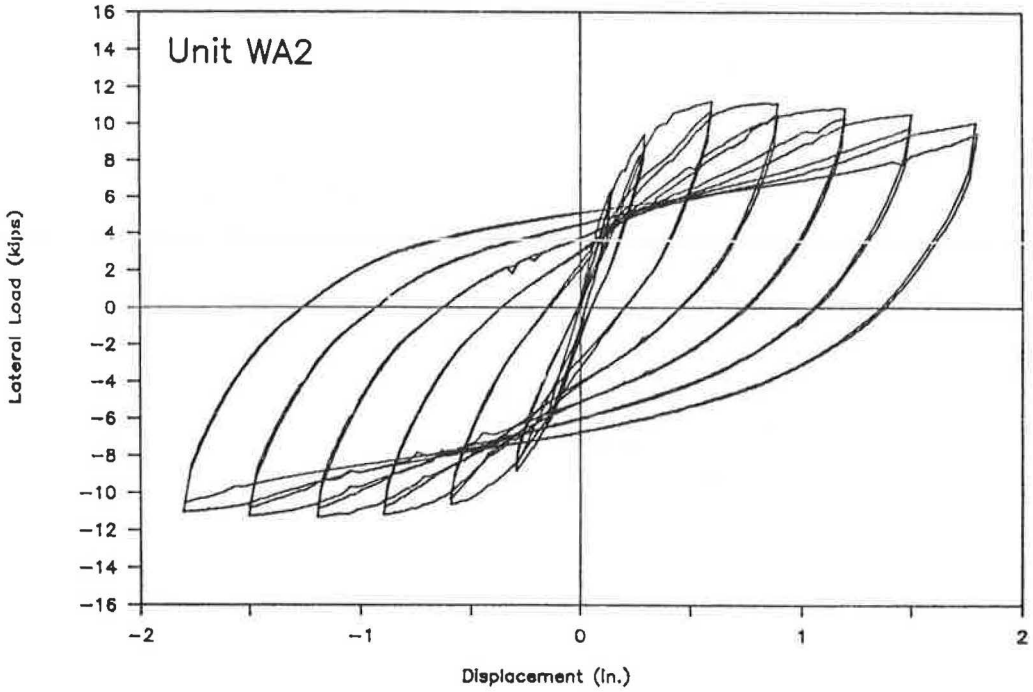

FIGURE 7 Lateral load-displacement hysteresis curves for Unit WA2.

ratios of 2.5 (Units WA1 and CA1) and 1.25 (Units WA2 and CA2) were compared. The hysteresis curves for Units WA1 and CA1 are shown in Figures 11 and 12, respectively. The hysteresis curves for the specimens with the higher aspect ratio are similar to those for the shorter specimens, indicating that flexure dominated the behavior of both sets of specimens. However, it can be seen in the plots that the curves for Unit CA1 are somewhat narrower than those for Unit WA1, indicating decreased energy dissipation characteristics in the column with the CA detail.

The shear strength envelope curves for Units WA1 and WA2 and Units CA1 and CA2 are shown in Figures 13 and 14, respectively. To account for the different lateral load levels associated with columns of different heights, the shear force, V, is plotted normalized with respect to the yield shear force, V_y. It can be seen in Figures 13 and 14 that greater degradation

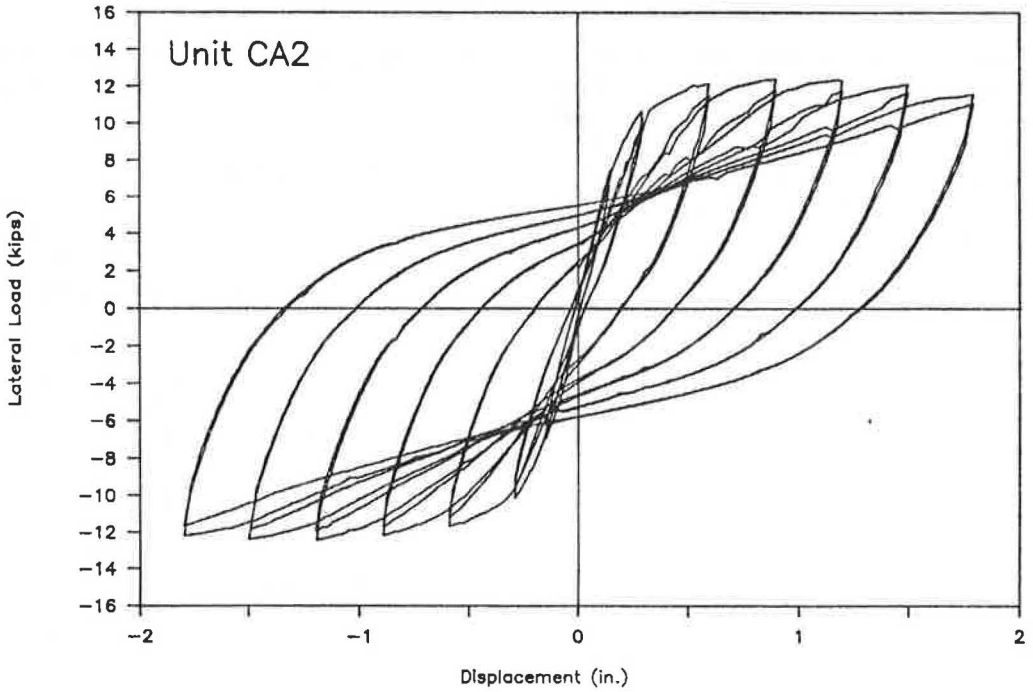

FIGURE 8 Lateral load-displacement hysteresis curves for Unit CA2.

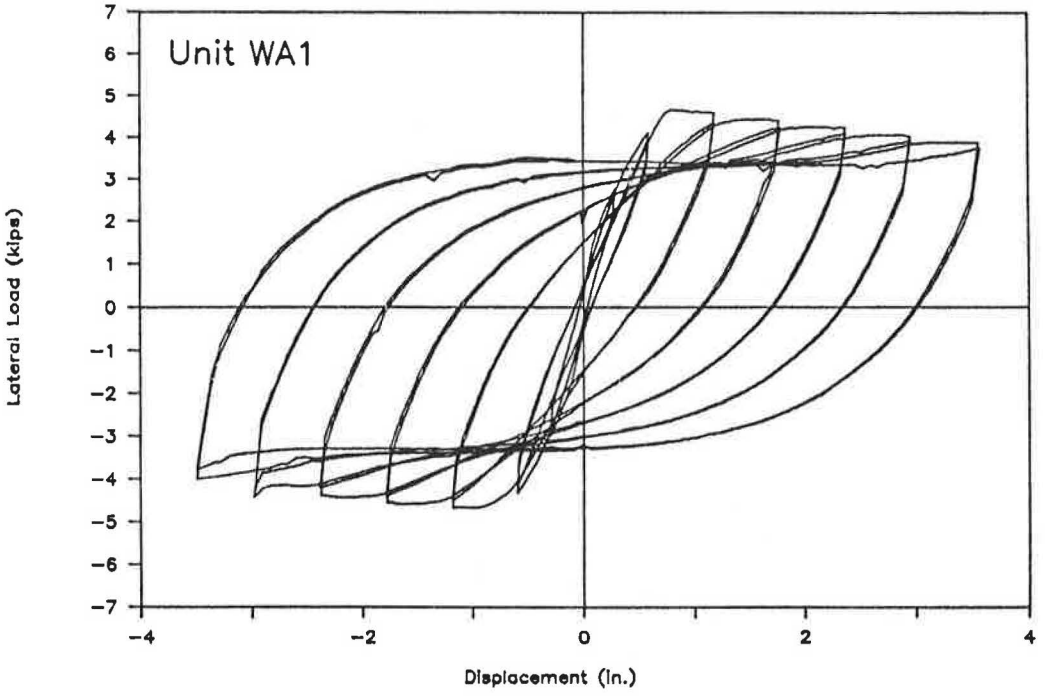

FIGURE 11 Lateral load-displacement hysteresis curves for Unit WA1.

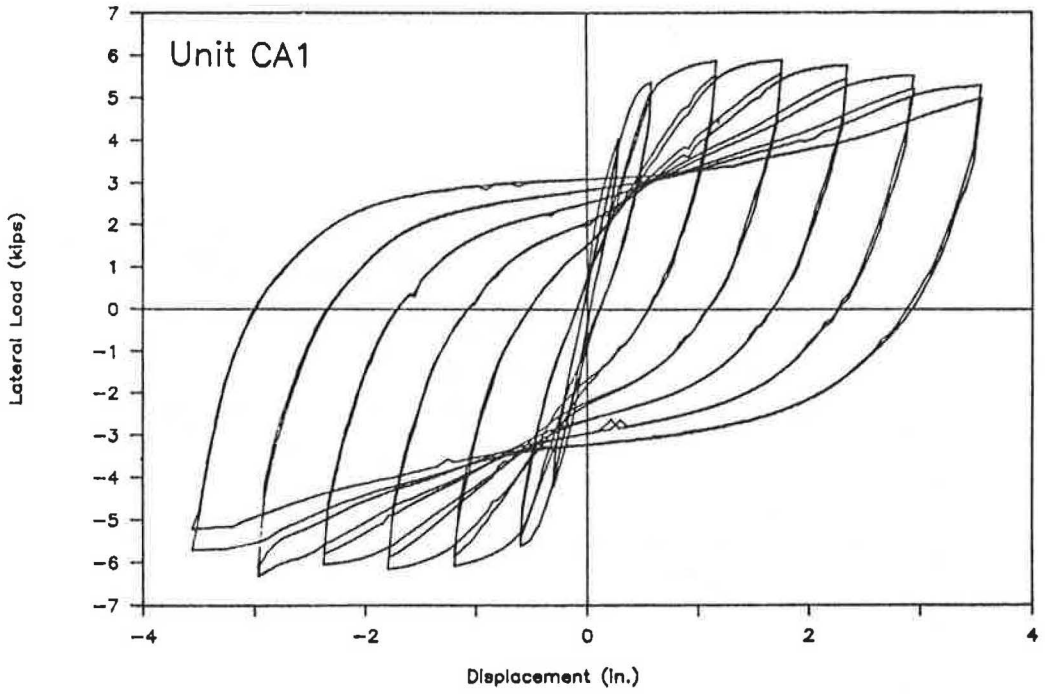

FIGURE 12 Lateral load-displacement hysteresis curves for Unit CA1.

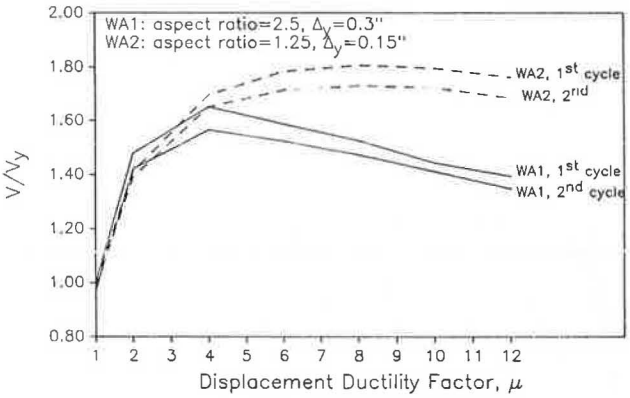

FIGURE 13 Shear strength envelope curves for Units WA1 and WA2.

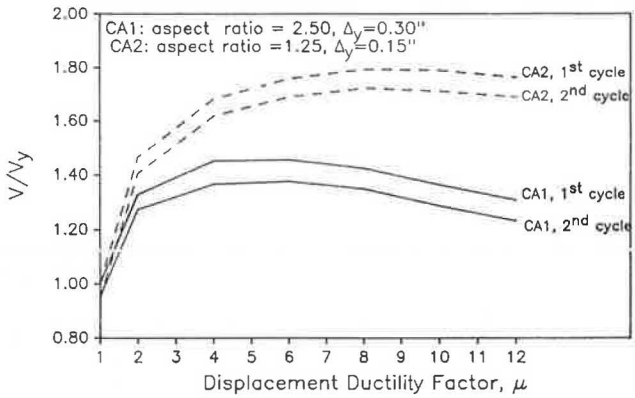

FIGURE 14 Shear strength envelope curves for Units CA1 and CA2.

these columns provides a measure of the repeatability of the test results. The shear strength envelope curves for Units WA2 and WA4 and Units CA2 and CA4 are shown in Figures 21 and 22, respectively. It can be seen that there is close agreement between the results from the two sets of tests.

Comparison of Energy Dissipation Characteristics

The energy dissipated by a column during a particular load cycle is represented by the area enclosed by the load-displacement hysteresis curve. The energy dissipated by a perfectly elastoplastic system during a complete displacement cycle, as shown in Figure 23, is the area of the parallelogram *BCDE*. For a particular displacement ductility factor, μ, the ideal plastic energy dissipated, E_p, can be computed as

$$E_p = 4(\mu - 1)V_p\Delta_y$$

where V_p is the maximum shear force attained at that displacement level (*3*).

In order to evaluate quantitatively the energy dissipation capability of the various hinge details, the measured energy dissipation was divided by the E_p-value of the column for the same displacement ductility factor. This ratio will be referred to as the relative energy dissipation index. Plots of E/E_p values versus the displacement ductility factor, μ, for Units WA2, CA2, and CON2 are shown in Figure 24. The low values of E/E_p at $\mu = 2$ and $\mu = 4$ for the control column, Unit CON2, are due to the inexactness in defining the actual yield dis-

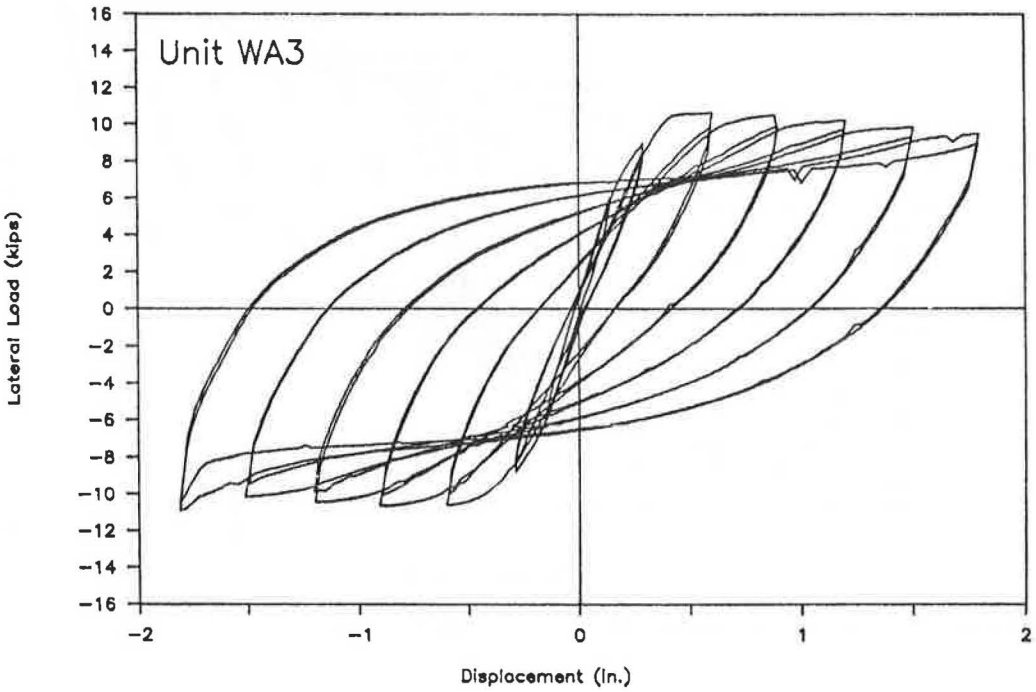

FIGURE 15 Lateral load-displacement hysteresis curves for Unit WA3.

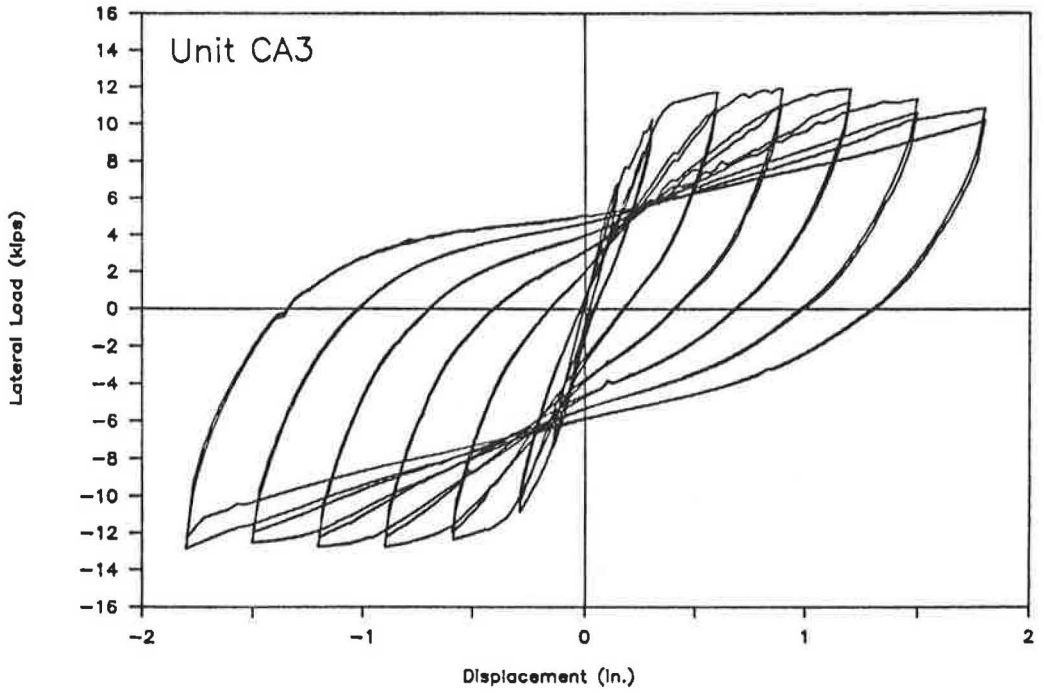

FIGURE 16 Lateral load-displacement hysteresis curves for Unit CA3.

placement in the different columns, with the result that the response of Unit CON2 is still largely elastic at these displacement levels. It can be seen in Figure 24 that the energy dissipation effectiveness is greatest for Unit CON2 and least for Unit CA2. The reduced effectiveness in the columns with the moment-reducing details may be due to a confining of the plastic action (i.e., reduction in length over which the plastic hinge is developing) at the base of the column, particularly for the CA detail.

SUMMARY AND CONCLUSIONS

The following observations and conclusions were made about the major variables investigated in this study.

1. When subjected to cycled inelastic displacements under constant axial load, the columns of this study with moment-reducing plastic hinge details, both those with the WA detail and those with the CA detail, displayed a hinging behavior that was very similar to the hinging behavior of an unmodified column with the same dimensions and reinforcement. Even at displacement levels of $\mu = 12$, the columns exhibited stable load-deflection hysteresis curves and continued to absorb energy.

2. Columns with the CA moment-reducing detail developed larger strain values in the longitudinal bars for the same level of displacement than did the columns with either the WA moment-reducing detail or the unmodified (control) detail. In addition, columns with the CA detail had lower energy dissipation effectiveness compared with the effectiveness of

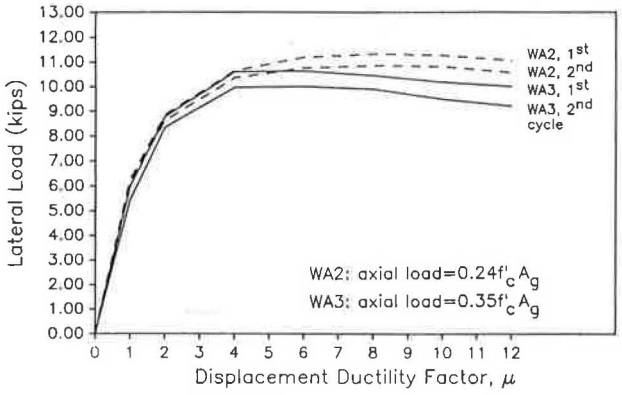

FIGURE 17 Shear strength envelope curves for Units WA2 and WA3.

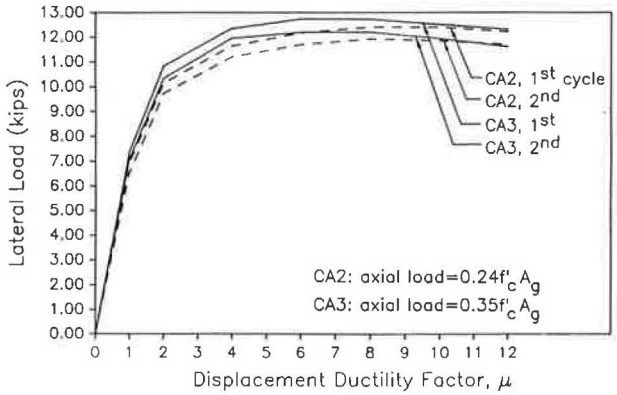

FIGURE 18 Shear strength envelope curves for Units CA2 and CA3.

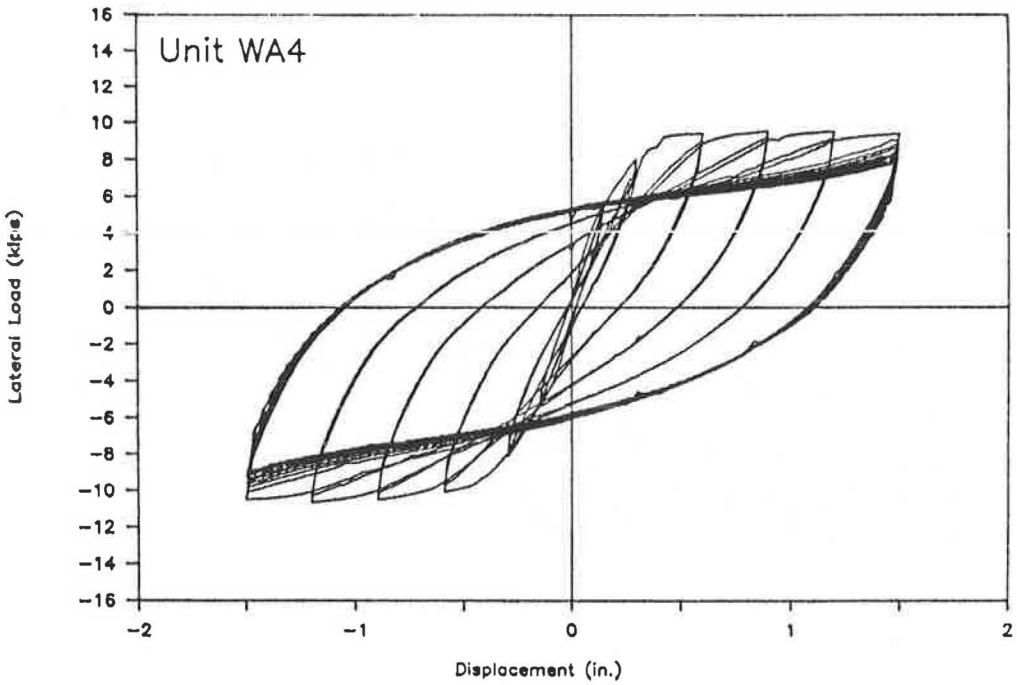

FIGURE 19 Lateral load-displacement hysteresis curves for Unit WA4.

the columns with the other details. Both the larger strain values and the lower energy dissipation effectiveness may be a result of a confining of the plastic hinging action in the columns with the CA detail.

3. Flexure dominated the behavior of all the columns of this study, including those with an aspect ratio of 1.25. However, the lower aspect ratio resulted in a greater drop in strength between the first and second cycle of loading at a particular displacement level in the columns with the WA detail.

4. Increasing the magnitude of the axial load by approximately 50 percent resulted in a slightly greater degradation of shear strength in the columns with the WA detail. However, the columns with the CA details were unaffected by the

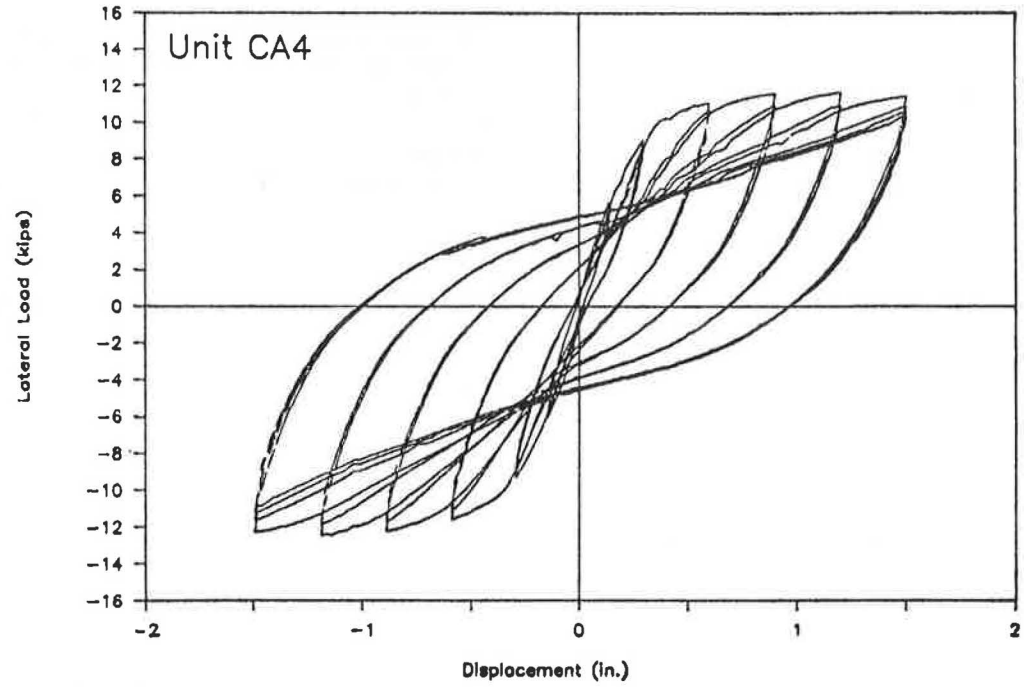

FIGURE 20 Lateral load-displacement hysteresis curves for Unit CA4.

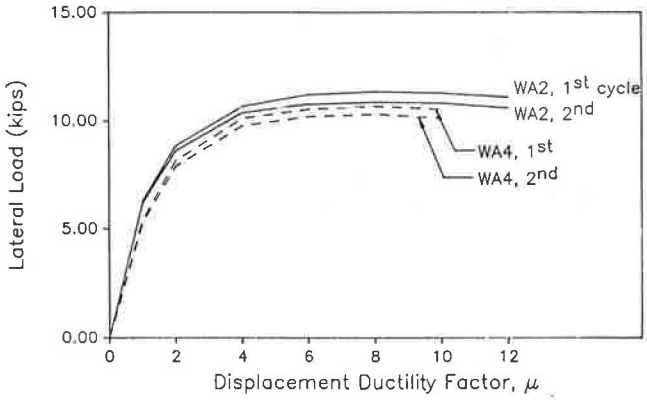

FIGURE 21 Shear strength envelope curves for Units WA2 and WA4.

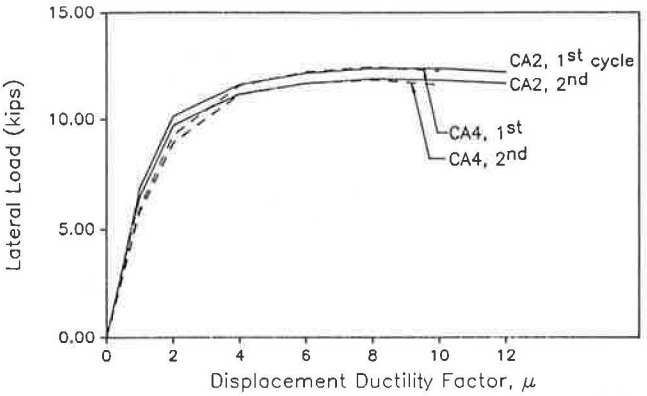

FIGURE 22 Shear strength envelope curves for Units CA2 and CA4.

increased axial load. This lack of effect was attributed to the confinement provided around the hinge by the outer architectural column.

5. In the low-cycle fatigue tests, no evidence of distress was observed in the columns with either the WA or CA details when units were cycled up to 16 times at a displacement level of $\mu = 10$.

ACKNOWLEDGMENTS

The research presented in this paper was funded by the Washington State Transportation Center (TRAC). The authors acknowledge the valuable advice and assistance of several people, including Umesh Vasishth of Arvid Grant and Associates Consulting Engineers; Robert Chen of the Washington State Department of Transportation; and Kurt Nelson, Yung-Ho Won, John Peterson, and Greg Lisle, graduate and undergraduate students in the Department of Civil and Environmental Engineering at Washington State University.

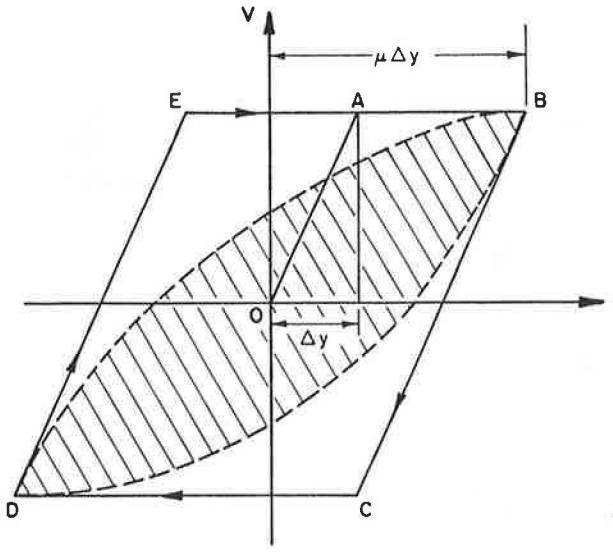

FIGURE 23 Actual and idealized perfectly elastoplastic hysteresis curves.

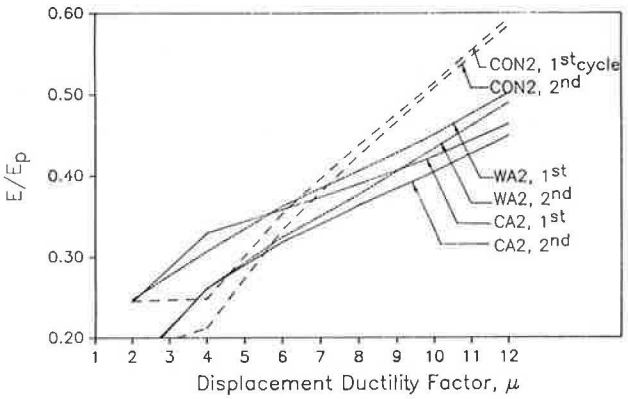

FIGURE 24 Relative energy dissipation index curves for Units CON2, WA2, and CA2.

REFERENCES

1. K. Y. Lim, D. I. McLean, and E. H. Henley. *Plastic Hinge Details for the Bases of Bridge Columns: Small-Scale Model Study*. Interim Project Report. Washington State Department of Transportation, Olympia, April 1989.
2. M. J. N. Priestley and R. Park. Strength and Ductility of Concrete Bridge Columns Under Seismic Loading. *ACI Structural Journal*, Jan.–Feb. 1987.
3. B. G. Ang, M. J. N. Priestley, and T. Pauley. *Seismic Shear Strength of Circular Bridge Piers*. Research Report 85-5. Department of Civil Engineering, University of Canterbury, Christchurch, New Zealand, July 1985.
4. R. Park and R. W. G. Blakely. *Seismic Design of Bridges: Bridge Seminar 1979*, Summary Vol. 3. Structures Committee, Road Research Unit, National Roads Board, New Zealand, 1979.

Publication of this paper sponsored by Committee on Concrete Bridges.

Use of High-Strength Concrete in Prestressed Concrete Box Beams for Highway Bridges

JOHN J. SCHEMMEL AND PAUL ZIA

A study was conducted to determine the structural and economic benefits of using high-strength (6,000 to 12,000 psi) concrete in box beams for highway bridges. The goal was to establish a range of application of various beam designs in terms of span capacity. The study focused on long-span, simply supported, prestressed concrete box beams. The application of high-strength concrete was investigated in two ways. First, high-strength concrete was substituted for normal-strength concrete in the design of standard beam sections. Second, to improve structural performance, modifications were made to the geometry of the standard beams in conjunction with use of the high-strength material. In both cases a parametric study was performed to identify the most structurally efficient designs. Results indicate that the maximum attainable span of the box beam can be significantly increased by using high-strength concrete in conjunction with a modified internal void shape. In addition, attainable span lengths were generally longer and had ½-in. rather than 0.6-in. strands for the beam sections studied. Those designs found to provide the greatest structural benefit were subsequently examined for their relative cost-effectiveness. Comparisons were made on the basis of a total superstructure cost per square foot of bridge deck. For shorter span lengths, spread box beams 3 ft wide were found to be the most cost-effective. For longer spans, the 4-ft-wide adjacent box sections were less costly. Strand size does not appear to significantly influence the cost of a box beam.

A recently concluded study (*1*) conducted for the North Carolina Department of Transportation (NCDOT) examined the use of high-strength concrete in highway bridge applications. Interest in such research stemmed from the need for long-span bridges in the coastal regions of the state, as well as a recognition of the potential structural and economic advantages of high-strength concrete.

Long-span bridges are often necessary in coastal areas in order to ensure that navigational requirements are met. Generally, steel bridges are used for most long-span installations along the coast of North Carolina, because reinforced and prestressed concrete bridges have not been found to be as economical. However, steel superstructures are particularly susceptible to corrosion in this environment; thus they require frequent maintenance.

The use of high-strength concrete in a highway bridge structure offers many benefits and advantages. From a structural viewpoint, span lengths can be increased and dead loads reduced with the use of lighter and more slender cross sections. In terms of serviceability, durability is improved and deflections may be reduced because of the increase in stiffness. From the standpoint of overall economy, total project costs may be reduced because fewer elements are required.

Realizing that the advantages of high-strength concrete could be directly applied to design situations in the state, NCDOT initiated a research project to assess the extent to which this material might prove beneficial in highway bridge construction. This project examined both standard and modified girder, beam, and pier elements. Results (*1*) for the girder and pier elements considered were similar to the findings of others (*2*,*3*). Because of space limitations, only the findings relative to the box beams are presented.

J. J. Schemmel, 4190 Bell Engineering Center, Department of Civil Engineering, University of Arkansas, Fayetteville, Ark. 72701. P. Zia, Box 7908, Department of Civil Engineering, North Carolina State University, Raleigh, N.C. 27695.

OBJECTIVE

The primary focus of this investigation was the use of high-strength concrete in the girder and pier systems of a simple stringer-type bridge. The main objectives were to identify the structural and economic benefits of utilizing concrete with a compressive strength between 6,000 and 12,000 psi in these types of structural elements. This was to be accomplished by first establishing the range of application for various girder and pier designs in terms of their span length and axial load capacity, respectively. Then the cost-effectiveness of selected designs was evaluated by comparing their cost of construction.

APPROACH

Parametric studies were conducted to identify those box beam designs that provided the greatest structural benefits. The study was confined to simply supported, precast, pretensioned members. In addition to the standard AASHTO box beams, a number of modified sections were investigated. The box beams were evaluated for their maximum span length and the number of prestressing strands required for any given span. High-strength normal-weight concretes of 6,000, 8,000, 10,000, and 12,000 psi at 28 days were considered.

In order to identify the most cost-effective box beams, an economic study was made for those designs that had demonstrated superior structural benefits. The beams were evaluated on the basis of a total cost per square foot of deck over a range of spans. Unit costs for materials and labor were estimated using data from a number of sources.

On the basis of the results of the parametric and economic studies, recommendations were made regarding the most beneficial beam designs.

PARAMETRIC STUDY

The goal of this study was to determine the effect of various structural parameters, such as concrete strength and cross-sectional shape, on the span capacity of a box beam. To accomplish this, a detailed flexural analysis was performed on each of the beam designs considered. To facilitate this effort, computer programs were developed to handle the input, analysis, and output.

Program Development

The following is a brief overview of the analysis process used in this study. A more detailed description of the computer programs can be found elsewhere (*1*).

In the parametric study each analysis began by using the preprocessing routine to define the geometric and material properties of the structure to be analyzed. This included data relative to the bridge cross section, beam cross section, concrete and steel material properties, prestressing strands, loadings, and deflection limits. An important feature of this routine is the option to select a standard box beam shape or directly define a cross section for analysis.

The flexural analysis itself begins with the computation of the cross-sectional properties, loads, and moments. A general strand pattern, which is used in the placement of the prestressing strands, is also established at this point. Then an incremental or iterative process is invoked to determine the maximum span length of the beam, along with the relationship between span length and the required number of prestressing strands. With each increment in span, strands are added to the cross section as necessary until the extreme fiber stresses, ultimate strength, minimum reinforcement, and deflection requirements (when specified) are satisfied. Checks are made at both mid-span and span ends. The initial camber and live load deflection were computed for all beam designs. Although no limits were specified in either case, the deflections were not found to be excessive. The span length is continually increased in small increments until at least one design criterion can no longer be satisfied, regardless of the number of prestressing strands added to the section. The analysis is then terminated. Data generated by the flexural analysis are sent to the postprocessing routine to be formatted and printed. Pertinent data are also stored for use in the subsequent cost analysis.

In general, the flexural analysis routine conforms to the latest AASHTO (*4*) and NCDOT (*5*) design specifications. Before this routine was written, it was necessary to determine which parts of these specifications, if any, required modification to account for the use of higher-strength concretes. It was concluded, after an extensive review of the literature, that the majority of the AASHTO and NCDOT specifications still applied to the design of a prestressed box beam when high-strength concrete was used. The most notable differences between normal and high-strength concrete related to the modulus of elasticity, modulus of rupture, and in some cases the creep of concrete. The equations recommended by ACI Committee 363 (*6*) for the modulus of elasticity (E_c) and modulus of rupture (f_r) were used in this study. These equations are

$$E_c = 40{,}000(f_c')^{1/2} + 1{,}000{,}000 \text{ psi} \quad (1)$$

$$f_r = 11.7(f_c')^{1/2} \text{ psi} \quad (2)$$

Some uncertainty remains regarding the creep of high-strength concrete. Although many studies report less creep with high-strength concrete, the effect of this on the loss of prestress has not been fully established. For this study it was assumed that the specific creep (creep strain/psi) would remain nearly the same as that for normal-strength concrete, because large prestressing forces would be required in some cases. Therefore, the prestress loss due to creep was based on the current AASHTO (*4*) equation. The AASHTO (*4*) equations for losses due to elastic shortening, shrinkage, and stress relaxation were also used. For shrinkage, the relative humidity was taken as 75 percent.

Scope

A typical 36-ft-wide bridge with two 12-ft traffic lanes, a cast-in-place deck, and standard New Jersey barriers was used in this study. The primary variables examined were the beam cross section, beam spacing, strand diameter, and concrete compressive strength.

The eight standard AASHTO box beams were investigated. A typical beam cross section is shown in Figure 1. These sections are either 3 or 4 ft wide with a depth that varies between 27 and 42 in. The shape, size, and location of the internal voids are such that thickness of the walls remains unchanged for all members. In addition to the standard shapes, two sections with modified internal voids were considered. The modified cross sections are shown in Figures 2 and 3. Type A has a bottom flange that is larger than the standard beam, as well as a thinner web. This cross section permits two rows of prestressing strand across the bottom. Type B has a wider web, which permits two columns of strand, and a slightly thicker bottom flange.

Both adjacent and spread box beam designs were investigated. For the spread box beams, only an 8-ft spacing was considered. This was in part because of the limits on spacing

Beam	D1	D2
BI36 or 48	27	16
BII	33	22
BIII	39	28
BIV	42	31

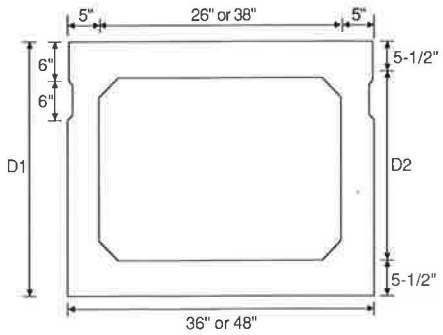

FIGURE 1 Standard AASHTO bridge box beams.

Beam	D1	D2
BI36 or 48	27	15.5
BII	33	21.5
BIII	39	27.5
BIV	42	30.5

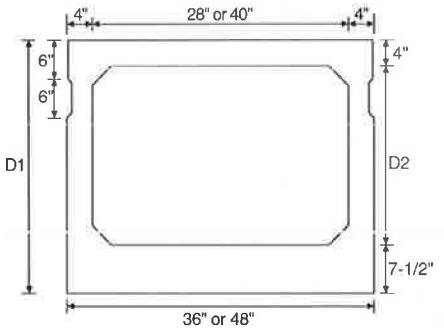

FIGURE 2 Modified Type A bridge box beams.

indirectly imposed by the AASHTO equations for the live load distribution factor. A 4-in. deck with No. 5 bars spaced at 8 in. on center was used with the adjacent beam designs. For the 8-ft beam spacing, a 7.5-in. deck with No. 5 bars spaced at 6 in. on center was specified.

Both ½- and 0.6-in. diameter seven-wire prestressing strands were used in the designs. (The authors recognize that currently there is a lack of sufficient information on the development length of the 0.6-in. strand.) Only low-relaxation Grade 270 strands were considered. A standard 2-in. grid was used in positioning the ½-in. strand, and a 2.5-in. grid was used for the 0.6-in. strand. An outside cover of 2 in. was used in all cases. To ensure that stresses did not become excessive, strands were assumed to be sheathed, as necessary, to prevent bonding and force transfer near the ends. In addition, two strands were located near the top fiber of each section, in order to control transportation and erection stresses.

Four combinations of release and 28-day concrete strengths were considered in this study. Release strengths varied from 4,000 to 7,000 psi in 1,000-psi increments. The corresponding 28-day strengths ranged from 6,000 to 12,000 psi in 2,000-psi increments. A study conducted at North Carolina State University (*7*) indicated that these strengths could be achieved by using locally available materials.

Other pertinent design assumptions included the following:

1. Flexure was assumed to govern the design of the beams. Shear was not examined. Erection camber and live load deflections were computed.
2. The bridge deck was assumed to develop full composite action with the beams in resisting any superimposed loads. In computing the section properties of the composite beam, the deck thickness was reduced by ¼ in. to allow for wearing of the deck.
3. A typical interior beam was used to determine the effective flange width and the magnitude of the superimposed loads.
4. The live load was the HS20 truck or lane load, whichever governed. (It is recognized that HS25 loading has replaced HS20 in some states. However, this is not the case in North Carolina.) The weight of the future wearing surface was taken as 20 psf. The dead weight of the barriers was distributed equally to all beams.
5. Prestress losses were computed according to NCDOT specifications. The loss due to concrete shrinkage was taken as 5,750 psi, which corresponds to 75 percent relative humidity.
6. The allowable tensile stress in the precompressed tensile zone was taken as 0 psi because of exposure to a corrosive marine environment.
7. Two intermediate diaphragms placed at the one-third points were used for all sections and span lengths.

Beam	D1	D2
BI36 or 48	27	18
BII	33	24
BIII	39	30
BIV	42	33

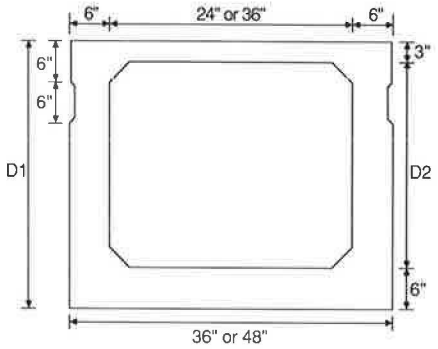

FIGURE 3 Modified Type B bridge box beams.

Results

In most cases, the maximum span capacity of a beam increased as the concrete strength was increased. Relative to that for 6,000-psi concrete, the increase in maximum span ranged from 0 to 25.8 percent for the individual beam designs investigated. Table 1 gives the average percent increase in maximum span for all standard 3- and 4-ft-wide beams and both strand diameters. It is clear from these data that when 0.6-in. strands are used, there is no advantage to using a compressive strength greater than 8,000 psi. However, with ½-in. strands, the maximum span length increased with the concrete strength, up to 10,000 psi. If the compressive strength is increased further to 12,000 psi, there is only a slight additional benefit.

In addition, the form of the relationship between span length and number of strands remains essentially the same as the concrete strength is increased. This can be seen in Figure 4

TABLE 1 PERCENT INCREASE IN SPAN LENGTH FOR STANDARD SECTIONS

	Concrete Strength (psi)	Average Increase in Maximum Span Over that for 6,000 psi Concrete: 1/2" Strand (%)	0.6" Strand (%)
3 Foot Beams			
	8,000	12.4	4.6
	10,000	17.8	4.6
	12,000	18.3	4.6
4 Foot Beams			
	8,000	12.2	3.5
	10,000	16.9	3.5
	12,000	17.3	3.5

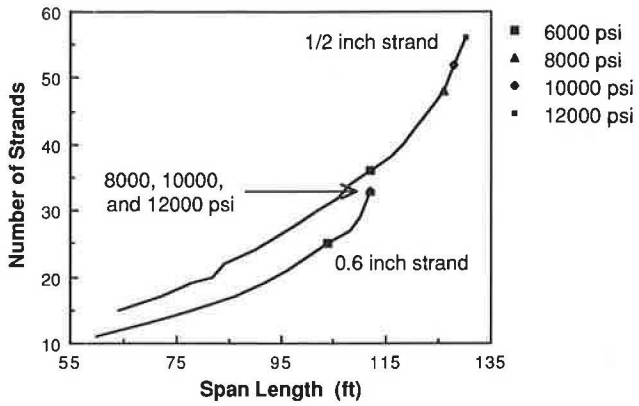

FIGURE 4 Span capacity curves for both ½- and 0.6-in. strands: AASHTO BIV36 adjacent box beams.

where, for an AASHTO BIV36 box beam, span-versus-strand curves are plotted for each concrete strength and both strand diameters. The maximum span length associated with each level of strength is identified on these curves. The plots show that a compressive strength is most beneficial within the range between its own maximum span and that of the next lowest strength.

Figure 4 also displays the main advantage of using 0.6-in. strands in box beams: Fewer 0.6-in. than ½-in. strands are required for the same span length. The difference in the number of strands required varies quite a bit with the span length and the cross section of the beam. However, for an otherwise similar design, maximum span lengths tend to be shorter with 0.6-in. strands.

In Figure 5, span-versus-strand curves are plotted for all of the standard box beams for the case of adjacent beam spacing, ½-in.-diameter strand, and 12,000-psi concrete. These plots show that the 4-ft-wide sections require more strands per beam than do their 3-ft-wide counterparts for the same span. Nonetheless, the total number of strands required for the bridge will be less with the 4-ft sections because fewer members are needed when adjacent box beams are used. Also, the total volume of concrete is less with the 4-ft beams in this case. When an 8-ft beam spacing is used, the 3-ft-wide sections require fewer strands per beam, fewer total strands for the bridge, and less concrete.

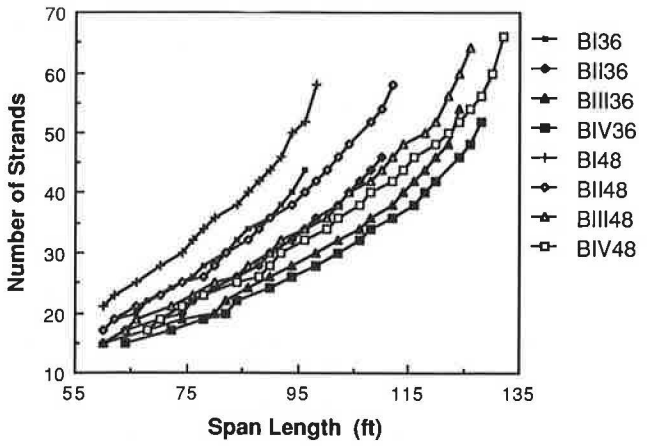

FIGURE 5 Span capacity curves for all standard box beams (f'_c = 12,000 psi; strand diameter = ½ in.).

Both of the modified sections considered in this study provided additional benefits over their parent box beams. The Type A sections were the most effective in almost every case. Relative to the parent beam, increases in the maximum span up to 29.7 percent were observed with the Type A section. Table 2 gives, for each level of concrete strength and both strand diameters, the average percent increase in maximum span for the Type A beam over that for the standard beams. The data indicate that the benefits of the modified sections increase with the concrete compressive strength. It is also clear that 0.6-in. strands can be used to greater advantage with the Type A sections than with the parent beams. A comparison of the span-to-strand relationships for the standard and modified sections also shows that, in general, the Type A sections reach longer span lengths and require fewer strands. Figure 6 shows the span-versus-strand curves for the standard and modified AASHTO BIII48 beams. In addition to the above, the Type A beams have a smaller cross-sectional area than does their parent section.

On the basis of the findings from this study, only the modified box beams were considered in the economic study, because they clearly provided the greatest structural benefits.

ECONOMIC STUDY

Although the constituent materials and production methods are essentially the same as those used for normal-strength concrete, high-strength concrete is generally a more costly material. This is primarily because of the increased material quantities and more stringent quality control procedures.

TABLE 2 PERCENT INCREASE IN MAXIMUM SPAN FOR MODIFIED TYPE A SECTIONS

	Average Increase in Maximum Span Over that for the Standard Section		
	Concrete Strength (psi)	1/2" Strand (%)	0.6" Strand (%)
3 Foot Beams			
	6,000	2.1	4.2
	8,000	4.0	12.8
	10,000	5.1	20.0
	12,000	10.1	21.9
4 Foot Beams			
	6,000	0.0	3.1
	8,000	1.1	13.7
	10,000	4.6	20.8
	12,000	9.5	23.4

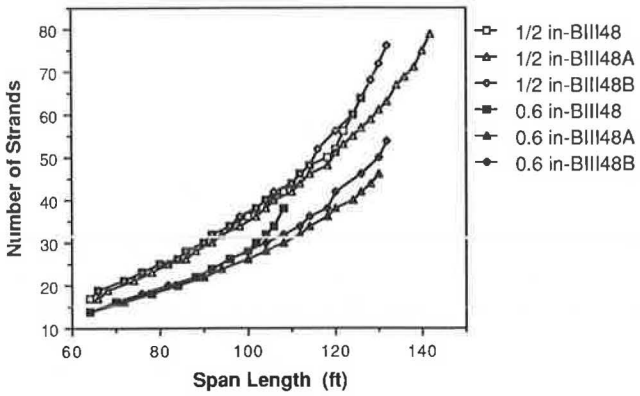

FIGURE 6 Span capacity curves for the standard and modified BIII48 box beams (f'_c = 12,000 psi).

Nonetheless, high-strength concrete can still be an economical construction material because of the structural benefits that can be realized with its use. In order to determine the cost-effectiveness of using high-strength concrete in prestressed box beams, an economic study was made of a number of selected beam designs.

Approach

When the economy of a beam design is evaluated, the overall cost of the bridge superstructure should be considered rather than the cost of a single beam element. This is important because the use of high-strength concrete in a box beam can influence other aspects of a bridge design. For this study, the superstructure was assumed to consist of only the bridge deck and the prestressed box beams. Components whose costs would be common for all bridge designs, such as the barrier rails, diaphragms, and future wearing surface, were not considered.

The cost-effectiveness of the modified box beams was evaluated by preparing a set of cost curves for each beam. These curves were created with the aid of a computer program written for this study. Using data from the parametric study as well as the specified unit costs for materials and labor, a total superstructure cost per square foot of bridge deck was computed for each increment in span length up to the maximum span. A total superstructure cost curve was developed for each combination of concrete strength, beam spacing, strand diameter, and beam cross section examined. Figure 7 shows the superstructure cost curves for an AASHTO BII36A beam with ½-in. strands. By connecting the points of least cost, an idealized cost curve can be created for the box beam. This approach eliminates the compressive strength and beam spacing as variables from the economic analysis. Idealized cost curves were created for each of the modified box beams and both strand diameters. A somewhat similar approach was used by Rabbat et al. (*2*) in their study of bridge girders.

By comparing the idealized curves, the most economical beam designs were identified as those being the least costly over a range in span length.

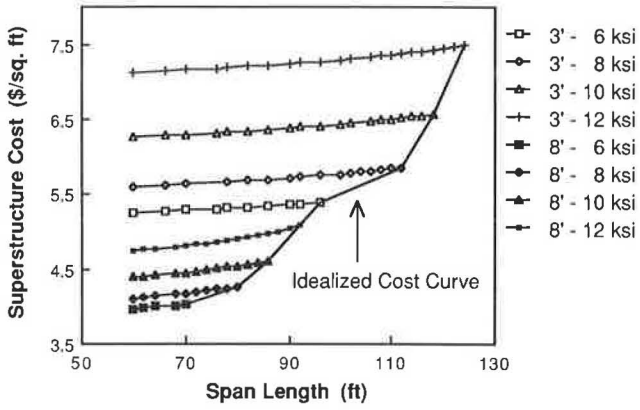

FIGURE 7 Cost curves for the BII36A modified beam with ½-in. strand.

Unit Costs

The primary materials used in the construction of a typical superstructure include normal-strength concrete and mild steel reinforcement for the bridge deck. The box beams require high-strength concrete, internal void material, sheathing, mild steel reinforcement, and prestressing strands. Labor costs should account for the setup and removal of formwork; placement of the reinforcement and prestressing strands; tensioning of the strands; mixing, placement, finishing, and curing of the concrete; quality control testing; storage; transportation; and erection. In addition to the material and labor charges mentioned, there are the indirect costs of overhead and profit to be considered.

In order to simplify the economic analysis, only those items listed below were included in the computation of the total cost for a superstructure:

1. Normal-strength concrete and primary flexural steel for the bridge deck,
2. High-strength concrete and prestressing strands for the box beams,
3. Labor charges for the production and placement of the concrete, and
4. Labor charges for the placement of the reinforcement or prestressing strands.

It was necessary to establish a typical, or average, unit cost for each of the items listed above. This was a more difficult task than it would first appear. With high-strength concrete being a state-of-the-art material and 0.6-in. strands having had relatively limited use, little hard data are available regarding unit costs for these items. In-place unit costs for the concrete, mild steel, and prestressing strands were estimated from data found in the literature and through private conversations with local precasters. The costs used in this study are shown in Table 3. Overhead and profit were not included. Because

TABLE 3 IN-PLACE UNIT COSTS FOR MATERIALS AND LABOR

Concrete Strength (psi)	$/cy
3,000	60
6,000	75
8,000	82
10,000	95
12,000	112
Strand Type	**$/ft**
1/2"-270-LR	0.30
0.6"-270-LR	0.35
Mild Steel	**$/lb**
#5 Bars	0.38

there were no readily available data, the unit cost for 0.6-in. strands was estimated from that for ½-in. strands.

Results

The cost curves for the AASHTO BII36A beam, shown in Figure 7, are typical of most of the modified box sections examined. These curves clearly show the economic benefit of using higher-strength concretes in conjunction with wider beam spacings. For example, the cost of a design using 12,000-psi concrete with an 8-ft spacing is, on average, 7.7 percent less than a design that uses 6,000-psi concrete and a 3-ft spacing while maintaining a similar span capacity. To reach longer span lengths, closer beam spacings and higher-strength concretes are necessary, however costly. In general, these results are similar to the findings of Rabbat (*2*) and Jobes (*3*) for the I- and T-shaped girder sections they considered.

Figures 8 and 9 show the idealized cost curves for the modified BII, BIII, and BIV sections for both beam widths and strand diameters. For clarity, the curves for the BI sections are not shown; these sections were found to be the most costly in nearly all cases. The curves in Figures 8 and 9 make clear which box beam sections are the most cost-effective. For span lengths up to about 95 ft, the 3-ft-wide beams, particularly the BII36A, are the most economical. For spans longer than 95 ft, the 4-ft-wide beams, in particular the BIV48A, are more economical. Except for the longest span lengths, there is actually little difference in cost among the three section depths for either beam width. These findings are true for both strand diameters. In fact, for the unit costs used in this study, the strand diameter has very small effect on the total cost of the superstructure.

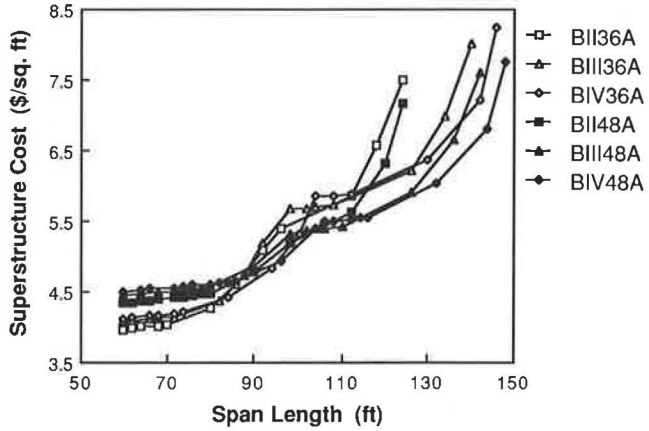

FIGURE 8 Idealized cost curves for 3- and 4-ft modified beams with ½-in. strand.

CONCLUSIONS AND RECOMMENDATIONS

On the basis of the results of this investigation, the following conclusions can be drawn with respect to the use of high-strength concrete in prestressed box beam bridges:

1. Most AASHTO design specifications still apply to high-strength concrete. The equations recommended by ACI Committee 363 for the modulus of elasticity and modulus of rupture were used in this study.
2. Span lengths longer than those previously attainable with normal-strength concrete can be reached with high-strength concrete. On average, the maximum span length of the standard box beams increased about 17 percent with an increase in the concrete strength from 6,000 to 12,000 psi. Some beams showed an increase of more than 25 percent.
3. With the modified Type A beams, maximum span lengths can be increased over the parent sections by about 10 percent with ½-in. strands and by about 22 percent with 0.6-in. strands. Some sections showed nearly a 30 percent increase in span capacity. The modified sections also required fewer strands for the same span and have a smaller cross-sectional area.

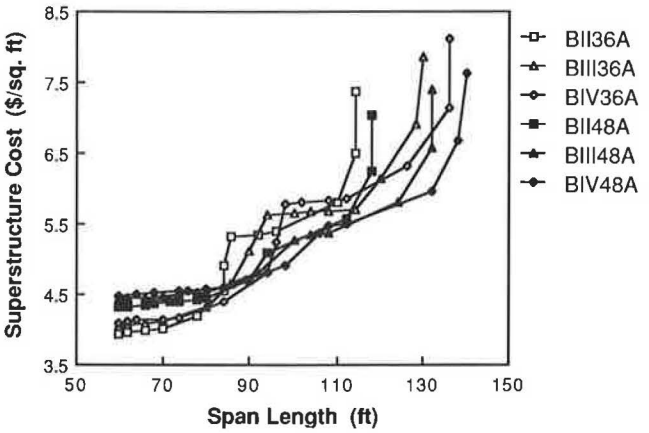

FIGURE 9 Idealized cost curves for 3- and 4-ft modified beams with 0.6-in. strand.

4. For the beams studied, longer span lengths can be reached with ½-in. strands but fewer 0.6-in. strands are required for any common span.

5. For spans up to about 95 ft, 3-ft beams at wide spacings are the most economical, but for longer spans the 4-ft beams spaced more closely are more economical.

The following recommendations are made with respect to the use of high-strength concrete in prestressed box beam bridges:

1. The modified Type A box beam sections should be used rather than the current standard. These sections allow for more strands along the bottom flange. They have a smaller cross section but larger section modulus than the parent sections. For span lengths up to 95 ft, the 3-ft-wide sections should be used. For longer spans, the 4-ft-wide sections should be used. Either ½- or 0.6-in.-diameter strands can be used.

2. Further modification of the standard box beam should be investigated. It was found that the 27-in.-deep sections were never as cost-effective as the others. The 42-in.-deep section, which is the largest, was one of the most economical for all span lengths. An even deeper section may provide further benefits.

3. Although many studies report less shrinkage and creep with high-strength concrete, the effects of this on the loss of prestress have not been fully established. Additional research is needed in this area.

4. The issue of acceptable live load deflections should be studied, because this serviceability requirement is not now addressed by the AASHTO standard specifications. The advantages of high-strength concrete could be greatly diminished if deflection criteria similar to those for steel bridges were imposed.

5. Finally, it is recommended that a few demonstration bridge projects be developed for which high-strength concrete would be specified. Either standard or modified sections could be utilized in these bridges.

ACKNOWLEDGMENTS

This research was conducted by the Center for Transportation Engineering Studies at North Carolina State University in cooperation with the North Carolina Department of Transportation and the Federal Highway Administration.

REFERENCES

1. J. J. Schemmel. The Application of High-Strength Concrete to Highway Bridges. Ph.D. dissertation. Department of Civil Engineering, North Carolina State University, Raleigh, May 1989.
2. B. G. Rabbat, T. Takayanagi, and H. G. Russell. *Optimized Sections for Major Prestressed Concrete Bridge Girders*. Report FHWA/RD-82/005. FHWA, U.S. Department of Transportation, Feb. 1982.
3. H. J. Jobes. *Applications of High-Strength Concrete for Highway Bridges*. Report FHWA/RD-82/097. Research and Development, FHWA, U. S. Department of Transportation, Oct. 1981, 228 pp.
4. *Standard Specifications for Highway Bridges*, 13th ed. American Association of State Highway and Transportation Officials, Washington, D.C., 1983.
5. *Design Manual*, Vol. 1. Structure Design Unit, Highway Design Branch, Division of Highways, North Carolina Department of Transportation, Raleigh, 1984.
6. ACI Committee 363. State-of-the-Art Report on High-Strength Concrete. *Journal of the American Concrete Institute*, Vol. 81, No. 4, July-Aug. 1984, pp. 364–411.
7. M. L. Leming. *Properties of High-Strength Concrete: An Investigation of High-Strength Concrete Characteristics Using Materials in North Carolina*. Final Report. North Carolina Department of Transportation, Raleigh, July 1988.

Publication of this paper sponsored by Committee on Concrete Bridges.

Bridge at Joigny: High-Strength-Concrete Experimental Bridge

YVES MALIER AND LUCIEN PLISKIN

An experimental bridge constructed of high-strength concrete has been built at Joigny, France. The project is part of a national research program bringing together the French Ministry of Public Works and Ministry of Research, the cement industry, university and state laboratories, and professional associations and institutions. The bridge has been instrumented in order to verify its long-term behavior and its durability in comparison with that of ordinary concrete bridges.

In 1985 the French Ministry of Public Works, in association with the Ministry of Research, launched the so-called Projets Nationaux de Recherche et de Développement (National R&D Projects) in the field of civil engineering. One of these projects was devoted to Voies Nouvelles du Matériau Béton (New Developments for Concrete). The objectives of this project are clearly defined by its title: to identify and develop new ways to use the materials that make up concrete.

The objectives of this project can be achieved through construction of experimental structures based on preliminary applied research and through instrumentation of these structures. The implementation of this project is based on four leading principles:

1. To ensure a continuous relationship among basic research, end-user-oriented research, experimental structures, codes, and development. The construction of experimental structures is necessary to demonstrate the actual usefulness of new materials, to evaluate their durability, to assess their economic input, to calibrate and update future codes, and to raise new subjects for further research.
2. To associate new materials with new design concepts.
3. To highlight the notion of "high-performance materials." A global approach to the various properties of concrete allows the adviser, the designer, or the owner to emphasize one or several specific properties of the material. If, as far as new concretes are concerned, their most familiar property is their high compressive strength, it should be borne in mind that other prominent properties should be considered, such as increased durability, frost-thawing resistance, abrasion resistance, or imperviousness to water and gas. This explains why the American high-strength concrete (HSC) has been termed "high-performance concrete" in France.
4. To stress the fact that, as a rule, these high-strength or high-performance concretes, because of their increased durability, will be specified more and more by clients.

Association Technique de l'Industrie des Liants Hydrauliques, 8, Rue Villiot, 75012 Paris, France.

To fulfill its objectives, the project brings together state and private owners such as the Ministry of Public Works, the French Electricity Board (EDF), and the Paris Airport Authority (ADP); the cement industry; large contractors; university, private, and state laboratories; as well as professional associations and institutions.

The project is funded by these members. The budget amounts to about $10 million (U.S.) for a 5-year period, excluding the cost of experimental construction. The Ministry of Public Works subsidizes the project by an incentive support of about $1.20 million (U.S.).

As a matter of fact, a highly valuable contribution is made by the Direction des Routes (Road Direction) of the Ministry of Public Works through its active support in helping to find possible construction sites for experimental HSC bridges.

THE BRIDGE AT JOIGNY

Extensive research and development carried out on HSC in several French civil engineering laboratories made it possible to consider the construction of an actual experimental bridge with HSC.

Aim of the Experiment

The French Ministry of Public Works agreed with the national project team on the following criteria for choosing the nature and location of the experimental bridge:

- The bridge should be representative of current bridge construction and not be exceptional in any way.
- The bridge should not be located near large towns or industrial areas, in which facilities would easily be found.
- The 28-day characteristic strength of the concrete should be 60 MPa (8,600 psi) (generally, French bridges use 35- to 40-MPa concretes).
- The bridge should be built using local cement and aggregates. Local ready-mixed concrete plants were to furnish the material so that their proper capabilities could be checked. The use of silica fume was excluded, because it had been proved that this material was not really necessary to obtain the specified HSC.
- The bridge should be designed according to French building code BPEL 83, which deals with prestressed concrete structures. All the possibilities offered by the enhanced strength of the concrete should be exploited.

• The bridge should be instrumented in order to collect data on its behavior and to verify the validity of the conceptual approach. This criterion led to the specification of cast-in-situ construction methods in order to avoid interference by construction temporary stress distribution.

To summarize these criteria, it can be said that the aim of the experiment was to demonstrate the feasibility of building a typical bridge using C 60 concrete and the unsophisticated means and materials that can be found everywhere in France.

Basic Features of the Bridge

Geometrical Description

The bridge crosses the Yonne River near the town of Joigny. Its concept is quite classical. Aesthetics as well as economics influenced the choice of a balanced, continuous, three-span bridge [i.e., 34, 46, and 34 m (112, 151, and 112 ft)] with a height of 2.2 m (87 in.) and an overall width of 15.8 m (52 ft).

The bridge double-tee cross section is made of two main beams with a trapezoidal cross section and an upper slab. The distance between beam axes is 8 m (26 ft). Their minimal width at the bottom chord is 0.5 m (20 in.).

Prestressing

The structure is prestressed longitudinally by 13 external tendons, each made of twenty-seven 1.5-cm (0.6-in.) strands. External tendons offer three advantages:

1. The width of the webs can be reduced to a minimal value determined chiefly by normal stress considerations. A lighter structure is thus obtained.
2. The tendons may be easily replaced if necessary. This is an advantage, because the C 60 concrete being more durable than ordinary concrete, the life span of the high-tensile steel may be shorter than that of the concrete.
3. In the case of an experimental structure, this layout allows simpler and more accurate prestressing force measurements in the tendons.

Design Stresses

The bridge was designed according to the French codes Béton Précontraint aux Etats Limites (BPEL) (Limit-States Design of Prestressed Concrete) and Béton Armé aux Etats Limites (BAEL) (Limit-States Design of Reinforced Concrete). These codes formerly dealt only with concretes up to C 40 but have been upgraded in order to incorporate C 60 concretes. Only minor adjustments to the codes had to be made, mainly concerning the creep coefficient, which was reduced from 2.00 to 1.50 for C 60 concretes.

The use of these codes, which include different safety factors, led to an actual maximal compressive stress of 30 MPa in the lower fiber of the midsection of the central span during the last stages of prestressing.

High-Strength Concrete Versus Ordinary Concrete

It should be emphasized that comparisons carried out during the preliminary studies of the bridge showed that the concrete quantities could be reduced from about 1395 m^3 (1,800 yd^3), when ordinary C 35 concrete was used to 985 m^3 (1,300 yd^3) with C 60 HSC. This 30 percent reduction in concrete volume led to a 24 percent load reduction onto the pier, abutments, and foundations.

The decreased dead weight also induces savings in the quantities of prestressing strands. Because the height-to-span ratios were slightly different in the two solutions, the steel savings were not as large as they could have been if these ratios had been identical.

Concrete Design

Exhaustive laboratory tests were run in order to define a mix design allowing the production of a ready-mixed concrete with the following properties:

• Mean 28-day strength of about 70 MPa with a minimal standard deviation,
• Ability to be transported and delivered fresh to a construction site 30 km (about 20 mi) from the concrete plant,
• Ability to be pumped in pipes 120 m (470 ft) long,
• High workability after a sufficient time.

The concrete batch constituents were as follows:

• Fine aggregate: sand from Yonne River, 0/4 mm; corrective sand, 0.080/0.13 mm;
• Coarse aggregate, 6/20 mm;
• Cement HS PC, 450 kg/m^3 (760 lb/yd^3);
• Water, 161 liters/m^3 (271 lb/yd^3);
• WRA and retarder.

Concrete Properties

Fresh Concrete

The water/cement (W/C) ratio, measured at the plant for every batch, remained between 0.362 and 0.377. The slumps, measured at the site, were over 200 mm for more than 2 hr. The entrained air contents were within 0.5 and 1 percent.

Hardened Concrete

Compressive Strength The concrete strength was measured on test samples. According to the French standards, these are cylinders with a diameter of about 160 mm (cross section of 20,000 mm^2) and a height of 320 mm, which were cast in metallic molds.

The mean compressive strength f_{cm} was as follows:

Age (days)	*Strength (MPa)*
3	26.10
7	53.60
8	78.00
57 (150-mm-diameter in situ cores)	86.05

At 28 days, the minimum and maximum strength values were 65.5 and 91.7 MPa, respectively, and the standard deviation σ reached 6.75 MPa. The French Construction Code (Fascicule 65) requires for this kind of ready-mixed concrete that

1. The mean strength be at least equal to the characteristic strength value f_{ck} plus a margin

$$f_{cm} \geq f_{ck} + 1.30\sigma$$

2. The minimum strength be larger than the characteristic strength f_{ck} minus a margin

$$f_{cmin} > f_{ck} - 3 \text{ MPa}$$

These 28-day strength requirements were easily met.

Comparative tests were carried out between different types of samples: ϕ 160- x 320-mm usual reference cylinders, ϕ 160- x 320-mm cylinders with ground bearing faces, ϕ 110- x 220-mm cylinders, ϕ 100- x 100- x 100-mm cubes, ϕ 150- x 300-mm in situ cores, ϕ 100- x 200-mm in situ cores, and ϕ 70- x 140-mm in situ cores.

The results were as follows:

Sample	*Strength (MPa)*
Reference	71.9
Ground	71.2
Cylinder	67.7
Cube	83.9
150-mm core	76.7
100-mm core	84.2
70-mm core	75.5

Tensile Strength The tensile strength was measured on cylinders with the Brasilian splitting test. The average tensile strength was 5.07 MPa on 28-day samples.

Placement of Concrete

The contract required that the concrete be poured in one continuous phase. In order to avoid any delay, two independent ready-mixed concrete plants were to deliver the same concrete. In this way, even if one of them was out of order, the nonstop pouring operations could be completed at a lower rate.

The 1000 m^3 (1,300 yd^3) of concrete was placed without any incident by two pumps in 24 hr, as planned.

Instrumentation

The bridge was instrumented in order to follow its behavior during a period of several years. The experimentation is being run by the Laboratoire Central des Ponts et Chaussées (Central Laboratory for Roads and Bridges), which is under the direction of the Ministry of Public Works.

The goals of the experimentation are threefold: to observe the thermal evolution of concrete during the setting phase, to determine prestressing forces and deformations, and to study creep and shrinkage of the concrete.

Thermal Evolution of Concrete

During the setting phase at the mid-central span and in the massive end blocks, the maximum temperatures measured were

- 73°C in the middle of the end blocks,
- 57°C in the webs, and
- 32°C in the upper slab.

A special finite-element program was run to check these values. In order to calibrate the finite-element calculations, a quasi-adiabatic test was carried out to obtain the temperature variations of a concrete specimen. The results of the calculations are in good accordance with the measurements.

Prestressing Forces and Deformations

The deformations of a cross section located near the middle of the central span were continuously recorded. The rotations of the same span were also measured and recorded. The measured deformations are currently 15 percent smaller than those predicted by calculation. This discrepancy can be attributed to an underevaluation of the Young's modulus.

The time evolution of the tensile forces in the longitudinal tendons was measured. The first measured values were 5.10 MN per tendon near the anchorages and 5.20 MN at the mid-central span. The calculations predicted 5.10 and 4.90 MN, respectively. These differences can be attributed to an overevaluation of friction at the deviator transverse beams.

Creep and Shrinkage of Concrete

A major part of the experiment was devoted to the study of the shrinkage and creep of the concrete. Sixteen tests are to be carried out during the next few years on various specimens:

1. On specimens made with the in situ concrete, two shrinkage tests, with and without drying, and two creep tests, with and without drying, loaded at 28 days.
2. On laboratory specimens made with a concrete using the site materials with the same composition as the in situ concrete, four shrinkage tests and eight creep tests loaded and unloaded at different ages.

The results of these tests will be available within a few years.

CONCLUSIONS

The first French prestressed concrete bridge designed and built with a 60-MPa characteristic strength concrete according to the French building codes was successfully completed by early 1989.

The bridge has been instrumented in order to verify the assumptions taken into account in the calculations, to check its long-term behavior, and more generally to assess its supposedly increased durability as compared with that of ordinary concrete bridges.

Economic comparisons made it clear that although its unit price per cubic meter is higher than that of ordinary concrete, HSC leads to reduced immediate total investments thanks to material savings and higher construction productivity. These conclusions were reached without taking into account immaterial and long-term added savings provided by the inherent enhanced durability of HSC.

It is worth stressing that the bridge, which was built for the Ministry of Public Works, is to be incorporated into one of the main French roads. This first achievement of the national project on new concretes is to be followed by further steps:

1. In accordance with the wishes of the French Road Direction, the utilization of C 60 concretes will be extended to the construction of most bridges in the coming years.
2. Other experimental bridges implementing HSC with higher characteristic strength will be built in the near future.

Publication of this paper sponsored by Committee on Concrete Bridges.

Modeling Fatigue Loads for Steel Bridges

A. G. TALLIN AND T. PETRESHOCK

Histograms of the gross vehicle weight (GVW) of trucks obtained from weigh-in-motion data for seven states are analyzed. These histograms are modeled by two bimodal distributions consisting of mixed pairs of lognormal distributions and a lognormal and a Type III largest extreme value distribution. Fatigue lifetimes for AASHTO categories A, B, C, and E details are calculated from these models of the distribution of GVW by approximating the Miner's stress as a linear function of the mth root of the mth expected moment of the GVW. The lifetimes based on the two models are compared with each other and with the results obtained by assuming a single lognormal distribution. The results show that the lifetimes estimated using the bimodal distributions differ little from each other but are significantly shorter than the lifetimes estimated from the single lognormal distribution. It was also noted that there are large differences between the estimated lifetimes of different AASHTO categories.

Load models appropriate for the estimation of bridge reliability due to fatigue life are different from those that are appropriate for the estimation of bridge reliability due to overloads. Although the occurrence of a single extraordinary load is important in the analysis of the ultimate capacity of a bridge, metal fatigue is concerned with the cumulative effect of loading at lower stress levels. As a result, a good fatigue model must be rich enough to model cumulative load effects.

The problem of modeling traffic loads for fatigue analysis has been studied by a number of researchers (*1–3*). Several fatigue load models developed from weigh-in-motion data compiled by Snyder et al. (*4*) are discussed and the consequences of assuming different models of the estimated lifetime of steel bridge components subject to fatigue loads due to trucks are examined.

Two distinct methods are used to estimate fatigue lifetimes (*5*). The first is the *S-N* approach, in which the lifetime in terms of stress cycles N is related to the mth power of the stress range S:

$$N = AS^{-m} \tag{1}$$

The second is the linear elastic fracture mechanics (LEFM) approach, in which the lifetime of a component is estimated from the relationship between the mth power of the stress intensity range ΔK and the rate of crack growth da/dN:

$$\frac{da}{dN} = C(\Delta K)^m \tag{2a}$$

$$= C[Y(a)^m S^m] \tag{2b}$$

In Equations 1 and 2 the exponent m and factors A and C are material constants. In Equations 2, $Y(a)$ is a function of the crack length a. Because of its simplicity, the first approach is used extensively for design calculations, for example, in the AASHTO specifications (*6*).

Whenever the stress range or stress intensity range cannot be assumed to be constant, the value for the stress range S in Equations 1 and 2 is modified to compensate for the time-varying loads. This is usually done by using an equivalent constant stress range such as the Miner's stress S_M, which has the form

$$S_M = \left(\frac{1}{N}\sum_{i=1}^{i=N} S_i^m\right)^{1/m} \tag{3}$$

where S_i is the stress range at the ith cycle and m is the exponent used in Equations 1 and 2. Because the number of cycles in fatigue problems is large and the stress range in each cycle is randomly distributed, the Miner's stress will approach the mth root of the mth expected moment of the underlying probability distribution for the stress range, or $[E(S^m)]^{1/m}$.

LOAD MODELS

The data analyzed here were collected by Snyder et al. (*4*) from weigh-in-motion studies performed in eight states in which calibrated highway bridges were used as scales. Each data set ranges from 1,377 to 6,547 observations, with a total of 24,179 observations. Figure 1 is a typical histogram of the gross vehicle weight (GVW) arbitrarily normalized so that a GVW of 1.0 is the weight of the AASHTO HS-20 design vehicle (72 kips). No information concerning the number of axles corresponding to the individual truck weights was included in the results of this study. The distribution of GVW is characterized by the two peaks or modes, which are a consequence of the distribution between heavier loaded trucks and lighter unloaded trucks. Although the lower mode appears to have a relatively wide peak, the upper mode is narrow and seems to have the shape characteristic of a negatively skewed distribution.

If one assumes that the mechanism for the dual peaks is due to two separate populations, loaded and unloaded trucks, an appropriate model for the GVW should be a mixed distribution with a probability density function (pdf) of the form

$$f_{GWV}(w) = pf_L(w) + (1 - p)f_H(w) \tag{4}$$

where $f_L(w)$ and $f_H(w)$ are the partial pdf's of light and heavy trucks, respectively, and p is the probability that an individual truck is a member of the light-truck population.

Two mixed distribution models were developed for each of the eight data sets. The first model (LN-LN) assumed that

Department of Civil and Environmental Engineering, Polytechnic University, 333 Jay St., Brooklyn, N.Y. 11201.

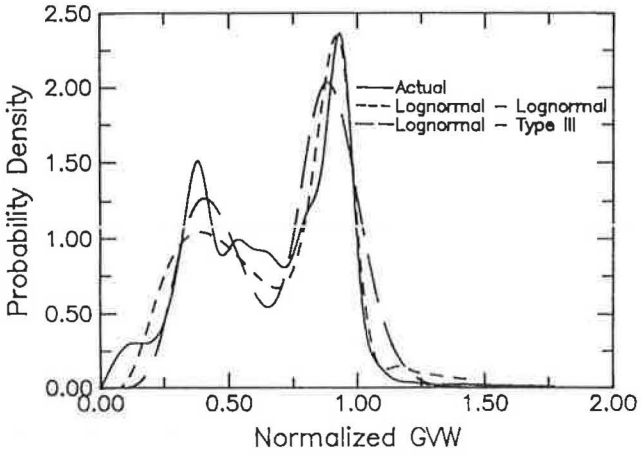

FIGURE 1 Comparison of estimated and measured histograms.

both the light and heavy trucks were distributed according to a lognormal distribution with a pdf of the form

$$f_Y(y) = \frac{1}{y(2\pi)^{1/2}\delta_Y} \times \exp\left\{-\tfrac{1}{2}\left[\frac{1}{\delta_Y}\ln(y/m_Y)\right]^2\right\} \quad y \geq 0 \tag{5}$$

where m_Y is the median of Y and δ_Y^2 is the variance of $\ln Y$.

In an attempt to model the left skewness of the distribution of the heavier trucks, the second model (LN-ET3) used a lognormal distribution for the light trucks and a Type III largest extreme value distribution for the heavy trucks with a pdf of the form

$$f_Y(y) = \frac{k}{w-u}\left(\frac{w-y}{w-u}\right)^{k-1} \times \exp\left[-\left(\frac{w-y}{w-u}\right)^k\right] \quad y \leq w \tag{6}$$

where k is the shape factor, u is the location parameter, and w is the upper limit of possible values.

The mean-squared error between the measured and mixed distributions LN-LN and LN-ET3 was used to measure goodness of fit:

$$\Sigma[f(w;\theta) - f_m(w)]^2 \tag{7}$$

where $f_m(w)$ is the measured density and θ is the vector of five or six parameters involved in the LN-LN and LN-ET3 models, $(p, m_{Y_1}, \delta_{Y_1}, m_{Y_2}, \delta_{Y_2})$ and $(p, m_{Y_1}, \delta_{Y_1}, k, u, w)$, respectively. Powell unconstrained optimization (*7*) was used for each set of data to find the optimal set θ resulting in the minimum of Equation 7.

The resulting parameters and the mean-squared errors are given in Tables 1 and 2 for the LN-LN and LN-ET3 models, respectively, for the distributions of normalized GVW for seven states tabulated by Snyder et al. The mean-squared errors associated with the LN-ET3 model are lower than those for the LN-LN model.

COMPARISON

To compare the effects of assuming each of the two postulated models, estimated lifetimes for AASHTO A, B, C, and E category details were calculated. Each detail was assumed to be designed for fatigue at the AASHTO maximum allowable stress range for the category. It is assumed that the stress range experienced by a detail is a linear function of the GVW of the truck causing the stress. If the fatigue criterion governs, the maximum allowable design fatigue stress range corresponds to the design truck weight and to the normalized truck weight of 1.0.

Using Equation 1 with the stress range equal to the Miner's stress $\approx [E(S^m)]^{1/m}$, the lifetime in years can be approximated by

$$L = \frac{AF_D^{-m}/E(W^m)}{\text{ADTT} \times 365} \tag{8}$$

where

A and m = material properties,
ADTT = average daily truck traffic,
L = detail life in years, and
F_D = fatigue design stress.

TABLE 1 ESTIMATED PARAMETERS FOR LN-LN MODEL

	Lognormal 1			Lognormal 2		
State	m_{y_1}	δ_{y_1}	p	m_{y_2}	δ_{y_2}	m.s.e
Arkansas	0.4491	0.3135	0.4293	0.8981	0.1323	1.552
California	0.3947	0.2638	0.5671	0.9660	0.1868	0.564
Georgia	0.3906	0.2551	0.5976	0.8383	0.1718	0.3478
Illinois	0.5236	0.3551	0.5077	0.9485	0.1935	0.1405
New York	0.4137	0.3129	0.6329	0.9654	0.1529	0.3187
Ohio	0.5038	0.3055	0.5792	1.0015	0.1255	0.2572
Texas	0.4265	0.3122	0.5290	1.0288	0.1857	0.5231

TABLE 2 ESTIMATED PARAMETERS FOR LN-ET3 MODEL

	Lognormal			Type III			
State	m_{y_1}	δ_{y_1}	p	w	u	k	m.s.e
Arkansas	0.5354	0.5404	0.6391	1.0578	0.8813	2.4144	0.9043
California	0.3808	0.2229	0.4798	1.2194	0.8054	1.6182	0.213
Georgia	0.3689	0.1601	0.3150	1.1520	0.5696	1.9122	0.07381
Illinois	0.4353	0.2449	0.2448	1.3958	0.7702	2.5764	0.07652
New York	0.3899	0.2587	0.5178	1.1728	0.7989	1.5873	0.1805
Ohio	0.4849	0.2759	0.5321	1.2504	0.9292	2.2981	0.1657
Texas	0.3908	0.1754	0.2622	1.2441	0.6717	1.3520	0.3285

TABLE 3 COMPARISON OF PREDICTED LIFETIMES

Property		Fatigue Sensitive Detail			
		A	B	C	E
F_D		24.0	16.0	11.0	5.0
m		2.31	2.55	3.10	2.80
A ($\times 10^9$)		6.07	3.72	12.17	1.04
State	Load Model	Lifetime in Years			
		A	B	C	E
Arkansas	LN-LN	19.53	16.55	40.19	61.42
	LN-ET3	17.97	14.77	32.49	52.58
	LN	23.59	21.12	58.99	83.53
California	LN-LN	20.85	17.34	39.92	62.90
	LN-ET3	23.26	19.70	47.37	72.85
	LN	27.97	25.40	72.99	85.37
Georgia	LN-LN	30.27	26.44	68.36	101.21
	LN-ET3	31.29	27.37	70.82	104.77
	LN	35.07	32.66	99.75	134.68
Illinois	LN-LN	16.66	13.81	31.75	50.00
	LN-ET3	17.67	14.79	34.82	54.14
	LN	18.96	16.60	43.95	64.03
New York	LN-LN	23.15	19.53	46.44	71.89
	LN-ET3	25.34	21.70	53.42	81.12
	LN	27.92	25.34	72.90	101.67
Ohio	LN-LN	17.95	14.99	35.01	54.66
	LN-ET3	18.96	15.95	37.97	58.66
	LN	19.64	17.26	46.05	66.79
Texas	LN-LN	16.41	13.40	29.59	47.64
	LN-ET3	29.26	24.49	37.64	73.40
	LN	21.86	19.32	51.59	75.12

The quantity $E(W^m)$ is the mth expected moment of the normalized GVW distribution.

$$E(W^m) = p\int_w^m f_L dw + (1 - p)\int_w^m f_H dw \quad (9)$$

The fatigue design stress F_D is a function of the detail type ranging from 2.0 ksi for cover plate terminus (Category E) to 24.0 ksi at web flange connections in rolled beams (Category A).

Shown in Table 3 are the estimated lifetimes based on the two double-mode models LN-LN and LN-ET3 developed here. For comparison purposes, lifetimes based on a single LN stress range distribution are also included in Table 3. For each of the seven states the lifetimes are estimated for four AASHTO detail categories A, B, C, and E. The ADTT was assumed to be 1,000 vehicles per day and the material constants are those tabulated by Nolan and Albrecht (*8*) from tests of a large number of typical fatigue-sensitive details in which run-out effects were ignored.

CONCLUSIONS

The results show that, except for the data set from Texas, the estimated lifetimes are insensitive to which double-mode stress range model was used. In the case of Texas, the low central value for f_H in the LN-ET3 model, $u = 0.67$, compared with the high median for f_H in the LN-LN model, $m_{Y_2} = 1.03$, results in large differences in the estimated lifetimes. However, in all other states the estimated lifetimes differ by less than 10 percent, which, in light of the precision of such methods, is insignificant. On the other hand, estimated lifetimes based on the single-mode distribution are all longer than the estimates based on the LN-LN and LN-ET3 stress range models. The greatest difference was for Category C details, which have the steepest *S-N* relationship, with $m = 3.1$.

The estimated lifetimes are highly sensitive to design stresses and material properties. Although the *S-N* curves are significantly higher for Category A details than for Category E details, the use of significantly lower design stresses for Category E details causes estimated lifetimes for Category E details to be much longer than those for Category A details. The results in Table 3 ignore any run-out or fatigue limit effects, and as a result, all stress cycles cause damage. This may account for short lifetime estimates and possibly the large differences in the estimated lifetimes between details. However, the results point to possible large discrepancies between the fatigue lifetimes for various categories.

The results presented here suggest that there are discrepancies between the lifetimes estimated from single-mode stress distributions and those estimated from the double-mode models proposed here. The results also suggest that more realistic modeling of the stress range may be even more important for richer fatigue models such as *S-N* curves combined with fatigue limits or Paris crack growth relations with threshold stress intensity ranges.

ACKNOWLEDGMENTS

The work described here was supported by grants from the National Science Foundation and A. S. Veritas Research.

REFERENCES

1. F. Moses. Probabilistic Load Modelling for Bridge Fatigue Studies. Presented at IABSE Colloquium on Fatigue of Steel and Concrete Structures, Lausanne, Switzerland, 1982.
2. W. Nyman and F. Moses. Calibration of Bridge Fatigue Design Model. *Journal of Structural Engineering*, Vol. 111, No. 6, 1985.
3. H. Shaaban and P. Albrecht. *Collection and Analysis of Stress Histograms Recorded on Highway Bridges*. Department of Civil Engineering Report. University of Maryland, College Park, 1985.
4. R. E. Snyder, G. E. Likins, and F. Moses. *Loading Spectrum Experienced by Bridge Structures in the United States*. Report FHWA/RD-85/012. FHWA, U.S. Department of Transportation, 1985.
5. J. W. Fisher. *Fatigue and Fracture in Steel Bridges—Case Studies*. John Wiley & Sons, New York, 1984.
6. *Standard Specifications for Highway Bridges*, 12th ed. American Association of State Highway and Transportation Officials, Washington, D.C., 1977.
7. W. H. Press, B. P. Flannery, S. A. Teukosky, and W. T. Vetterling. *Numerical Recipes in C: The Art of Scientific Computing*. Cambridge University Press, Cambridge, England, 1988.
8. C. S. Nolan and P. Albrecht. *Load and Resistance Design of Steel Structures for Fatigue*. Department of Civil Engineering Report. University of Maryland, College Park, 1983.

Publication of this paper sponsored by Committee on Steel Bridges.

Crack Detection at Cover Plate Ends and Welded Splices Using Ultrasound Technology

PATRICK D. ZURASKI

Many steel bridges constructed before 1970 are now of concern because they contain welded fabrication details that are highly susceptible to the formation of fatigue cracks. It is imperative that nondestructive evaluation methodology be available to examine such bridges, especially those with more than 25 years of service history and high volumes of truck traffic. Within Ohio a large number of bridges were fabricated with welded splices and cover plates located over the piers of continuous-beam bridges. Commonly accepted analytical models indicate that the average fatigue life has already been exceeded in some situations. Unfortunately, unaided visual inspection allows no opportunity for early crack detection because the critical top flange surface is embedded in the concrete deck. Research conducted on behalf of the Ohio Department of Transportation has demonstrated that ultrasonic testing procedures may be used to determine whether cracks have been initiated within a top flange surface that is embedded in concrete. Three Interstate highway bridges experiencing high volumes of truck traffic and containing AASHTO Category E′ cover plate details were examined during 1989. Application of the ultrasound technology is described and the results of this field investigation are presented.

Existing steel bridges designed with welded connection details and constructed before 1970 are a source of concern for their owners because frequently they must be considered highly susceptible to the formation of fatigue cracks when viewed in the light of current fatigue design standards and specifications. Figure 1 shows a field-welded detail used extensively in Ohio that consists of welded cover plates plus full-penetration, vertical-seam welds located over the piers of continuous-beam bridges. Commonly accepted analytical models indicate that the average fatigue life has already been exceeded in some situations. Unfortunately, unaided visual inspection allows no opportunity for early crack detection because the critical top flange surface is embedded in a concrete deck.

On the one hand, it is essential that any necessary corrective measures be undertaken to maintain an adequate level of safety. On the other, it would be inappropriate to embark on an extensive rehabilitation program based solely on the predictions of analytical models, which may indicate that the fatigue life of a particular detail has reached, or is nearing, exhaustion. Considering the wide statistical scatter in many of the key fatigue-life parameters and the influence of the volume of truck traffic, it could be many years (if ever) before sufficient damage has accumulated to cause distress, such as a fatigue crack, to actually occur. Nondestructive evaluation strategies may be employed to assist bridge owners in making difficult economic decisions consistent with requirements for safety.

The welded connection shown in Figure 1 was a standard splice detail in Ohio's expressway construction from the late 1950s to the mid-1960s, some of which detail was eventually incorporated into the Interstate system. Frequently, the stress range at the end of the top flange cover plate, calculated using the standard HS-20 design vehicle, is much higher than that allowed by the AASHTO specifications (*1*). Considering that the majority of cover plate terminations within this study are AASHTO Category E′ details and that one-way traffic volumes exceed 4,000 trucks per day, it is quite difficult to find any acceptable location within a tension zone for terminating the cover plates.

Confronted with a calculated stress range greater than that allowed, one may select from alternative, probability-based methods for computing the remaining life at the ends of these cover plates. Procedures recently proposed by Moses et al. (*2*) allow for considerable latitude in selecting the distribution factor, the weight of the fatigue-evaluation truck, the truck traffic volume, the degree of composite action, and other factors. Moses et al. indicate that computed "estimates of remaining life provide a useful indication of fatigue safety and facilitate reasonable cost-effective decisions regarding repair, rehabilitation, or replacement." Thus, because fatigue lives are probabilistic rather than deterministic, calculated values primarily provide a basis for priority ranking and planning. For maximum effectiveness, however, such calculations should be complemented with physical evidence gathered during an on-site examination before extensive rehabilitation or costly repairs are initiated.

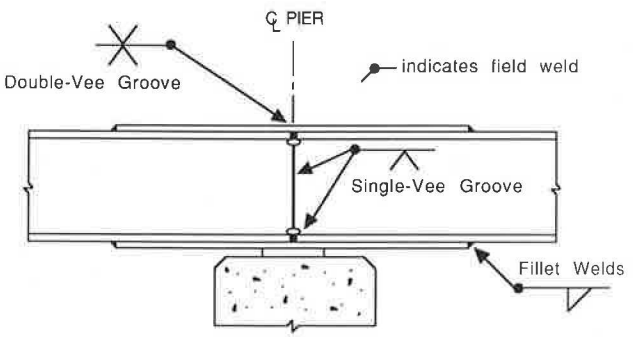

FIGURE 1 Welded splice and cover plate detail.

Department of Civil Engineering, University of Akron, Akron, Ohio 44325-3905.

The primary objective of the research reported here was to demonstrate that ultrasound technology may be effectively used to detect any cracks that may have initiated at the ends of welded cover plates or within butt-welded flange splices embedded in a concrete deck. A brief validation was conducted in the laboratory followed by an on-site examination of 20 cover-plated and weld-spliced beams selected from three different bridges (six, counting the structure for each traffic direction separately).

A brief description of the characteristics of ultrasound waves and their role in crack detection is provided below, followed by discussion of the work that was conducted in the laboratory and at the three bridges. Specific findings regarding the application of ultrasound technology to nondestructive bridge evaluation are reported.

ULTRASOUND

Sound is the mechanical vibration of particles in a medium, and it travels as an elastic wave. Particles of the medium do not travel with the wave but only react to its energy (*3*) and vibrate about a fixed point. Thus, it is the energy of the wave that moves through the material. For many applications, ultrasound waves are generated by crystalline materials, which exhibit a piezoelectric effect in which the application of an alternating voltage through the thickness of a "crystal" causes it to expand and contract. Thus, a sound wave may be created and transmitted from one medium into another by direct contact with the crystal or through an intervening medium. It is noteworthy, especially in applications of nondestructive testing, that the reverse phenomenon also occurs. An ultrasonic wave incident on a crystal (hereafter referred to as a transducer) causes it to vibrate, producing an alternating current across the faces of the transducer (*4*). Defects (cracks, inclusions, etc.) cause sound waves to be reflected back to a transducer, and the resulting voltage serves notice that a defect is present.

The normal audible frequency range of sound is approximately 20 Hz to 20 kHz. In contrast, the ultrasonic frequency (beyond the range of the human ear) employed during this study was 2.25 MHz. Utilizing a lead zirconate titanate (PZT) crystal, the propagation velocity employed was approximately 9,500 ft/sec.

Basic Application

The most basic application of ultrasonics in flaw detection involves transmitting a sound wave with a zero-degree angle of incidence (measured from the normal to the surface) into a medium, such as the plate shown in Figure 2. In the study described here, ultrasound was transmitted as a series of extremely short pulses, and a single transducer functioned as both transmitter and receiver. The transducer detected reflected signals between transmissions.

Voltage traces are viewed on a cathode-ray oscilloscope. The screen shown in Figure 2(a) corresponds to an ultrasound scan conducted away from the interior defect. Only the initial voltage burst and echo from the bottom surface of the plate appear. When the transducer occupies a position above the defect, an additional voltage "spike" appears corresponding to reflection of sound from the defect, as shown in Figure 2(b).

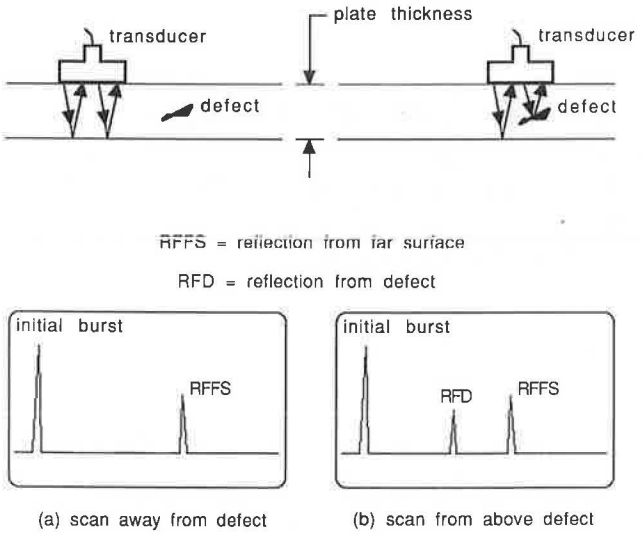

FIGURE 2 Typical oscilloscope traces for ultrasound scans.

Because air greatly impedes sound transmission, a thin film of liquid couplant, or gel, must be brushed onto the surface of an element before ultrasonic examination. This ensures intimate contact with the surface of the transducer and provides for efficient sound transmission into the test part. Preferably, the gel may be applied to smooth, bare metal. Paint removal is briefly discussed later in the section entitled "Field Study."

Most often, applications of ultrasonics are more complex than those shown in Figure 2. Sound frequently is transmitted with a nonzero angle of incidence, and it may be necessary to interpret multiple reflections. Orientation of the defect with respect to the direction of sound travel is one primary consideration for requiring sound to be transmitted along an oblique path. Detailed consideration of types of sound waves and reasons for employing them is beyond the scope of this paper; nevertheless, a brief discussion is provided in the next section. A thorough discussion is available, however, in the literature (*3–6*).

Oblique Sound Path

The strongest indication of cracks and line-type flaws is obtained when the sound is directed at right angles to the defect. That optimum orientation is not possible, however, for a fatigue crack located at the toe of a cover plate weld (Figure 3). The crack is nearly vertical and the sound must be transmitted toward the crack at an oblique angle, as shown. The sound is shown as being directed from the bottom surface of the top flange because it is typical construction practice to embed the top flange within the concrete deck, with only the bottom surface exposed.

The angle at which an ultrasonic wave is refracted and travels through an object is controlled by the angle of incidence (Figure 4). Furthermore, the sound may travel as either a longitudinal wave or a shear wave, or both, and possibly

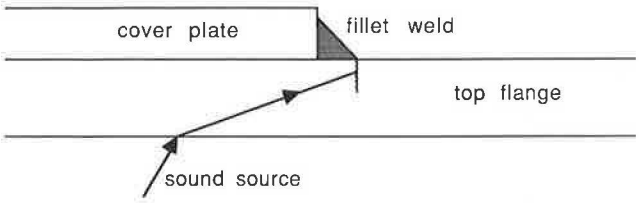

FIGURE 3 Sound path at oblique angle to fatigue crack in beam flange.

even as a surface wave, also depending on the angle of incidence.

Longitudinal waves differ from shear waves with respect to the direction of particle excitation. For the former, particle motion (recalling that this is about a fixed position, not travelling with the wave) is parallel to the direction of the sound path, and for the latter, particle motion is perpendicular to the sound path. Surface waves (a shear wave with refraction angle of 90 degrees) travel along the surface at a shallow depth. A complete discussion may be found elsewhere (*5*).

A range of incident angles above a certain critical angle exists such that only one type of wave, the shear wave, is transmitted into the object being inspected. For such angles, the longitudinal wave is totally reflected from the surface. Transmitting only one type of wave is crucial because the presence of two types of waves would give confusing results (*4*). Sound wave refraction, a function of the angle of incidence and velocities in the respective mediums of transmission, is governed by Snell's law. A standard physics text (*7*) or the literature previously cited may be consulted for detailed treatment.

Determining Defect Position with Shear Waves

For shear waves transmitted into plates containing no defects, only one spike, the initial voltage burst, appears on the oscilloscope screen. Nothing is directed back to the transducer because the sound wave is totally reflected at the plate surfaces (metal-air interfaces) (*4*), as shown in Figure 5(a). For a plate containing a crack, a second spike appears because sound is directed back toward the transducer from irregular features (very small, intermittent concave surfaces) along the

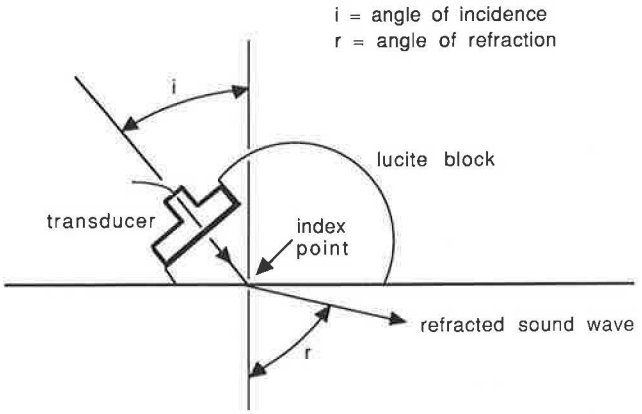

FIGURE 4 Sound wave geometry.

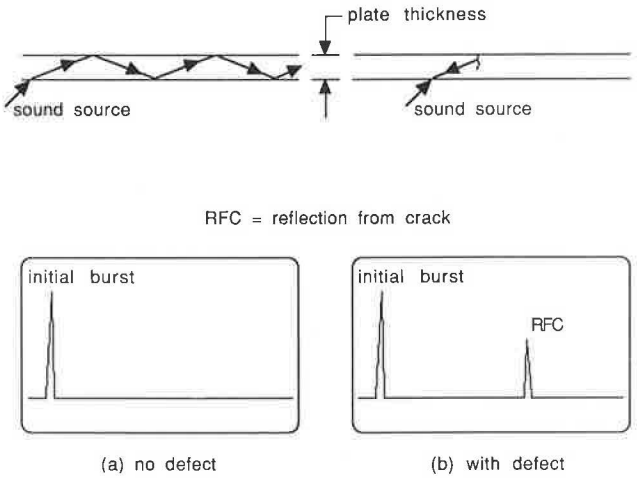

FIGURE 5 Oscilloscope activity with shear waves.

side face of the crack. This is shown in Figure 5(b) (although the minute concave surfaces do not appear because of the scale of the figure).

Reflections may also occur from sources other than a crack, including irregular surface features of the weld, the heel of the weld, an undercut, or the corner of the cover plate. Procedures for interpreting sound wave reflections and identifying the source of the reflections are discussed in the subsection devoted to examining cover plate ends in the "Field Study" section of this paper.

The horizontal distance between spikes in Figure 5(b) corresponds to the elapsed time between the initial sound transmission and subsequent reception. The time may be easily converted to the horizontal distance between the index point of the transducer and the location of the defect because the angle of the sound path and velocity of the shear wave in steel are known. In fact, by utilizing a calibration block containing precision-machined "defects" at accurately known depths and adjusting the sweep settings on the oscilloscope, one may directly read actual distance on the horizontal axis of the screen.

One may determine crack depth as well as crack location. The change in transducer position from the time the crack is first detected until the last indication may be noted. Then when the transducer translation and the refraction angle are known (*6*), the crack height may be computed.

LABORATORY EXAMINATION

A laboratory validation of nondestructive evaluation with ultrasound was performed before the field work was conducted at existing bridges. Two test plates (with dimensions comparable with the components in the bridges) with welded cover plates were subjected to cyclic loading in a servohydraulic material test system until a crack was initiated at one weld toe. The welds at the ends of the cover plates were subjected to ultrasonic examination, and dye penetrant examination was also performed. Subsequently, one of the plates was cast into a surrounding mass of concrete, simulating embedment of a top flange within a concrete deck, and reevaluated with ultrasonic examination. Once again the cracks

were detected in a reliable manner. Several aspects of this work are described below.

The test specimens, fabricated from ASTM A36 steel, consisted of a cover plate 18 in. long welded all around to a base plate 36 in. long with a ½-in. fillet weld deposited using the submerged arc process. The cross section of the base plate was 8 in. by ⅞ in. and that of the cover plate was 6.5 in. by ¾ in. The specimen configuration is shown in Figure 6.

The plates were subjected to repeated cycles of three-point bending rather than axial load as an expeditious way of initiating a crack at the toe of a weld, that is, within the base metal along the transverse weld at an end of the cover plate. The plate was inspected periodically under bright light and with a magnifying glass to determine the presence of a crack.

The plates were examined with ultrasound by moving the transducer on the surface of the larger plate on the side without the cover plate. The locations of crack indications were recorded and a confirming evaluation was performed with dye penetrant. The results were consistent with one another.

The dye penetrant indicated the presence of a crack (manifested as a red stain against a white developer background) in the same zones that were indicated by the ultrasound. The depth of the cracks indicated by the ultrasonic inspection varied depending on location; the depth was found to be in the range of ⅛ in. to 5/16 in.

A limited magnetic particle inspection was also conducted, but very quickly discontinued. The concentration of iron filings characteristic of a crack was occurring in weld toe zones that had provided no indication of cracks by either ultrasonics or dye penetrant examination. Perhaps a dissimilarity between base metal and weld metal might have caused such a "false indication," but it was not within the scope of the investigation to pursue the matter further.

A general guideline in ultrasound technology is that an ultrasonic beam being transmitted in metal is reflected by an internal defect (void or nonmetallic inclusion) if the size of the defect is greater than one wavelength. Thus, cracks within plate surfaces covered with concrete (or cracks containing concrete debris) may be readily detected from the opposite surface if the defects are at least as large as the 1.25-mm wavelength employed in this study.

To demonstrate that cracks could be detected within components embedded in concrete, one cracked plate was cast in

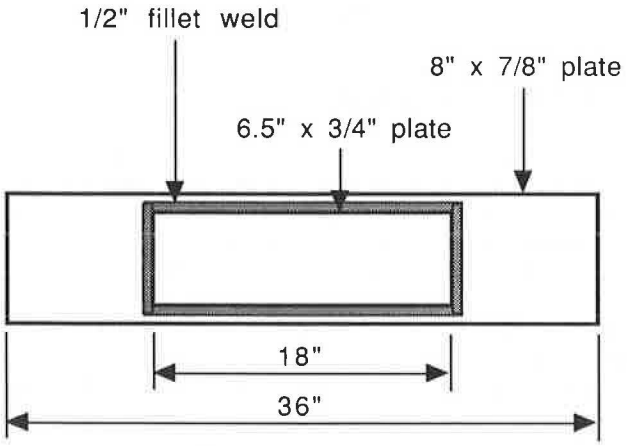

FIGURE 6 Welded cover plate test specimen.

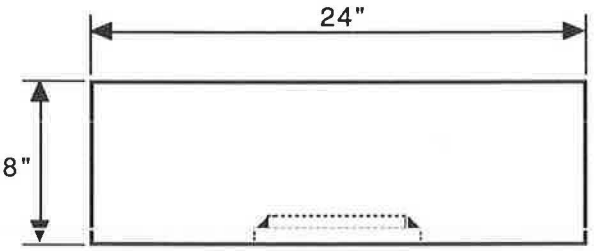

FIGURE 7 Cover plate specimen cast within concrete.

a central position within a block of concrete 2 ft wide by 3.3 ft long by 8 in. deep (Figure 7). After being cured, the block was turned over to provide access to the plate. The ultrasound transducer was moved over the exposed plate surface and indications of cracks were obtained that essentially matched the results from the previous examination of the plate that had been conducted without the covering of concrete.

FIELD STUDY

Three urban Interstate highway bridges that have been in service for approximately 25 years were examined with ultrasound. Each structure is a continuous-beam bridge with W33 or W36 wide flange sections that incorporate the welded-splice and cover plate detail shown in Figure 1. Two bridges have three spans, and one has four spans, and the beam spacing is approximately 7.75 ft. All three bridges are of noncomposite construction and are located within 3.5 mi of one another on the same segment of Interstate highway. All flange thicknesses exceed 0.8 in. except for the exterior spans in one bridge, which have a thickness of 0.7 in. Therefore, the most severe AASHTO fatigue classification, Category E′, applies in most instances for the cover plate ends. The full penetration flange splices are nominally Category B, but only when weld soundness is established by nondestructive inspection.

Further discussion regarding fatigue performance characteristics of the bridges is provided below, followed by a summary of the findings from the ultrasound examination. No fatigue cracks were detected at the ends of the cover plates. Some weld-root flaws and crack-type indications were detected within the full penetration butt welds connecting the top flanges. It was necessary to properly interpret certain "false indications," however, to conclude that cracks were not present at the ends of the cover plates. The observations gathered in the field will be described in detail.

It is possible that fatigue cracks could already have been initiated at a cover plate end and not have been detected by visual inspection because the top flange (tension surface) is embedded in the concrete deck. A combination of a high volume of truck traffic (more than 4,000 trucks per day in each direction) and a calculated stress range that exceeds 10 ksi in some situations [AASHTO specifications allow 2.6 ksi for Category E′ (*1*)] provided the justification for a careful field examination. Even according to recently proposed, reliability-based fatigue evaluation (*2*) and design (*8*) procedures that more properly account for actual service conditions (compared with the current design specification), the mean fatigue life has already been exceeded for one of the bridges. (The

FIGURE 8 Beam lines with deck removed.

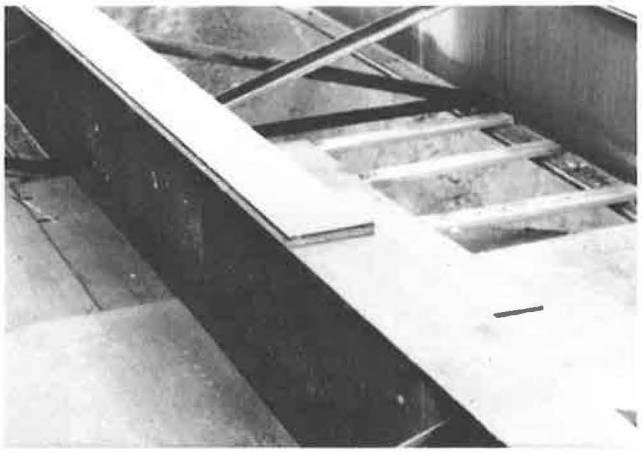

FIGURE 9 Termination of top flange cover plate.

fatigue life analysis of these bridges will be reported in a subsequent paper.)

These bridges presented a special opportunity, because their concrete decks were being removed as part of a routine construction contract. The field work was conducted at that time so that access would be available to both the top and bottom surfaces of the top flange. None of the field work was conducted while the deck was still in place.

Four beam lines within one of the bridges, exposed after deck removal, are shown in Figure 8, which also shows the angle-type cross bracing frames between the girders. The termination of a typical top flange cover plate is shown in Figure 9. Falsework was installed between bottom flanges of the girders to protect the roadway below during deck removal. It also provided convenient access to the cover plates for ultrasound examination.

Calibration and Preparation

The first operations conducted at each bridge site were to calibrate the ultrasound transducer and to remove the paint from the surfaces over which the transducer would be moved. Setting up the instrumentation and calibrating the transducer required less than 30 min at each site. The time required for paint removal was approximately 15 min at each cover plate end.

Calibration involves the simple operation of moving the transducer over a calibration block containing narrow slits located at a precisely specified depth. Because the distance to the slit, the angle of the sound path, and the sound velocity are known, sweep settings may be adjusted on the oscilloscope of the accompanying instrumentation so that actual distances are shown instead of time.

Paint should be removed from the surface over which the transducer is moved for a distance of approximately 5 in. on each side of the transverse weld toe. Separate techniques with small power tools, wire wheels, and disks covered with coarse aluminum oxide grit were employed for the removal. The last method provided the best results. Paint removal is not necessary for obtaining a trace on the oscilloscope screen, but it greatly enhances the quality of the signal. Figure 10 shows the transducer positioned on the bottom surface of a cover-plated flange, and Figure 11 shows actual usage of the instrumentation.

Examination of Cover Plate Ends

Even though no cracks were detected at the ends of the cover plates, indications (spikes) did appear on the oscilloscope screen during the examination. It was discovered that certain undulations in the surface of the weld (sometimes referred to as "rollovers"), shown schematically in Figure 12 and in a

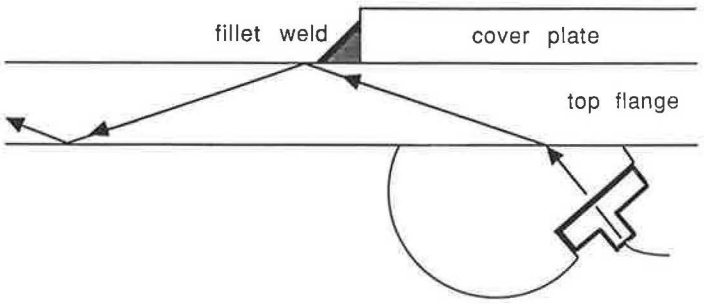

FIGURE 10 Inspection at end of welded cover plate: scan of cover plate end.

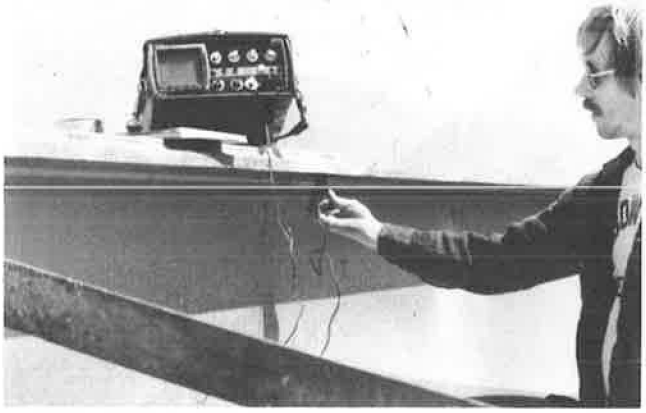

FIGURE 11 Inspection at end of welded cover plate: ultrasound instrumentation.

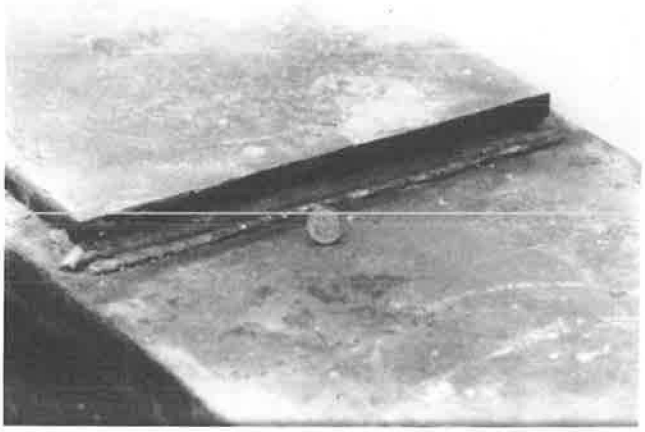

FIGURE 13 Irregularity in weld surface at end of cover plate.

photograph in Figure 13, provide false indications. The sound incident to the concave surface in Figure 12 is focused by the corner-like trap back toward the transducer, and an indication appears on the screen.

Undercutting is another potential source of false indications. This type of defect is associated with the unintentional introduction of a groove (left unfilled by weld metal) into the base material adjacent to the toe of a weld. Such a disruption in the flange surface may also focus sound back toward the transducer.

The indication caused by a rollover does not differ from that caused by a real crack, such as the one shown in Figure 14. The corner created by the intersection of the crack and surface of the top flange focuses the sound back toward the transducer in a manner similar to the rollover. It is possible, however, to distinguish between a real crack and a false indication by conducting the ultrasound scan from both sides of the weld. The crack shown in Figure 14, representative of a fatigue crack at the end of a cover plate, causes an indication to appear for scans conducted from both the left and right sides of the weld. When a scan is conducted from the right side of the weld in Figure 12, there is no indication because the sound is no longer incident on a trapping surface feature.

Two other methods were used to reject the indications caused by the rollovers. First, after several indications (not known to be false at the time), the end of the cover plate was subjected to dye penetrant examination. There was no evidence of a crack. Second, a procedure referred to as "damping" was used to distinguish between alternative locations as the source of a crack. Damping involves applying a small amount of the liquid couplant to one's finger and tapping on the surface near the toe of the weld. (When the finger is in contact with the surface, a portion of any incident sound is refracted into the finger.) The transducer was translated until a spike appeared on the screen and was then held stationary. Tapping on the weld at the rollover caused the spike on the screen to jump. Tapping on the base metal of the top flange at a slight distance from the weld toe did not cause the spike to jump.

One must usually rely on scanning from both sides of the weld, however, as a basis to reject the false indications, because the top surface is not visible in most situations. With the deck in place, it is not possible to tap on the weld or to conduct a dye penetrant examination.

Considering a typical situation, in which the top surface of the beam is not visible, the first important step before an ultrasonic examination would be to establish the position of the toe, or end, of the weld. The design drawings would indicate the distance from the flange butt-weld splice to the end of the cover plate. Next, the precise position of the end weld may be established by directing a longitudinal wave into the flange at an incident angle of zero degrees. The beginning of the weld can be accurately established (within approximately 1/64 in.) by watching for a change in signal on the screen. Therefore, any indication detected with a shear wave transducer that is not located right at the weld toe must be something other than an end-of-plate fatigue crack.

In a few situations, a false indication came from the top corner of the cover plate from sound that was directed toward the weld with the transducer on the left side of the weld (as

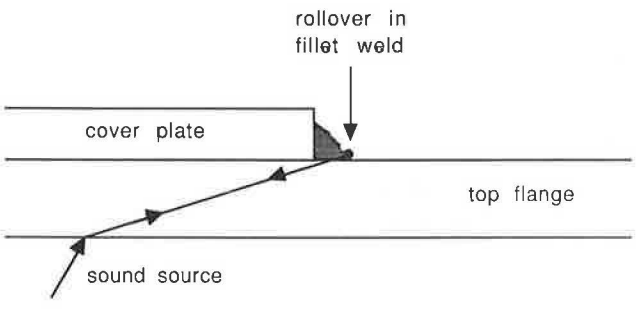

FIGURE 12 Sound reflection from irregularity in weld surface: rollover in fillet weld.

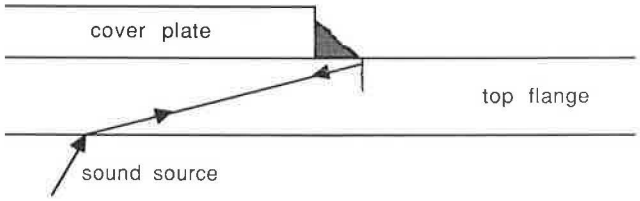

FIGURE 14 Sound reflection from fatigue crack at weld toe.

in Figure 12). Damping the sound by tapping the surface at the corner and watching the spike jump revealed that the source of the indication was not at the end of the weld. However, the same conclusion could have been reached without access to the surface by noting the distance from the transducer to the source of the indication and by noting further that the location of the source did not coincide with the toe of the weld.

Examination at Flange Splices

Indications of voids and defects within the full penetration butt welds joining the top flanges were detected at several locations by ultrasonic examination. In the majority of cases the defects were restricted to the center-depth regions of the flange, which pointed toward incomplete fusion, lack of penetration, or a similar fabrication flaw as the source of the indications. Very little depth ($\leq 1/8$ in.) makes it possible that these defects have been present since fabrication of the welded splices 25 years ago and that an active crack front is not present.

At three locations, however, indications were detected that revealed a through-thickness dimension extending from the center of the flange to near its top surface. It becomes difficult to assess the full extent of the flaw as it nears the surface because of interference from the metal-air interface at the top of flange and irregularities in the flange surface. In one instance, there was evidence from the ultrasound that a defect had travelled to within 1/64 in. of the surface of the top flange. The evidence indicated the type of crack shown in Figure 15. There was no way to confirm this finding by visual methods, because the cover plate and side fillet welds obscured the top flange surface from view.

Radiographic (x-ray) examination was conducted on the three butt welds with the largest flaw depth in an attempt to confirm the findings from the ultrasonic examination. The radiographic film did not show any evidence of cracks. It is not proper to state, however, that a crack was not present, because when viewed from above, the crack could be "lost" in the background. That is, any crack propagating vertically from a lack-of-fusion defect would likely be obscured in the film within the dark region that characterizes the defect zone.

To ensure safety and preserve the overall integrity of the negative moment connection, a bolted flange splice was installed at the location where ultrasonic examination revealed that the defect had nearly reached the surface. Other locations with flaws of significant depth will be closely monitored.

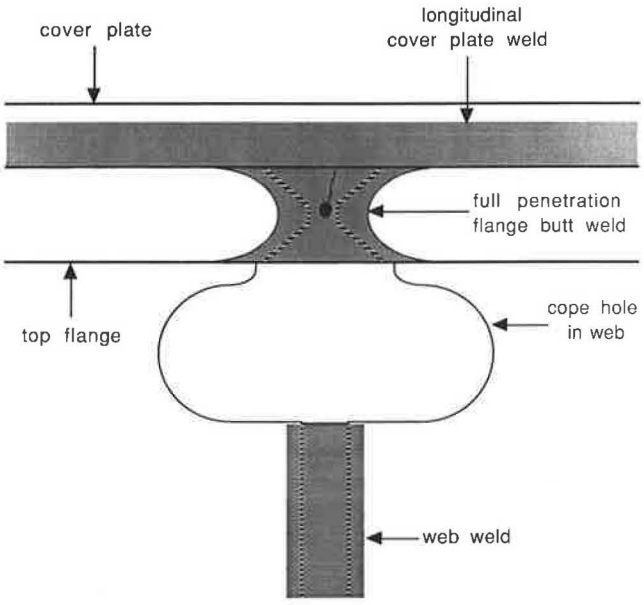

FIGURE 15 Crack propagation from flaw within root of flange splice butt weld.

CONCLUSIONS

Ultrasound may be effectively employed as a nondestructive evaluation tool for crack detection in existing bridges. Embedment of the cracked surface of an element in concrete does not alter the ability of the ultrasound testing to detect a crack, as long as a scanning surface is exposed. Before an agency initiates an ultrasonic inspection program, a test specimen composed of a welded cover plate and a base plate should be fabricated to provide guidance. By incorporating welds with smooth surfaces, welds with rollovers, and cracks at some locations in the weld toes, the test specimen simulates conditions that may be encountered in the field. This provides control and helps in interpreting the field results.

ACKNOWLEDGMENTS

This project was funded by the Ohio Department of Transportation (DOT) and the Federal Highway Administration. Vikram Dalal and Florian Euteneuer were liaison representatives for the Ohio DOT. Ultrasonic testing and the other nondestructive tests described in this paper were conducted by Glitsch Field Services/NDE, North Canton, Ohio.

REFERENCES

1. *Standard Specifications for Highway Bridges*. American Association of State Highway and Transportation Officials, Washington, D.C., 1989.
2. F. Moses, C. G. Schilling, and K. S. Raju. *NCHRP Report 299: Fatigue Evaluation Procedures for Steel Bridges*. TRB, National Research Council, Washington, D.C., 1987.
3. *Nondestructive Testing—Ultrasonic*, 2nd ed. Classroom Training Handbook CT-6-4. General Dynamics, Convair Division, 1981.
4. J. B. Hull and V. B. John. *Non-destructive Testing*. Springer-Verlag, New York, 1988.
5. P. E. Mix. *Introduction to Nondestructive Testing—A Training Guide*. Wiley, New York, 1987.
6. D. Ensminger. *Ultrasonics—Fundamentals, Technology, Applications*. Marcel Dekker, Inc., New York, 1988.
7. F. W. Sears, M. W. Zemansky, and H. D. Young. *University Physics*, 7th ed. Addison-Wesley, Reading, Mass., 1987.
8. *Guide Specifications for Fatigue Design of Steel Bridges*. American Association of State Highway and Transportation Officials, Washington, D.C., 1989.

Publication of this paper sponsored by Committee on Steel Bridges.

Wheel-Load Distribution Results from AISI-FHWA Model Bridge Study

MARK MOORE, KARL A. STRAND, MICHAEL A. GRUBB, AND LLOYD R. CAYES

An experimental test program to evaluate the behavior of a 0.4-scale model of a two-span continuous plate-girder bridge with modular precast prestressed concrete deck panels has recently been completed. The bridge, designed according to Alternate Load Factor Design (ALFD), or Autostress Design, procedures, utilizes noncompact plate girders with slender webs that fall beyond the present limits of the ALFD guide specification. A comprehensive plan was followed to subject the model to a series of tests to evaluate specific responses at simulated AASHTO service load, overload, and maximum load levels. At elastic service-load stress levels, live-load lateral-distribution factors were computed from experimentally developed influence surfaces. These factors were compared with factors computed from a finite-element model, from current AASHTO procedures, and from proposed empirical formulas. The factors computed from the experimental and finite-element model data were generally in close agreement. The factors computed from the proposed empirical formulas for the interior girder also agreed closely with the experimental data. The factors computed using AASHTO procedures were quite conservative for the interior girder and less so for the exterior girders. Neither the proposed nor the current AASHTO procedures were found to account for the observed slight variation of the distribution factor along the span. The data would seem to indicate that finite-element analysis and the proposed empirical formulas are both plausible methods for computing elastic girder wheel-load distribution factors. For similar tests conducted after the formation of automoments along with subsequent shakedown at overload, the computed distribution factors varied less than 10 percent. Thus it appears that elastic distribution factors may still be used at overload, even though controlled local yielding is allowed in ALFD procedures. In addition, for similar tests conducted with selected cross-frames removed, changes in the computed distribution factors were less than 10 percent in the positive-moment region for both interior and exterior girders. For the interior girder in the negative-moment region, distribution factors varied up to an average of 15 percent for the tests conducted with cross-frames in place and with selected cross-frames removed. This suggests that the load was distributed primarily through the concrete deck.

In 1982 a jointly funded bridge research program was initiated between the American Iron and Steel Institute (AISI) and the Federal Highway Administration (FHWA). The primary purpose of the large experimental test program was to study experimentally the behavior of a scale model of a two-span continuous plate-girder bridge designed according to Alternate Load Factor Design (ALFD), or Autostress Design, procedures (*1*) and built with modular precast prestressed concrete deck panels. In ALFD, a designer is permitted to utilize some of the substantial postyielding reserve strength that is available in continuous plate-girder bridges. Currently, an AASHTO guide specification (*2*) permits the use of ALFD for the design of continuous bridges using rolled-beam and comparable welded-beam sections that satisfy specific compactness requirements. As part of an ongoing research program to extend the ALFD procedures to noncompact sections, the model bridge test was designed using plate-girder sections that do not satisfy the current compactness requirements of the ALFD specification.

Testing of the model bridge included the development of elastic influence surfaces for the computation of lateral live-load distribution factors for interior and exterior girders in positive and negative bending at AASHTO service load levels. The three-dimensional influence surfaces were computed for selected reactions, moments, and shears in the model bridge (*3*). Three-dimensional influence surfaces were also developed for measured axial forces in the bottom flange of selected girders. These bottom-flange forces, which are a measure of the bending moment in the girder, were then used to compute lateral distribution factors. Initially, tests placed at specific locations to determine these elastic influence surfaces for a single concentrated load were completed. These tests were conducted immediately following construction of the model bridge. Following the completion of testing at the AASHTO overload level, in which controlled local yielding and subsequent shakedown were observed in the girders after several cycles of simulated overload live load plus impact, these influence surfaces were developed again. The influence surfaces were also developed by repeating the tests with selected cross-frames removed.

This paper provides a summary of these three influence surface tests. Live-load distribution factors computed from the experimental data are compared with factors computed using a mathematical finite-element model, current AASHTO procedures, and empirical formulas and recommendations recently developed as part of National Cooperative Highway Research Program (NCHRP) Project 12-26 on lateral live-load distribution.

M. Moore and K. A. Strand, Wiss, Janney, Elstner Associates, Inc. 3100 Premier Drive, Suite 200, Irving, Tex. 78063. M. A. Grubb, AISC Marketing, Inc., 650 Smithfield Street, Suite 750, Pittsburgh, Pa. 15222-3907. L. R. Cayes, Federal Highway Administration, 6300 Georgetown Pike, HNR-10, McLean, Va. 22101.

BACKGROUND OF MODEL BRIDGE STUDY

The model bridge study is part of an extensive research program in progress to extend the ALFD concepts to noncompact plate-girder sections with slender webs that fall outside the compactness limits of the current ALFD guide specification (*4–8*). The experimental study involved the laboratory testing of a 0.4-scale model of a two-span continuous plate-girder highway bridge. The prototype bridge was designed by industry personnel using ALFD procedures. The model bridge consisted of two 56-ft spans, each with three plate girders. The girders supported 4-in.-thick modular precast concrete deck panels made composite with the plate girders using stud shear connectors. The panels were prestressed both transversely and parallel to the bridge axis. Components for the bridge were fabricated in two commercial shops and erected by a steel fabricator in the FHWA Structures Laboratory at the Turner Fairbank Highway Research Center in McLean, Virginia. Construction of the model bridge was completed in April 1987.

A comprehensive test plan was developed with the objective of evaluating specific responses of the model bridge at each of the three load levels specified by AASHTO—service load, overload, and maximum load. These load levels are used in ALFD and in the current AASHTO limit-states design approach known as Load Factor Design (LFD) (*9*). In both LFD and ALFD, specific structural performance requirements must be satisfied at each of the three load levels.

DESCRIPTION OF MODEL BRIDGE

Design of the model bridge began with design of a full-scale prototype. The prototype was designed according to ALFD procedures. The prototype bridge configuration used was a two-span continuous structure with equal spans of 140 ft. Overall deck width was 48 ft. The roadway width of 44 ft 6 in. allowed for three design lanes. The deck consisted of uniform 10-in.-thick precast concrete panels 8 ft wide by 48 ft long.

The superstructure consisted of three parallel flange (68-in. web depth) steel plate girders spaced at 17 ft, with a deck overhang beyond the exterior girders of 7 ft. Unpainted ASTM A588 weathering steel, 50 ksi nominal yield, was assumed in the design. Because the prototype bridge girders were designed using ALFD procedures, it was possible to use a prismatic girder section over the interior pier for this particular bridge configuration.

The bridge was designed for AASHTO HS-20 live loading plus the alternative military loading specified by AASHTO for bridges on the Interstate system. An AASHTO Case I roadway was assumed for checking fatigue. The prototype bridge was also designed using improved elastic live-load lateral distribution factors generated using a three-dimensional finite-element model of the bridge. Live-load distribution factors developed for one lane loaded were used to check fatigue details for over 2,000,000 cycles for truck loading, as specified by AASHTO for a Case I roadway. The improved live-load distribution factors showed some significant reduction over factors computed using current AASHTO procedures, particularly for the interior girder. Details of the prototype bridge design may be found elsewhere (*10,11*).

Details of the model bridge design, fabrication, and erection have also been reported previously (*10,11*). The scale factor of 0.4 used for the model bridge was determined by physical characteristics of the FHWA Structures Laboratory, fabrication techniques, and availability of plate material. A typical cross section of the model bridge is shown in Figure 1, and an elevation view of one span is shown in Figure 2. Details of the model-bridge girders and precast panels are given below.

Girders

The top flange of each girder in the model bridge was ¼ in. by 5⅝ in. throughout. The web of each girder was ¼ in. by 27 3/16 in. throughout. The bottom flange of each girder was 9/16 in. by 8 in. throughout, except 11 ft 2 in. from the abutments where the flange thickness decreased to 5/16 in. All the above dimensions are nominal. Material tests were conducted on specimens taken from the actual plate material in the model to determine the static yield strengths of the webs, flanges, and stiffeners. Because it was desired to achieve average mea-

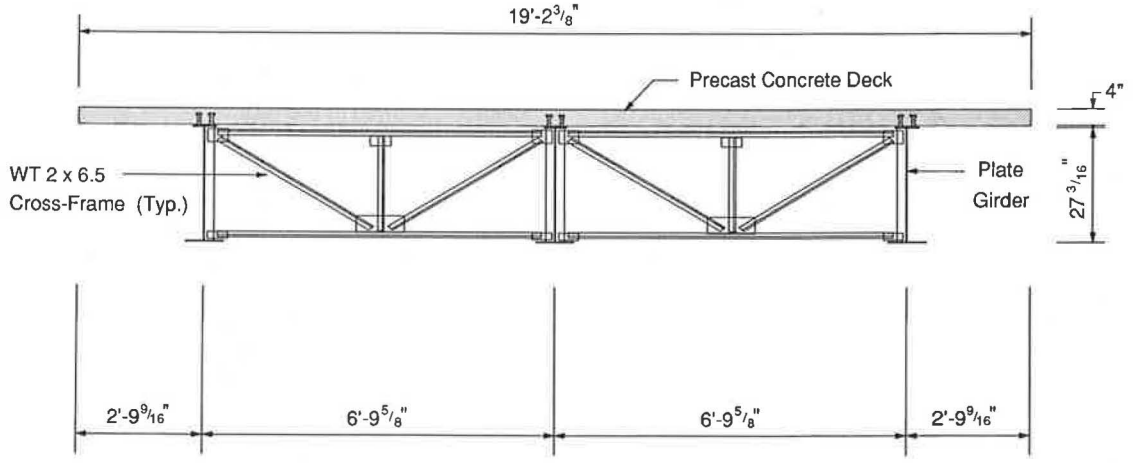

FIGURE 1 Cross section of model bridge.

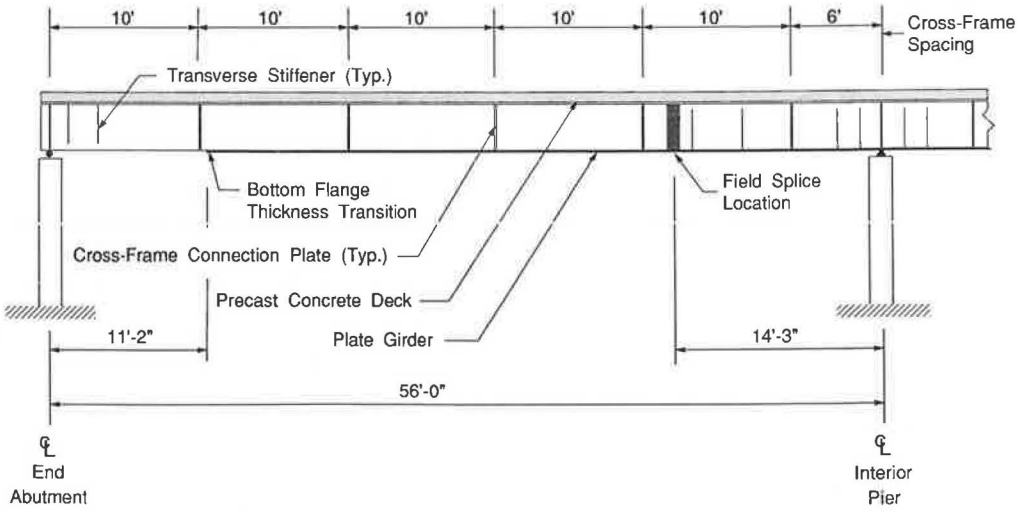

FIGURE 2 Elevation of model bridge.

sured static yield strengths as close as possible to the specified nominal yield strength of 50 ksi, and actual measured yield strengths are often higher than the specified nominal yield strength, ASTM A36 material was used for the girders. The average measured static yield strengths of the plate material used varied from 42.1 to 55.9 ksi.

Bearing stiffeners were located on both sides of the web of each girder over the supports. Cross-frame connection plates were located at 10-ft intervals, measured from the abutments, along the interior girder on both sides of the web and along each exterior girder on the inside face of the web only. This corresponds to a 25-ft cross-frame spacing in the prototype bridge, which is currently the maximum allowed by the AASHTO specification. Fillet welds were used to connect the cross-frame connection plates rigidly to the girder top and bottom flanges, as required by AASHTO. The cross-frames were composed of diagonals, top and bottom horizontal members, and a vertical post, all WT2 × 6.5 rolled sections. The cross-frame members were welded to ¼-in.-thick gusset plates, which were bolted to 5/16-in.-thick connection plates. Because only a limited number of rolled tee sections were available, the cross-sectional areas of the individual components of the cross-frames were not scaled down exactly from the prototype bridge. To evaluate the effect of improperly scaled down cross-frames, the stiffness of the cross-frame assemblages was varied in the finite-element model of the model bridge and found to have a negligible effect on the computed live-load distribution factors. Intermediate cross-frames were located 6 ft from each side of the interior pier. The cross-frames adjacent to the pier were spaced according to AI.FD criteria to brace the bottom (compression) flange and ensure adequate inelastic rotation capacity at maximum load.

Each girder had a bolted field splice 14 ft 3 in. on each side of the interior pier composed of ¼-in. splice plates fastened with ¾-in.-diameter ASTM A325 high-strength bolts. Each girder was supported on roller bearings at both abutments and on fixed bearings permitting rotation but no translation at the interior pier. Each end-abutment bearing was a 2-in.-diameter roller placed between two ¾-in. sole plates. The interior-pier bearing consisted of a ¾-in. sole plate, a plate with a rounded top surface, and two pintels. The top sole plates were welded to the bottom flange of the girders, and the bottom sole plates rested on circular load cells supported on concrete piers. The load cells were used to measure the girder reactions. Instrumentation on the steel girders included numerous strain gauges, deflection transducers, and rotation gauges.

Precast Panels

The 35 modular precast deck panels on the model bridge were each 4 in. thick, 3 ft 2 in. wide, and 19 ft 2⅜ in. long. The deck panels were pretensioned in the transverse direction using a 7/16-in.-diameter low-relaxation strand and posttensioned along the full length of the bridge after erection using a 0.60-in.-diameter low-relaxation strand. The bridge deck panels were designed on the basis of normal-weight concrete with a 28-day compressive strength of 6,000 psi. A "double-female" type of joint was used at the transverse panel-to-panel interface and grouted before posttensioning. After posttensioning, a 12-day waiting period was observed to allow for some of the concrete creep and shrinkage to occur before the panels were made composite with the girders. Grout was then placed in the 5/16-in. separation between the top of the girders and the bottom of the deck panels and in each pocket around the ⅝-in.-diameter, 3-in.-long stud shear connectors to achieve composite action. Leveling and hold-down devices were provided as specified in the prototype design. Two additional test panels were cast to obtain independent data on concrete creep and shrinkage. Instrumentation in the panels included strain gauges mounted on mild reinforcement bars embedded in the panels and numerous surface-mounted Whittemore points.

The average compressive strength of the concrete in the panels varied from 6,520 to 8,020 psi over the duration of the bridge tests. The average measured ultimate strength of the 7/16-in.-diameter prestressing strand was 281.7 ksi, and the average yield strength measured at 1 percent elongation was 247.8 ksi. The average measured ultimate strength of the 0.60-in.-diameter prestressing strand was 271.8 ksi, and the average yield strength measured at 1 percent elongation was 253.6 ksi. Measured yield strengths for both the 7/16-in.- and 0.60-in.-

diameter strands exceeded the minimum requirements for yield strength of 90 percent of the rated strand capacity for low-relaxation strands specified in ASTM A416.

Finite-Element Model

By using the general purpose finite-element program MSC/NASTRAN (*12*), a three-dimensional mathematical model of the model-bridge superstructure was generated. The three plate girders were modeled with three bar elements, one for the web and one for each flange. The three bar elements were rigidly connected to act as a single beam. A total of 40 grid divisions per span was used lengthwise along the model. The cross-frames were modeled with bar elements pinned at the ends to resist only axial loads.

The deck panels were modeled using four-node isoparametric plate elements that resist plane bending and membrane forces. Two plate elements were used transversely between each girder, and one plate element was used to model the deck overhang on one side of each of the exterior girders. Composite action was simulated by offsetting the flange and web bar elements from the concrete deck nodal points by the actual distance between them. It was assumed in the model that the concrete stiffness was fully effective throughout. A structural thickness of 10 in., a Poisson's ratio of 0.15, and a modulus of elasticity of 4,700 ksi were assumed for the deck-panel elements. Appropriate boundary conditions were input at each girder support.

COMPENSATORY DEAD LOADS

Because of the correct scaling of only the model-bridge geometry and applied loads, and not the weight density of the materials (concrete and steel), actual dead-load stresses in the model bridge were only about 40 percent of the computed dead-load stresses in the prototype bridge. To satisfy the rules of similitude, it was important to model critical dead-load moments and shears as closely as possible. Therefore, concentrated loads were applied to each girder at three locations in each span to simulate a compensatory uniform dead load. The loads were applied at approximately the 0.4, 0.6, and 0.8 point in each span of each girder, measured from the abutments. Noncomposite compensatory dead loads were applied to the bottom flanges of steel girders at these locations immediately after erection of the steel framing. These loads, applied to the noncomposite structure, compensated for the fact that the weight density of the steel girders and precast deck components in the model bridge could not be scaled correctly with a single linear scale factor. These noncomposite compensatory dead loads were maintained as constant as possible during erection of the deck panels.

Following erection, posttensioning, and grouting of the deck system, additional compensatory dead loads were applied to the composite structure. The composite dead loads were also applied to the bottom flanges of the girders and compensated for the loads due to the barrier curbs, railings, and future wearing surface that were included in the prototype design but were not physically present on the model bridge. Although it was recognized that elements such as parapets, curbs, and sidewalks may influence the distribution of live loads, it was beyond the scope of this research program to evaluate the possible effect of these elements, which was considered secondary compared with the effects of girder spacing, cross-frame spacing, and deck thickness.

The combined noncomposite and composite compensatory dead loads were maintained throughout the influence surface tests using a hydraulic loading system. After the service load tests, these loads were transferred from the bottom flanges of the steel girders to the top of the precast deck panels and maintained during the subsequent influence surface tests. A complete discussion of the compensatory dead-load system used may be found elsewhere (*10*).

INFLUENCE SURFACE TESTS

Lateral live-load distribution to the steel girders of the model bridge at elastic service load stress levels was evaluated by generating a series of influence surfaces for the bottom-flange axial force in each girder at selected locations. These bottom-flange forces were used as a measure of the bending moment in each girder. Deck-panel distribution behavior is not discussed here.

To generate the influence surfaces, a single concentrated load of 16.6 kips made of lead weights was applied to the top surface of the bridge deck at locations longitudinally spaced approximately every one-fifth of the span along the full length of the bridge. The magnitude of the load was selected so that measured strains could be recorded without causing yielding in the girders. The magnitude of the weight used is not related to an AASHTO wheel load or concentrated load. The lead weight was placed on two 4-in. by 12-in. wood blocks spaced 12 in. apart during testing. Figure 3 shows the lead weight used and the bearing blocks. In the transverse direction, the applied load was placed near the edge of the deck overhangs, directly over each girder, and halfway between the girders.

The elastic axial forces in the bottom flange of each girder caused by a single concentrated load placed at each location shown in Figure 4 were measured at the interior-pier section and at the approximate maximum positive-moment section of the west span. The line at the 0.4 point was assumed to be critical for bottom-flange axial forces in the positive-moment region, and the line at the 0.6 point was assumed to be critical for bottom-flange axial forces in the negative-moment region. Bottom-flange axial forces at each section were computed from the average of four measured strains at each bottom flange location. The measured forces were then used to compute critical elastic live-load distribution factors according to a method previously reported (*13*). To illustrate that lateral distribution factors vary along the span, distribution factors at critical positive-moment and negative-moment regions of the bridge for both interior and exterior girders were computed. Factors were computed for only one exterior girder, because the bridge is symmetrical. These factors were then compared with (a) factors computed from corresponding bottom-flange axial forces from a finite-element analysis of the model bridge using the same method, (b) factors computed using current AASHTO procedures, and (c) factors computed from proposed empirical formulas and recommendations

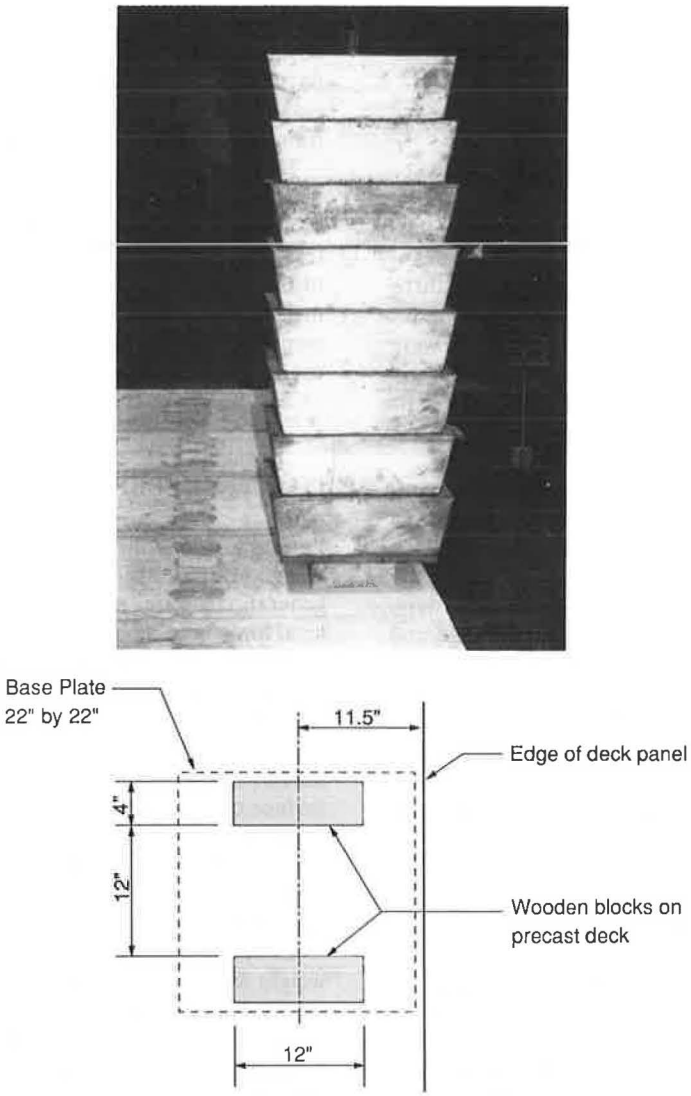

FIGURE 3 Details of dead weight for simulated wheel loadings.

developed in Phase I of NCHRP Project 12-26 on wheel-load distribution (*14*).

A series of three tests was conducted to develop influence surfaces for evaluation of the lateral live-load distribution to the girders in both positive-moment and interior-pier regions. The initial series of elastic influence surface tests, designated Test 1, was completed immediately following erection and instrumentation of the model bridge and application of the compensatory dead loads. In Test 1, all cross-frames in the model bridge remained in place.

Subsequently, the model bridge was subjected to multiple lanes of simulated AASHTO overload lane and truck loadings plus impact. The overload tests were designed to cause the formation of automoments and to illustrate shakedown under repeated loadings. After shakedown, the bridge behaves elastically again under subsequent loads not exceeding the initial overload (*1*). Permanent deformations due to controlled local yielding allowed at interior piers may be included in the dead-load camber. The stabilization of the controlled permanent deformations in the continuous steel girders during automoment formation and subsequent shakedown was observed and documented. The results of the overload testing were reported by Moore and Grubb (*11*). Following the completion of the overload tests, the second series of influence surface tests, designated Test 2, was conducted. The purpose of Test 2 was to evaluate the lateral live-load distribution to the steel girders after formation of the automoments and shakedown of the bridge. These lateral live-load distribution factors were compared with the distribution factors computed before the overload tests.

The third series of influence surface tests, designated Test 3, was conducted immediately following Test 2. For Test 3, selected intermediate cross-frames in the positive-moment regions of both the east and west spans were removed. The purpose of this test series was to evaluate the lateral live-load distribution to the girders with fewer cross-frames than required by the current AASHTO specification. In the west span, cross-frames designated D2–D5 (see Figure 4) were removed. In the east span, cross-frames designated D9–D12 (see Figure 4) were removed. The critical intermediate cross-frames adja

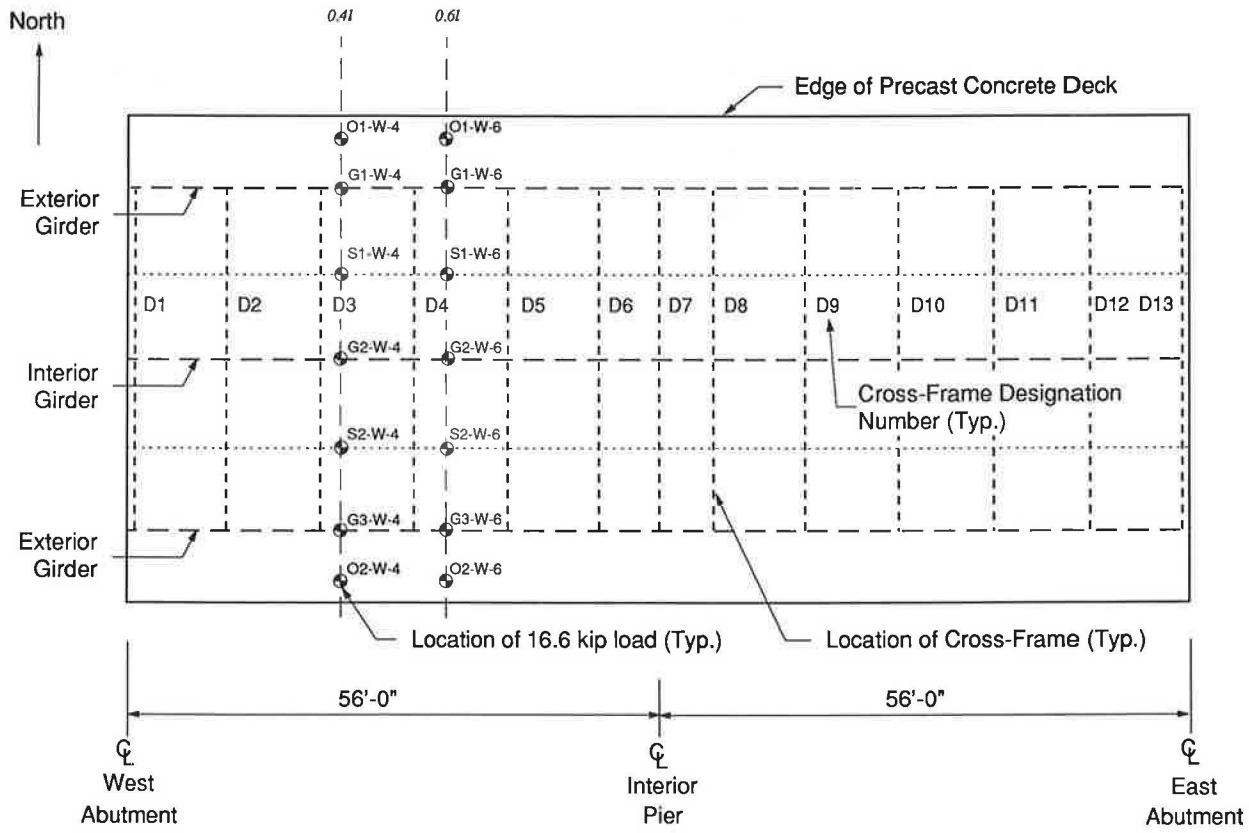

FIGURE 4 Plan view of model bridge showing the locations of the applied loads during the elastic influence surface tests.

cent to the pier, designated D6 and D8 in Figure 4, were not removed. These cross-frames brace the bottom (compression) flange in this region.

MEASURED BOTTOM-FLANGE AXIAL FORCES

Positive-Moment Region

To determine the critical distribution factors in the positive-moment region for each test, bottom-flange forces were computed from strains due to the 16.6-kip concentrated load measured at the 0.4 point of the west span (measured from the abutment) in the exterior and interior girders. The concentrated load was applied across the section at the 0.4 point in the west span. Figure 5 presents the bottom-flange forces in each test measured at the 0.4 point of an exterior girder in the west span for the loads applied across the section at the 0.4 point in the west span. Similarly, Figure 6 presents the bottom-flange forces in each test measured at the 0.4 point of the interior girder in the west span. Also shown in each figure are the corresponding bottom-flange forces from the finite-element model of the model bridge.

For the exterior girder, the bottom-flange forces in all three tests measured in the positive-moment region were generally within 10 percent of the bottom-flange forces predicted using the finite-element model. From Figure 5, no significant differences were observed in measured bottom-flange forces in the exterior girder at the 0.4 point for the tests completed before and after shakedown at overload, Tests 1 and 2. In addition, no significant differences were observed in measured bottom-flange forces in the exterior girder at the 0.4 point for the tests completed after shakedown with cross-frames in place and with selected cross-frames removed, Test 2 and 3.

For the interior girder, no significant differences were observed in bottom-flange forces measured at the 0.4 point for tests completed before and after shakedown at overload, Tests 1 and 2. When selected cross-frames were removed and the load was applied directly over the interior girder, the bottom-flange force in the interior girder measured at the 0.4 point increased 12 percent in Test 3 as compared with Test 2. For the load applied directly over an exterior girder, the bottom-flange force in the interior girder measured at the 0.4 point decreased 11 percent in Test 3 as compared with Test 2.

Negative-Moment Region

To determine the critical distribution factors in the negative-moment region for each test, bottom-flange forces were computed from strains due to the 16.6-kip load applied across the section at the 0.6 point of the west span measured at the interior pier in the exterior and interior girders (measured from the abutment). Figure 7 presents the bottom-flange forces in each test due to the application of the concentrated load across the section at the 0.6 point in the west span measured

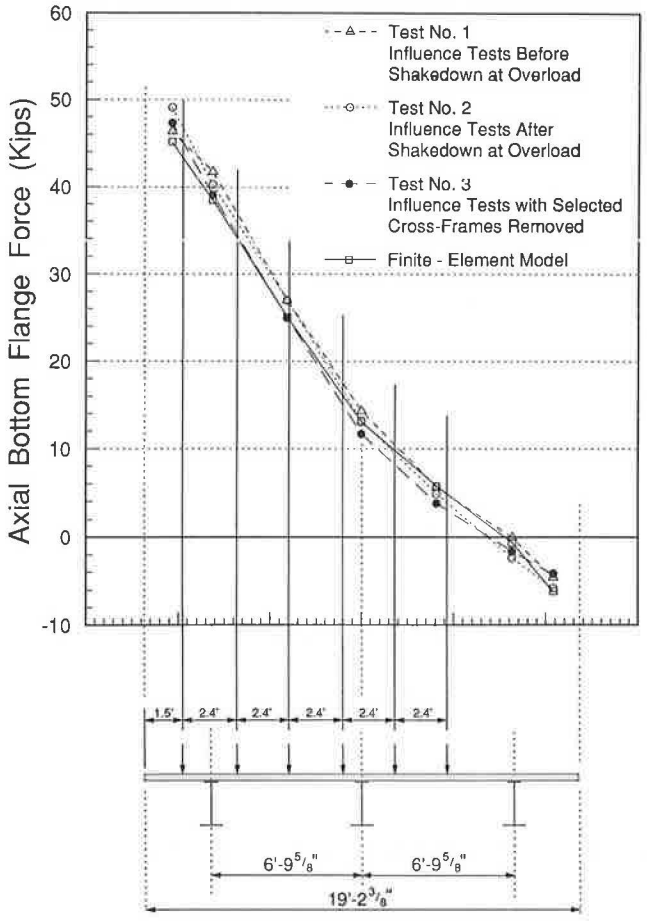

FIGURE 5 Comparison of bottom-flange forces at 0.41 (west span) from measured test data and the finite-element model for an exterior girder with the 16.6-kip load applied across the section at 0.41 (west span).

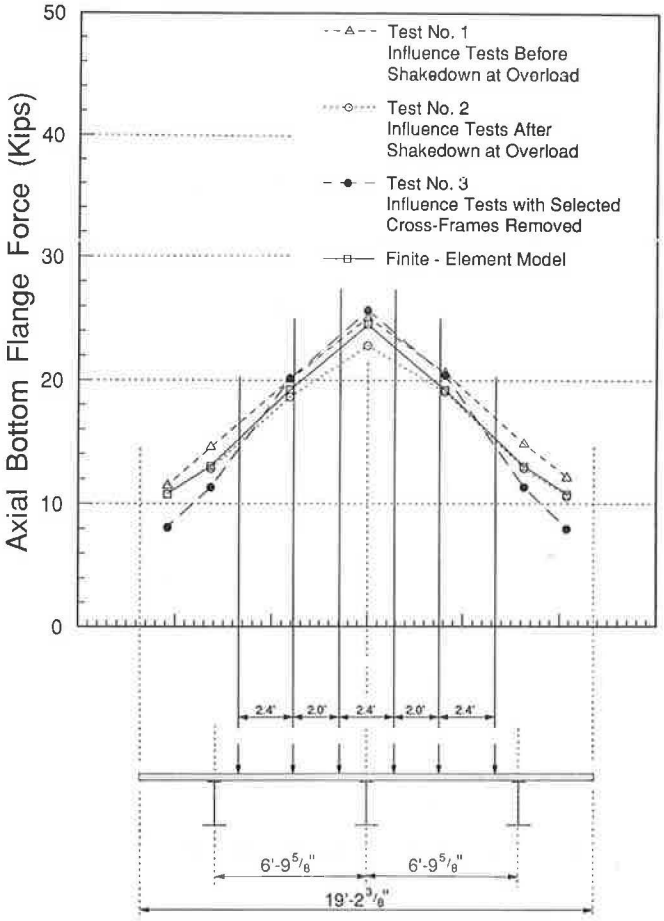

FIGURE 6 Comparison of bottom-flange forces at 0.41 (west span) from measured test data and the finite-element model for the interior girder with the 16.6-kip load applied across the section at 0.41 (west span).

at the interior-pier region of an exterior girder. Similarly, Figure 8 presents the bottom-flange forces measured in each test at the interior-pier region of the interior girder. Also shown in each figure are the corresponding bottom-flange forces from the finite-element model.

For both the exterior and interior girders, no significant differences were observed in bottom-flange forces measured at the interior pier in Tests 1 and 2, completed before and after shakedown at overload. For the case in which the load is applied directly over the interior girder, the bottom-flange force in the interior girder, measured at the interior pier, was approximately 24 percent higher in the test with selected cross-frames removed (Test 3) as compared with the test with all cross-frames in place (Test 2). For the load applied directly over an exterior girder, the bottom-flange force in the interior girder, measured at the interior pier, decreased 13 percent in Test 3 as compared with Test 2. In general, the bottom-flange forces predicted by the finite-element model underestimated the bottom-flange forces measured in each of the experimental tests.

DISTRIBUTION FACTORS

Once the plots discussed above were developed, the total bottom-flange axial force due to a single axle line of scaled-down AASHTO HS vehicles was computed for each location. [A single axle line had been determined to be sufficient in previous studies (*13*).] This scaled-down single axle line for three lanes of AASHTO HS vehicles is shown at the bottom in Figures 5–8. For each girder, the axles are shifted in their design lanes according to AASHTO rules to cause the worse loading on that girder. From each plot, contributing bottom-flange forces under each wheel were computed and summed for one, two, and three lanes loaded. Each wheel load was equal to the largest AASHTO HS scaled-down wheel load divided by 16.6. For three lanes loaded, the sum was reduced by 10 percent as allowed by AASHTO to account for the probability of coincident loading. Each sum was then divided by the theoretical elastic bottom-flange force at either the 0.4 point of the span or the interior pier, developed from a single-line-girder finite-element model loaded with the largest AASHTO HS scaled-down single axle load. The result was then multiplied by 2 to determine the corresponding distribution factor in units of wheels (*13*).

Wheel-load distribution factors for an exterior girder are summarized in Table 1. The distribution factors were computed using experimental data from each of the three tests and the method discussed above. In addition, Table 1 lists for comparison the wheel-load distribution factors computed using the same method with data from the finite-element model,

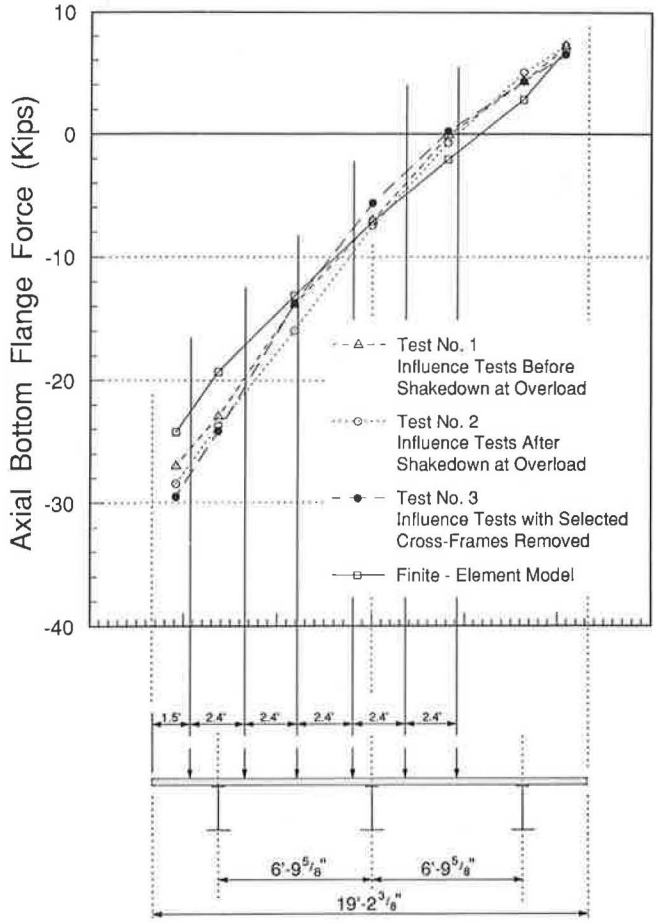

FIGURE 7 Comparison of bottom-flange forces at the interior pier from measured test data and the finite-element model for an exterior girder with the 16.6-kip load applied across the section at 0.61 (west span).

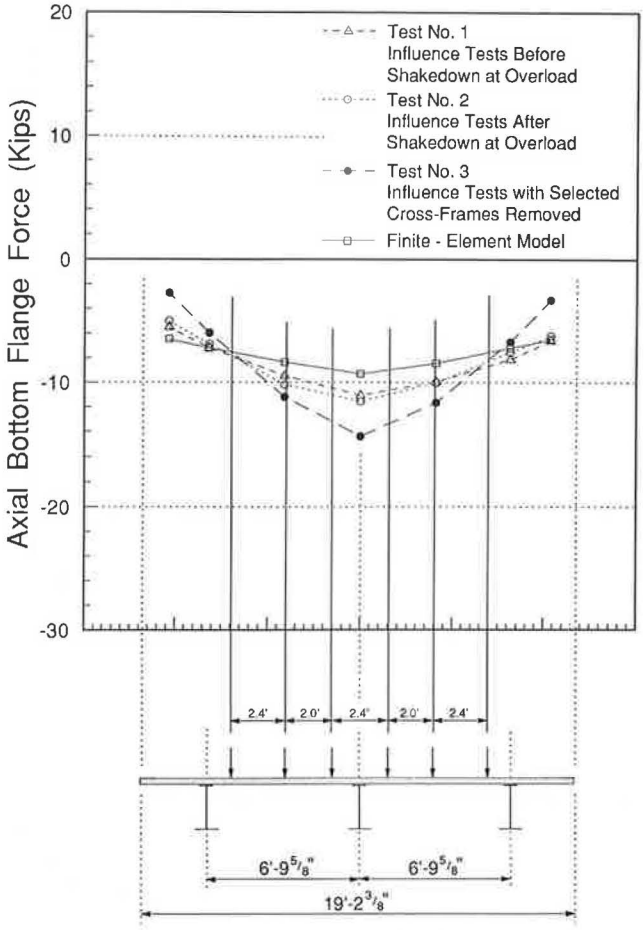

FIGURE 8 Comparison of bottom-flange forces at the interior pier from measured test data and the finite-element model for the interior girder with the 16.6-kip load applied across the section at 0.61 (west span).

factors computed according to the current AASHTO specification procedures, and factors computed from empirical formulas and recommendations proposed in NCHRP Project 12-26. The agreement between the factors computed from the experimental and finite-element analysis is well within 10 percent in the positive-moment region. For an exterior girder at the interior-pier region, the larger deviations of up to approximately 20 percent between the experimental and finite-element based factors appear to relate to some overestimation of the transverse stiffness of the model bridge by the elastic finite-element model. For the exterior girder, the current AASHTO provisions based on assuming the deck to act as a simple span between the girders provide wheel-load distribution factors that agree reasonably well with the experimental data, at least for more than one lane loaded. For multiple lanes loaded, the AASHTO factors were slightly conservative. It is recommended in the NCHRP Project 12-26 report (*14*) that this same approach be used for exterior girders until further research has been completed. According to the current AASHTO design-lane rules, a distribution factor cannot be computed for the case of three lanes loaded. As shown in Table 1, the observed slight variation in the distribution factor along the span is not considered in either the current AASHTO provisions or the proposed NCHRP formulas.

Table 2 summarizes similar data for the interior girder at both the positive-moment and interior-pier regions of the bridge. For the interior girder, factors computed on the basis of data from the three experimental tests and the finite-element analysis were well within 10 percent in the positive-moment region. Again, in the negative-moment region, the larger deviations of up to approximately 32 percent between the experimental and finite-element based factors appear to relate to some overestimation of the transverse stiffness of the model bridge by the elastic finite-element model. As with the exterior girder, the distribution factors for the interior girder vary slightly along the span of the bridge. For both the positive-moment region and the interior-pier region, the current AASHTO provisions produce very conservative distribution factors when compared with the factors computed on the basis of the experimental data and the finite-element analysis. On the basis of current AASHTO specifications, the deck is assumed to act as a simple span between girders because the girder spacing in the prototype exceeds 14 ft. The empirical formulas for interior girders proposed in NCHRP Project 12-26 for one lane loaded and for multiple lanes loaded produce distribution factors that are in close agreement with the experimental and finite-element data. The multilane formula proposed in NCHRP Project 12-26 does not differentiate between two and three lanes loaded.

TABLE 1 SUMMARY OF WHEEL-LOAD DISTRIBUTION FACTORS OF AN EXTERIOR GIRDER

	Positive - Moment Region			Interior - Pier Region		
	Number of Lanes Loaded			Number of Lanes Loaded		
	One Lane	Two Lanes	Three Lanes	One Lane	Two Lanes	Three Lanes
Experimental Results:						
Test No. 1 Influence Tests Before Shakedown at Overload	1.593	2.455	2.475	1.909	2.850	2.693
Test No. 2 Influence Tests After Shakedown at Overload	1.598	2.441	2.429	2.009	3.069	2.923
Test No. 3 Influence Tests with Selected Cross Frames Removed	1.538	2.309	2.274	2.025	2.915	2.706
Finite - Element Model	1.500	2.297	2.321	1.669	2.575	2.552
Current AASHTO Procedures	2.029	2.647	----	2.029	2.647	----
Procedures Proposed in NCHRP Project 12-26	2.029	2.647	----	2.029	2.647	----

---- denotes inapplicable

In NCHRP Project 12-26, limits of applicability were established for the proposed empirical formulas. The prototype bridge falls within the span-length limitation of 200 ft and the slab-thickness limitation of 12 in. However, it is important to recognize that other characteristics of the prototype bridge fall outside the limits of applicability for the empirical formulas proposed in NCHRP Project 12-26. The proposed formulas are only applicable to cross sections with four or more girders and a maximum transverse girder spacing of 16 ft. The model bridge tested in this research program was based on a prototype bridge utilizing only three girders and a transverse girder spacing of 17 ft. Nevertheless, the agreement between the experimental data and the proposed empirical formulas is quite good.

For both the interior and exterior girders in the positive-moment and interior-pier regions, the computed wheel-load distribution factors based on the influence surface tests conducted before and after shakedown at overload (Tests 1 and 2, respectively) varied less than 10 percent. In general, there was a trend for the distribution factors before shakedown to

TABLE 2 SUMMARY OF WHEEL-LOAD DISTRIBUTION FACTORS OF THE INTERIOR GIRDER

	Positive - Moment Region			Interior - Pier Region		
	Number of Lanes Loaded			Number of Lanes Loaded		
	One Lane	Two Lanes	Three Lanes	One Lane	Two Lanes	Three Lanes
Experimental Results:						
Test No. 1 Influence Tests Before Shakedown at Overload	0.909	1.642	2.122	0.881	1.663	2.154
Test No. 2 Influence Tests After Shakedown at Overload	0.832	1.499	1.940	0.921	1.693	2.211
Test No. 3 Influence Tests with Selected Cross Frames Removed	0.923	1.608	2.058	1.111	1.952	2.478
Finite - Element Model	0.880	1.555	2.008	0.748	1.421	1.879
Current AASHTO Procedures	1.647	2.824	2.806	1.647	2.824	2.806
Procedures Proposed in NCHRP Project 12-26	1.027	2.122	2.122	1.027	2.122	2.122

decrease slightly in positive-moment regions and increase slightly at the interior-pier regions after shakedown. This could be a result of some minor concrete cracking that may have occurred at the interior pier during the overload test.

In general, for both the interior and exterior girders, the distribution factors changed very little in the tests conducted after shakedown with the cross-frames in place and with selected cross-frames removed (Tests 2 and 3, respectively). For the case of the exterior girder in the interior-pier region, the computed distribution factors were reduced up to approximately 7.5 percent from the values after shakedown when the cross-frames were removed. For the case of the interior girder at the interior-pier region, the computed distribution factors increased an average of about 15 percent from the values after shakedown when the cross-frames were removed. These trends were slightly less pronounced in the positive-moment regions.

SUMMARY AND CONCLUSIONS

A large experimental test program has recently been completed to evaluate the behavior of a 0.4-scale model of a two-span continuous plate-girder bridge with precast prestressed modular concrete deck panels. The bridge, designed according to Alternate Load Factor Design (ALFD), or Autostress Design, procedures, utilizes noncompact plate girders with slender webs that fall beyond the current limits of the ALFD guide specification. A comprehensive test plan was followed to subject the model bridge to a series of tests designed to evaluate specific responses at simulated AASHTO service load, overload, and maximum load levels.

At elastic service-load stress levels, live-load lateral-distribution factors for the exterior and interior girders in positive and negative bending were computed from experimentally developed influence surfaces for the bottom-flange axial forces. These factors were compared with factors computed from a finite-element model, from current AASHTO procedures, and from proposed empirical formulas for interior girders. In positive-moment regions, the factors computed from the experimental and finite-element model data generally agreed within 10 percent. The larger deviations between the experimental and the finite-element model factors, in both interior and exterior girders, at the interior-pier region were probably caused by overestimation of cross-frame stiffness in the finite-element model. The interior-girder factors computed from the proposed empirical formulas also agreed reasonably well with experimental data, even though the prototype bridge used in this study falls outside the established range of applicability for the proposed formulas.

The factors computed using current AASHTO procedures were quite conservative for the interior girder, and less so for the exterior girders. The AASHTO factor for one lane loaded, used to check fatigue details for over 2,000,000 cycles of truck loading on Case I roadways, appeared to be extremely conservative in all cases. Neither the proposed nor the current AASHTO procedures accounted for the observed slight variation of the distribution factor along the span, but because the variation was small, this is probably justified. The data would seem to indicate that finite-element analysis is a plausible method for computing elastic wheel-load girder distribution factors. Also, the proposed empirical formulas appear to give reasonable results.

For tests conducted before and after shakedown at overload, the computed distribution factors varied less than 10 percent. This appears reasonable, because the bridge behaved elastically again after shakedown. The distribution factors before shakedown decreased slightly in postive-moment regions and increased slightly in negative-moment regions after shakedown, probably because of some minor concrete cracking that may have occurred over the interior pier during the overload testing. Thus, the data would seem to indicate that elastic distribution factors may still be used at overload, even though controlled local yielding is allowed in ALFD procedures.

For the tests conducted after shakedown with all cross-frames in place and with selected cross-frames removed, the computed distribution factors were generally reduced less than 7.5 percent in the exterior girders. For the interior girder, distribution factors increased up to an average of about 15 percent in negative-moment regions and an average of up to about 8 percent in positive-moment regions for the tests conducted with cross-frames in place and with selected cross-frames removed. However, the fact that the distribution factors did not vary significantly overall when the cross-frames were removed suggests that the load is primarily distributed through the concrete deck, at least for bridges without skewed supports.

ACKNOWLEDGMENTS

The work reported in this paper was part of a cooperative investigation sponsored by the Federal Highway Administration (FHWA) and the American Iron and Steel Institute (AISI). The study was conducted with the assistance of Sue Lane, Mary McGrath, and the staff of the FHWA Structures Laboratory. Additional assistance in testing the model bridge, reduction of test data, and data analysis efforts was provided by Pedro Albrecht and Kamal Elnahal of the University of Maryland and Chi Associates, Inc., Arlington, Virginia.

Design of the model bridge, load fixtures, instrumentation, and test plan was carried out by personnel from the steel industry and by Wiss, Janney, Elstner Associates, Inc. (WJE), retained by AISI to coordinate the technical aspects of the project. A. C. Kuentz of AISI and M. E. Moore of WJE served as co-principal investigators during the model bridge study. The staff of the study included M. A. Grubb of AISC Marketing, Inc.; R. P. Knight of Dynamic Isolation Systems, formerly of Bethlehem Steel Corporation; R. W. Lautensleger of ARMCO; and K. A. Strand of WJE.

The entire project was conducted under the guidance of an AISI Advisory Panel. The members of this panel were J. M. Barsom (Chairman) of U.S. Steel, a division of the USX Corporation; R. S. Fountain of Parsons-Brinckerhoff; G. Haaijer of the American Institute of Steel Construction; E. V. Hourigan of Parsons-Brinckerhoff, formerly of the New York Department of Transportation; C. L. Loveall of the Tennessee Department of Transportation; R. L. Mion of AISC Marketing, Inc.; B. T. Yen of Lehigh University; P. Zia of North Carolina State University; and I. M. Viest of Bethlehem, Pennsylvania.

Fabrication and erection of the model bridge was completed by Atlas Machine and Iron Works, Gainesville, Virginia. Precast components were fabricated by Shockey Bros. of Winchester, Virginia, and posttensioning was completed by VSL Corp., Springfield, Virginia. Load fixtures for the model bridge were fabricated by Salisbury Steel, Salisbury, Maryland.

REFERENCES

1. G. Haaijer, P. S. Carskaddan, and M. A. Grubb. *Suggested Autostress Procedures for Load Factor Design of Steel Beam Bridges*. Bulletin 29. American Iron and Steel Institute, Washington, D.C., April 1987.
2. *Guide Specification for Alternate Load Factor Design Procedures for Steel Beam Bridges Using Braced Compact Sections*. American Association of State Highway and Transportation Officials, Washington, D.C., 1986.
3. M. K. Elnahal, P. Albrecht, and L. R. Cayes. *Load Distribution in a Two-Span Continuous Bridge*. Report FHWA-RD-89-101. FHWA, U.S. Department of Transportation, June 1989.
4. A. Vasseghi and K. H. Frank. *Static Shear and Bending Strength of Composite Plate Girders*. Final Report AISI Project 320A, Phil M. Ferguson Structural Engineering Laboratory Report 87-4. University of Texas, Austin, June 1987.
5. C. G. Schilling. *Moment-Rotation Tests of Steel Bridge Girders*. AISI Project 188. American Iron and Steel Institute, Washington, D.C., April 1985.
6. C. G. Schilling. *Exploratory Autostress Girder Designs*. AISI Project 188. American Iron and Steel Institute, Washington, D.C., July 1986.
7. C. G. Schilling and S. S. Marcos. *Moment Rotation Tests of Steel Girders with Ultracompact Flanges*. AISI Project 188. American Iron and Steel Institute, Washington, D.C., July 1988.
8. C. G. Schilling. *A Unified Autostress Method*. AISI Project 51. American Iron and Steel Institute, Washington, D.C., Nov. 1989.
9. *Standard Specifications for Highway Bridges*, 13th ed. American Association of State Highway and Transportation Officials, Washington, D.C., 1986.
10. M. E. Moore and I. M. Viest. Laboratory Tests of a Continuous Composite Bridge. In *Proceedings of Conference on Composite Construction in Steel and Concrete*, Henniker, N.H., American Society of Civil Engineers, New York, June 1987.
11. M. E. Moore and M. A. Grubb. Behavior of a Two-Span Continuous Plate Girder Bridge Designed by the Alternate Load Factor Method. In *Proceedings of the National Engineering Conference*, Nashville, Tenn., American Institute of Steel Construction, Chicago, Ill., 1989.
12. C. W. McCormick. *MSC/NASTRAN User's Manual*. MacNeal-Schwendler Corporation, Los Angeles, Calif., April 1982.
13. P. S. Carskaddan and M. A. Grubb. *Live-load Lateral Distribution for the Approach Spans for the Cooper and Wando River Bridges*. U.S. Steel Research Bulletin. U.S. Steel, June 1983.
14. R. V. Nutt, R. A. Schamber, and T. Zokaie. *Distribution of Wheel Loads on Highway Bridges*. Final Report, NCHRP Project 12-26. TRB, National Research Council, Washington, D.C., April 1988 (available on a loan basis from NCHRP).

Publication of this paper sponsored by Committee on Steel Bridges.

Laboratory Investigation of the Coefficient of Friction in the Tetrafluorethylene Slide Surface of a Bridge Bearing

T. I. CAMPBELL, W. L. KONG, AND D. G. MANNING

A laboratory study of the influences of four parameters—contact pressure, temperature, speed of travel, and roughness of the stainless steel surface—on the coefficient of friction in a tetrafluorethylene–stainless steel interface is described. The coefficient of friction is found to be a maximum during the first cycle of movement, to decrease rapidly during the next four cycles, and to show little variation thereafter. The coefficient of friction increases with an increase in speed of travel and roughness of the steel surface and with a decrease in contact pressure and temperature. It is concluded that the values of the coefficient of friction for tetrafluorethylene given in the Ontario Highway Bridge Design Code follow the proper trend and are conservative, but not unduly so, under the combination of low temperature, high speed of travel, and rough mating surface.

Bearings using tetrafluorethylene (TFE) to provide slide surfaces are widely used in bridge structures. A low-friction TFE surface is used to provide either rotation, by sliding over a curved surface, or translation, by sliding on a plane surface, or a combination of both. Stainless steel is commonly used for the surface mating with the TFE.

The coefficient of friction is the prime parameter in the design of a TFE sliding bearing for a bridge because it dictates the magnitude of the forces transmitted from the superstructure to the substructure of the bridge. A state-of-the-art report (*1*) has identified 14 parameters that affect the coefficient of friction of TFE sliding on a metallic plate. These parameters are lubrication, contact pressure, speed of travel, eccentric loading, temperature, creep, roughness of the mating surface, type of TFE, attachment of the TFE to the backing plate, surface contamination, length of the travel path, load and travel history, specimen size, and wear. The influence of some of these parameters is not clearly documented in the literature and contradictory statements exist, particularly in the case of lubricated surfaces.

Results from a laboratory testing program undertaken to study the influence of some of the parameters judged to be the most influential on the coefficient of friction of TFE are reported in this paper. The testing was carried out at Queen's University under the sponsorship of the Ministry of Transportation of Ontario with the aim of refining the provisions in the Ontario Highway Bridge Design Code (OHBDC) (*2*) in relation to TFE slide surfaces.

T. I. Campbell, Department of Civil Engineering, Queen's University, Kingston, Ontario, Canada K7L 3N6. W. L. Kong, McNeely Engineering and Structures Ltd., Kingston, Ontario, Canada K7L 1G6. D. G. Manning, Research and Development Branch, Ministry of Transportation, Downsview, Ontario, Canada, M3M 1J8.

LABORATORY TEST PROGRAM

A suggested expression (*1*) for the coefficient of friction, μ, of TFE is

$$\mu = QP^{n-1} \quad (1)$$

where Q and n are parameters and P is the contact pressure on the TFE. It has been reported that Q is primarily a function of temperature and speed of travel, whereas n, which has a value less than unity, is mainly a function of filler content of the TFE, surface lubrication, surface finish of the metallic sliding plate, and loading history (*3,4*). Validation of such a relationship would simplify the requirements for the coefficient of friction for TFE slide bearings in bridge design codes.

The Ontario specification for bearings (OPSS 1203, 1988) stipulates that only dimpled, unfilled TFE resin with a silicone grease lubricant conforming to U.S. Military Specification Mil-S-8660C (1983) should be used in the slide surface of a bridge bearing. The parameters investigated in the test program were limited to contact pressure, temperature, speed of travel, and roughness of the metallic sliding plate. Loading history was kept uniform throughout the test program.

The ranges of the parameters considered for the test program are given in Table 1. These ranges reflect the conditions to which TFE slide bearings are likely to be subjected in practice and also limitations of the available test equipment. Maximum pressures of 30 MPa and 45 MPa are specified (*2*) for TFE slide surfaces in bridge bearings under dead load and total load, respectively. A temperature of -25°C represents the lowest temperature attainable in the cold room facility at Queen's University. The range of speed of travel covers that from the relatively slow temperature-induced movement to the expected relatively fast speed during passage of traffic on a bridge structure, and are within the capabilities of the testing rig. A 0.25-μm (arithmetic average) finish is required for a plane surface of the metallic plate, according to the Ontario specification for bearings (OPSS 1203, 1988). The two selected roughnesses (0.03 and 0.34 μm), measured perpendicular to the direction of polishing, correspond to those for commercially available Nos. 8 and 4 finish stainless steel plates (ASTM A480-82a, 1982), respectively. The surface roughness is highest perpendicular to the direction of polishing. A No. 8 finish is normally used for the stainless steel plate in bridge bearings in Ontario.

The ranges of parameters given in Table 1 were covered in the series of 12 tests outlined in Table 2. In each series, five

TABLE 1 RANGES OF PARAMETERS

Parameter	Range
Pressure, P (MPa)	10, 15, 25, 30, 45
Temperature, T (°C)	-25, 20
Speed of travel, V (mm/s)	0.08, 1, 20
Roughness of metallic plate, R (μm)	0.03, 0.34

TABLE 2 DETAILS OF TEST SERIES

Series	Temperature (°C)	Surface Roughness (μm)	Travel Speed (mm/s)
1	20	0.03	0.08
2	20	0.03	1.0
3	20	0.03	20.0
4	20	0.34	0.08
5	20	0.34	1.0
6	20	0.34	20.0
7	-25	0.03	0.08
8	-25	0.03	1.0
9	-25	0.03	20.0
10	-25	0.34	0.08
11	-25	0.34	1.0
12	-25	0.34	20.0

individual specimens of lubricated, dimpled TFE were tested under contact pressures of 10, 15, 25, 30, and 45 MPa, respectively, whereas temperature, surface roughness, and speed of travel were maintained as indicated, giving a total of 60 tests. The contact pressure was computed using the gross area of the TFE surface.

The specimens of dimpled, lubricated TFE resin had a diameter of 75 mm and a thickness of 4.5 mm, and were recessed to a depth of 2.5 mm in a rigid steel backing plate. A diameter of 75 mm appears to be the accepted standard for TFE tests in Europe, and the minimum thickness and free height of the TFE specimens are stipulated in the Ontario specification for bearings. A dwell of load period of 12 hr was used before testing, as required by the American Association of State Highway and Transportation Officials (*5*).

The TFE-stainless steel interface was subjected to a certain number of cycles of movement, using a stroke of ±10 mm/cycle to give a travel path of 40 mm/cycle. Fifty cycles were selected for the slow speed (0.08 mm/sec) tests in order to limit the test to a reasonable time period. Three hundred cycles were usually completed in the intermediate speed (1.0 mm/sec) tests and a minimum of 8,000 cycles completed in the fast speed (20 mm/sec) tests.

A diagrammatic representation of the self-straining rig used for the testing program is shown in Figure 1. This rig is capable of subjecting a TFE-stainless steel interface to cyclic sliding movement at different speeds under different levels of contact pressure. The TFE specimen is compressed against a stainless steel plate by means of a vertical hydraulic ram acting through a spherical bearing to ensure concentric loading. This plate is attached to a sliding platform that moves horizontally on steel rollers. The speed and stroke of the horizontal movement are controlled by an MTS closed-loop testing system. A triangular displacement-time function was used to provide a uniform speed over the stroke. Load cells were used to measure the vertical and horizontal loads transmitted to the TFE

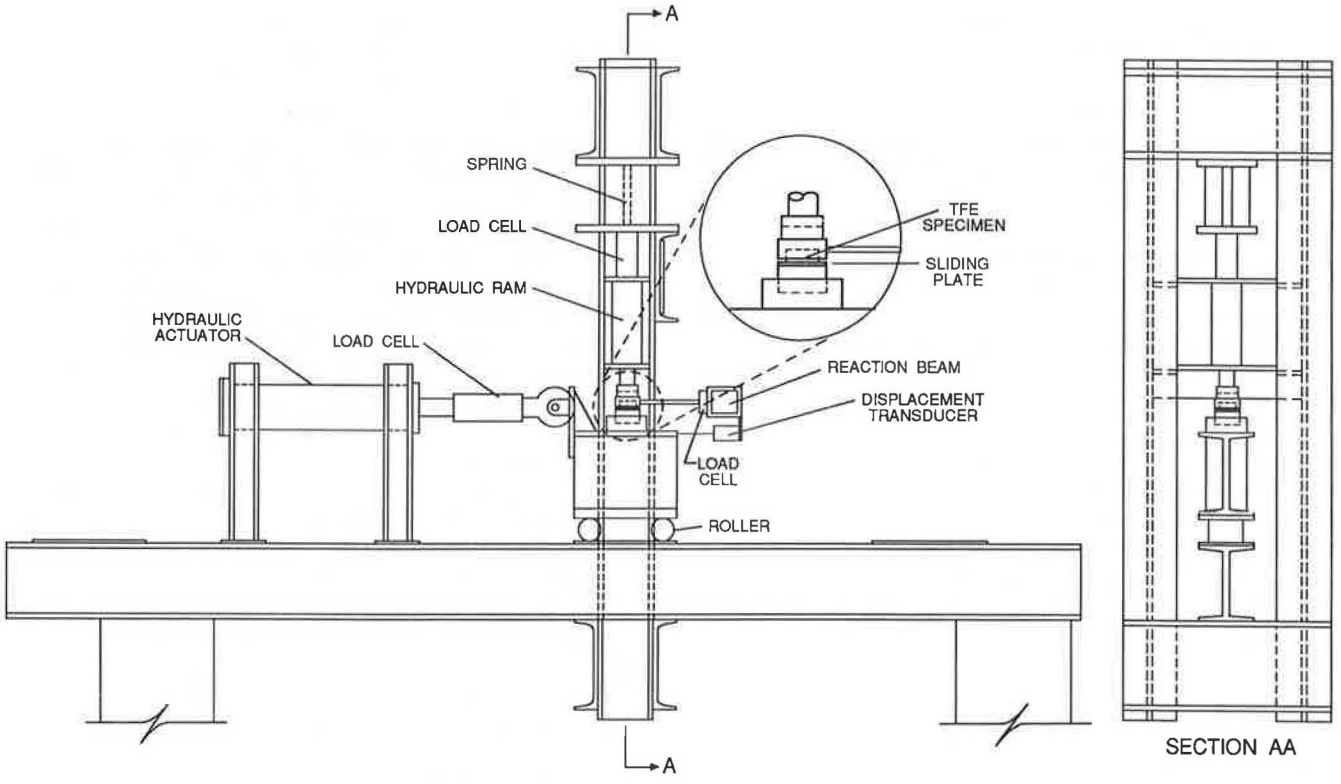

FIGURE 1 Diagrammatic representation of testing rig.

specimen. The temperature of the TFE-stainless steel interface was monitored, together with the temperature and the humidity of the environment of the rig. The tests at −25°C were conducted with the rig located in a cold room facility.

The coefficient of friction at the TFE-stainless steel interface is determined from the ratio of the horizontal to the vertical load in the interface. A typical variation of the coefficient of friction over a complete cycle of movement is shown in Figure 2. The static and dynamic coefficients of friction, which relate to the forces required to initiate movement and to maintain movement, respectively, are identified. The static coefficient is taken as the maximum value and the dynamic coefficient as the minimum value.

The TFE, stainless steel, and lubricant used in the tests were obtained from the same sources as those used by a Canadian bearing manufacturer. The dimples on the TFE surface have a diameter of 8 mm and a depth of 2 mm, and are arranged in the pattern shown in Figure 3. Molykote 44, which is a silicone oil thickened with lithium soap, was used as the lubricant. The stainless steel specimens were mounted on the sliding platform so that the direction of movement was perpendicular to the direction in which the stainless steel was polished. The backing plate containing the TFE specimen was placed on the stainless steel plate in the test rig, with the TFE specimen aligned so that the direction of the movement of the TFE relative to the stainless steel was as indicated in Figure 3. This alignment of the dimples ensured that the lubricant was smeared uniformly over the entire region of movement of the TFE.

OBSERVATIONS FROM TEST DATA

Data from all 60 tests have been presented and discussed in detail (*6*). Phenomena observed during the tests and trends exhibited by the test data are summarized as follows.

During the tests using the rough (No. 4 finish) stainless steel plate, the lubricant became darker in color and stiffer in consistency with the increasing number of cycles compared

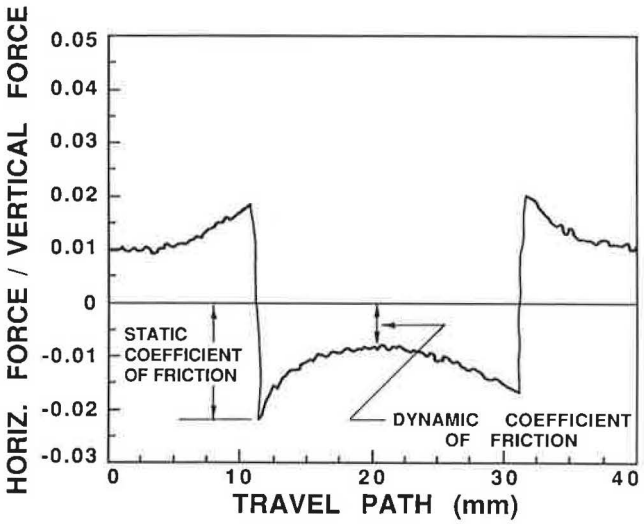

FIGURE 2 Variation of the ratio of horizontal to vertical force over a cycle.

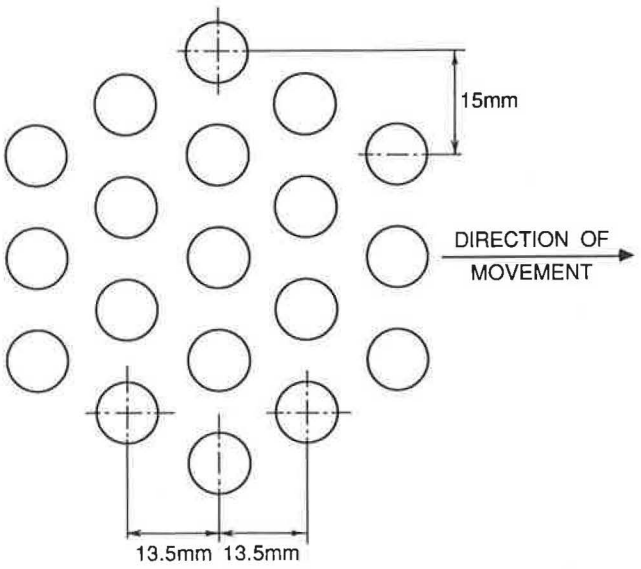

FIGURE 3 Arrangement of grease dimples.

with the corresponding tests using the smooth (No. 8 finish) stainless steel plate. The grease from the smooth stainless steel plate tests was found to be discolored by the presence of embedded particles of TFE. The color of the grease from the tests using the rough stainless steel plate was very dark, presumably as a result of contamination with residuals of the abrasive used in polishing the stainless steel.

Significant wear of the TFE was observed in the test carried out using a smooth stainless steel plate at a contact pressure of 45 MPa, a sliding speed of 20 mm/sec, and a temperature of −25°C. Wear was characterized by a deposit of flakes of TFE on the stainless steel plate at each end of the stroke. A loss in weight of 4 percent was measured after 8,000 cycles in this test. By comparison, in the corresponding test using the rough stainless steel, the loss in weight was only 0.5 percent. The reason for the significantly larger amount of wear with the smooth stainless steel plate was not immediately obvious. Traces of wear were also observed in the test using the smooth stainless steel plate at a contact pressure of 30 MPa, a sliding speed of 20 mm/sec, and a temperature of −25°C. No wear, as characterized by TFE deposits, was detected in any other test.

The shape of the force ratio–displacement trace for a cycle differed, particularly during the early cycles of movement, for the rough and smooth stainless steel plates. Figure 4 shows traces from the second cycle of movement in tests with a smooth stainless steel plate [Figure 4(a)] and a rough stainless steel plate [Figure 4(b)]. Figure 4(b) shows a more pronounced difference between the ratio of the horizontal to the vertical force at mid-stroke and at the end of the stroke than does Figure 4(a). After about 30 cycles, the shape of the trace for the rough plate approached that of the smooth plate.

The temperature ot the TFE specimen increased with the number of cycles in the fast speed tests using both smooth and rough stainless steel plates. After 8,000 cycles at 20°C, the increase was approximately 2°C for the smooth plate and 3°C to 4°C for the rough plate, whereas at −25°C the corresponding increase was from 5°C to 10°C for both plates and the temperature increased with contact pressure.

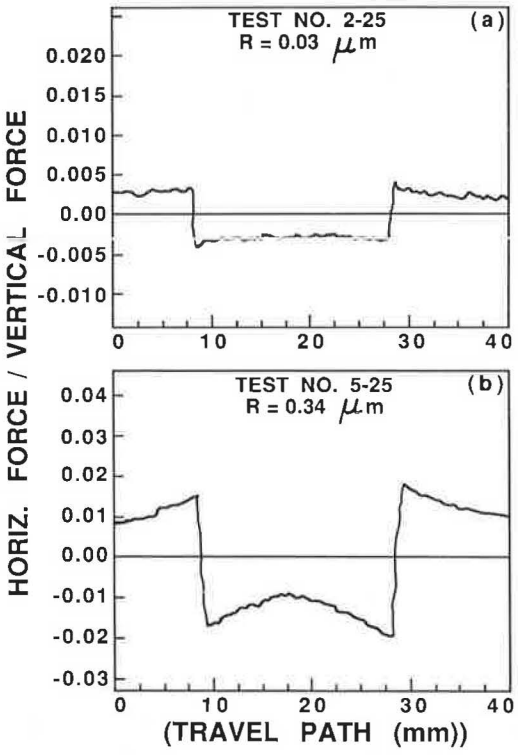

FIGURE 4 Traces of variation of horizontal to vertical force ratio for rough and smooth stainless steel plates.

Typical data obtained from one of the tests (Test 6-30) are shown in Figure 5. Test 6-30 is the test in Series 6 using a contact pressure of 30 MPa. Values for both the static and dynamic coefficients of friction, obtained after various cycles in the tests at 20°C and −25°C, are given in Tables 3 and 4, respectively.

Generally, the highest value of the coefficient of friction, both static and dynamic, was recorded during the initial movement from the mid-stroke position. A rapid drop in the magnitude of both coefficients of friction occurred after 1 cycle of movement, and the magnitude of the drop increased with speed of movement. A further decrease occurred up to about 5 cycles, after which both coefficients appeared to stabilize and remain fairly constant up to 50 cycles. For each test, the difference between the static and dynamic coefficients of friction remained fairly constant with increasing number of cycles. Data obtained beyond 50 cycles indicated an increase in both the coefficients of friction up to about 1,000 cycles, after which the values stabilized and remained fairly constant up to as many as 18,000 cycles. However, some exceptions to this general trend were observed.

In Series 4 and 5, at low and intermediate speeds, respectively, as can be seen from column (1)/(2) of Table 3, the initial static coefficient of friction was lower than that at 50 cycles, except in Tests 5-15 and 5-45. The maximum value of the static coefficient of friction in each of these two tests was recorded at the end of the stroke during the first cycle rather than at initial movement from the mid-stroke position. Subsequent to the first cycle, the static coefficient decreased and stabilized after about 5 cycles. On the other hand, in all the tests of Series 4 and 5, the dynamic coefficient of friction increased over the first 5 cycles and then stabilized. This deviation from the general trend may be due to the effectiveness with which the lubricant is spread during the first cycle of movement of the TFE on the rough stainless steel plate. The lower value of the static coefficient of friction occurred at mid-stroke when the lubricant had been present under pressure for the 12-hr preloading period, whereas the peak coefficient of friction occurred at the end of the stroke when part of the surface of the stainless steel plate was receiving lubricant for the first time. The absence of this deviation in the Series 6 tests suggests that, for the rough plate, the influence

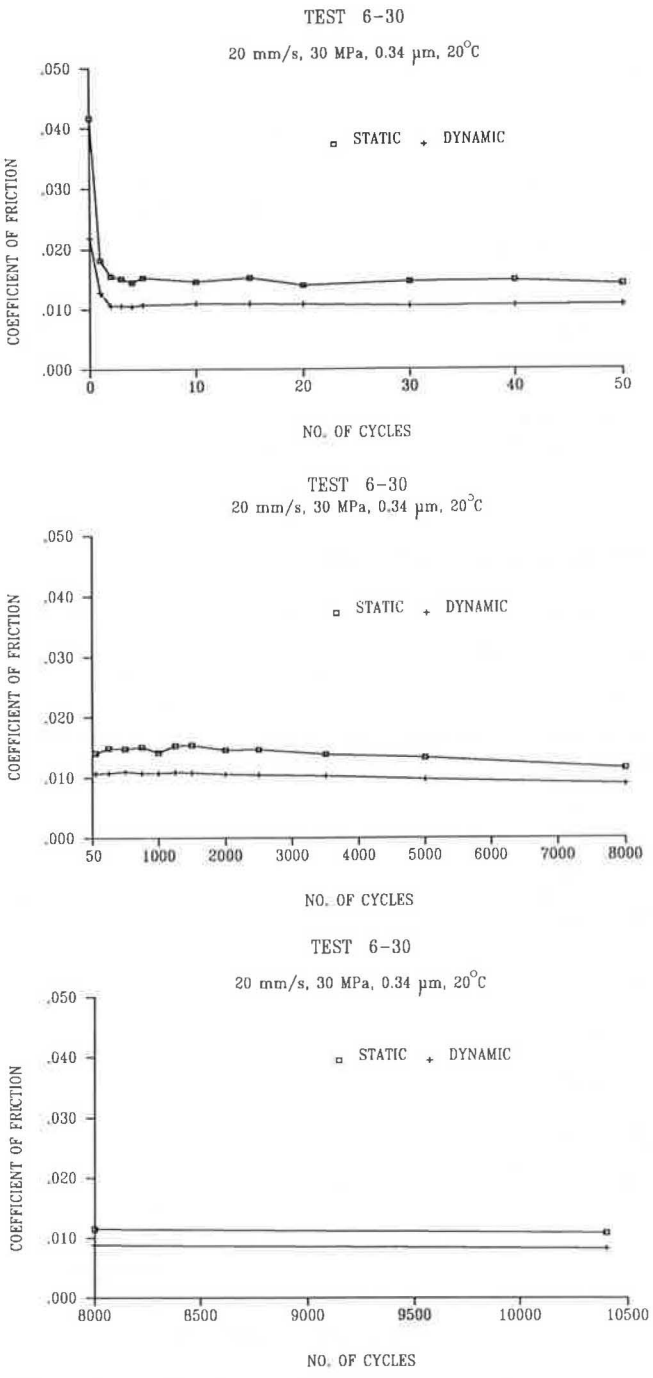

FIGURE 5 Typical test data.

TABLE 3 COEFFICIENTS OF FRICTION AFTER VARIOUS CYCLES AT 20°C

TEST NO.	COEFFICIENT OF FRICTION							RATIOS		
	INITIAL		AT 50 CYCLES		AT SPECIFIED CYCLES					
	STATIC (1)	DYNAMIC	STATIC (2)	DYNAMIC (3)	STATIC (4)	DYNAMIC	CYCLES	(1)/(2)	(4)/(2)	(3)/(2)
1-10	.0116	.0087	.0108	.0080				1.07		.74
1-15	.0135	.0820	.0072	.0051				1.88		.71
1-25	.0058	.0046	.0038	.0028				1.53		.74
1-30	.0055	.0037	.0038	.0027				1.45		.71
1-45			.0031	.0021	.0033	.0025	106		1.06	.68
2-10	.0136	.0068	.0077	.0050	.0100	.0060	375	1.77	1.30	.65
2-15	.0140	.0092	.0052	.0032				2.69		.62
2-25			.0040	.0026						.65
2-30			.0040	.0018						.45
2-45	.0086	.0079	.0033	.0011				2.61		.33
3-10	.0334	.0172	.0126	.0064	.0198	.0112	8000	2.65	1.57	.51
3-15	.0473	.0258	.0081	.0028	.0127	.0041	8000	5.84	1.57	.35
3-25	.0338	.0181	.0063	.0035	.0106	.0065	8000	5.37	1.68	.56
3-30	.0290	.0175	.0066	.0044	.0120	.0078	18000	4.39	1.82	.67
3-45	.0230	.0160	.0045	.0030	.0059	.0040	5000	5.11	1.31	.67
4-10	.0149	.0100	.0169	.0112				.88		.66
4-15			.0146	.0101						.69
4-25	.0089	.0063	.0092	.0066				.97		.72
4-30	.0062	.0039	.0082	.0060				.76		.73
4-45	.0054	.0054	.0062	.0047				.87		.76
5-10	.0167	.0132	.0253	.0212	.0318	.0250	400	.66	1.26	.84
5-15	.0430	.0280	.0300	.0260	.0253	.0208	360	1.43	.84	.87
5-25	.0146	.0118	.0176	.0140	.0201	.0153	400	.83	1.14	.80
5-30	.0114	.0095	.0141	.0128	.0175	.0142	360	.81	1.24	.91
5-45	.0143	.0125	.0124	.0106	.0117	.0910	305	1.15	.94	.85
6-10	.0689	.0530	.0387	.0310	.0406	.0276	8000	1.78	1.05	.80
6-15	.0528	.0381	.0274	.0233	.0270	.0217	10600	1.93	.99	.85
6-25	.0331	.0191	.0169	.0136	.0170	.0140	10600	1.96	1.01	.80
6-30	.0417	.0218	.0141	.0107	.0109	.0830	10400	2.96	.77	.76
6-45	.0328	.0185	.0104	.0078	.0077	.0610	8000	3.15	.74	.75

Blanks indicate that data were not available

TABLE 4 COEFFICIENTS OF FRICTION AFTER VARIOUS CYCLES AT −25°C

TEST NO.	COEFFICIENT OF FRICTION							RATIOS		
	INITIAL		AT 50 CYCLES		AT SPECIFIED CYCLES					
	STATIC (1)	DYNAMIC	STATIC (2)	DYNAMIC (3)	STATIC (4)	DYNAMIC	CYCLES	(1)/(2)	(4)/(2)	(3)/(2)
7-10	.0603	.0279	.0286	.0213				2.11		.74
7-15	.0232	.0140	.0172	.0118				1.35		.69
7-25	.0225	.0112	.0183	.0136				1.23		.74
7-30	.0143	.0105	.0097	.0070				1.47		.72
7-45	.0084	.0055	.0080	.0059				1.05		.74
8-10	.0549	.0251	.0220	.0168	.0341	.0233	335	2.50	1.55	.76
8-15	.0387	.0197	.0200	.0149	.0253	.0187	335	1.94	1.26	.75
8-25	.0576	.0420	.0254	.0200	.0267	.0220	200	2.27	1.05	.79
8-30	.0229	.0139	.0103	.0080	.0125	.0874	136	2.22	1.21	.78
8-45	.0537	.0340	.0178	.0155	.0225	.0193	235	3.02	1.26	.87
9-10	.1000	.0526	.0328	.0290	.0814	.0686	7400	3.05	2.48	.88
9-15	.1120	.0673	.0277	.0223	.0552	.0467	8000	4.04	1.99	.81
9-25	.0809	.0489	.0265	.0230	.0317	.0270	9546	3.05	1.20	.87
9-30	.0844	.0505	.0266	.0238	.0331	.0128	8000	3.17	1.24	.89
9-45	.0590	.0395	.0187	.0163	.0280	.0263	8000	3.16	1.50	.87
10-10	.0420	.0247	.0291	.0154				1.44		.53
10-15	.0264	.0161	.0299	.0159				.88		.53
10-25	.0158	.0102	.0156	.0078				1.01		.50
10-30	.0256	.0173	.0252	.0196				1.02		.78
10-45	.0156	.0109	.0208	.0167				.75		.80
11-10	.0660	.0528	.0648	.0488	.0613	.0476	350	1.02	.95	.75
11-15	.0486	.0259	.0372	.0276	.0461	.0336	300	1.31	1.24	.74
11-25	.0469	.0307	.0267	.0226	.0340	.0293	235	1.76	1.27	.85
11-30	.0240	.0166	.0148	.0118	.0259	.0223	358	1.62	1.75	.80
11-45	.0296	.0225	.0205	.0165	.0296	.0257	350	1.44	1.44	.80
12-10	.1480	.0770	.0500	.0434	.0573	.0434	8200	2.96	1.15	.87
12-15	.0945	.0559	.0430	.0365	.0680	.0570	8000	2.20	1.58	.85
12-25	.0928	.0515	.0432	.0370	.0468	.0382	8000	2.15	1.08	.86
12-30	.0704	.0467	.0220	.0212	.0350	.0303	8000	3.20	1.59	.96
12-45	.0796	.0595	.0247	.0209	.0240	.0209	8000	3.22	.97	.85

Blanks indicate that data were not available

of the lubricant on the coefficient of friction may not be as significant during the initial cycles at higher speeds.

The trends in the Series 7 and Series 10 tests were similar to those in Series 4 and 5. In the Series 7 tests, both the static and dynamic coefficients decreased over the first 2 cycles but increased and stabilized after about 10 cycles. The general trend in the Series 10 tests, carried out at −25°C using No. 4 stainless steel, was for an increase in the static coefficient of friction over the first 5 cycles followed by relatively stable values up to 50 cycles. The appearance of this trend in Series 7, where the smooth stainless steel plate is used, indicates that the spread of the lubricant may be hindered by the lower temperature of this test. However, the lack of this trend in the comparison Series 11 tests, in which rough stainless steel plate is used, suggests that the influence of the lubricant on the coefficient of friction is less pronounced at low temperature. The behavior in the low temperature tests may also be influenced by icing in the TFE-stainless steel interface.

ANALYSIS OF TEST DATA

On the basis of the preceding observations, it may be concluded that, with the exception of the first 5 cycles of movement, the values of the coefficients of friction after 50 cycles of movement are representative. Consequently, further analyses are based on the static coefficient of friction at 50 cycles. Both static and dynamic values appear to follow the same basic trends.

The column headed (1)/(2) in both Tables 3 and 4 shows that the ratio of the initial coefficient of friction to that at 50 cycles does not appear to be dependent on contact pressure. However, this ratio increases with speed of movement and was as high as 5 in the Series 3 tests, in which the speed of movement was 20 mm/sec. The ratios in column (4)/(2) of Tables 3 and 4 indicate in most cases an increase in the coefficient of friction beyond 50 cycles. From column (3)/(2) in Tables 3 and 4 it can be seen that the ratio of the dynamic to static friction at 50 cycles varies from an average of 0.54 in Series 2 to 0.88 in Series 12. This ratio appears to be independent of contact pressure.

Data at 50 cycles from a number of the test series are presented in Figures 6, 7, and 8 in the form of plots of coefficient of friction against contact pressure. Also shown on each plot is the best fit to the data of the relationship given in Equation 1. It can be seen that reasonable fits are obtained for the data, particularly from the tests at 20°C. More scatter is apparent in the data from the tests at −25°C. Values of

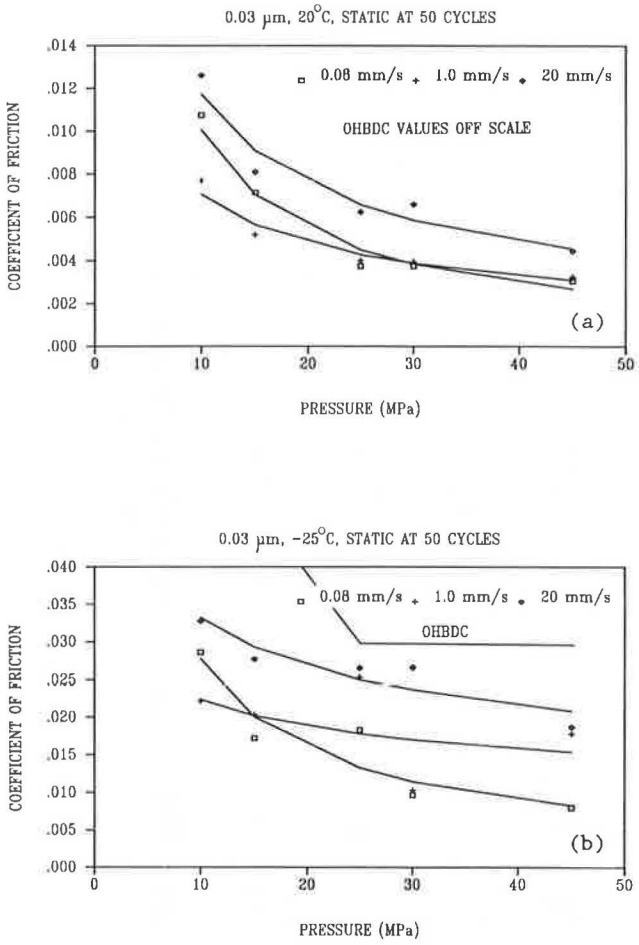

FIGURE 6 Influence of pressure, speed of movement, and temperature on the coefficient of friction.

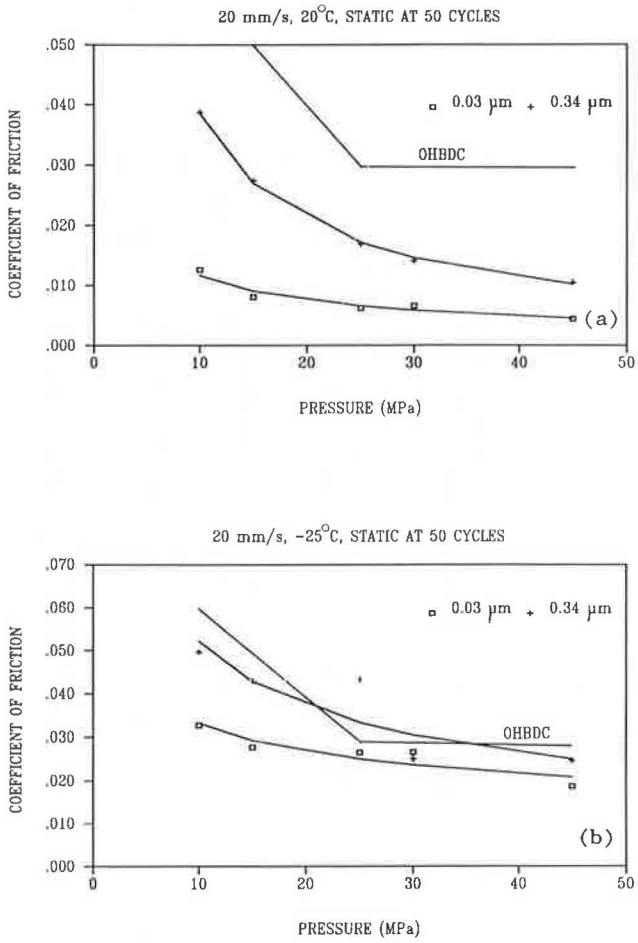

FIGURE 7 Influence of pressure, surface roughness, and temperature on the coefficient of friction.

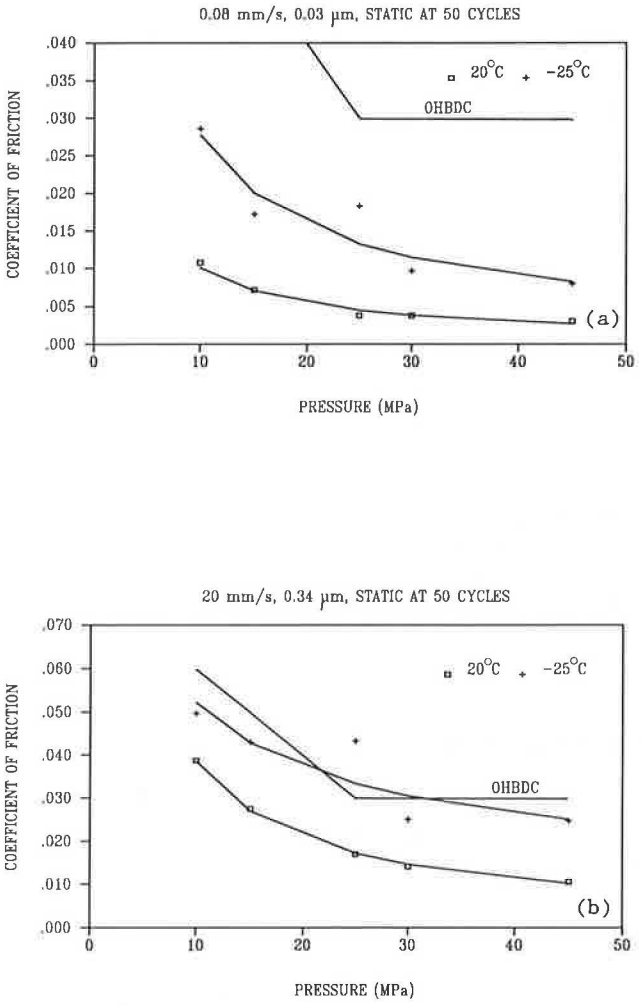

FIGURE 8 Influence of pressure, temperature, and surface roughness on the coefficient of friction.

the coefficient of friction specified in the Ontario Highway Bridge Design Code (*2*) for unfilled lubricated TFE sliding surfaces are shown on most of the plots in Figures 6, 7, and 8.

The influence of speed of movement for a particular temperature and surface roughness of the stainless steel is indicated in Figure 6, whereas the influence of surface roughness for a particular temperature and speed of movement and the influence of temperature for a particular speed of movement and surface roughness are indicated in Figures 7 and 8, respectively. All the plots in Figures 6, 7, and 8 show the established trend, in that the coefficient of friction of TFE decreases with increasing pressure under all conditions.

Data from tests using No. 8 finish stainless steel at 20°C and −25°C, respectively, are shown in Figures 6(a) and 6(b), which reflect the general trend observed by others that the coefficient of friction increases with speed of movement. It can be seen, however, that this is not the case under all conditions. Figure 6(a), relating to the tests at 20°C, indicates that the coefficient of friction at 0.08 mm/sec is greater than that at 1 mm/sec at contact pressures below 25 MPa, whereas Figure 6(b), relating to the tests at −25°C, indicates a similar trend at contact pressures below 15 MPa. Further, it can be seen in Figure 6 that for the relevant combinations of the parameters, all measured values of the coefficient of friction are less than the specified values for unfilled TFE in the OHBDC (*2*).

The coefficient of friction is higher for the rougher (No. 4 finish) stainless steel, as seen in Figure 7. However, it appears that for a particular contact pressure the difference between the values of the coefficient of friction for the two finishes (Nos. 4 and 8) is similar at −25°C and 20°C. It is indicated in Figure 7(b) that the measured coefficient of friction exceeds the OHBDC value at contact pressures in the 20- to 30-MPa range at −25°C with a No. 4 finish stainless steel plate and a speed of movement of 20 mm/sec. However, this finish (0.34 μm) is rougher than the 0.25-μm finish permitted by the OHBDC.

It can be seen from Figure 8 that the coefficient of friction is larger at −25°C than at 20°C. Also it appears that the rate of decrease in the coefficient of friction with increasing contact pressure is lower for the rough stainless steel plate.

A single value of each of the two parameters, Q and n, used in Equation 1 to relate the coefficient of friction and the contact pressure, was obtained from each of the test series by means of a regression analysis. These 12 data points were insufficient to develop general relationships for the variation of Q and n with speed for the two conditions of temperature and roughness of the stainless steel. More test data are required.

RECOMMENDATIONS FOR DESIGN AND FURTHER RESEARCH

The values of the coefficient of friction for unfilled TFE, as given by the OHBDC, are higher than those obtained after 50 cycles for all conditions simulated in the test program, with the exception of the high-speed tests at −25°C using a rough stainless steel plate in the 20- to 30-MPa range. Because smooth (No. 8 finish) stainless steel is normally used for bearings manufactured in Ontario, the OHBDC values may be considered conservative for temperatures as low as −25°C and speeds of movement up to 20 mm/sec, provided that it is permissible to design structures for the static coefficient of friction at 50 cycles.

A comparison between the values of the initial static coefficient of friction from the tests using the No. 8 finish stainless steel and those specified in the OHBDC is shown in Table 5. It can be seen that if structures are to be designed for the initial level of friction, the OHBDC values may be unconservative, particularly at a temperature of −25°C and a speed of 20 mm/sec (Series 9 tests). The initial coefficient of friction in this case may be as high as 2.8 times the OHBDC value.

Because the coefficient of friction decreases rapidly during the first few cycles of movement and changes little between 5 and 50 cycles, it appears that significant benefits, in the form of a reduction in the specified coefficient of friction for design, could be achieved if the initial coefficient of friction of TFE could be reduced. This may be possible by subjecting the sliding surface to cyclic movement before installation of a bearing. Other possible means of reducing the initial coefficient of friction should also be explored.

TABLE 5 COMPARISON OF TEST AND OHBDC VALUES FOR THE COEFFICIENT OF FRICTION

Test No.	Coefficient of Friction		Initial/OHBDC
	Initial	OHBDC	
1-10	0.0116	0.06	0.193
1-15	0.0135	0.05	0.270
1-25	0.0058	0.03	0.193
1-30	0.0055	0.03	0.183
1-45		0.03	
2-10	0.0136	0.06	0.227
2-15	0.0140	0.05	0.280
2-25		0.03	
2-30		0.03	
2-45	0.0086	0.03	0.287
3-10	0.0334	0.06	0.557
3-15	0.0473	0.05	0.946
3-25	0.0338	0.03	1.127
3-30	0.0290	0.03	0.967
3-45	0.0230	0.03	0.767
7-10	0.0603	0.06	1.005
7-15	0.0232	0.05	0.464
7-25	0.0225	0.03	0.750
7-30	0.0143	0.03	0.477
7-45	0.0084	0.03	0.280
8-10	0.0549	0.06	0.915
8-15	0.0387	0.05	0.774
8-25	0.0576	0.03	1.920
8-30	0.0229	0.03	0.763
8-45	0.0537	0.03	1.790
9-10	0.1000	0.06	1.667
9-15	0.1120	0.05	2.240
9-25	0.0809	0.03	2.697
9-30	0.0844	0.03	2.813
9-45	0.0590	0.03	1.967

The ratio of the initial coefficient of friction to that at 50 cycles increases with sliding speed, as shown in Columns (1)/(2) of Tables 3 and 4. Sliding speeds at the bearings of typical bridge structures should be determined from field tests in order to establish upper limits for the sliding speed.

CONCLUSIONS

On the basis of the coefficient of static friction after 50 cycles of movement, unless otherwise stated, the following conclusions may be drawn from the data obtained in this test program:

1. The coefficient of friction decreases with increasing pressure over the range 10 to 45 MPa.
2. The general trend is an increase in the coefficient of friction with sliding speed over the range 0.08 to 20 mm/sec.
3. The coefficient of friction increases with roughness of the stainless steel plate over the range 0.03 to 0.34 μm.
4. The coefficient of friction increases with decrease in temperature over the range 20° to 25°C.
5. Values of the coefficient of friction given for unfilled TFE in the OHBDC indicate the proper trend and are conservative except for the rough stainless steel plate at −25°C and a travel speed of 20 mm/sec.
6. The initial coefficient of friction can be as high as five times that after 50 cycles of movement.
7. The coefficient of friction generally decreases rapidly during the first 5 cycles of movement, remains fairly constant up to 50 cycles, increases slightly from 50 to 1,000 cycles, and then again remains fairly constant up to as many as 10,000 cycles.
8. The dynamic coefficient of friction is lower than the static coefficient but follows the same trend with an increasing number of cycles.
9. The relationship of Equation 1 gives a reasonably good fit to the test data, but more data are required in order to establish values of the parameters Q and n.
10. Possible means of reducing the initial coefficient of friction should be explored.

ACKNOWLEDGMENT

This paper is based on work sponsored by the Ministry of Transportation of Ontario at the Queen's University at Kingston, Ontario, Canada.

REFERENCES

1. T. I. Campbell and W. L. Kong. *TFE Sliding Surfaces in Bridge Bearings*. Report ME-87-06. Ministry of Transportation and Communications, Downsview, Ontario, Canada, July 1987, 57 pp.
2. *Ontario Highway Bridge Design Code*, 2nd ed. Ministry of Transportation and Communications, Downsview, Ontario, Canada, 1983.
3. M. E. Taylor. *PTFE in Highway Bridge Bearings*. Report TRRL-LR-491. Transport and Road Research Laboratory, Crowthorne, Berkshire, England, 1972, 62 pp.
4. W. I. J. Price. *Transmission of Horizontal Forces and Movements by Bridge Bearings, Joint Sealing and Bearing Systems for Concrete Structures*. ACI Publication SP-70, Vol. 2. American Concrete Institute, Detroit, Mich., 1982, pp. 761–784.
5. *Standard Specifications for Highway Bridges*, 13th ed. American Association of State Highway and Transportation Officials, Washington, D.C., 1983.
6. T. I. Campbell and W. L. Kong. *Laboratory Study of Friction in TFE Sliding Surfaces for Bridge Bearings*. Report MAT-89-04. Ministry of Transportation, Downsview, Ontario, Canada, Feb. 1989, 66 pp.

Publication of this paper sponsored by Committee on General Structures.

Integral Bridges

MARTIN P. BURKE, JR.

In the United States and Canada, integrated bridge construction is becoming one of the bridge engineer's primary responses to joint-related bridge damage caused by the use of deicing chemicals and the restrained growth of rigid pavements. The relative success that has been experienced with integral bridges—bridges without deck joints—is now being reflected not only in the increasing number of longer integral bridges, but also in the integral conversion of existing jointed bridges. It appears that the initial success of such techniques would be an accelerated use of integrated conversion as an effective alternative to bridge joint rehabilitation.

Integral bridge construction may be defined as the practice of constructing bridges without deck joints. When such construction is used to eliminate intermediate joints in multiple-span bridges, it is accepted that the continuity achieved by such construction will subject superstructures to secondary stresses. These stresses are caused by the response of continuous superstructures to thermal and moisture changes and gradients, settlement of substructures, posttensioning, and so on. When such construction is used to eliminate deck joints at abutments, it is likewise accepted that such structures will, in addition, be subjected to secondary stresses due to restraint provided by abutment foundations and backfill against the cyclic movement of bridge superstructures. The justification for such construction is based on the recognition that for short- and medium-span bridges of moderate lengths, significantly more damage and distress has been caused by the use of deck joints than by the secondary stresses these joints were intended to prevent. In addition, elimination of costly joints and bearings and the details and procedures necessary to permit their use generally results in more economical bridges. Consequently, more bridge engineers are now willing to relinquish some of their control of secondary stresses primarily to achieve simpler and less expensive bridges with greater overall integrity and durability.

CONTINUOUS SUPERSTRUCTURES

Current design trends received their primary impetus and direction almost six decades ago. In May 1930, a brief 10-page paper (*1*) published in the *Proceedings of the American Society of Civil Engineers* generated considerable discussion in academia. It also created a minor revolution in the design and construction of short- and medium-span bridges. In this paper, Cross presented a simple and quick method for the analysis of integral-type structures such as continuous beams and frames. The method was quickly adopted by bridge engineers, and the bridge practices of many transportation departments began to change. Before Cross' "moment distribution," multiple-span bridges were generally constructed as a series of simple spans. Following the introduction of moment distribution, bridge engineers began eliminating troublesome deck joints at piers by providing continuous superstructures.

On the basis of a recent mail survey (*2*), it appears that the Ohio Department of Transportation was one of the first agencies to initiate the routine use of continuous construction (Figure 1). Its experience provides an informative background for this movement toward the use of fully integrated continuous construction. At first, riveted field splices were used to integrate adjacent spans and achieve full continuity for steel stringer bridges. By 1934, the department had devised its first butt-welded field splice. Following this first tentative application, the welded field splice was continuously improved and used almost exclusively for more than 30 years for the erection of steel stringer bridges. In the late 1950s, high-strength bolted field splices were adopted for the Patterson-Riverside Bridge at Dayton, Ohio, one of the first bridge applications for high-strength bolting in the United States. By 1963, high-strength bolting replaced field butt welding in Ohio as the method of choice for integrating multiple-span steel bridges to achieve full continuity. Consequently, by riveting, field welding, and high-strength bolting, Ohio has employed continuous construction almost exclusively on multiple-span steel bridges for close to 50 years. Because continuity can be achieved more readily with cast-in-place concrete, Ohio has been building continuous concrete bridges for close to 60 years.

Figure 1 shows the beginning of the routine use of continuous construction in the United States and Canada and the per-decade increase in the number of transportation departments that have adopted the use of continuous construction. As shown in Figure 1, 26 of 30 departments responding to the recent mail survey (*2*), or 87 percent of responding departments, now routinely use continuous construction for short- and medium-span bridges.

Currently the state of Tennessee appears to be leading the way in constructing long continuous bridges. For example, the Long Island Bridge at Kingsport was constructed in 1980 by using 29 continuous spans without a single intermediate joint. The total length of this bridge is about 2,700 ft center to center of abutment bearings. Deck joints and movable bearings have been furnished, but only at the two abutments. It has been aptly named "The Champ."

INTEGRAL BRIDGES

During the past two to three decades, many bridge engineers have become acutely aware of the relative performance of bridges built with deck joints at abutments and those built without them. In most respects, bridges without joints—inte-

Burgess & Niple, Limited, 5085 Reed Road, Columbus, Ohio 43220.

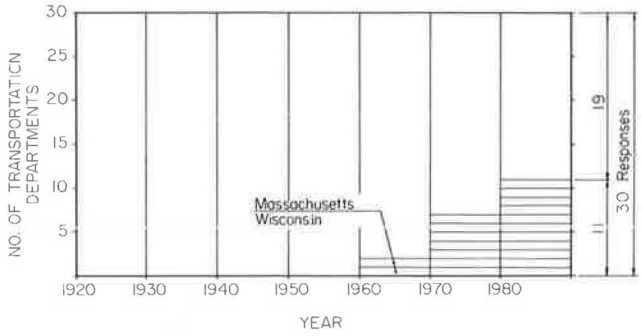

FIGURE 1 Design trends for continuous bridges: early conversion of simple spans to continuous spans.

gral bridges—have performed more effectively, because they remain in service for longer periods of time with only moderate maintenance and occasional repairs. Some of this experience was forced upon bridge engineers by circumstances beyond their control.

Because of the growth and pressure generated by jointed rigid pavement, many bridges built with deck joints at abutments have been and are being severely damaged. After deck joints are closed by pavement growth, bridge decks are squeezed by the generation of pavement pressures. These pavement pressures can easily exceed 1,000 psi or cumulatively the total force due to such pressures can exceed 650 tons per lane of approach pavement (*3*). When the design of abutments for nonintegral-type bridges—bridges with deck joints at abutments—is considered, the forces of these magnitudes are irresistible. Many abutment backwalls have been fractured. Other abutments have been split from top to bottom. In longer bridges with intermediate deck joints, piers have been cracked and fractured as well.

In geographical areas with low seasonal temperatures and an abundance of snow and freezing rain, the use of deicing chemicals to maintain dry pavements throughout the winter season has also had a significant effect on the durability and integrity of bridges built with deck joints. Open joints and sliding plate joints of shorter bridges and open finger joints of longer bridges have allowed deck drainage, contaminated with deicing chemicals, to penetrate below deck surfaces and wash over supporting beams, bearings, and bridge seats. The resulting corrosion and deterioration have been so serious that some bridges have collapsed and others have had to be closed to traffic to prevent their collapse. Many bridges have required extensive repair; most of the bridges that have remained in service have required almost continuous maintenance to counteract the adverse effects of these chemicals. To help minimize or eliminate these corrective efforts, a whole new industry was created.

Beginning in the early 1960s, the first elastomeric compression seals were installed in bridges in the United States to seal deck joints. Since these first installations, numerous types of elastomeric joint seals have been developed and improved in an attempt to achieve a joint seal design that would be both effective and durable. Most designs have been disappointing. Many leaked. Some required more maintenance than the original bridge built without seals. By and large, the many disappointments associated with various types of seals have caused bridge engineers to consider other options.

Costs of various types of bridges showed marked differences. For two bridges built essentially the same except that one was provided with separate abutments and deck joints and the other was provided with integral abutments, the jointed bridge was usually more expensive. In addition, bridges with integral abutments suffered only minor damage from pavement pressure, were essentially unaffected by deicing chemicals, and functioned for extended periods without appreciable maintenance or repair. Consequently, more bridge engineers began to appreciate the merits of integral bridges for short to moderate bridge lengths. Gradually, design changes were made and longer integral bridges were built and evaluated. In 1946 Ohio's initial length limitation for its standard continuous concrete slab bridges was 175 ft. In a 1973 study of integral construction (*4*), 4 states responded that they were using steel bridges and 15 states that they were using concrete bridges in the 201- to 300-ft range. In a 1982 study (*5*), even longer bridges were reported:

> Continuous steel bridges with integral abutments have performed successfully for years in the 300-foot range in such states as North Dakota, South Dakota, and Tennessee. Continuous concrete structures, 500 to 600 ft long with integral abutments have been constructed in Kansas, California, Colorado, and Tennessee.

Currently, 11 states are building continuous bridges with integral abutments in the 300-ft range. Missouri and Tennessee report even longer lengths. Missouri reports steel and concrete bridges in lengths of 500 and 600 ft, respectively, and Tennessee reports lengths of 400 and 800 ft for similar bridges. Finally, Figure 2 shows that 20 of 30 transportation departments, or 60 percent of those responding to the survey, are now using integral construction for continuous bridges.

The attributes of integral bridges have not been achieved without cost. Parts of these bridges operate at very high stresses, stresses that cannot easily be quantified. These stresses are significantly above those permitted by current design specifications. In this respect, bridge engineers have become rather pragmatic. They would rather build cheaper integral bridges and tolerate these higher stresses than build the more expensive jointed bridges with their vulnerability to destructive pavement pressures and deicing chemical deterioration. In 1985, Loveall, then Engineering Director for the Tennessee

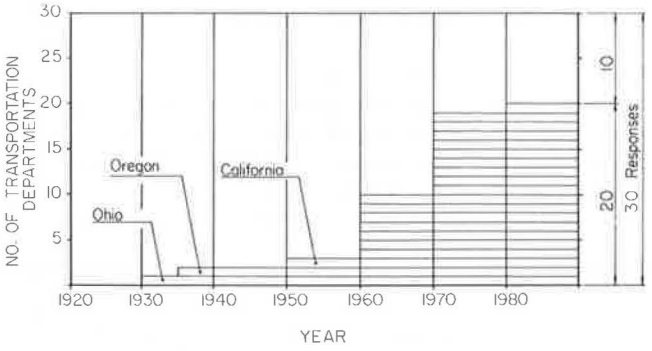

FIGURE 2 Design trends for continuous bridges: early use of integral abutments.

Department of Transportation, reflected this attitude when he wrote (*6*):

> In Tennessee DOT, a structural engineer can measure his ability by seeing how long a bridge he can design without inserting an expansion joint. . . . Nearly all our newer (last 20 years) highway bridges up to several hundred ft have been designed with no joints, even at the abutments. If the structure is exceptionally long, we include joints at the abutment but only there. . . . Joints and bearings are costly to buy and install. Eventually they are likely to allow water and salt to leak down onto the superstructure and pier caps below. Many of our most costly maintenance problems originated with leaky joints. So we go to great lengths to minimize them.

Even though bridge engineers have conditioned themselves to tolerate higher stress levels in integral bridges, occasionally their design control is not sufficient to prevent these high stresses from resulting in structural distress and structural fracture.

STRUCTURAL DISTRESS

Responses to an early survey about construction of continuous bridges with integral abutments indicated a rather widespread concern by bridge engineers for the potentially high stresses that would be present in longer bridges (*4*). This concern, more than any other, appeared to be responsible for the early lack of enthusiasm for using integral abutments for longer continuous bridges. Although the majority of bridges with integral abutments perform adequately, many of them operate at high stress levels. For instance, an abutment supported on a single row of piles is considered flexible enough to accommodate longitudinal thermal cycling of the superstructure and dynamic end rotations induced by the movement of vehicular traffic. Nevertheless, the steel piles of such an abutment are routinely subjected to axial and flexural stresses approaching, equaling, or exceeding yield stresses (*5,7*). Occasionally, a combination of circumstances results in visible distress.

Responding to a 1973 survey, a number of bridge engineers said that some integral abutment wingwalls had minor cracks (*4*). This problem was corrected by more generous wingwall reinforcing steel. Other engineers reported pile cap cracking, which appears to have been eliminated by rotating steel H-piles to place the weak axis normal to the direction of bridge movement.

In a recent article in *Concrete International*, Gamble (*8*) emphasizes the importance of considering restraint stresses in cast-in-place construction. He discusses cracking that occurred in a continuous concrete frame bridge. Even though concrete in this structure was considerably below the specified cylinder strength and shear reinforcement did not meet current requirements, failure of the structure was attributed to its stiffness and resistance to shrinkage and contraction of the bridge deck. Failures of this type emphasize the necessity of achieving flexibility in substructure design and conservative reinforcement to withstand secondary stresses induced by foundation restraint and superstructure shortening.

Currently, precast concrete or prefabricated steel superstructures are generally replacing small cast-in-place bridges in many states and provinces. Consequently, problems associated with initial shrinkage are gradually being eliminated. However, where cast-in-place construction continues to be used, flexibility of substructures remains a critical part of bridge design. For example, Loveall said (*6*):

> Structural analysis of our no joint bridges indicates that we should have encountered problems, but we almost never have. Once we tied the stub abutment of a bridge into rock, and the structure cracked near its end, but we were able to repair the bridge and install [a] joint while the bridge was under traffic. The public never knew about it. That was one of few problems.

Development of new forms of construction will be accompanied by instances of structural distress, and this has certainly been true for continuous bridges with integral abutments. However, as shown in Figure 2, the increased use of integral abutments suggests that 60 percent of transportation departments are satisfied with the performance of integral construction and are using such construction in one form or another for longer and longer bridges. With continued care and consideration, the trend shown in Figure 2 will no doubt continue.

INTEGRAL BRIDGE DETAILS

Figures 3–8 show integral abutment details used by six transportation departments. It is probably not accidental that a fair amount of similarity is evident in these designs, because structural details from early successful designs are adapted by other bridge engineers for use by their departments. Even though there are similarities, there are also differences, which reflect the types of bridges being built and the care and concern being given to the choice and development of specific details. It should also be realized that these sketches are "bare bones" presentations. They do not reflect other important design aspects such as skew and construction procedures, which are considered in the application of these details for specific bridges. These aspects cannot be illustrated and properly described in a paper as brief as this one. Nevertheless, because these aspects can have a considerable effect on the performance, integrity, and durability of integral designs, it is appropriate to mention at least passive pressure and pile stresses for those engineers considering such designs for the first time.

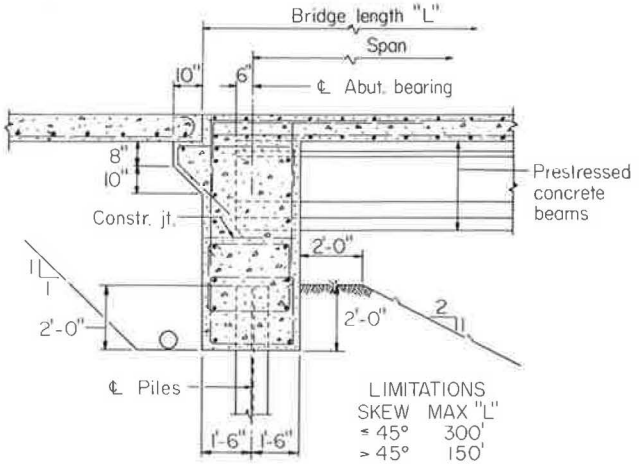

FIGURE 3 Integral abutments: Iowa.

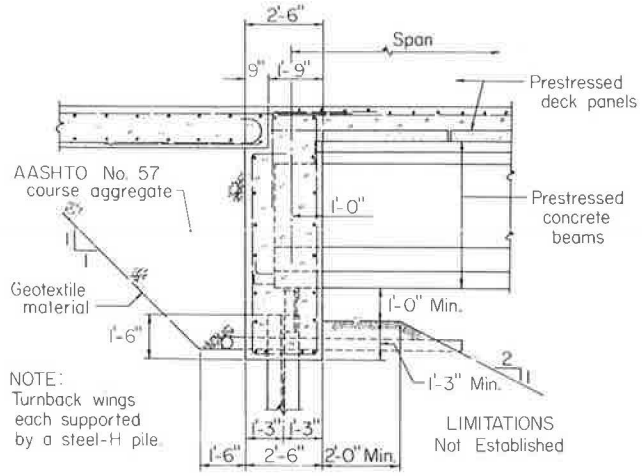

FIGURE 4 Integral abutments: Pennsylvania.

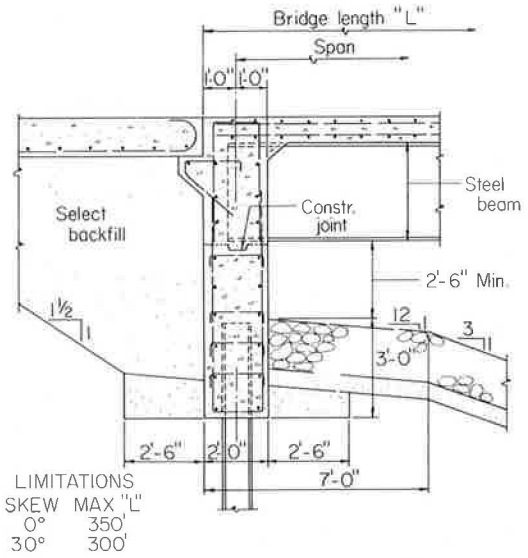

FIGURE 5 Integral abutments: North Dakota.

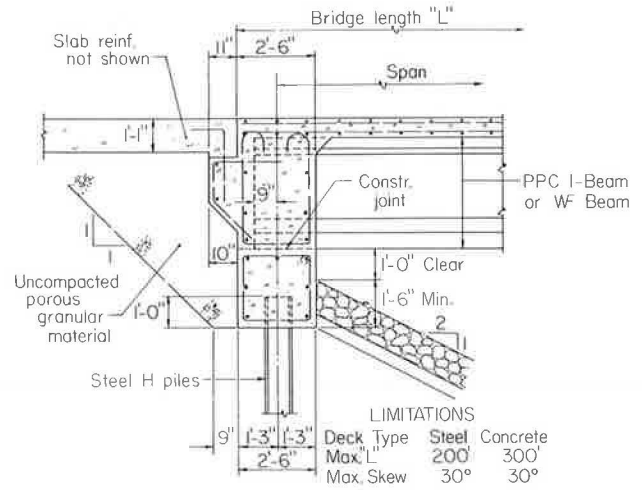

FIGURE 6 Integral abutments: Illinois.

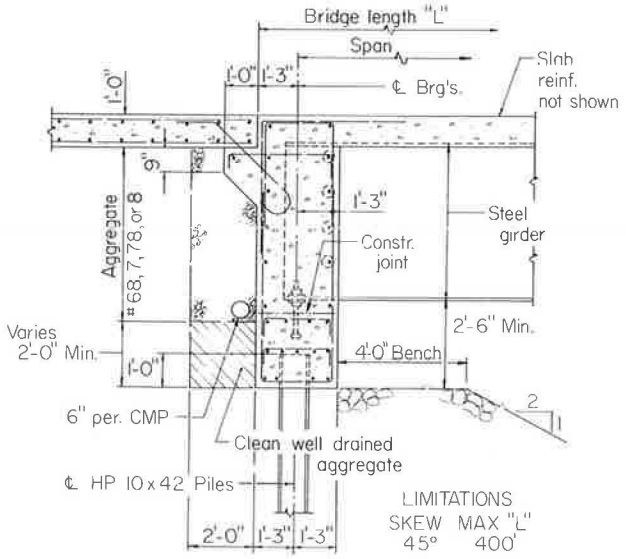

FIGURE 7 Integral abutments: Tennessee.

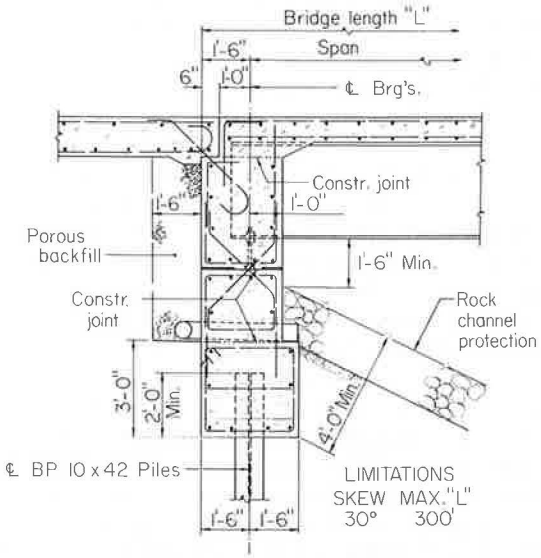

FIGURE 8 Integral abutments: Ohio.

Passive Pressure

To minimize the passive pressure developed in abutment backfill by an expanding integral bridge, design engineers have used a number of controls, devices, and procedures. Including but not limited to the following, they have (a) limited bridge length, structure skew, and the vertical penetration of abutments into embankments; (b) used select granular backfill and uncompacted backfill; (c) provided approach slabs to prevent vehicular compaction of backfill or to permit the use of backfill voids behind abutments; (d) used embankment benches to shorten wingwalls and used suspended turn-back wingwalls; and (e) used semiintegral abutment designs (Figure 4) to eliminate passive pressure below bridge seats.

Pile Stresses

Knowing that longitudinal forces in superstructures are somewhat directly related to the resistance of abutment pile foundations to longitudinal movement, design engineers have (a) limited the foundation of integral bridges to a single row of slender vertical piles, (b) limited the pile types, (c) oriented the weak axis of H-piles normal to the direction of movement, (d) used prebored holes filled with fine granular material for piles, (e) provided an abutment hinge to control pile flexure, (f) limited structure skew, and (g) used semiintegral abutment designs for longer bridges (Figure 9) to minimize foundation restraint to longitudinal movement.

Surveys

A number of questionnaires about integral bridge practices have been circulated in recent years. The responses reflect the policies, attitudes, and opinions of those engineers responsible for bridge design policies. They also show how some of those attitudes and opinions have changed during the last decade. In 1973, Emanual et al. (*4*) received responses about their current design practices from 43 transportation departments. In 1982, Wolde-Tinsae et al. (*5*) used a questionnaire as part of an investigation into nonlinear pile behavior. Responses from 29 transportation departments were presented in tabular form. In 1983, Greimann et al. (*9*) elicited responses from 30 transportation departments on their pile orientation practices for skewed integral bridges. In 1987, Wolde-Tinsae and Klinger (*10*) solicited responses from selected transportation departments in the United States, Canada, Australia, and New Zealand. (The reports by Wolde-Tinsae et al., Greimann et al., and Wolde-Tinsae and Klinger also contain valuable bibliographies for those interested in a more in-depth study of current research on behavior of integral bridges and performance of abutment pilings.) Last, in 1987 the author received responses from 30 transportation departments describing the limitations that these departments use to control the behavior and performance of integral bridges (*2*).

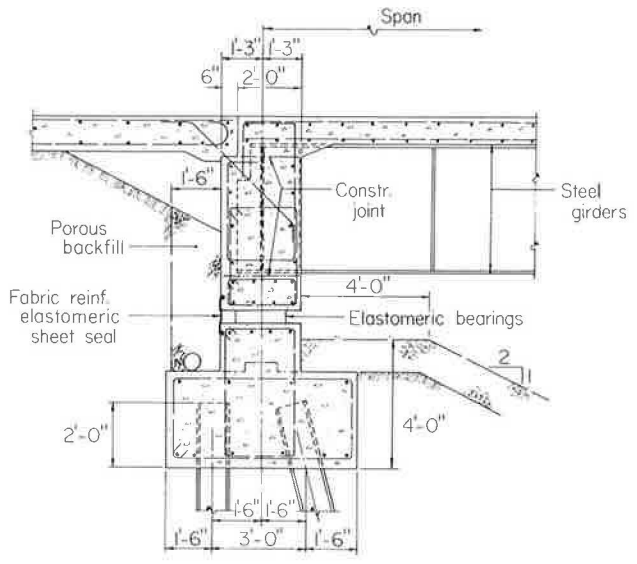

FIGURE 9 Semiintegral abutment details: Ohio.

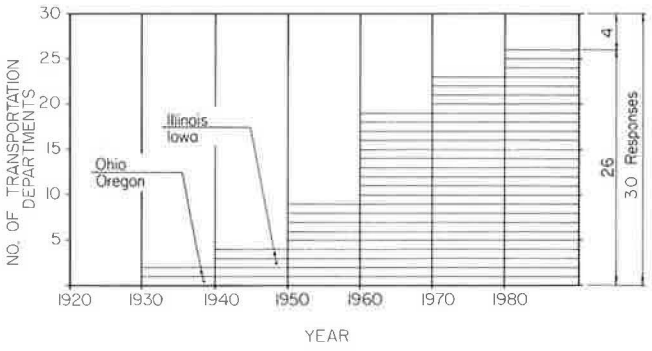

FIGURE 10 Design trends for continuous bridges: routine use of continuous construction.

INTEGRAL CONVERSIONS (RETROFITTING)

Following the trend toward the use of continuous construction and the use of integral abutments, as shown in Figures 1 and 2, transportation departments are also beginning to convert existing multiple-span bridges from simple to continuous spans. Figure 10 shows that this effort began with Wisconsin and Massachusetts in the 1960s and has gathered strength in the past two decades. Currently 11 of 30 departments, or about 30 percent of the transportation departments, have converted one or more bridges from multiple simple spans to continuous spans.

Although the chart in Figure 10 suggests considerable activity, it actually shows only the relative number of departments that have made such conversions. It is not indicative of the number of bridges that have been converted. For example, positive responses were received from only two departments in response to the following question (*2*): "In recent years, have you converted any bridges from multiple simple spans to continuous spans to eliminate intermediate deck joints?" The Ontario Ministry of Transportation and Communications responded:

> We are modifying a few structures from simple spans to continuous spans, eliminating the intermediate deck joints in the process. . . .

The Texas Department of Highways and Public Transportation responded:

> In recent years, we have eliminated numerous intermediate joints. Generally, this is done while replacing the slab. We simply place the slab continuous across the bents. On a few occasions, we have removed only the joint and surrounding deck area, added reinforcing, and replaced that portion of the deck thus tying the adjacent spans together.

The Tennessee Department of Transportation also has been actively converting simple span bridges to continuous spans. In a recent paper, Wasserman, Engineering Director of Structures at the Tennessee Department of Transportation describes and illustrates a number of such conversions (*11*).

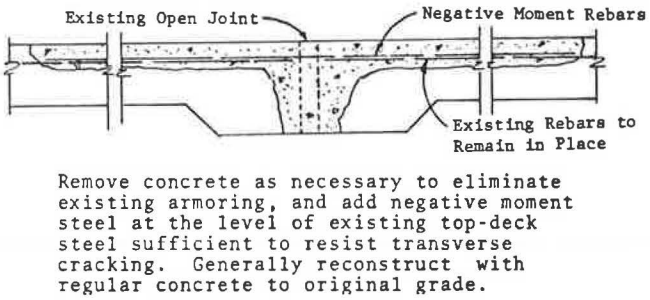

FIGURE 11 Integral conversions at piers: Texas.

To give this movement some direction, the Federal Highway Administration has issued a Technical Advisory on the subject (*12*). That advisory in part recommends that a study of the bridge layout and existing joints be made "to determine which joints can be eliminated and what modifications are necessary to revamp those that remain to provide an adequate functional system. . . ." For unrestrained abutments,

> a fixed integral condition can be developed full length of the shorter bridges. An unrestrained abutment is assumed to be one that is free to rotate, such as a stub abutment on one row of piles or an abutment hinged at the footing. . . . [W]here feasible, develop continuity in the deck slab. Remove concrete as necessary to eliminate existing armoring, and add negative moment steel at the level of existing top-deck steel sufficient to resist transverse cracking [Figure 11].

The detail shown in Figure 11 reflects the procedure described by Texas. Note that the detail shows that only the slab portion of the deck is being made continuous. The simply supported beams remain simply supported. For such construction, it is important to ensure that one or both of adjacent bearings supporting the beams at a joint are capable of allowing horizontal movement. Providing for such movement will prevent horizontal forces from being imposed on bearings from rotation of the beams and slab continuity.

The state of Utah also has converted some simple span bridges to continuous ones by using a design similar to the one shown in Figure 12. For deck slabs with a bituminous overlay, a membrane can be used to waterproof the new slab section over piers. With a design like this, it is understood that the deck slab would be exposed to longitudinal flexure from rotation of the beam ends responding to the movement

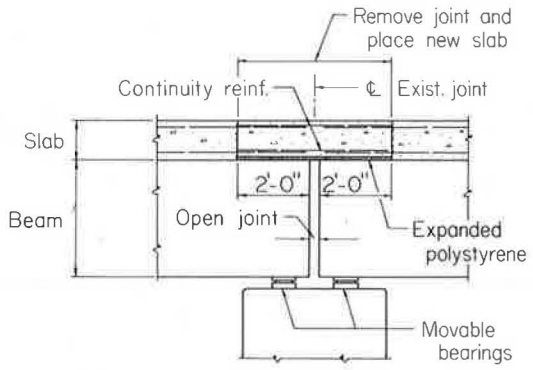

FIGURE 12 Integral conversions at piers: Utah.

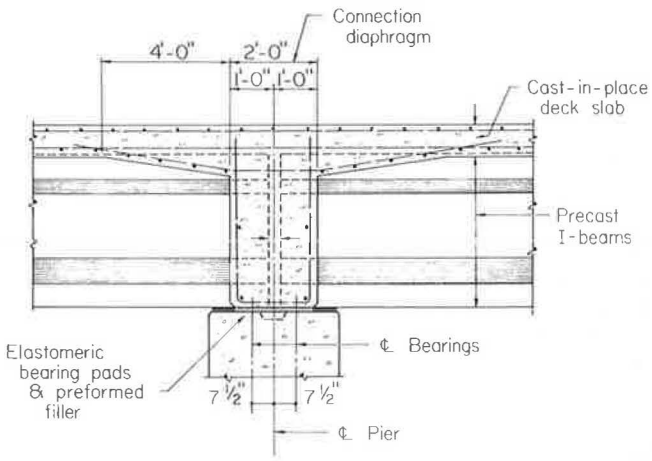

FIGURE 13 Integral conversions at piers: Wisconsin.

of vehicular traffic. However, for short- and medium-span bridges, the deck cracking associated with such behavior is preferred by some over the long-term adverse consequences associated with an open joint or a poorly executed sealed joint.

In new construction, conversion of simple spans to continuous spans is rather commonplace. Figure 13 shows the design detail used in Wisconsin for prestressed I-beam bridges. A substantial concrete diaphragm is placed at piers between the ends of simply supported prestressed beams of adjacent spans. It extends transversely between parallel beam lines. Then a reinforced concrete deck slab is placed to integrate the beams and deck slab, thereby providing a fully composite continuous structure. This type of prestressed I-beam construction appears to be standard for many transportation departments.

Figure 14 shows the standard design detail used by the state of Ohio to achieve continuity for simply supported prestressed box beams. These box beams are placed side by side and then transversely bolted together. Finally, continuity reinforcement is placed and the concrete closure placement is made.

In a 1969 paper, Freyermuth (*13*) gives a rather complete description of the considerations necessary to achieve continuity in a bridge composed of a continuously reinforced concrete deck slab on simply supported precast prestressed beams.

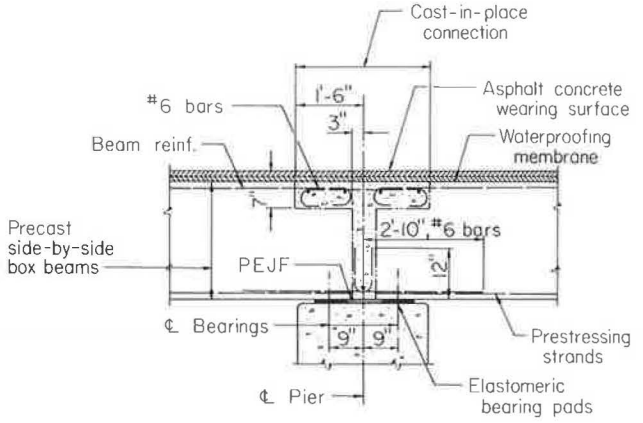

FIGURE 14 Integral conversions at piers: Ohio.

Conversion of existing bridges either by replacing the deck completely or by replacing portions of the deck adjacent to deck joints over piers can be accomplished by following the procedures developed for new structures. Obviously, for existing bridges, creep effects will be negligible. Shrinkage effects for other than complete deck slab replacements should also be negligible. Not only does such continuous conversion eliminate troublesome deck joints, the continuity achieved also results in a slightly higher bridge load capacity because positive moments due to live load are reduced by continuous rather than simple beam behavior.

Although too recent to consider in terms of a design trend, conversion of nonintegral to integral or semiintegral abutments for both single- and multiple-span bridges has begun. Figures 15 and 16 give design details used for a number of recent conversions by the Ohio Department of Transportation. Reconstruction of these abutments was made necessary by the substantial damage induced by pavement growth and

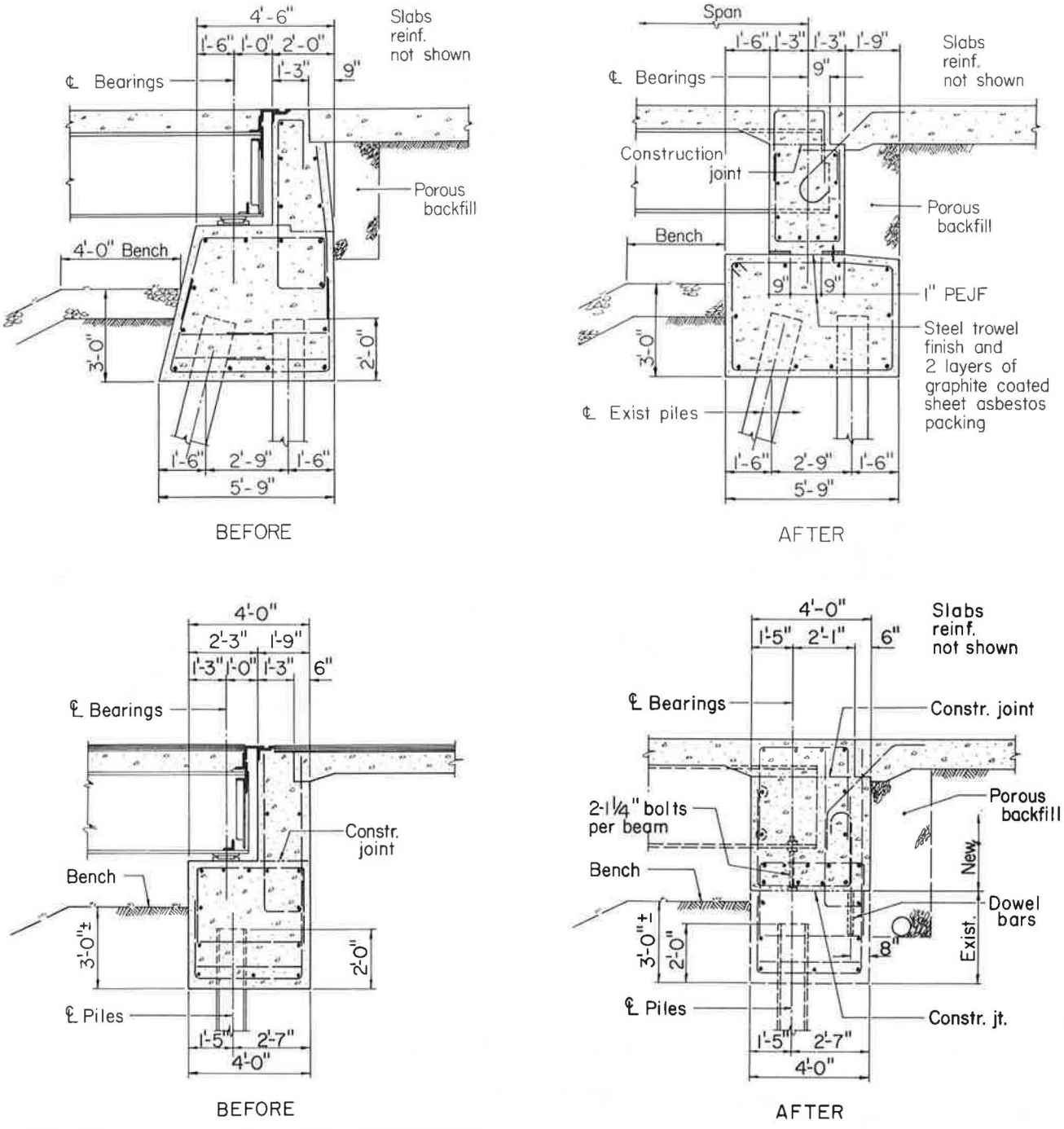

FIGURE 15 Integral conversions at stub-type abutments.

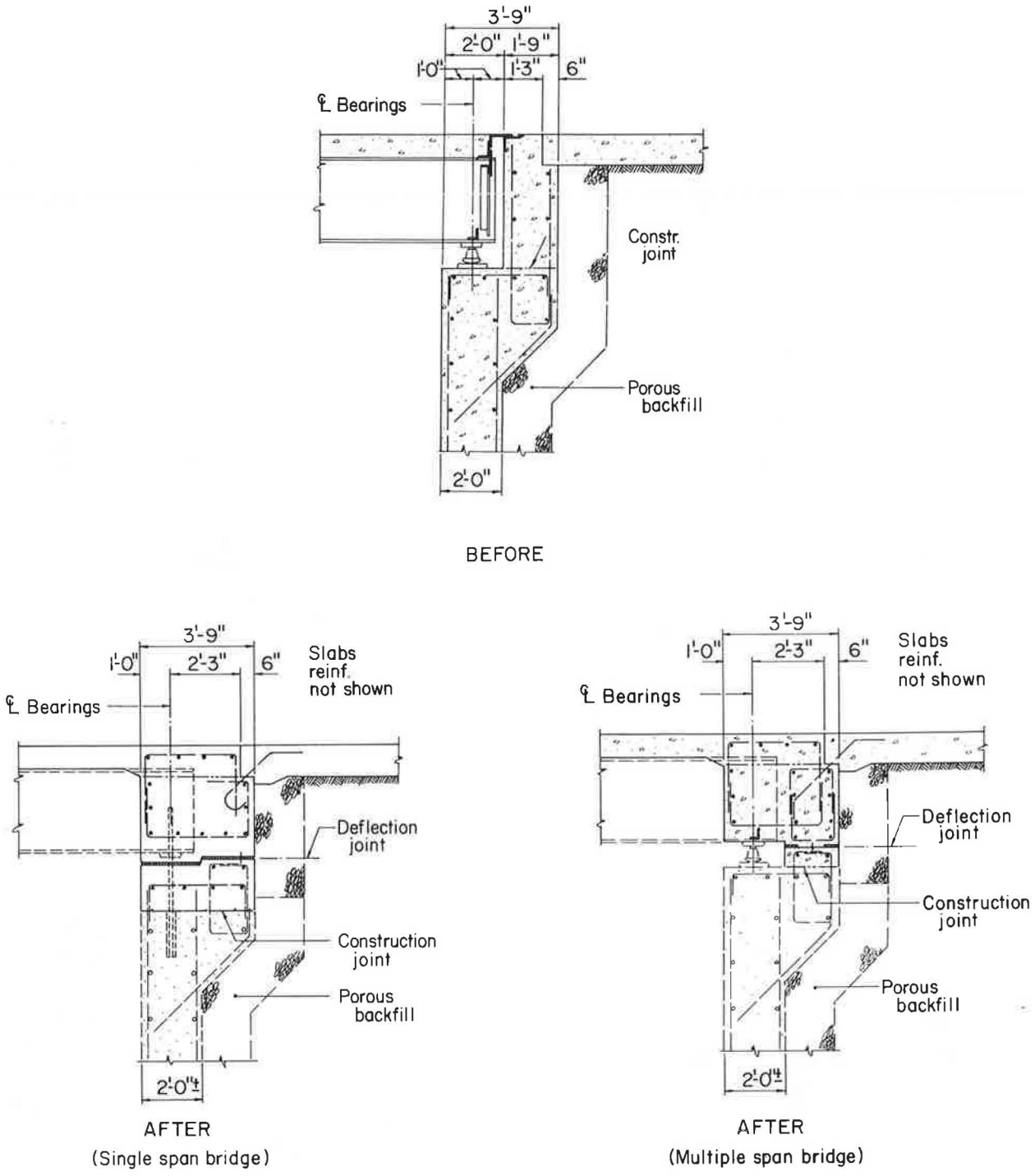

FIGURE 16 Integral conversions at wall-type abutments.

pressure, by deicing chemical deterioration, or by both. Instead of replacing backwalls and joints, and in some cases bearings and bridge seats as well, it was decided to pattern the reconstruction after the design details used by the department for its new integral bridges. In this way, subsequent concern about the effects of pavement pressure and deicing chemical deterioration has been minimized.

SUMMARY

As the trend shown in Figure 1 continues, it appears that the use of continuous construction for multiple-span bridges will become standard for all transportation departments in the very near future. It also appears that the use of integral abutments for single- and multiple-span bridges (Figure 2) will

increase when comprehensive and conservative guidelines for their use become more readily available and when their long-term performance has been more fully documented.

Because design and construction of fully continuous bridges have become routine and continuous conversion of simple spans in new construction is becoming more commonplace, it is surprising that similar conversion techniques are not used more often to convert existing jointed bridges to continuous bridges. Presumably, the next decade or two will see a burgeoning in retrofitting simple multiple-span bridges to continuous bridges (Figure 10) and from nonintegral to integral abutments. When more information on the operating stress levels of integral bridges has been developed and when more fully described design details and procedures for integral conversions have become available, bridge engineers will be able to more fully justify their consideration of such construction. Until then, much intuition and prudent judgment will continue to be used to ensure that integral construction and conversion techniques will provide the service life needed to justify their adoption and continued use.

REFERENCES

1. H. Cross. Analysis of Continuous Frames by Distributing Fixed-End Moments. *Proc., American Society of Civil Engineers*, May 1930.
2. M. P. Burke, Jr. *NCHRP Synthesis of Highway Practice 141: Bridge Deck Joints*. TRB, National Research Council, Washington, D.C., Sept. 1989.
3. M. P. Burke, Jr. Bridge Approach Pavements, Integral Bridges and Cycle Control Joints. In *Transportation Research Record 1113*, TRB, National Research Council, Washington, D.C., 1987.
4. J. H. Emanual, J. L. Hulsey, J. L. Best, J. H. Senne, and L. F. Thompson. *Current Design Practice for Bridge Superstructures Connected to Flexible Substructures*. University of Missouri-Rolla, 1973.
5. A. M. Wolde-Tinsae, L. F. Greimann, and P. S. Yang. *Nonlinear Pile Behavior in Integral Abutment Bridges*. Iowa State University, Ames, 1982.
6. C. L. Loveall. Jointless Bridge Decks. *Civil Engineering—ASCE*, 1985, pp. 64–67.
7. J. L. Jorgenson. Behavior of Abutment Piles in an Integral Abutment Bridge. In *Transportation Research Record 903,* TRB, National Research Council, Washington, D.C., 1983.
8. W. L. Gamble. Bridge Evaluation Yields Valuable Lesson. *Concrete International*, June 1984, pp. 68–74.
9. A. M. Greimann, D. M. Wolde-Tinsae, and P. S. Yang. Skewed Bridges with Integral Abutments. In *Transportation Research Record 903*, TRB, National Research Council, Washington, D.C., 1983.
10. A. M. Wolde-Tinsae and J. E. Klinger. *Integral Abutment Bridge Design and Construction*. Report FHWA/MD-87/04. Maryland Department of Transportation, Annapolis, 1987.
11. E. Wasserman. Jointless Bridges. *Engineering Journal*, Vol. 24, No. 3, 1987.
12. *Bridge Deck Joint Rehabilitation (Retrofit)*. Technical Advisory T5140.16. FHWA, U.S. Department of Transportation, 1980.
13. C. L. Freyermuth. Design of Continuous Highway Bridges with Precast Prestressed Concrete Girders. *ACI Journal*, Vol. 14, No. 2, 1969.

Publication of this paper sponsored by Committee on General Structures.

West Seattle Swing Bridge

THOMAS A. KANE, THOMAS F. MAHONEY, AND JOHN H. CLARK

Construction is under way on a double leaf concrete swing bridge across the Duwammish River in Seattle, Washington. This bridge represents a revival of a type of movable bridge long out of favor and incorporates some new concepts in machinery and movable-bridge technology. The structure and its site are described and some of the factors that led to this novel design are detailed. Construction progress to date is reviewed.

The West Seattle Swing Bridge connects two portions of the industrial port area of Seattle across one of its major shipping channels. Prospects for widening the current 150-ft-wide ship channel to 250 ft required replacement of the existing bascule, built in 1927. In 1988 navigation traffic required approximately 10 openings per day of the existing bridge, which provides 45 ft of vertical clearance over high water. Increasing the vertical clearance from 45 ft for the existing bascule bridge to 55 ft for the new bridge is predicted to be sufficient to reduce the number of openings to an average of seven per day, primarily for large ocean-going barges and ships.

Vehicular traffic crossing the waterway bound for residential areas in the western part of Seattle had previously been routed over a new high-level bridge (140-ft vertical clearance). Construction of the high-level bridge had been long planned but was finally precipitated when an inbound freighter struck the bascule bridge that originally parallelled the bascule bridge being replaced by the swing bridge. The high-level bridge did not, however, provide for the local traffic between the two industrial areas on either side of the waterway because of the difficulty of providing adequate ramps to the elevated structure. This local traffic was 3,500 vehicle a day, 15 percent trucks, before closure of the existing bascule and is predicted to increase to 11,600 vehicles a day by the year 2000. Pedestrians and bicycles are also provided for on the new swing span but are excluded from the high-level bridge. The total structure width of 49 ft 9 in. provides for two traffic lanes and one combined bicycle-pedestrian way of 12 ft 0 in.

SITE DESCRIPTION

The swing bridge alignment was placed on the existing bridge alignment to minimize required right-of-way and revisions to the existing street network. This alignment results in skewing of the bridge axis approximately 45 degrees to the channel. A total of 19 different alignments in the vicinity and three basic structure types was evaluated before selection of the swing bridge for final design development. Other structure types investigated in the preliminary design stages were a vertical lift bridge and a bascule bridge. The vertical lift bridge was believed to be aesthetically incompatible with the immediately adjacent high-level bridge. A vertical clearance of 140 ft would have been required and the towers would have extended above the level of the deck of the adjacent bridge. The 45-degree skew of the channel alignment to the street alignment would have required a lift span length of approximately 460 ft. A double leaf bascule bridge was also investigated. The required span length was approximately 380 ft trunion to trunion, with a skew of 30 degrees between the channel and the roadway. The alignment shift to reduce the skew from 45 to 30 degrees would have added two reverse curves to the street and required additional right-of-way.

The 480 ft center to center of pivot piers for the swing bridge was established by the width of the open west leaf and the location of a column of the high-level bridge (see Figure 1). The east leaf is then symmetrical about the center line of the channel. The tail span length of 173 ft was also set by the column of the high-level bridge. Once the alignment was chosen, the span lengths were fixed. The west approach length is determined by the need to cross over a railroad track and intersecting street, the east approach by grades. Stair towers for pedestrian access are provided on each approach. A control tower for the bridge operator is adjacent to, but separate from, the west pivot pier. The control tower is a 120-ft-high structure so that the bridge operator has an unrestricted view of the channel and all of the approach roadway.

The crossing site is near the mouth of the Duwammish River. Soils encountered at the site range from hydraulic fill and recent alluvial sands and silts to heavily preconsolidated glacial till. Depth to the till varies from 50 ft on the west end of the project to 200 ft on the east end. Lenses of loose silt exist erratically throughout the alluvium layer. The loose surficial silts and hydraulic fill are deemed susceptible to liquefaction in major seismic events. Densification by Vibrofloatation was specified to prevent such liquefaction.

Seismicity of the area is moderately active (UBC Zone III seismic acceleration coefficient $A = 0.25$). The seismicity studies and the seismic design of the high-level bridge were discussed in a previous paper (*1*) along with details of the geology and foundation conditions at this site.

STRUCTURE

Considerations in the choice for the superstructure design were construction economy, maintenance costs, traffic safety, and aesthetic compatibility with the adjacent high-level bridge (a concrete box girder). Two designs were prepared and advertised for bids, a posttensioned segmental concrete box girder and a steel box girder with a precast prestressed concrete deck made composite after erection. Typical cross sections of the two alternatives are shown in Figure 2. Five bids were received for the concrete box girder alternative; they ranged from $33,537,636 to $37,583,660 including all approach

Andersen Bjornstad Kane Jacobs, Inc., 220 West Harrison, Seattle, Wash. 98119.

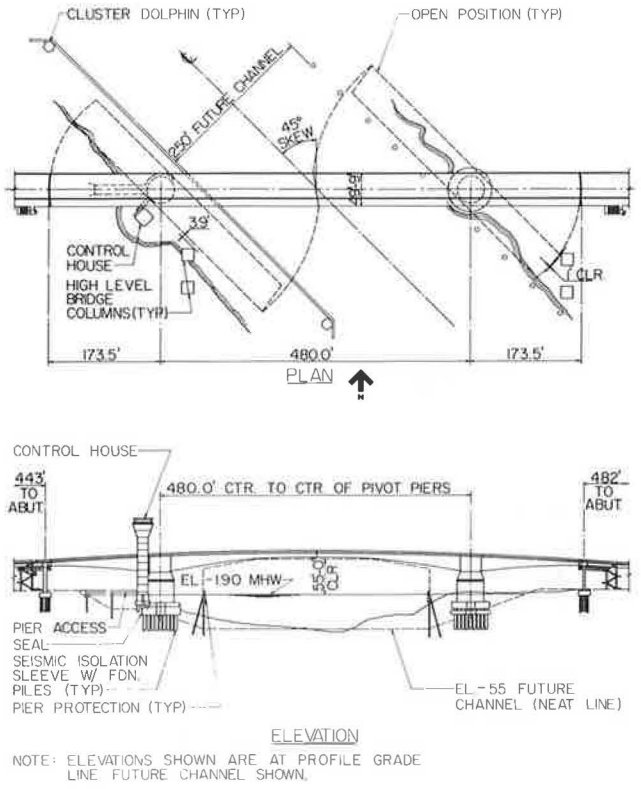

FIGURE 1 West Seattle Swing Bridge: plan and elevation.

work and site work. The concrete box girder was awarded. Principal construction quantities are given in Table 1, and the cost breakdown for major work categories (based on the low bid) is presented in Table 2. Bids received and the engineer's estimate are given in Table 3.

A major concern regarding the design of the concrete box girder bridge was control of long-term deformations. Provisions for control of both long-term and short-term deformations included additional posttensioning beyond that required for stress control, some unbonded tendons, additional future tendons, adjustment of approach span elevation at the tail span joint, vertical adjustment of each leaf as a whole, and specifications requiring nearly simultaneous construction of the two movable leaves.

The first line of defense against unwanted long-term deformation was the adoption of the principle of load balancing for the design of the longitudinal posttensioning. The amount of prestress provided is the amount required to provide 100 percent load balancing for the final dead load condition. This required approximately 30 percent more posttensioning than the amount required to satisfy service load stress conditions. The deck of the box girder is posttensioned transversely and vertical posttensioning is included in the webs. The additional longitudinal posttensioning reduced the need for vertical posttensioning in some areas. The box girder cross section is similar to that adopted for the adjacent high-level bridge.

Static balance of each leaf about the pivot pier is achieved by thickening component section elements in the tail span and by adding ballast concrete so that the last 40 ft of the tail span is solid except for a 4-ft-square access shaft. Some precast ballast blocks are provided for adjustment of the static balance. As-built measurements after casting of each section are required so that the final static balance can be closely predicted. The 42-ft-diameter pier house (see Figure 3) carries the superstructure loads to the foundations and houses the drive machinery, emergency generators, and part of the control system. Pier house walls are 32 in. thick and heavily reinforced.

The pier table element of each leaf is supported by a transition element that provides two load paths to the foundation. The closed position path (serving vehicular traffic) is from the superstructure pier table through a conical shell to the walls of the pier house. Service bearings made of steel plates with reinforced elastomers separate the transition element from the roof of the pier house. The operating position load path is from the pier table through the center portion of the transition element to the 12-ft-diameter pivot shaft. The pivot shaft is a concrete-filled steel shell that rests on the hydraulically operated lift-turn cylinder. It is maintained in the vertical position by guide bearings at the roof and operating floor level of the pier house. In the operating position, the whole movable leaf, including transition element and pivot shaft, are raised approximately 1 in. to transfer the load from the service bearings to the pivot shaft. A reinforced-concrete footing founded on 36-in.-diameter concrete-filled steel pipe piles completes both load paths.

The piling system incorporates 48-in.-diameter steel pipe sleeves around each foundation pile. The purpose of these sleeves is to control the elevation at which the foundation piling begins to receive lateral support from the surrounding soil. The annular space is excavated to a set elevation. The location of the piers is in the slope area of the channel excavation. Without the sleeves, the depth from the footing to the slope surface would vary from zero to 15 ft. Lateral stiffness of the piles would thus vary and significant torsional response to seismic excitation would result from the eccentricity between the center of mass and the center of stiffness. The sleeves eliminate this variation in lateral stiffness and the resulting eccentricity. The sleeves also support the tremie seal, which is separated from the footing.

Twin hydraulic slewing cylinders rotate each movable leaf from the closed position to the open position to allow for passage of ships. The operational cycle is based on a normal 2-min slewing time; the total cycle, which includes setting traffic lights and lowering gates, is approximately 4½ min. Friction is minimized because the structure is supported on the hydraulic fluid of the lift-turn cylinder. The principal source of friction is the pivot shaft in vertical alignment.

Power for raising and rotating the movable leaf is provided by three 100-hp, 125-gal/min hydraulic pumps in each pier house. Normal operation is with two pumps; the third pump alternates as a spare. Other redundancies built into the system include the ability to slew the bridge using only one slewing cylinder (with increased cycle time) and even to slew the bridge against the friction of the service bearings should the lift-turn cylinder fail to operate. This latter redundancy is an extraordinary condition to be undertaken only in extreme emergency. It requires manual overrides of pressure relief valves in the hydraulic system and would require replacement of part of the service bearings. The center lock and tail locks are driven and pulled by local hydraulic cylinders operated by separate pumps. Design for the locks included the ability to be driven against a 1-in. misalignment. Torsional stiffness of the box girder is sufficient so that locks are required only at the center line.

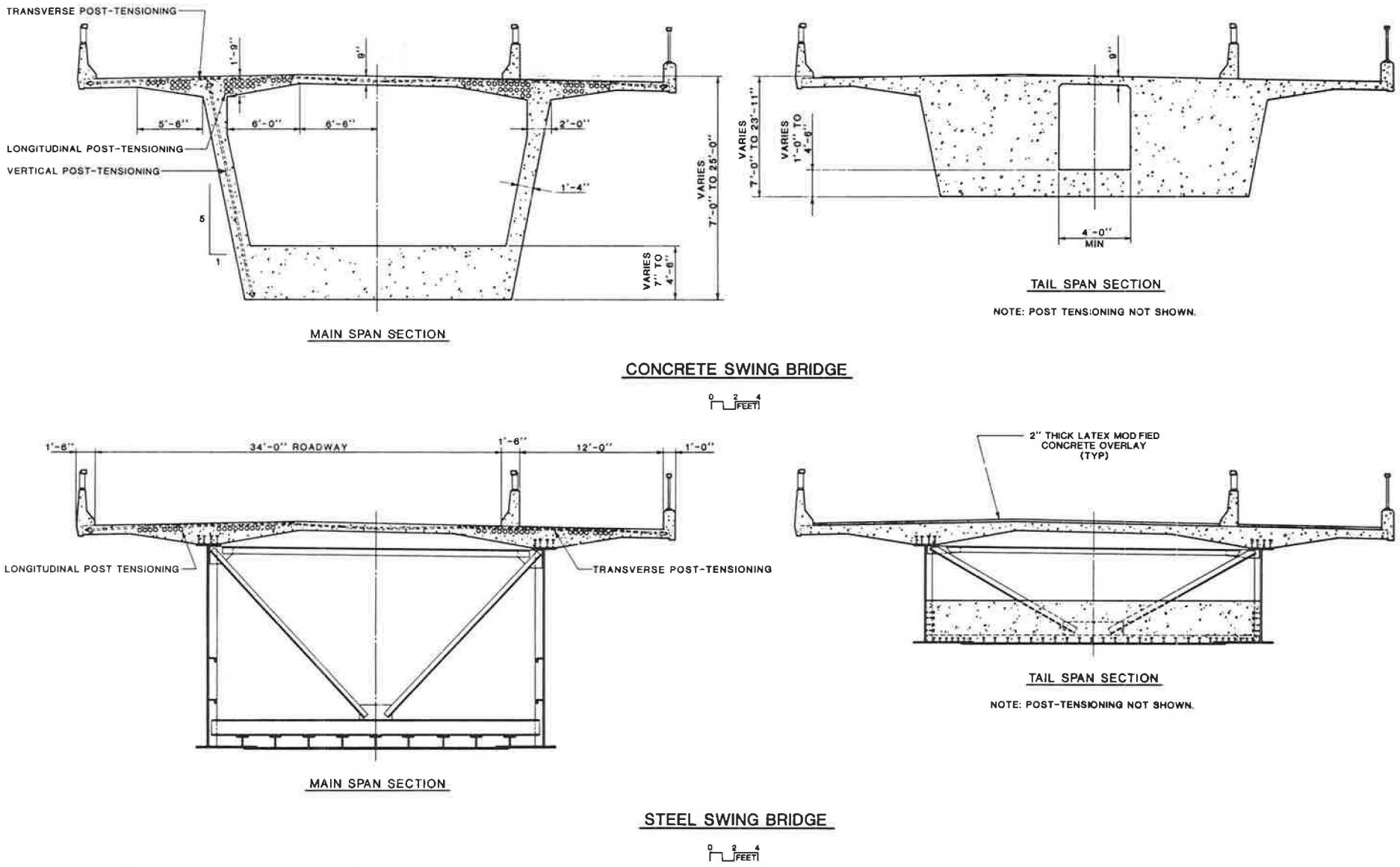

FIGURE 2 Cross sections of alternative designs: concrete and steel swing bridges.

TABLE 1 PRINCIPAL CONSTRUCTION QUANTITIES (STRUCTURAL)

Item	Unit	Approaches Sub Struc	Approaches Super Struc	Swing Spans Sub Struc	Swing Spans Super Struc
Structural Excavation	cy	3200		5220	
Shoring	sf				
Soil Densification	cy	38600		18900	
PSC Piling 16.5" Dia	lf	19335			
PSC Piles 16.5" Dia	ea	290			
Steel Piling 36" Dia	lf			10120	
Steel Piles 36" Dia	ea			64	
Concrete Cl D	cy			1372	
Concrete Cl C	cy			186	82
Concrete Cl B	cy				
Concrete Cl AX	cy	2880	1370	3284	65
Concrete Cl PC 5000	cy	275	606	1195	
Concrete Cl PC 6000	cy			237	6604
PSC Girder S4	lf		911		152
PSC Girder S120	lf		2750		
PSC Girder M120	lf		3404		
Reinf Steel	Ton	337	115	347	420
Rein Steel, Epoxy Ct'd	Ton		115		92
Prestressing Steel, Bar	Ton			1.3	14.6
Prestressing Steel, Strand	Ton				267
Concrete Barriers	lf		3496		2475
Metal Railing	lf		3035		
Latex Mod Concrete	sy				4450
Control System	LS				
Hydraulic System	LS				
Lift/Turn Cylinders	ea			3	
Pivot Shafts	ea		2		
Control Tower	LS				

TABLE 2 COST BREAKDOWN

	LOW BID
1. Mobilization	$2,800,000
2. Demolition	3,761,566
3. Civil (Streets, Utilities, Traffic)	3,395,615
4. Approach Spans	4,659,520
5. Swing Piers	6,868,280
6. Swing Spans	5,601,985
7. Machinery	3,977,000
8. Electrical	1,055,895
9. Controls, Control Tower	941,000
10. Pier Protection	476,775
	$33,537,636

TABLE 3 BIDS RECEIVED

BIDDERS	Concrete Alternate	Steel Alternate
Engineer's Estimate	$33,330,749.40	$36,621,554.40
Kiewit - Global	33,526,192.00	No Bid
General Construction Co./ 3A Industries, J.V.	33,750,799.50	No Bid
Guy F. Atkinson Const. Co.	34,854,453.00	No Bid
S.J. Groves & Sons Co.	36,803,487.00	No Bid
Paschen Contractors, Inc.	37,560,625.88	No Bid

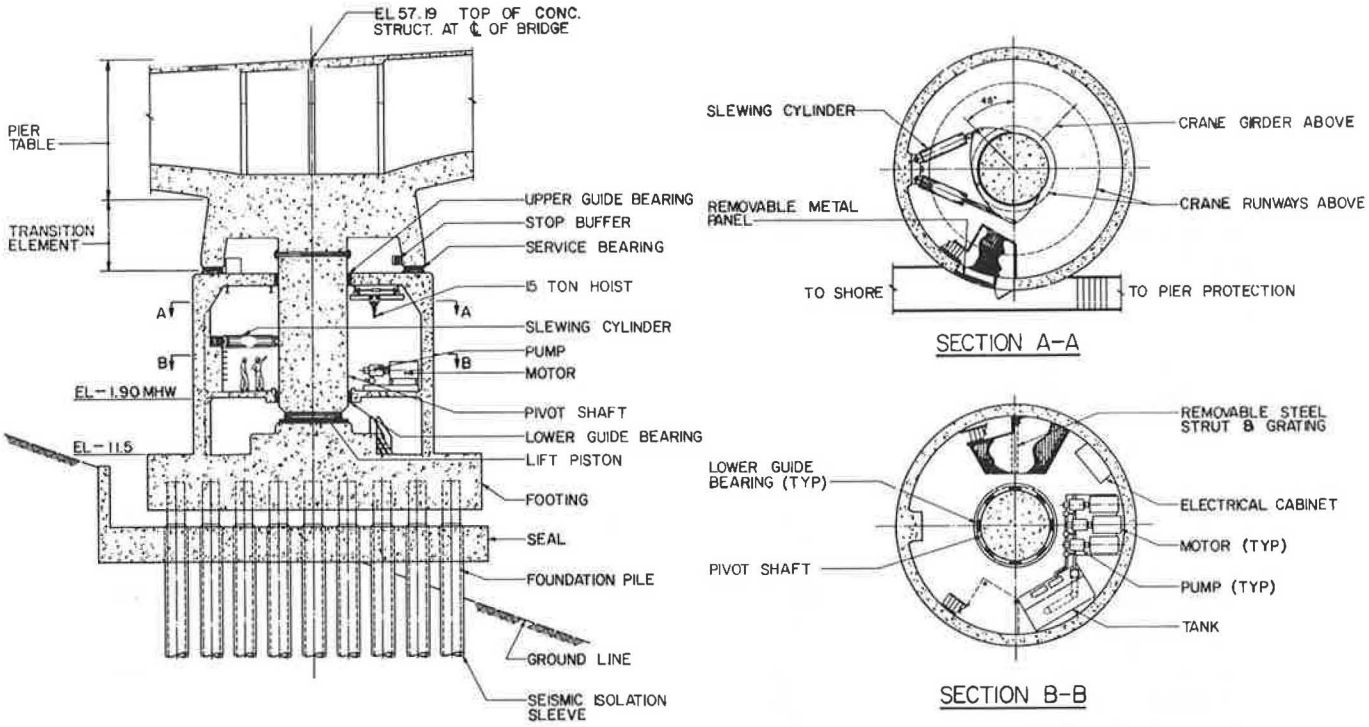

FIGURE 3 Pivot pier section.

Hydraulic system components are designed to operate at a normal pressure of 1,700 psi and an emergency (slewing against the service bearing friction) pressure of 6,000 psi.

Hydraulic buffers are designed to stop the leaf moving at full rotation speed of 0.57 degree per second in 0.44 degree of travel. Open position buffers are located on the roof of the pier house and contact stops on the inner surface of the transition element cone. Tail span buffers are located on the approach span piers and contact the tail span. Normal closing speeds at buffer contact are 35 percent of normal speed; thus normal operation buffer loads are small.

The control unit is a programmable controller that sequences operations and provides status information to the bridge operator. The primary position control is limit switches that initiate braking through the controller. The dynamics of the operating structure (large inertia, low damping) were not deemed suitable for dynamic feedback control. The control system is essentially the same as manual operation except that the controller "pushes the buttons," checks interlocks, and announces the status on a monitor. Manual override is possible for most steps of the operation.

Diesel-powered emergency generator sets (350 kW) are provided in each pier house on the lower floor. Fuel is stored in above-ground enclosed tanks on shore.

One of the design exercises of great value was a study of maintenance actions to ensure provision for access to all items. Adequate openings were provided for removal and replacement of each piece of machinery and all pieces of equipment and areas of the bridge had a means of safe access for inspection and maintenance.

CONSTRUCTION PROGRESS

Bids for the construction of the project were taken in September 1988. Five bids were received (Table 3). The contract was awarded to Kiewit-Global on September 28, 1988, and notice to proceed was given on March 1, 1989. The contract calls for a 22-month construction schedule. Construction progress as of May 1990 included machinery fabrication, demolition of the existing bascule superstructure, site utiity work, and substructure construction. Scheduled completion date is January 1991.

The project was designed by the joint venture West Seattle Bridge Design Team composed of Andersen Bjornstad Kane Jacobs, Inc.; Parsons Brinckerhoff, Quade, and Douglas; and Tudor Engineering. Contech Consultants were responsible for the segmental box girder design. Hamilton Engineering, Inc., designed the hydraulic machinery and Elcon provided the electrical design. The project sponsor is the Seattle Engineering Department, and Frank Yamagimachi is project engineer for the city.

REFERENCE

1. J. H. Clark. Foundation Design: West Seattle Bridge. In *Transportation Research Record 982*, TRB, National Research Council, Washington, D.C., 1984.

Publication of this paper sponsored by Committee on General Structures.

Development and Testing of an Experimental Stressed-Timber T-Beam Bridge

BARRY DICKSON AND HOTA V. S. GANGARAO

New types of timber bridges are being designed and constructed on the basis of a new joining technique called laminating. At West Virginia University, designers have combined this new technology with a new timber product, laminated veneer lumber, to create a T-beam bridge. The process of designing this bridge required a limited research project because of the lack of design guides. The tests performed are described and many of the results of these tests are included. The bridge was constructed in May 1988, after which a monitoring program was initiated. These tests are also described and results tabulated. Short-term performance of the bridges appears excellent; the long-term performance remains unmeasured. Costs of this bridge are included, as are the authors' recommendations for future bridges of this type.

Timber has been rediscovered as an effective bridge-building material. The stamina and beauty of the early covered timber bridges, many of which remain in service today, are well known. Modern timber design and construction techniques are revitalizing the timber bridge industry and expanding the market for lower-grade structural hardwoods.

In West Virginia, a state blessed with an ample supply of hardwood timber but burdened with many lightly traveled bridges in poor condition, timber is a natural choice for new bridges and rehabilitation projects. A nationwide program, initiated by Congress and administered by the U.S. Department of Agriculture-Forest Service (USDA-FS), has been promoting the use of locally grown timber by funding a series of conferences on timber bridges across the country. Coupled with these conferences is the building of demonstration bridges, which, in most cases, are funded by local or state highway departments.

It was through this program that a modern timber bridge was built in Charleston, West Virginia. The site required a structure capable of spanning 75 ft with a 22-degree skew. The demonstrative function of the project required the use of locally grown timber (primarily hardwoods). The lack of design aids required experimentation, modeling, and field monitoring after construction.

STRESS-LAMINATED TIMBER

Originating in Canada over 10 years ago, stress-laminated timber has proved to be a practical method of combining relatively short and narrow timber planks (laminations) into a strong, resilient, and inexpensive bridge. To create a stressed-timber deck bridge (a bridge consisting only of a thick, laminated timber slab), multiple laminations are squeezed together by high-strength steel bars that pass through predrilled holes in the laminations. The bars are tensioned using a hydraulic jacking system similar to the systems used for posttensioning concrete. The compression within the timber laminations and the frictional resistance to sliding are the only mechanisms required to create a timber "plate," thus eliminating traditional mechanical fasteners. Either steel bearing plates or steel channels are required to distribute the high local compressive stress from the steel bars to the outer timber laminations. The compressive stress is then transmitted to the inner laminations. Figure 1 shows the configuration of a stressed-timber deck.

This method of construction has many advantages over conventional timber construction but unfortunately is limited to fairly short spans, usually less than 45 ft. Although there is great demand for short-span bridges, especially in a mountainous state such as West Virginia, the span requirements of the demonstration bridge exceeded the capacity of stress-laminated decks.

PROPOSED DESIGN: STRESS-LAMINATED TIMBER T-BEAMS

The demand for structurally reliable, long, wide timber components cannot be met by the solid sawn timber available today. This need has given rise to many "reconstituted" timber products, including plywood, glued laminated beams, and stress-laminated decks. Timber materials can be combined to use the material properties to maximum advantage. However, producing high-strength, high-reliability timber products is usually expensive and thus should be done only when these features are most necessary.

The T-beam concept was proposed because the material combination was very efficient. A high-strength, high-reliability stringer combined with a deck composed of lower-cost, lower-quality timber appeared to be the combination that best met the bridge site and demonstration requirements. High-strength steel bars not only compress the deck laminations together, as is done in stressed timber, but also connect the stringers and the deck. The longitudinal orientation of the deck planks should add substantially to the strength of the stringers while also serving as a riding surface.

Constructed Facilities Center, West Virginia University, Morgantown, W. Va. 26506-6101.

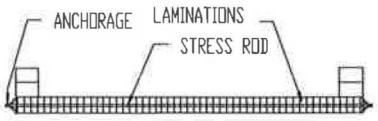

FIGURE 1 Stressed deck.

To span the 75 ft required, a glue-laminated timber product, laminated veneer lumber (LVL), was selected. LVL is a high-quality structural timber material composed of thin (1/10-in. thick), vertical laminations glued together to form beams up to 48 in. deep and 80 ft long. By adding laminations, any desired thickness can be created.

A stress-laminated timber T-beam is formed by using high-strength steel bars to join a stress-laminated deck and an LVL beam. Figure 2 shows the orientation of the components and how the high-strength steel bars tie the timber components together.

Assuming full composite action between the decking and the stringers, an effective flange width equal to half of the clear span between stringers, and a load-sharing fraction of 0.4, an initial design was prepared. A summary of the proposed design follows:

- Center of bearing to center of bearing, 73.25 ft, 17 ft width (one lane), 22-degree right forward skew;
- Seven LVL stringers, each 73.25 ft long, 42 in. deep, and 6 in. wide with 3 in. of camber;
- Northern red oak deck laminations between stringers, 18, each 9 in. deep, 1½ in. wide, and a maximum of 16 ft long;
- Steel bars, ¾-in. diameter, 150 ksi (ultimate stress) on 36-in. center;
- LVL diaphragms on 25-ft centers, each 6 in. wide, 31 in. deep, and 27 in. long;
- Timber guardrail system designed and crash tested by others.

The experimental program described in the following section was undertaken to test the design assumptions.

MODEL TESTING

Because the proposed design was new and untried, a model test program was performed at the Major Units Laboratory of West Virginia University. Time constraints restricted the test program to the most critical areas involving the safety

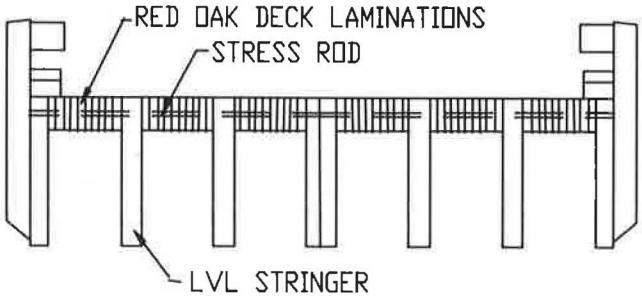

FIGURE 2 T-beam section.

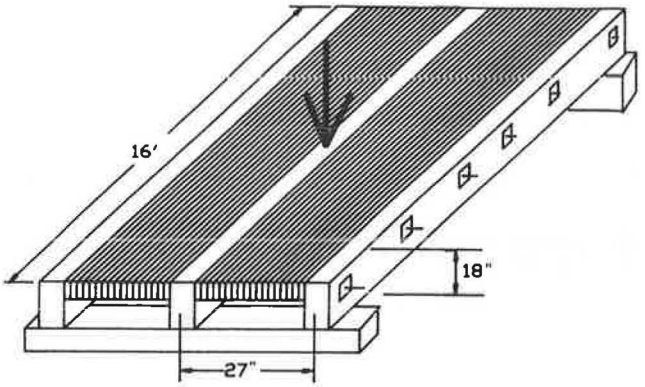

FIGURE 3 Experimental set-up.

and performance of the design: (a) composite action, (b) load sharing, and (c) creep of the system due to prestress forces.

A 16-ft-long, three-stringer model (see Figure 3) was built to simulate the full-scale structure. The model was not built to scale but rather was designed to simulate a worst case. The spacing of the model stringers was identical to that of the planned full-size structure, but the deck depth was greatly reduced, butt joints were located at every other lamination, low-quality red oak was used, and the laminations were left unnailed. The model was simply supported at the ends (15 ft 6 in. from center of bearing to center of bearing) and static loading was applied by a hydraulic jack at various locations.

Timber is usually modeled as an orthotropic material with vastly superior bending properties in the longitudinal axis than in the radial or tangential axes. In traditional timber bridge construction, the decking would be placed on top of the stringers and perpendicular to them; thus the stronger bending strength of the decking is perpendicular to the stringers. The traditional configuration gives good load transfer from stringer to stringer but decreases the live-load-carrying capacity of the stringers by adding dead load. However, the T-beam differs dramatically from this usual orientation; the load transfer from deck to stringer may depend only on shear forces between elements of an "articulated plate."

Composite Action

One reason for the choice of the T-beam configuration was to minimize the total amount of timber required. By orienting the deck timber laminations in the same direction as the stringers, the stronger bending strength of the timber decking acts in combination with the stringers to form a composite structure. Thus, the deck laminations serve as both a riding surface and a load-carrying component.

One test for composite action of a system is to measure the strains at the upper and lower surfaces of a stringer. If composite action exists, the strain diagram (see Figure 4) will indicate a neutral axis location higher than that which would be found for a simple rectangular cross section.

Bending tests performed on both the stringer alone and the stringer-deck combination indicated almost complete composite action for the T-beam unit tested. Figure 4 indicates that the experimentally determied neutral axis of the test model nearly coincides with the calculated neutral axis found

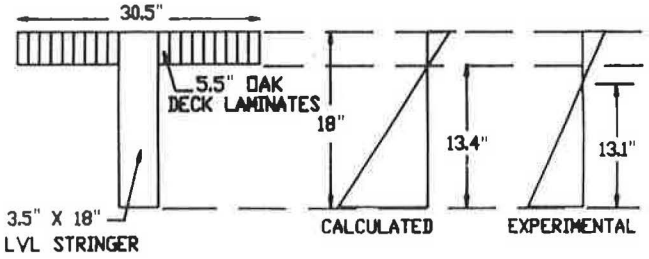

FIGURE 4 Location of neutral axis.

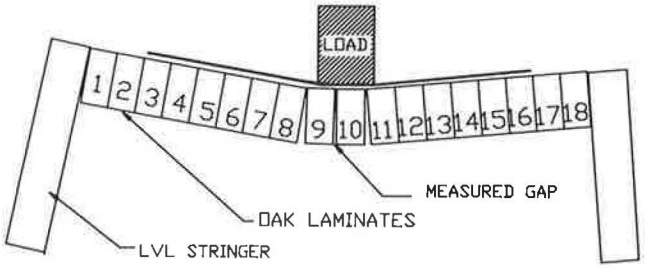

FIGURE 6 Gap measurement test.

using the geometric properties of a T-beam section with flange width equal to 30.5 in.

Load Sharing

The gain realized by orienting the decking parallel to the stringers has the disadvantage of decreasing the ability of the deck to transfer load to neighboring unloaded stringers. The bridge design code of AASHTO and the Ontario Highway Bridge Design Code (OHBDC) (*1*,*2*) do not offer any guidelines for this type of structure; thus, a test program was necessary.

This stressed deck system can be considered an "articulated" system (i.e., load sharing is accomplished through shear transfer only) or a plate with both shear and moment transfer. Both the moment and shear transfer ability are closely linked to the tension force levels of the posttension system.

The limited test program included three types of testing: (a) the "laminate slip" test (see Figure 5) to establish the normal force required to prevent slipping of laminates relative to neighboring laminates, (b) the "laminate gapping" test (Figure 6) to establish to what degree the prestressing bars prevent the opening of gaps between laminations on the tension side of the deck, and (c) the "load sharing" test in which the deflection of loaded stringers and the simultaneous deformation of neighboring, unloaded stringers were measured (Figure 7). From these tests the load distribution response of the system was established.

The test results accentuated the importance of maintaining posttension force levels. The time limitations of the test program precluded the comprehensive testing required to establish accurate, quantitative information necessary to determine the exact minimum levels of posttension force required, but the trend was quite clear. The observed results correlated well with the OHBDC (*2*), in which a posttension force equal to 12 percent of the allowable compressive strength of the timber laminates is the expected permanent force level. Testing performed at this posttension force level, under loads equal to an HS-20 wheel load, indicated excellent shear transfer (Figure 5) and only minor gapping (Figure 6). Measurements of deflections (Figure 7) indicated that the load transfer to adjacent components decreased as the load increased; at the maximum applied load of 16 kips the fraction of the load carried by the directly loaded stringer was approximately two-thirds of the total load.

Creep from Prestressing

Creep is the time-dependent deformation of a body under constant load. Timber is particularly sensitive to this phenomenon, and because the performance of a stressed timber deck relies so heavily on the force level holding the laminates together, understanding the creep behavior of the system due to prestressing is of vital importance to the structural integrity of prestressed timber bridges.

In stressed timber decks and stressed T-beam systems, the tensioned, high-strength steel bars and bulkhead system exert a constant compressive force on the timber laminations. When the system gradually loses compressive strength over some period of time, the timber loses some amount of width and

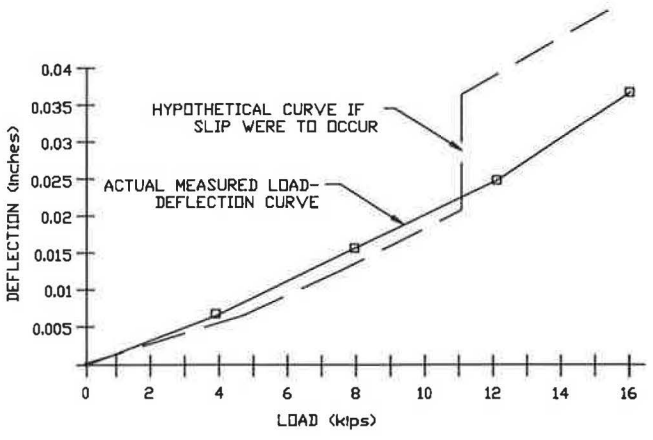

FIGURE 5 Load deflection (of deck planks).

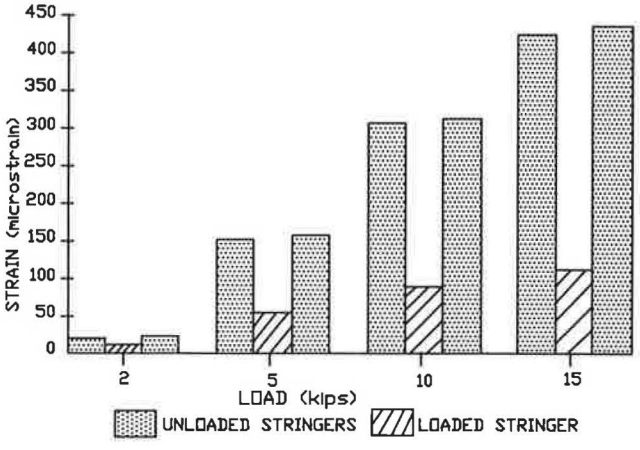

FIGURE 7 Load sharing between stringers.

the force in the steel bars is then reduced. The rate of creep loss is quite high in timber early in the load history (as it is in most materials) and then decreases as time passes.

The OHBDC design methodology includes provisions to compenstate for the loss of compressive strength when timber bridges are designed using several species of softwoods, but data for hardwoods are not included. In this study simple experiments were performed to gauge the creep effects in red oak. In the model, tension bars were loaded to a force level (18 kips) that created a compressive stress of 107 psi within the timber. Load cells were placed on two rod ends between the anchor plates and the bulkhead. Force level readings were taken for a 32-day period.

The data in Figure 8 show a loss of force over 32 days. Unfortunately, the timber deck of the model was found to be losing moisture (drying) as well as compressive strength; thus, it was impossible to determine which losses caused what share of the total. The test results did, however, emphasize the absolute necessity of checking the tensile bar force levels of the steel bars at regular intervals. On the basis of the experimental results, it was decided to follow OHBDC recommended stressing procedures and sequences and to monitor the bar forces on the actual bridge after installation.

ANALYTICAL PROCEDURES

The information accumulated during the model-testing program is only useful if it can be transformed to design values and guidelines. To accomplish this transformation, two mathematical methods were employed: a finite-element computer program and a system of generalized plate equations. Both mathematical procedures varied the ratio of the longitudinal modulus to the transverse modulus of elasticity until the deformations of the mathematical models approximated the deformations of the scale model. The most representative E_L/E_T ratio values then served as the final design material constant.

For this design project, the authors concentrated on two modeling methods: finite-element (FE) methods using the ANSYS computer program and generalized plate equations developed by GangaRao (*3*). Results from both methods correlated quite well with experimental data. The analytical models provided accurate predictions of moments in both the longitudinal and the transverse directions as well as deflections and distribution width.

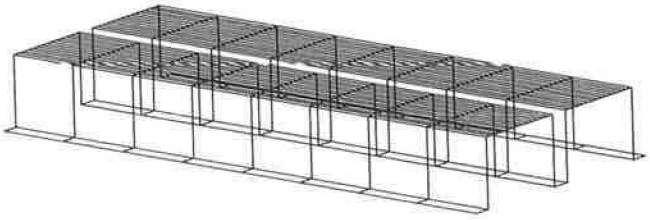

FIGURE 9 Finite-element configuration.

Finite-Element Method

Several attempts were made before an accurate FE model was found. The final model utilizes quadrilateral shell elements with both membrane and bending capabilities. In addition, to create compatibilty between the deck elements and the stringer, a thin "interface" element was introduced. Figure 9 shows the arrangement of model elements.

The model bridge was divided into a total of 800 elements, with each node (four nodes per element) having 6 degrees of freedom. Reduction of the number of simultaneous equations was possible by constraining the displacements in the X- and Y-directions as well as rotation about the Z-axis. Symmetry of the model and support boundary conditions further reduced the number of equations.

The assumed orthotropy of timber requires nine separate elastic constants to calculate the complete status of stresses and deflections. The FE analysis with ANSYS required only four elastic constants because only these values affect the calculation needed. E_L for this model was approximated at 1.7×10^6 psi for the red oak and 2.0×10^6 psi for the LVL. E_T for red oak was varied from $\frac{1}{10}E_L$ to $\frac{1}{25}E_L$, and G_{LT} was set at $0.06E_L$. These values are lower than the elastic constants for the individual members, to compensate for the effects of joints. Figure 10 compares the FE displacement profile with the experimental response and the plate-solution predictions. Although the maximum value of deflection, near the center of the loaded span, is not quite as large as the experimental value (0.27 versus 0.38 in.), the shape of the profile and the

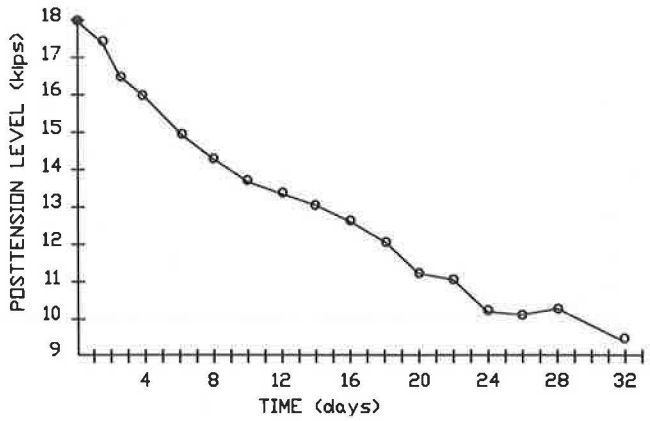

FIGURE 8 Creep losses.

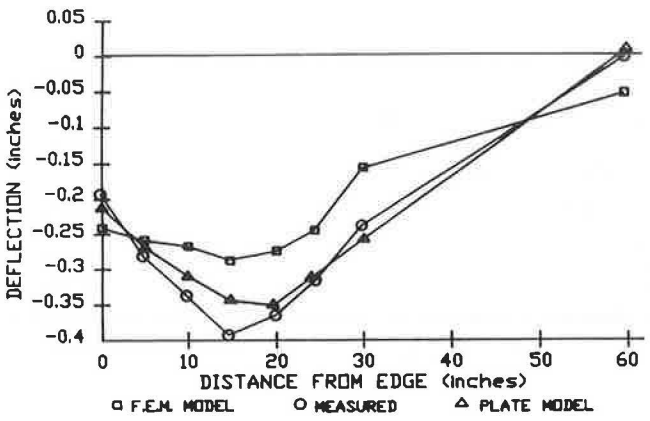

FIGURE 10 Transverse deflected profiles.

deflection of the stringers match very well. Because the deflections of the FE analysis (with $E_T = \frac{1}{20}E_L$) are less than the experimental values, the conclusion can be reached that the transverse stiffness of the deck is less than the estimated stiffness of the individual planks.

Generalized Plate Equations

A system of design equations was developed by GangaRao specifically to analyze steel grid decks, but it can be applied to any orthotropic bridge deck (*3*). These design equations account for most of the parameters affecting the plate behavior of a bridge, such as the aspect ratio of the deck, the orthotropic properties of the deck, loading conditions, number of lanes, and stringer spacing.

Very briefly, the generalized design equations are based on the premise that the bridge can be modeled as an orthotropic plate having two edges simply supported and two edges stiffened by edge beams. The solution form of the governing plate-bending equation is developed for a general load using Fourier and polynominal series; compatibility of deflections of the stringer and decking is assumed to analyze the system. The output of the analytical model includes both moments and deflections at any desired location for any applied load. To test the accuracy of this analytical method, the same input was used as that of the FE model discussed earlier except E_T, which was taken as $\frac{1}{25}E_T$. Because the applied load on the model structure simulated only one rear wheel (the model bridge was not wide enough to accommodate the standard 6-in. spacing of wheel loads), the loading of the analytical model was a combination of symmetric and antisymmetric cases. Superposition of the symmetric and antisymmetric loads produced the deflected profile shown in Figure 10. As in the FE model, the input value of E_T for the red oak in the transverse direction was varied to produce the best correlation with the experimental value. The best correlation of experimental deflections and analytically determined deflections was achieved when a value of $E_T = \frac{1}{25}E_L$ was used.

REVISED DESIGN

The second (and essentially the final) design was based on the test program data and observations and on the information generated by the analytical models. The T-beams were sized by working stress methods using simple beam-bending theory and assuming full composite action. The applied moments were computed for AASHTO loading and then reduced by the load-sharing factor found experimentally (and verified analytically). The live-load moments were not adjusted for impact, because AASHTO does not require this adjustment for timber structures.

For ease of fabrication, transportation, and erection, the bridge was designed to be constructed in two symmetric halves. The stressing system was designed with safety as the primary consideration. High-strength ⅝-in.-diameter steel bars were spaced on 24-in. centers and checked for their ability to prevent a catastrophic failure as well as their capacity to provide the normal force required for the timber laminations to transmit stresses.

Diaphragms, built of LVL timber like the stringers, were located at 18-ft centers. These were designed to provide lateral stability to the T-beam system and also serve as a backup load transfer mechanism in the event of a failure of the stressing system.

The guardrail system was based on a 10-kip crash-tested timber system developed by Wheeler Consolidated. Coal tar creosote preservative was specified for all wood components, and all steel items were galvanized. The final design is as follows:

- Six LVL stringers, each 73.25 ft long, 45 in. deep, and 6 in. wide with 3½ in. of camber;
- One LVL double wide stringer consisting of two stringers, each 73.25 ft long, 45 in. deep, and 4½ in. wide with 3½ in. of camber;
- Northern red oak deck laminations between stringers, 18, each 9 in. deep, 1½ in. wide, and a maximum of 16 ft long;
- Steel bars ⅝-in. diameter, 150 ksi (ultimate stress) on 24-in. centers;
- 8 × 20 steel channel bulkheads with 6 × 6 × ½ in. anchor plates;
- LVL diaphragms on 18-ft centers, each 6 in. wide, 36 in. deep, and 27 in. long;
- Timber guardrail system designed and crash tested by others.

FABRICATION AND ERECTION

Fabrication of the T-beam bridge was by Burke Parson and Bowlby (BPB) of Spencer, West Virginia. LVL stringers, purchased from Trus-Joist, Inc., of Boise, Idaho, were predrilled, preservative treated, and then shipped by rail and truck to the fabrication plant at Spencer. The deck planks, which were also predrilled and preservative treated, were nail laminated to each other and to the stringers and then temporarily posttensioned with mild steel rods in every second hole. Three 6-in.-wide stringers and one 4½-in.-wide stringer were assembled with the required decking to create half of the bridge. The process was repeated to create the other half, and the two halves were trucked to the bridge site.

At the bridge site, the abutments from the previous structure were repaired and modified to accept the new timber T-beams. A 140-ton crane and an 80-ton crane were located on either side of the span; the 140-ton crane lifted one half of the bridge from the truck trailer and placed it in position on the abutments. The smaller crane was used as an emergency backup in the event that the long reach required of the primary crane caused it to overturn. Although the smaller crane proved to be unnecessary, it was useful in positioning the end of the bridge half.

After the second half-section was craned to its position on the abutments, full-length, high-strength rods were inserted; then the temporary rods were removed and the entire structure was posttensioned. Installation of guardrails and concrete abutment backwalls was followed by the restressing operations; paving the surface with asphalitc concrete completed the job.

FIGURE 11 Completed structure.

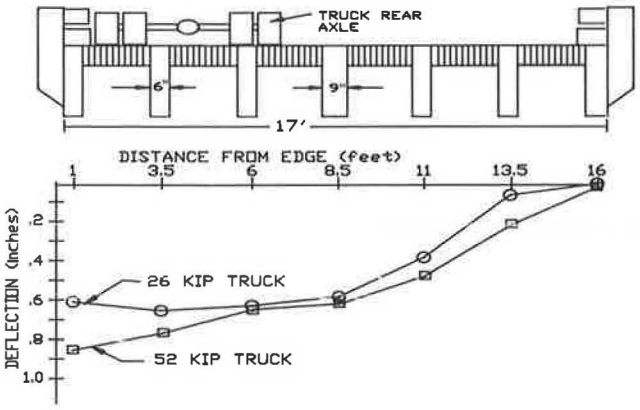

FIGURE 12 Transverse deflection profiles.

MONITORING PROGRAM

Figure 11 shows the completed timber T-beam structure. The bridge has been in service for 1 year and is apparently functioning well. It is, however, still an experimental structure and as such requires careful monitoring.

A short-term monitoring program (July 1, 1988, to December 30, 1988) consisted of six live-load tests and measurements of several of the bridge's responses. The live-load tests were designed to determine (a) the load deflection response of the stringers and the deck, (b) the stresses in the exterior stringer, (c) slip between laminates, and (d) skew effects. Other measured performance characteristics were stress level within the posttension system, dead-load deflection changes with time (creep), and moisture content fluctuations. In addition to these measurements and tests, simple visual observations and photographs were compiled to record the weathering of the exposed surfaces and general condition of the structure. The most recent visit to test posttension levels was made in May 1989.

MONITORING RESULTS

The short-term test program has provided a large body of data both for analysis of the bridge performance and as a datum from which long-term behavior can be measured. In addition to the data accumulated, valuable experience was gained in field monitoring techniques and in the unique problems of on-site experimentations. The test program was not completely successful, however. Portions of the results from several of the tests were clearly erroneous; the cause of these errors has been determined and changes will be made in future testing to eliminate these mistakes.

Stringer Deflection

Four separate load tests were performed in which a loaded truck was parked with its wheels on an outside stringer. Figure 12 shows transverse deflected profiles for two of these tests. There are some inconsistencies in the data, which show unreasonably lower deflections immediately below wheel loads. For example, the deflection 1 ft from the edge (see Figure 12) is directly beneath one of the wheel loads and should be greater than the deflection 3.5 ft from the edge. Taking deflection readings with a transit from the uneven top surface of the deck, particularly at the location of the test vehicle, was difficult and led to inaccuracies.

Maximum deflections generally occurred at the loaded exterior stringer, as is expected. The maximum deflection of 0.84 in. was due to the largest load of the test series (52,100 lb), which is approximately 83 percent of the AASHTO HS-20 truck load. The maximum deflection is quite small (equal to $L/865$) and much lower than was expected for a timber highway bridge. Part of the unforeseen stiffness is undoubtedly due to the double center stringer (9 in. thick), which was added to allow the bridge to be constructed in two symmetric halves. The large (8- × 12-in.) wheel rail and guardrail probably also contribute to the stiffness of the bridge.

Deck Deflection

Results of two deck deflection tests are shown in Figure 13. The data indicate a maximum deflection in both tests of only 0.02 in. for wheel loads of 8 and 10 kips.

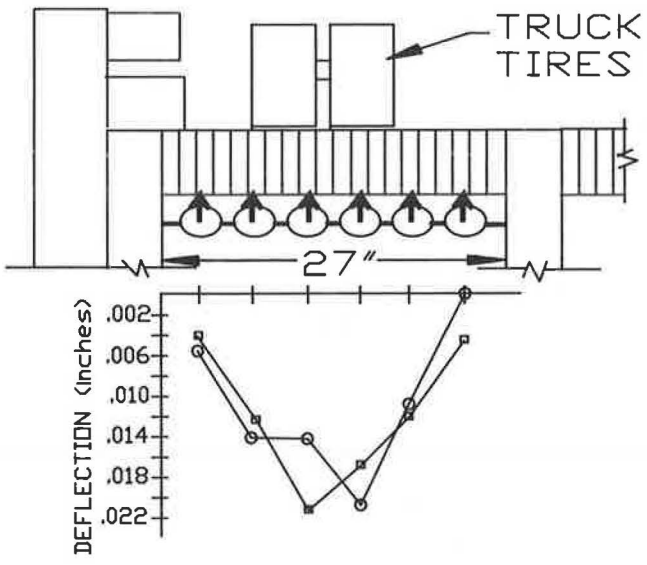

FIGURE 13 Deck deflection profile.

One benefit of this high deck stiffness is the ability of the deck to transfer the live load to the stringers more directly and to then transfer load from one stringer to another, providing a more even load distribution. A second benefit is that a small deformation is less likely to cause cracking of an overlay (asphaltic concrete). However, this degree of stiffness is probably more than is necessary and, of course, comes at some increased cost.

Stringer Stress Level

Strain measurement in the exterior stringer was one of the most difficult procedures to perform in the field and, unfortunately, the results cannot be considered very reliable. Figure 14 shows the data gathered for two live-load tests and includes the maximum calculated stress value. The readings show a strain increase in the gauges closer to the bottom of the stringer, as was expected, but in both tests the No. 4 gauge, located at the extreme lower face, exhibited a decrease in strain.

Despite the inconsistencies of the test results, the low strain measured by the six other gauges is indicative of a reasonable stress level in the most heavily loaded stringer. Simple calculations to convert the maximum measured strain to stress indicate a stress level of about 700 psi. The approximate load on that stringer was 15,000 lb. The problem of bonding strain gauges to creosote-treated timber can be overcome by use of clip-on strain gauges. A reliable, economical, and reusable strain transducer for field measurements [developed by Laferski et al. (*4*)] will be used in future monitoring projects.

Laminate Slip

The same testing done for deck load deflections was also used to locate any laminate slip. Although the graph in Figure 13 shows abrupt changes in deflection, the scale of the graph is highly distorted, with very small divisions on the ordinate compared with divisions on the abscissa. A graph with identical *X*- and *Y*-scales would show only a very slight curvature with no discontinuities.

Resistance to slip is dependent on the maintenance of a minimum posttension level. There is no evidence of laminate slip from either load tests or visual observations. After the load tests, all deflected deck planks returned to their unloaded positions.

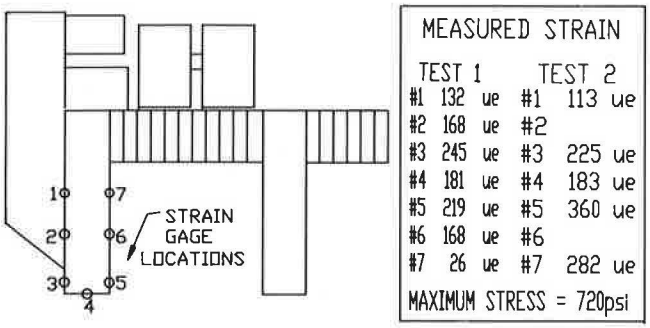

FIGURE 14 Strain measurements.

As a field check, the tension in one of the high-strength steel bars was released; the bar was able to move freely through the laminations indicating that the original hole clearance was intact and that no slippage had occurred.

Skew Effects

Due to the skewed bridge geometry, the possibility of an uplift force exists when a diagonally opposite corner is loaded. To test for this possibility, a truck load was placed at one corner and a dial gauge located below the opposite corner was monitored as the truck crossed the bridge. If the bridge skew had been an influence on the deflection response, an initial upward deflection would have been apparent. However, the dial gauge showed an immediate downward deflection of 0.002 in. when load was applied at the corner diagonally opposite. This deflection remained consistent as the truck traveled the length of the bridge; thus, no evidence of uplift was found.

Posttension Levels

Because the tension level in the posttension system is such an important factor in the response of the bridge, this testing was perhaps the most important of the monitoring program. Unfortunately, problems with equipment used to measure the tension level during the initial testing period reduced the amount of data. However, the amount of data gathered during the initial 6-month monitoring period combined with the data collected 1 year after the installation of the structure were sufficient to establish the prestressing system behavior.

Erection of the structure on May 7 and 8 was followed by an initial stressing on May 10, 1988. Information from the contractor indicated an initial tensile force of approximately 32 kips in the high-strengh steel bars. The second and third stressings were performed on May 18 and July 8, 1988, at which time the tensile force applied was again about 32 kips. Force levels from one load cell on one bar were measured from October to December 1988. In addition, an average tensile force from 15 bars tested in May 1989 was estimated by tensioning the rods until the anchor nuts were free to turn, rather than by using a load cell.

The early force levels from the single load cell, installed in October 1988, 5 months after the bridge was first stressed, are lower than expected (see Figure 15). The average force measured on May 1989 was 21.8 kips, or 67 percent of the jacking force. An extended period of rain before the test date may have caused some moisture-induced swelling and, consequently, an increased tension force level in the rods. If this was the case, another testing of the rods after a dry period should show a reduced force level. This procedure was tentatively planned for late summer 1989.

The long-term ability of the system to maintain the necessary tension level is a crucial element in the structural and economic performance of the bridge. Should the tension level fall below an acceptable level, the rods can be retensioned, but the intention of the design is to reduce this maintenance expense to a minimum. The structural consequences of inadequate tension level are serious. Complete loss of tension in one rod should not cause catastrophic failure (a safety feature

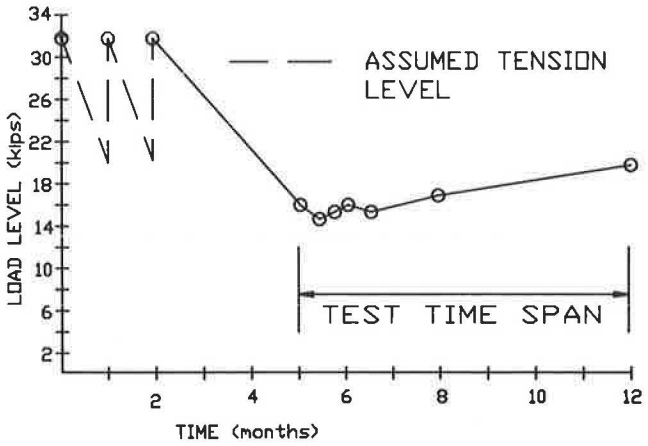

FIGURE 15 Posttension system losses.

of the design), but the ability to distribute load to the laminates and stringers can be seriously decreased.

Creep Deflection

Data for the creep deflection test were accumulated over the 6-month period of the monitoring program. Six months is a relatively short time span in the intended life of the structure, and there is, at this time, only slight evidence of loss of camber through creep losses.

Figure 16 indicates the loss of 0.03 ft (0.36 in.) of midspan elevation over 5 months. This is the maximum loss of the seven locations measured (top of each stringer at the bridge center line); the average value is 0.02 ft (0.24 in.). As in the previous tests, these data are not completely consistent, but the trend is well established. All of the stringers showed some loss of elevation from the first to the last reading. Each of the stringers maintained an upward camber, but the readings reveal that the bridge has an unequal camber when viewed across the section; that is, the center-line elevation of the center stringers is lower than that of the edge stringers.

The relatively short time span of this creep test prevents an accurate prediction of the rate of creep loss over the life span of the structure. Most materials exhibit a more rapid rate of loss early in the life span, which then levels off with time. It remains to be seen if this bridge will behave similarly.

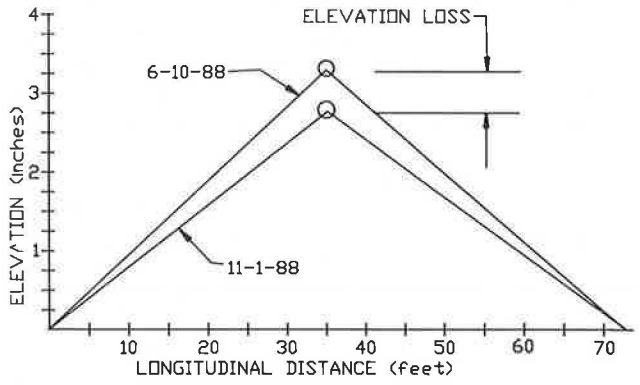

FIGURE 16 Creep deflection.

Moisture Levels

The timber and LVL materials used in the bridge were kiln dried to a moisture content of 19 and 8 percent, respectively, and then creosote treated. Exposure to the environment has increased the moisture content, as expected, with the greatest effect on the riding surface of the deck planks and LVL stringers.

At the time of this test, the timber deck surface was exposed to the weather; since that time, the surface has been covered with asphaltic concrete. Moisture levels were tested on the guardrail, top surface of decking, top surface of stringers, inside surfaces of stringers, and underside of deck planks. The variation of moisture levels was from 18 to nearly 40 percent, with the greatest variation in the LVL stringers. The highest readings were found on the upper surface of the stringers, which were subjected to the most adverse weather conditions. The moisture level in the oak decking was more consistent, averaging 22 percent. There did not appear to be a significant change in moisture levels from one test to the next, but the time span between tests was inadequate to show any relationship.

Weathering and General Condition

Visual observation showed very little noticeable weathering of the deck or stringers. However, the large timbers that make up the curb and the guardrail checked and split as they dried; some of these splits are extensive and much deeper than the penetration of the creosote.

Only minimal corrosion of the hardware has been observed. This insignificant corrosion was found on the high-strength bars where the couplers used in the stressing operation rubbed off some of the galvanizing material. A comprehensive inspection was not done, but the one rod that was removed and reinstalled was in excellent condition.

The galvanized steel pipe and neoprene washers used as a weatherproof covering for the anchoring hardware appear to be effective when installed correctly. Unfortunately, a large number of the installations were done incorrectly, and moisture has entered the covering devices. No serious corrosion was noted, however, even on the poorly protected anchors. These covering devices can do more harm than good, because they may retain moisture around the anchoring hardware rather than prevent its entrance.

Visual observation of the two exterior stringers indicated them to be off the vertical (not perpendicular to the abutments) when viewed from the abutments. By measuring this misalignment with a carpenter's 4-ft level, the maximum distance from the vertical was found to be 2¼ in. Discussions with the contractor indicate that the cause of this substantial distortion was either the erection procedure, in which one half of the bridge was "pulled" a small distance to mate with the previously anchored first half, or the retensioning operations, in which the top portion of the structure was squeezed together while the lower portion remained stationary.

COSTS

Information from the West Virginia Department of Highways shows the cost of the 73-ft timber T-beam bridge to be as follows:

Item	*Cost ($)*
Timber contractor, fabrication and delivery	78,800.00
Crane rental	10,125.00
Labor for erection	14,400.00
Equipment for erection	2,400.00
Materials for abutment alterations	1,185.00
Total	106,910.00

Although a breakdown of the contractor costs is not available, a large portion of the $78,800 was for the LVL beams and their transportation to the fabrication site. Labor and equipment for erection costs are for a 16-day period.

SUMMARY AND RECOMMENDATIONS

Results of the field monitoring program indicate that the stressed-timber T-beam bridge is performing very well. Most important, the force level in the high-strength steel bars is being maintained at a safe level. The deck deflection is minor and the stringer deflection appears to be acceptable. Weathering of the decking and stringers is, at this time, negligible.

From a performance perspective, the dead-load deflection (creep) is the most apparent problem and may not be significant over the long term. This will require future monitoring (as will the posttension force level). From a construction and fabrication perspective, the misalignment (not perpendicular to the abutment) of the stringers and the less cambered central stringer are serious problems that must be addressed in future T-beam projects. Several other minor construction problems can be easily rectified for future bridges.

The problem of high costs is not so easily resolved. This particular structure had very high crane rental costs and transportation charges. LVL is an excellent product with very good performance characteristics, but it is an expensive component. Much of the LVL costs were for transportation; if this cost could be reduced, the use of this product would be more cost-competitive.

The design of the structure also played a large role in the high cost. Because there were no guidelines to follow, the design had to be very conservative to guarantee public safety. There is little doubt that with the information now available, a more economical structure can be designed.

Recommendations for designers and fabricators of timber T-beam bridges include the following:

1. Use for shorter spans (40 to 60 ft). Although there is no performance problem, the high cost of transporting long components to treatment plants and then to the fabricator becomes prohibitive. Also, costs for large cranes are much higher than those for smaller cranes.
2. Increase the spacing distance between stringers to about 36 in. The deck stiffness is sufficient to transfer the live load more than the 27 in. span of this structure. The stringer capacity is not being utilized as fully as possible by the 27-in. spacing.
3. Choose stringer and deck material by geographic location as well as by load capacity and preservative treatability. Other possible materials (glued laminated timber, for example) may be less expensive and may be located closer to treatment facilities and fabricators.
4. Use a different rigging method when craning the bridge halves. This erection method used spreader beams to support the bridge halves; an "eye hook" rigging method would allow the crane operator to place the bridge segment exactly where required.
5. Do not anchor bridge halves to abutments until after second stressing sequence. Once this second stressing is complete, almost all of the compression of the timber deck will have taken place and there should be no more appreciable distortion.

With some additional monitoring, analytical work, and cost analysis, the timber T-beam can become a successful alternative to conventional bridge construction. A combination of low-cost local timber for the decking, high-reliability manufactured timber products for the stringers, and precision fabrication and erection techniques should provide a safe, long-lasting, and economical structure.

ACKNOWLEDGMENT

The authors appreciate the time and effort of Julio Davalos, West Virginia University, in editing and proofreading this paper.

REFERENCES

1. *Standard Specifications for Highway Bridges*, 13th ed. American Association of State Highway and Transportation Officials, Washington, D.C., 1983.
2. *Ontario Highway Bridge Design Code*. Ontario Ministry of Transportation, Downsview, Ontario, Canada, 1983.
3. P. Raju. *Wheel Load Distribution for Highway Bridges*. M.S. thesis. College of Engineering, West Virginia University, Morgantown, 1989.
4. J. R. Laferski, J. F. Davalos, and V. Vaddma. A Laboratory-built Clip-on Strain Gauge Transducer for Testing Wood. *Forest Products Journal*, Vol. 39, No. 9, 1989.

Publication of this paper sponsored by Committee on General Structures.

Structural Research and Testing in Florida

M. El Shahawy and A. M. Garcia

At present, interest is increasing in the evaluation of existing structures and the development of new and economical types of construction. This is a direct result of the rapid change in the environment and scarce financial resources, which necessitate the development of better and safer structures and expansion of the life of existing structures. Also, spectacular developments in computers have provided engineers with a powerful tool for modeling and analyzing complex structures on the basis of a variety of assumptions. The verification of these computer models can only be done through field and laboratory testing, which is now more important than ever before. The Florida Department of Transportation (FDOT), recognizing the importance of structural research, undertook the creation of an engineering group dedicated to structural research and testing. The primary responsibilities of the structural research group are to conduct field and laboratory testing, evaluate existing bridges and structural components, and develop new design concepts and ways to cut construction cost and time. The state-of-the-art structural research laboratory therefore becomes an essential element in keeping FDOT in the engineering forefront. In this paper FDOT's current research program and available capabilities are described, and the necessary components for successful laboratory and field testing are discussed in detail. A brief description of research projects in which both laboratory and field testing were utilized to develop a new economical bridge system is given.

Historically, Florida's bridges have been among the least expensive in the nation, on the basis of cost per square foot. This low cost is due to many factors, among them favorable weather conditions and lower labor costs. However, the main factor has been willingness to adapt new construction techniques and design philosophies while still maintaining public safety as uppermost in importance. It is therefore essential to encourage structural research for evaluation of these new techniques and design philosophies before they are implemented.

Challenges from abroad have pointed out a general deficiency in research spending, which would inevitably lead to inferior products. Transportation research, although more difficult to compare with commercially oriented industrial research, has suffered even more. Nationally, in medium-sized industries, research expenditure has averaged approximately 1 percent of product cost. In some western European countries and Japan, this expenditure is 5 percent. Heavy dependence on engineering in the United States suggests that the level of transportation research should compare with the level of research in these medium-sized industries.

The Florida Department of Transportation (FDOT), recognizing the importance of structural research, undertook the creation of an engineering group dedicated to structural research and testing. The importance of structural research was brought to the forefront by several structural problems that occurred on the then recently completed Keys segmental bridges and other bridges across the state. It was decided that if FDOT was to continue as a leader in bridge and structures design, it would be essential to give proper attention to structural research.

Florida Department of Transportation, 605 Suwannee Street, Tallahassee, Fla. 32399-0450.

OBJECTIVES

The primary objectives of the structural research group were to (a) conduct laboratory tests to develop new design and construction concepts and (b) conduct field testing and evaluation of existing bridges. A brief description of these tasks follows.

Laboratory Testing

FDOT's research laboratory consists of a structural engineering laboratory with an attached office building that houses the researchers, support group, computer laboratory, and electronic workshop. The structural research laboratory has a 60- × 125-ft area served by two traveling cranes, each with a capacity of 20 tons. The primary component of the structural laboratory is a strong floor, which is a 3.5-ft-deep, heavily reinforced concrete mat with dimensions of 110 × 50 ft. The floor has a grid of one hundred and forty-four 150-kip anchor points at 6-ft centers. Each anchor point consists of four inserts anchored to channels at the base of the 3.5-ft-thick floor slab. All loading systems are driven by hydraulic power. This power is supplied by a 55-gal/min pump that serves two 55-kip, two 22-kip, and one 550-kip capacity actuator through a hard line network including five independent channels of controls.

The laboratory has two testing frames. One testing frame, covering an area of 10 × 58 ft, has a total static capacity of 1,000 kips in the vertical direction and 500 kips in the longitudinal direction. Details of the loading frame are shown in Figure 1. This frame allows the experimental testing of any structural component or bridge model up to 55 ft long and 12 ft wide. The loads are applied by eight 125-kip capacity hydraulic jacks. Jacks are mounted in pairs on a traveling frame that allows free movement of each jack in both the X- and Y-directions. The unrestricted movement of the jacks allows the application of any desired load combination to simulate actual field conditions. Details of the loading apparatus are shown in Figure 2. The second frame is a servocontrolled closed-loop testing system with static and dynamic capacity of 550 kips. Figure 3 shows a ½-scale bridge model during testing.

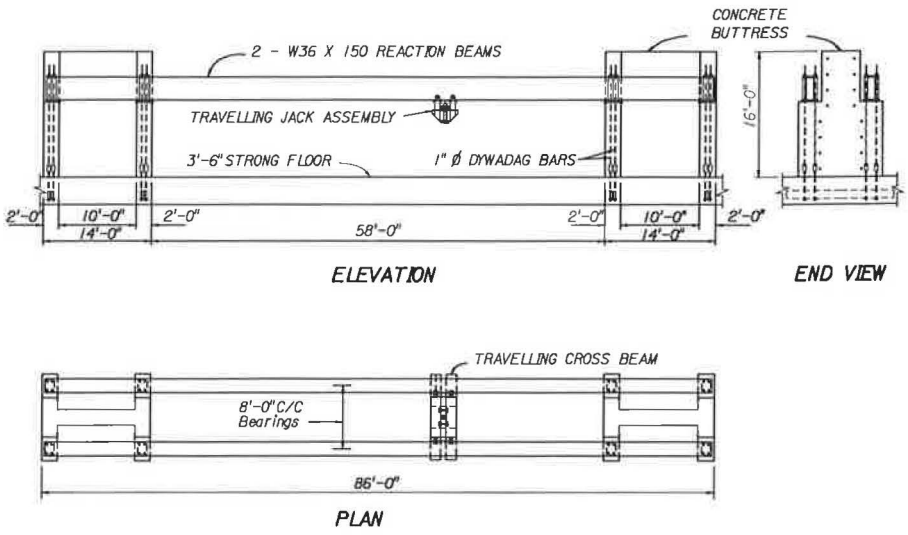

FIGURE 1 Dimensions of loading frame.

Two data acquisition systems are available. The first system is used to control and collect the test data from the 550-kip hydraulic testing frame. The second system is housed in a 23-ft motor home and is used for laboratory as well as field testing. The computer laboratory consists of a minicomputer with an extended memory and a graphic work station capable of handling large finite-element models. Also included in the laboratory are several IBM-AT and Hewlett Packard work stations with a large variety of software that provide the computational capabilities for the research group. FDOT's IBM mainframe computer is also available.

With its present capabilities, the structural research laboratory will facilitate static and dynamic load tests of large-scale bridge models and full-scale structural components. The results of such tests will serve in identifying serviceability and load capacity problems of highway bridges and in evaluating new concepts for inspecting and rehabilitating bridges and increasing their load capacity.

The research facility is one of a few in the United States and the only laboratory in Florida fully dedicated to structural research.

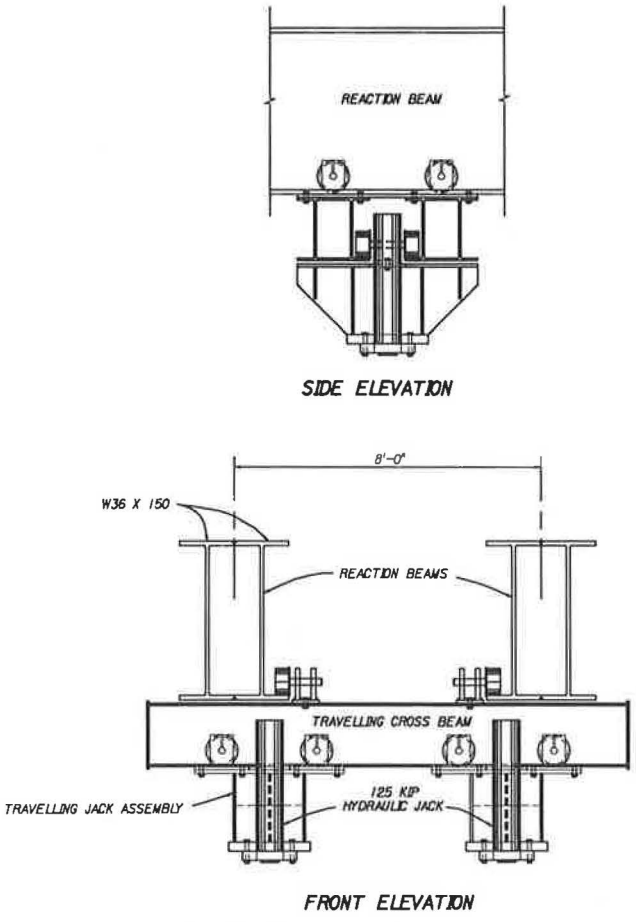

FIGURE 2 Details of loading apparatus.

Bridge Load Testing

It is estimated that of 500,000 existing bridges in the 50 states, nearly 105,000 are rated critically deficient (*1*,*2*). In Florida, thousands of the existing highway bridges are older than 20

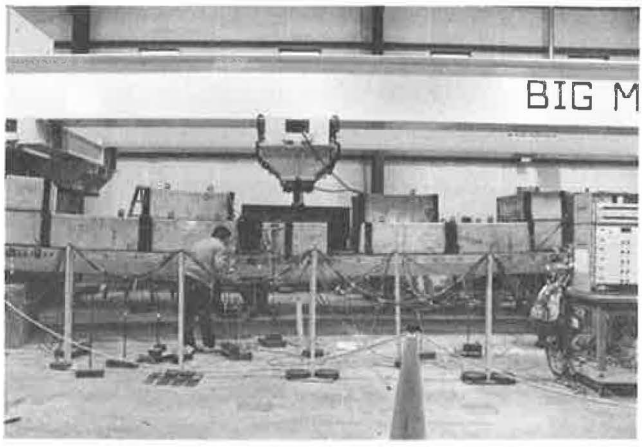

FIGURE 3 Half-scale model during testing.

years. Throughout the state, there are a number of bridges that, for one reason or another, are posted for loads lower than the original design loads. In many cases, the proper rating of a bridge cannot be achieved by the current methods of analysis. In most cases, the bridge is small and may be on an off-system road, so that it does not seriously affect commercial users. However, those that are on major systems and the resulting detours affect both the public and the commercial users.

Bridges of questionable strength that are posted for lower loads or scheduled to be replaced can be examined through a load test. The information collected from such a test can be analyzed to evaluate the true strength of the structure.

In bridge testing, various elements need to be examined. The strength of these elements is generally determined by placing strain or transducer gauges at critical locations along the elements. The bridge is then incrementally loaded to induce maximum effects. The data collected from the various instruments can be used to establish the strength of each component as well as the load distribution.

Testing Apparatus

The bridge load-testing apparatus consists of two testing vehicles, a mobile data acquisition system, and a mobile machine shop. The two testing vehicles were designed to deliver the ultimate live loads specified by the AASHTO code. Each vehicle is a specially designed tractor-trailer combination weighing in excess of 200,000 lb when fully loaded with concrete blocks. The detailed dimensions of the test vehicles are shown in Figure 4. Each vehicle can carry a maximum of 72 concrete blocks, each weighing approximately 2,150 lb. Incremental loading is achieved by adding blocks with a self-contained hydraulic crane mounted on each truck. Each truck contains a remote control system, allowing driverless operation when a bridge's strength is in question.

Testing Procedure

Once a bridge has been identified for load testing, a site survey and an analysis of existing plans and inspection reports give further information on the feasibility of such a test. The plans and details of instrumentation and loading locations are then established. The next step is to mobilize all testing equipment and personnel at the bridge site. The instrumentation [e.g., strain or transducer gauges, linear variable displacement transformers (LVDTs)] is placed at critical locations on the structure and tested for functional response.

The testing vehicles are loaded with an initial number of concrete blocks, established from the preliminary analysis of the existing structure. The vehicles are then driven to critical locations on the bridge while the data acquisition system monitors the instrumentation during loading. Figure 5 shows the two load-testing vehicles during testing. The data are immediately analyzed, displayed, and compared with the theoretical prediction to ensure the safety of the bridge, equipment, and testing personnel. After each load step, if the results compare favorably with the theoretical prediction, a specified number of blocks is added to the vehicles and the test is repeated until the ultimate AASHTO load is achieved. The data gathered can then be analyzed and a report of the findings prepared. Bridges that carry both vehicles without apparent distress are considered structurally safe.

RESULTS AND BENEFITS

One of the primary reasons for the establishment of the department's structural research program is the potential cost-saving benefits. In the short time that the laboratory has been in existence, the cost savings to the taxpayers have more than offset the expenditures.

Following are a few examples that show how Florida has already received significant cost savings and potential future savings.

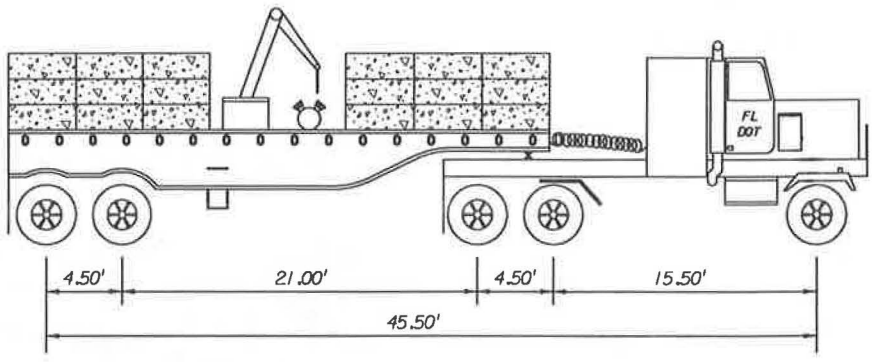

WEIGHTS		LOAD TRANSFER	
72 ballast blocks	154,800 lb.	5th wheel	82,350 lb.
Equipment	8,200 lb.	Steering axle	15,630 lb.
Trailer	24,000 lb.	Drive tandem	83,720 lb.
Tractor	17,000 lb.	Trailer tandem	104,650 lb.
Total	204,000 lb.		

Note: All weights and dimensions are approximate and for information only.

FIGURE 4 Detailed dimensions of testing vehicle.

FIGURE 5 Load-testing vehicles.

Load Testing

The results to date have shown that load limitations imposed by theoretical analysis are not representative of the structure's real capacities. Design engineers and the existing codes have made conservative assumptions in the mathematical analysis of a bridge. This is not an unexpected finding. What has not been established, though, is a more accurate understanding of the extent of that conservatism and what it represents.

With higher loads expected in the future and the fact that, in spite of all attempts at policing these loads, overweight vehicles use the roads and bridges every day, what is needed is the knowledge of what these bridges can actually carry safely.

The bridge load-testing program will allow a satisfactory overall strength evaluation of any bridge under question. The information provided will greatly increase selective rehabilitation rather than the current practice of replacement of the entire structure. Proof loading has consistently indicated that structures have greater residual strength. It is estimated that about 85 percent of bridges with load restrictions do have adequate load-carrying capacity and subsequently do not need to be posted or replaced.

According to the department's program and resource plan, approximately $850,000,000 will be spent on bridge replacement and maintenance during the next 10 years. If this amount could be reduced by only 10 percent through the proof testing of bridges thought to be structurally deficient, the potential exists to save an estimated $85,000,000 during the 10-year period.

Florida Bulb-Tee Beam

The Florida bulb-tee beam was developed in house through extensive analysis and testing. The 72-in.-tall beam is the most effective ever designed or built in the United States. It was first incorporated in the Eau Gallie Bridge, which carries State Road 518 over the Atlantic Intercoastal Waterway, called the Indian River in Melbourne, Florida (*3*). The bridge consists of twenty 145.0-ft spans and carries four designated traffic lanes, two emergency lanes, and a 5.0-ft sidewalk. The bridge is subdivided into five independent structures, each continuous over four spans. Continuity was achieved by longitudinal posttensioning, which was carried out in two phases, one before and one after the slab was placed.

The development process included the physical testing of a full-scale, two-span continuous beam. The test beam carried the full AASHTO service load with no cracking. At ultimate, the beam carried 130 percent dead load and 490 percent live load, thus greatly exceeding AASHTO requirements.

The bridge was built in two stages. In the first stage, approximately two-thirds of the superstructure was constructed and opened for traffic. In the second stage, the old bridge was removed and the remaining part of the superstructure was built. Before the first stage of construction was opened to traffic, the bridge was load tested. The Eau Gallie Bridge won a certificate of special recognition from the Prestressed Concrete Institute in 1987.

In a competition for building the Howard Franklin Bridge over Tampa Bay, a design utilizing the Florida bulb-tee won, with a direct savings to FDOT of approximately $2,000,000. These savings, coupled with the estimated savings over conventional AASHTO or segmental beams on both the Eau Gallie Bridge ($800,000) and the Apalachicola Bridge, now under construction ($1,000,000), totals almost $4,000,000 in benefits already received by the department.

Isotropic Deck Reinforcement

The testing of both prototype and model bridge slabs showed that the mode of failure is not governed by flexure, as suggested by the AASHTO specifications, but by punching shear (*4*). Accounting for that fact in the design of bridge slabs will permit decreasing slab reinforcement by at least 50 percent. The research work is essentially complete. Adopting the new method of design will save approximately $4,500,000 a year for the state of Florida.

Transversely Posttensioned Double-Tee Bridges

The double-tee bridge system was developed through a cooperative effort between industry and the FDOT structural research group (*5,6*). The fully precast, prestressed double-tee beams are tied together by transverse posttensioning through

simple grout-filled V-joints. The system provides for complete transverse continuity. This new system is aimed at state and Interstate highways with spans up to 80 ft.

In addition to analytical development, two series of physical tests were carried out. In the first (*5*), a half-scale bridge model was statically tested to investigate the overall behavior of the new system. In the second series (*6*), four fatigue tests were performed on a two-span 1:3.5 scale continuous bridge model at Florida Atlantic University. On the basis of both studies, a new design method was developed for short-span bridges.

The new design was utilized in the construction of two bridges for the city of Tallahassee. Both bridges were then load tested. The test results suggest that this new design is one of the most efficient for short-span bridges.

This new bridge type will save as much as $5/ft over current AASHTO designs for short-span bridges. It is estimated that a savings of $50,000,000 over the next 10 years may be possible using this new design.

CONCLUSIONS

Structural research is essential to transportation. Deficiency in research spending will only lead to inferior products. For many years, funding for transportation research in the United States has not been sufficient to support innovative product development as demanded by the public. The United States has become a copier and user of technology developed by others rather than a leader.

Increased research funding and long-term planning are critical for the United States to compete with other western European countries and Japan and to become once more a leader in this field. The Florida research program is only a small step in that direction and should be considered by other states in planning for the future. The benefits and the long-term cost savings are obvious.

ACKNOWLEDGMENT

Many people have been instrumental in the development of the Florida research program. The authors would like to thank all of them and specifically Paul F. Csagoly and Henry T. Bollmann for their valuable contributions.

REFERENCES

1. K. R. White, J. Minor, K. N. Derucher, and C. P. Heins, Jr. *Bridge Maintenance Inspection and Evaluation*. Marcel Dekker, Inc., New York, 1981.
2. F. Moses and D. Verma. *NCHRP Report 301: Load Capacity Evaluation of Existing Bridges*. TRB, National Research Council, Washington, D.C., Dec. 1987.
3. H. T. Bollmann and P. F. Csagoly. *The Eau Gallie Bridge Replacement—New Design Concepts*. Florida Department of Transportation, Tallahassee, Jan. 1984.
4. C. O. Hays, J. M. Lybas, and J. O. Guevara. *Test of the Punching Shear Strength of Lightly Reinforced Orthotropic Bridge Decks*. Structures and Materials Research Report 88-3. University of Florida, Gainesville, Aug. 1988.
5. M. El Shahawy, P. Csagoly, and W. Nickas. *Development of Double-Tee Bridge System for Interstate Highways*. Structural Research Report SRR-0001-87. Florida Department of Transportation, Tallahassee, 1987.
6. D. Reddy and M. Arockiasamy. *Static and Cyclic Behavior of Joints in Precast Prestressed Concrete Double Tee Bridge Systems*. Research Project 99700–7364. Florida Atlantic University, Boca Raton, 1987.

Publication of this paper sponsored by Committee on General Structures.

Methodology for Assessment of Vessel Impact Energy on Bridge Piers and Spans

PETER BEIN

Relevant risk factors are reviewed and a methodology is presented for determination of vessel impact energies and return periods for bridges located over navigable waters. The approach integrates vessel traffic and operating characteristics, bridge geometry, marine environment conditions, and aberrance frequencies of vessels. The method is generic and can be applied to multispan as well as to short bridges located either in a marine environment or over inland waterways. Main and side piers and spans are considered the objects of vessel impact threats. The analysis can be useful in bridge planning and in selection of design criteria for impact loads on bridge elements. The methodology recommends calculation of impact velocities of vessels by the application of mechanistic equations describing the behavior of errant vessels in wind, currents, and waves as a function of the vessels' operating speed and location at the instance of aberrance. The method can also be used if the impact velocity distributions are assumed by judgment. Examples from two Canadian bridge projects are given.

The determination of vessel impact forces is crucial for planning and design of bridges over navigational waters, but it requires extensive data. Some bridge risk assessments mix loss of human life with economic efficiencies (*1*, pp. 24–34). An alternative approach (*2*, pp. 297–306) selects vessel impact design criteria on the basis of socially acceptable risk levels and requires an assessment of possible impact energies and recurrence intervals. Multispan bridges pose special problems in the assessment. Vessels straying from a navigational channel have a high probability of approaching the flanks of a bridge. Often the side elements cannot, for reasons of economy, be designed to the same standards as the main piers and spans. Marine exposure creates additional risk factors, which are not normally present in inland waterways. This paper reviews vessel impact risk factors for a long bridge located in a marine environment and presents a method for assessing impact energy and recurrence. Potential damage to a bridge depends on the striking vessel's kinetic energy and also on dissipation of this energy in the process of deformation and displacement of the vessel, bridge elements, and protective devices. Energy dissipation and impact force generation are not the subject of this paper. The approach is illustrated with two cases: the Northumberland Strait Crossing on Canada's eastern seaboard and the Annacis Channel Bridge in Vancouver, British Columbia.

In this paper, a vessel "casualty" means a collision, grounding, flooding, capsizing, foundering, sinking, fire, explosion, ice damage, or other misfortune. Casualties and near-casualties are "incidents." "Collision" is contact between two or more vessels, whereas "striking" is contact between a vessel and a stationary object. "Aberrance" means that a vessel is out of control or on an error course.

3955 West 14th Avenue, Vancouver, B.C., Canada V6R 2X2.

RISK FACTORS AND IMPACT ENERGY

A review of sources on marine and bridge casualties, which is discussed elsewhere (*3*), revealed that the following factors may aggravate the risk of vessel impacts on multispan bridges in a marine environment:

1. Mixed use of the waterway, involving fishing, recreation, and commercial vessels;
2. The presence of towed barges and ships under ballast in the traffic;
3. Tides, currents, winds, floating ice, and reduced visibility;
4. Sabotage and vandalism; and
5. A large number of spans and piers posing an obstacle to safe transit of a large vessel on a stray course.

Casualty Statistics and Limitations

The review also established that casualty statistics cannot be exported uncritically between regions, particularly under conditions of low vessel traffic volume. The statistics are based on past occurrences and reflect marine conditions, ship technology, and navigational aids specific to the time and place of data collection. Human differences between the navigators in foreign waters and at a study bridge site may also be a limitation, because the human factor is the leading cause of incidents.

Computational methods based on mechanistic models and fault-tree analysis of a vessel's systems are not adequate either, because they miss the human error. These limitations pose a dilemma, because strikings of bridges are rare events, and a risk analyst would gladly use any available data. Vessel casualty data banks, such as those operated by marine insurance companies or the Canadian and U.S. coast guards, provide a sound basis to establish statistics reflecting local factors. In North America, the law requires the reporting of all incidents through appropriate channels, but near-casualties would not always be reported. Canadian Coast Guard reports of 77 marine incidents (Table 1) in the Northumberland Strait were analyzed. Although fishing vessels appear accident-prone, they are significantly safer than other vessels if one considers their length of time at sea.

TABLE 1 CASUALTIES IN NORTHUMBERLAND STRAIT, 1976–1986

Year	No. of Incidents[a] Total	Fishing[c]	Other[d]	No. of Casualties[b] Total	Fishing[c]	Other[d]
1976	2	0	2	2	0	2
1977	0	0	0	0	0	0
1978	1	0	0	1	0	1
1979	2	1	1	2	1	1
1980[e]	10	4	6	9	4	5
1981	11	10	1	11	10	1
1982	10	7	3	9	7	2
1983	7	6	1	7	6	1
1984	12	9	3	10	8	2
1985	16	8	8	15	8	7
1986[f]	5	4	1	5	4	1
Total	77	49	28	72	48	23

Notes:
(a) Excluding ferries, confined waters, and harbors.
(b) As [a] but multiple vessels involved are counted as one event.
(c) Including trawlers, draggers and seiners.
(d) General cargo, tankers, dredges, towed barges and work boats, icebreakers, tenders, and research vessels.
(e) New reporting procedure introduced.
(f) Incomplete annual report.

Bridge Striking Data

Half the time, the human factor was the main cause in major Canadian bridge strikings. The human factor was a secondary contributor to the environmental factors; thus human error was involved in most of the incidents (*4*). Contrary to conventional design practice, ships choose to ram the side piers and spans more often than the main piers (*5*). Only 6 of 19 serious strikings worldwide involved main piers, and 13 involved side piers and superstructures (*6*). Bridges over waterways may create or aggravate difficult areas of navigation (*7*).

Sea Ice Factor in Casualty Statistics

Ice conditions were found to make a significant contribution to vessel casualties in Canada and in Europe (*3*). In Table 1 most of the incidents involving more than one vessel occurred in ice. In Canada, ice was the primary cause in three major bridge casualties (*4*). Table 2 shows that in Northumberland Strait the risk of vessel casualty in winter is about seven times greater per transit than in the ice-free season. Whether an incident in ice will become a casualty at a bridge depends on the buffer effects and the movement of ice surrounding the vessel.

TABLE 2 RELATIVE HAZARD OF SEA ICE IN NORTHUMBERLAND STRAIT

Season	Vessel Movements	Incidents	Incident Frequency
Ice-free	189	10	0.053
Winter	21	8	0.381
Total	210	18	

Note:
1980-1985 casualty records for Northumberland Strait, Canadian Coast Guard. Number of vessel movements based on 1978-1986 annual average, 10% of which take place in winter.

Impact Energy Equation

The impact energy E_{ij} is given by

$$E_{ij} = 0.5 \cdot k_m \cdot m_i \cdot v_j^2 \quad (1)$$

where

k_m = added mass coefficient,
m_i = mass of vessel, and
v_j = impact velocity of vessel.

The impact mass includes both the vessel and a water volume surrounding the hull. The coefficient k_m ranges from 1.1 for head-on to 1.4 for broadside strikings in deep water. For a clearance under the keel smaller than the vessel's draft, k_m can exceed a value of 2. Modern laden tankers meet such conditions in many navigational channels. At side piers, which are usually located in shallower water, most of the laden cargo ships will engage a high added mass of water. If a ship is trapped in sea ice, the mass of ice moving with the ship should be included in m_i.

Many factors specific to site conditions and vessel operation determine magnitude and direction of v_j, as follows:

$$v_j = f_i\,(v_o, l_o, S_e, S_i) \quad (2)$$

where

i = vessel under consideration;
v_o, l_o = vessel's operating speed and location before aberrance, respectively;
S_e = modifying effects of wind, currents, and waves as the vessel closes in on the bridge; and
S_i = vessel's geometric and dynamic characteristics.

It is expedient to determine v_j by simulation with equations describing vessel behavior under wind, current, and wave forces. A range of starting speed and location is assumed from data on vessel operation. Each starting condition is analyzed for the full range of possible environmental conditions that cause the vessel to advance toward the bridge. Advanced hydrodynamic equations can also be used, but then the vessel data inputs may be too demanding. A set of curves as in Equation 2 was developed for laden and empty barges (*2*). Each curve describes v_j as a function of the closing distance, current, and wind speed and direction. One set of such curves is shown in Figure 1.

Environmental Factors and Vessel Behavior

The marine environment can be a powerful determinant of vessel speed and aberrant behavior. Currents may be due to tidal, wind-stress, and storm surge currents, which are independent and add up if superimposed. Currents increase in passages and narrows, where bridges are most often located. The resultant flow depends on the hydrography and bathymetry and on the meteorological conditions in a bridge site area. Currents combined with wind and waves determine drift velocities of disabled vessels and vessel course-keeping on approaches to the bridge. In winter, floating ice interferes

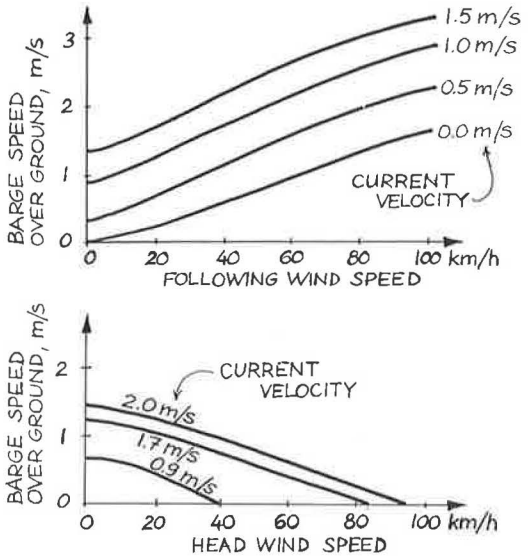

FIGURE 1 Impact velocity curves for laden barges becoming aberrant at 700 m closing distance.

with navigation. More detailed discussions have been presented elsewhere (*3*).

PROBABILITY MODEL FOR STRIKING A MULTISPAN BRIDGE

Three conditions are required for a vessel to strike a bridge:

1. Aberrance: the vessel must either become out of control or disabled or start an erroneous course anywhere on the approach to the bridge.
2. No evasion: the vessel must continue sailing and must reach the bridge location rather than somehow avoid it.
3. Geometry: once at the bridge, the vessel must make contact with some bridge elements.

Besides the probability of striking, mass and impact velocity of the vessel influence the extent of potential damage to the bridge. Thus, three pieces of information are needed to assess the probability of impact energy: (a) probability of striking, P_s; (b) probability of impact mass, P_m; and (c) probability of impact velocity, P_v. For Vessel i, these probabilities are independent and the total probability of impact energy E_{ij} due to mass m_i and velocity v_j is

$$P(E_{ij}) = P_{si} \cdot P_{mi} \cdot P_{vj} \tag{3}$$

Annual basis is used for all three probabilities because the objective of the analysis is to calculate annual probability distributions of impact energy from which return periods can be obtained.

Probability of Striking

The probability of striking is a product of three probabilities:

$$P_{si} = p_{1i} \cdot p_{2i} \cdot p_{3i} \tag{4}$$

where

p_{1i} = annual probability of aberrance of the vessel type under consideration,
p_{2i} = probability of no evasion; and
p_{3i} = geometric probability.

Probability of Aberrance

How far from the bridge a vessel gets out of control is irrelevant from the risk analysis viewpoint, as long as the aberrance is a potential threat to the bridge. The aberrance frequency is specific to type of vessel and local conditions. Barges or other vessels on tow are more prone to get out of control, as are large ships under ballast. Adverse weather and currents, and the presence of sea ice, increase the chance of aberrance of any vessel. Local data on aberrance frequencies account for both the local vessel factor and local site conditions. If available, such data should be used rather than data from foreign waterways, because the specific local environmental and operating conditions are locked into the statistics.

Probability of No Evasion

Evasive actions may be taken on board the stray vessel if the crew realizes the danger. Some possibilities include dropping an anchor, steering away from the bridge, or reversing the engine. Human intervention could also come from outside, for example, by deflecting a stray vessel or stopping it with tugs. Evasion may also occur by chance if the aberrant vessel is stranded, sinks, or is grounded on shallows before reaching the bridge. Depending on incident-reporting practice, vessel aberrance statistics now available may or may not include the effects of human intervention on evasion. In most risk analyses, p_{2i} is assumed to equal 1.0 unless there are vessel-monitoring and tug intervention systems in place at a bridge site. Such systems would make sense for long bridges with low-clearance side spans because the likelihood of striking side spans and piers is high.

Geometric Probabilities

Geometric probability of striking a bridge element depends on the size of the vessel and on bridge dimensions. For piers, the probability is

$$p'_{3i} = (B + w_i)/L \tag{5}$$

where

B = pier base or protective island diameter,
w_i = effective width of vessel, and
L = bridge span center to center.

The vessel's effective width is a random variable equal to the width projected on the longitudinal axis of the bridge. It ranges from vessel breadth for bow-on and stern-on impacts to vessel length for impacts broadside. Ambitious studies with sufficient data can assume a probability distribution for w_i, but

generally the following judgmental formula for an average value should suffice:

$$w_i = (l_i + b_i)/a_i \quad (6)$$

where

l_i = vessel's length overall,
b_i = vessel's breadth (beam), and
a_i = judgmental constant greater than 1.0.

The judgmental constant depends on vessel and pier type. Strikings tend to be oblique at a sharper angle at main piers, whereas they would be more broadside at side piers. In the Northumberland Strait study, $a_i = 3$ was adopted for ballasted and for towed vessels, and $a_i = 4$ for all other vessels. Corresponding to relatively sharp angles of vessel attack, these constants are particularly relevant to main piers. Smaller values would be more appropriate for side piers. The constant and the effective width of vessels have a greater effect on Equation 5 when the pier diameter is small compared with vessel size, and for that reason the estimation should then be more careful.

The geometric probability of striking the spans, p''_{3i}, depends on a vessel's superstructure. The topmost "soft" elements, such as antennas and masts, are not necessarily a serious threat, and the height of the vessel can be suitably reduced for risk analysis of spans. At sites with tidal variation of water level, the vertical clearance of a span has a frequency distribution. The same vessel may clear the available height at low tides but not at high tides. The general expression for p''_{3i} is

$$p''_{3i} = P(h_i > H) = 1 - P(h_i < H) = 1 - F_h(H) \quad (7)$$

where

h_i = elevation of uppermost limit of vessel's "hard" elements above water line,
H = span vertical clearance,
P = probability, and
$F_h(H)$ = cumulative distribution function, that is, the probability that vessel height h_i is equal to or less than the available vertical clearance under a span.

The latter distribution can be constructed from the frequency distribution of tidal elevations.

Probability Relation to Closing Distance

All three probability components of bridge striking by a vessel are related to its distance from the bridge. In general, this function is

$$p_k = f_k(d) \quad (8)$$

where k refers to aberrance, evasion, or geometric probability and d is the closing distance from the vessel to the bridge. In most analyses it would be pragmatic to take average values for each p_k.

For long bridges, the geometric probability of striking main piers decreases with the closing distance, whereas for side piers and spans, it increases. A schematic in Figure 2 helps

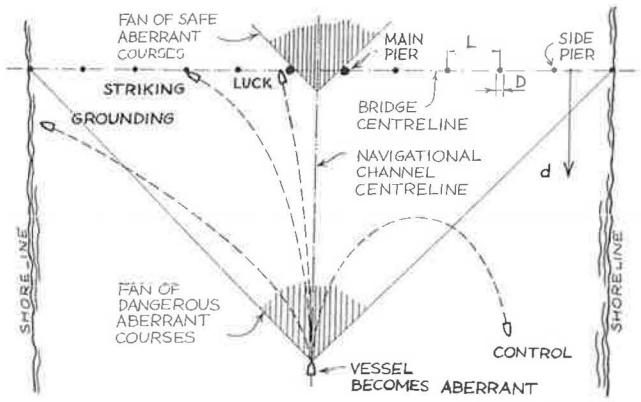

FIGURE 2 Situation graph for probabilistic model.

to calculate the geometric probabilities. Assume that each pier is represented by a circle of diameter D equal to the width of the pier base plus a characteristic average vessel dimension, as defined in Equation 5. Diameter D can be different for main and side piers. All errant paths of a vessel are equiprobable straight lines fanning out from the point at which loss of control started. If there are reasons to believe that the errant paths are not equally likely, a different probability distribution can be introduced.

When the outside of the fan glances the inside of the main pier circles, there are no strikings. When the outside of the fan intersects the bridge approaches at the shoreline, the upper limit of the number of potential strikings is reached. Moving the fan farther away will strand the vessel. Intuitively, between the two limits there are strikings of the bridge, and their geometric probability can be calculated by counting the number of bridge elements swept by the fan placed at successively increasing distances from the bridge.

The geometric probabilities are shown in Figure 3 for the case of a navigational channel centered about the bridge length and all spans of equal length. For aberrance occurring up to about 1.5 span lengths from the bridge, main piers are prime targets. As the distance increases, the likelihood of hitting one of the side piers increases. The results are for a 90-degree fan. For a navigational channel located close to one shore, there will be about 50 percent reduction of frequency of strik-

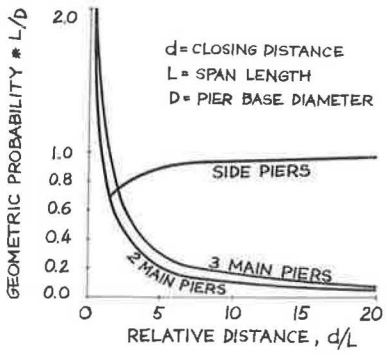

FIGURE 3 Relative likelihood of striking piers when all span lengths are equal.

ing the side bridge element. Similar results can be shown for striking the spans.

The tendency to hit piers and spans will be countered by possible successive evasions. The chance of taking an evasive action diminishes at shorter distances, which do not leave as much time to act compared with longer closing distances. For lack of data, one can assume a probability of no evasion, $p_{2i} = 1.0$ at $d = 0$, decreasing to $p_{2i} = 0.0$ at a large distance, which should be determined by judgment.

The distance to the farthest point of aberrance that could result in striking is large in the case of long bridges. In Figure 2, the distance is equal to about half of the bridge total length, that is, 6 km for the case of the Northumberland Strait Crossing. Published aberrance frequency statistics relate to vessel passage by a critical location, but for long bridges it would be more meaningful to express the frequency in terms of distance traveled by a vessel. It is not a particular location that is critical to aberrance, but rather a certain long distance on both approaches to a bridge. This alternative approach to estimating aberrance frequency requires both vessel incident and travel data from the study area.

Probability of Impact Mass

Probability of impact mass is

$$P_{mi} = f_i \cdot p_{mi} \tag{9}$$

where f_i is the relative frequency of vessel type under consideration in the traffic volume and p_{mi} is the probability of added mass. The total annual traffic volume is classed into a number of typical vessels on the basis of operational characteristics and size. An allowance should be made for traffic growth and for possible introduction of new types of vessels in the future.

Probability p_{mi} is conditional on the same factors that affect the total mass at impact. These factors are the ratio of water depth to vessel draft and the inclination of the striking vessel relative to bridge elements. The ratio depends on vessel loading condition and location at the bridge, and the inclination depends on vessel type, loading, and weather and currents.

It may be too cumbersome to determine p_{mi} conditional on so many factors. Unless Equation 3 proves to be sensitive to this parameter, p_{mi} can be disregarded. The annual traffic volume is then classed on the basis of both vessel operational characteristics and behavior when aberrant in the marine environment, and an average added mass coefficient is used in Equation 1. The Northumberland Strait preliminary study, for example, subdivided all vessels into freighters, tankers, passenger ships, barges, and other vessels. The cargo vessels were classed by size as laden or ballasted to account for the behavioral factor and the depth-to-draft ratio. A total of 14 types resulted, and the fraction of each vessel type in the annual volume was estimated from past traffic statistics and future projections.

Probability of Impact Velocity

Given the relationship in Equation 2, v_j has a joint probability of operating conditions v_o and l_o and environmental factors S_e. In general, the vessel's operating speed depends on S_e, and consequently,

$$P_{vj} = P(v_o|S_e) \cdot P(l_o) \cdot P(S_e) \tag{10}$$

where $P(v_o|S_e)$ is probability of operating speed in a given marine environment. Vessel characteristics S_i are implicit in Equation 10, which is specific to vessel type but not indexed with i for simplicity.

Variables v_o and S_e have those particular values that produce impact speed value v_j. Specifically,

$$P(S_e) = P(u_j|w_j) \cdot P(w_j) \cdot P(c_j) \tag{11}$$

where

u = wave conditions;
w = wind speed, direction, and duration;
c = currents; and
j = specific values resulting in the value v_j of impact speed.

For example, a certain vessel described by a set of characteristics S_i, westbound and becoming aberrant at l_o = (1.5 km east of the bridge) and v_o = (7 m/sec over ground or 5 m/sec through water), and experiencing w_j = (side wind, 40 km/hr), c_j = (westerly current, 2 m/sec; cross-current, 0.5 m/sec at 1-km intervals) could have an impact velocity v_j = 3 m/sec while inclined 60 degrees.

Waves need not always be considered, because they do not affect impact velocity of larger vessels. If considered, their probability is normally conditional on wind, unless other wave sources such as swell occur at a bridge site.

An example of a P_{vj} distribution for barges (*2*) is shown in Figure 4. The impact speed is a function of wind; river and tidal currents; four segments of barge routes, some of which involve turning; variable operating speeds; selected operating hours; and two distinct sources of aberrant vessels, namely, moored barges and towed barges. The complexity of operating conditions was reduced to two variables, v_o and l_o, which were classed into intervals with relative frequencies known from analysis of the operations. Occurrence of currents was determined for the operating hours. Frequency distributions for currents and winds were derived from past statistics. Environmental and operating conditions that drove the vessels away from the bridge or led to $v_j = 0$ were consolidated and their joint probability is shown in Figure 4 at impact speed 0 m/sec.

Return Period of Impact Energy

Calculation of the return periods is trivial once all the steps required to obtain $P(E_{ij})$ in Equation 3 have been completed for all possible impacts. All values of E_{ij} are arranged in descending order, and the probabilities of each event are added to arrive at the annual exceedence probability for a given impact energy. A reciprocal of the annual exceedence probability is the return period of the impact energy.

In some bridge risk analyses, there may be two or more distinct sources of possible strikings of bridge elements by vessels. Examples include a navigational channel and a vessel mooring site; a combination of independent navigational channels; or a combination of different marine activities, such as fishing and navigation. There may also be a number of

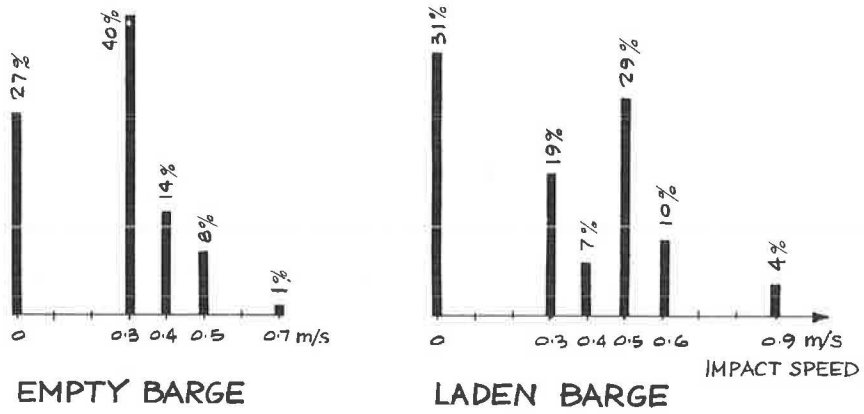

FIGURE 4 Probability of barge impact velocity.

segments within the shipping lanes with different vessel operating characteristics. Regardless of the real-world complexities, it is usually possible to break the problem down so that the energies, the associated probabilities, and the return periods can be calculated.

Such analysis has been done (*2*) for complex conditions. The impact energies associated with 200- and 500-year return periods were of particular interest for design. The bridge supports an urban arterial road, which serves as a lifeline facility in case of earthquake or other emergencies. The highway authority specified the 200-year event for designing structures to the elastic limit. A 500-year recurrence was specified for vessel impacts that can cause permanent structural damage, but without collapse and loss of human life.

Example

The Abegweit Passage of Northumberland Strait between Prince Edward Island and mainland Canada is 13 km wide. In preliminary planning, a number of generic bridge designs were considered. This example refers to an alternative with 43 spans, each 300 m in length (*3*). The navigational channel is located close to one shore. The side spans have a clear height of 14 m, but the main span permits transit of large ships. The main piers are protected by islands 100 m in diameter (including the effect of underwater slope), and the calculated impact energies are applied to design of the berms. Side piers are 15 m at the base.

Environment

Two ebbs and two floods move through the passage each day. The flood rates range from 0.4 to 1 m/sec, depending on the season. Surge currents caused by storms in the Gulf of St. Lawrence occur on 5 days per month on the average. The surges can reach 1 m/sec and last a long time if driven by major storms. Rip currents caused by crosswinds can be a major factor in loss of control of ballasted or towed vessels at the site. Wind conditions are not sufficient to develop Sea State 5 or rougher. Ice conditions are among the most difficult of all approaches to Canadian ports and last 10.5 weeks on the average. Even the most powerful ships may then experience difficulty, and lower-powered vessels become beset by the moving sea ice.

Vessel Traffic

The vessels in the navigation channel range from occasional passenger cruisers and large cargo ships and tankers to fishing trawlers and barge tows. Typical vessels are described in Table 3. The base case traffic volume is 260 vessel movements per year, of which 10 percent occur in ice conditions. Barges constitute 20 percent of the total traffic. The cargo vessels were assumed fully laden in 65 percent of movements and ballasted in 35 percent, and tankers and barges fully laden in 50 percent of movements.

Aberrance frequencies based on "vessel-kilometers" rather than "passing by a geographic point" could not be calculated for lack of vessel travel data.

Assumptions

Data were not available in sufficient detail to warrant determination of relative frequencies of all relevant environmental factors. Instead, P_{vj} was adopted by judgment of site and navigational conditions. The base case assumes a three-point distribution with 2, 4, and 6 m/sec impact speed and probability mass of 25, 50, and 25 percent, respectively. For barges and other vessels, the three points are 1, 2, and 3 m/sec. The low speed represents impacts in head currents, whereas the high speed represents impacts in following currents. To account for the dislocation of stray vessels under wind and current, which were not modeled mechanistically, a "path probability"

TABLE 3 CHARACTERISTICS OF TYPICAL VESSELS IN NORTHUMBERLAND STRAIT

Vessel Type	Displacement, tonnes		Length, m	Beam, m	Air Draft, m	
	Laden	Ballasted			Laden	Ballasted
Freighter	4000-18000	700-5200	91-134	13-20	18-32	20-34
Tanker	10000-16000	2800-3800	119-132	16-20	23-30	25-32
Passenger	3700	NA	98	16	24	NA
Barge	7400	1300	100	20	6	9
Other	1000	NA	46	9	21	NA

Note: NA = not applicable

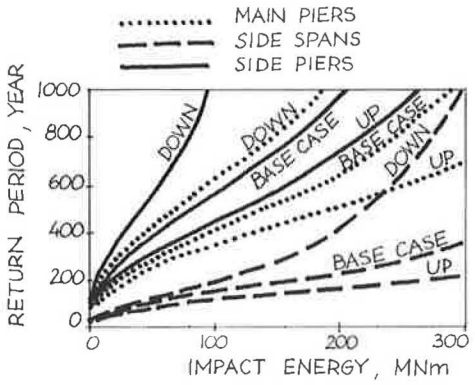

FIGURE 5 Effects of changing impact velocity by 1 m/sec up or down.

was introduced. It refers to the likelihood of an aberrant vessel transit within the main channel and piers. Other paths lead to side piers and spans. In the base case, 50 percent of aberrant courses are within the main channel, except ballasted freighters and ballasted tankers, and all barges are assumed to have this probability reduced to 30 percent owing to their steering difficulties.

Analysis

The analysis was carried out for main piers, side piers, and side spans using a microcomputer spreadsheet. None of the vessels can reach the underside of the main span, even at high tide. The return periods were computed from cumulative probability mass functions of impact energies and the results were smoothed out. The sensitivity of results was tested relative to impact speeds, traffic, aberrance frequencies, path probability, and bridge geometry. The results were graphed with the return period as a function of the impact energy. A graph can be entered with a predetermined return period and the corresponding impact energy can be found.

Results

The most severe loads can be expected on side spans, for which the corresponding curve has the smallest slope (Figures 5 and 6). A 500-year energy is 400 MNm on side spans, but it is only 140 MNm on main pier islands and 60 MNm on side piers in the base case. This agrees with intuition, because the side spans "catch" all vessels that cannot clear the height of the side spans above water level. Side piers receive less energy than main piers for a given return period, owing to higher main channel path probability assigned to the larger vessels, and higher geometric probability of striking the main pier island than the side piers. Changing the range of speeds from low to high doubles or triples the impact energy for a fixed return period (Figure 5). Changing the skewness of the speed distribution from left to right has a similar effect (not shown), because right skew of the distribution implies more frequent occurrences of higher speeds.

Doubling the barge traffic (Figure 6) has a negligible effect because the number of barge movements increases at the expense of the other vessel movements, whereas the total number of vessels remains unchanged. This simulates a mode shift from the smaller freighters and tankers to the barge. The small deviations from the base case reflect changes in vessel mass distribution. Doubling annual traffic, however, triples or quadruples the base case energies within the 200- to 500-year range (Figure 7).

Path probabilities have a strong effect (Figure 8), but the example uses extreme cases, which are not very likely in practice. The path effect is not comparable with the effect of aberrance frequencies, which are probably closer to the actual situation. A high probability of main channel path drastically increases the energy corresponding to 200 years, whereas a low probability reduces the impact energies on the protective islands to nil. A weaker effect in the same direction is due to aberrance frequency. The approximate magnitudes of these deviations from the base case vary greatly with the return period because the slope of the graphs is highly variable. For side piers and spans, the opposite trend is true for path probabilities (not shown), while aberrance probability changes have similar effects to those in Figure 7 in percentage terms.

The effect on side piers of changing side span length by 10 percent and of doubling pier base diameter was found to be minor. However, decreasing the 14-m clearance to 10 m (a saving of some 160 vertical m of side pier structures) does not practically change the risk of collisions with the "hard" elements of vessels.

Effect on Planning

As a result of the preliminary risk study, it was decided to relocate the navigational channel closer to the center of the

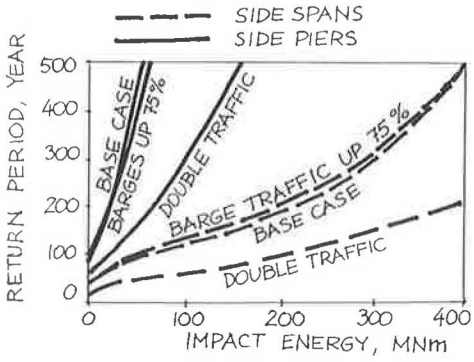

FIGURE 6 Effects on side piers and spans of changing impact velocity.

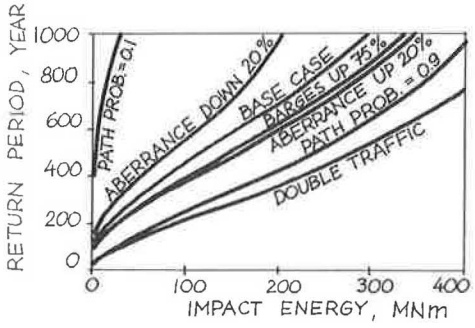

FIGURE 7 Effects on main spans of changing impact velocity.

bridge. The height of the side spans was increased to allow clearance for hard elements of the largest vessels under high-tide conditions. The sensitivity analysis findings pointed to the importance of vessel speed determination for future phases of the project. A 20 percent underestimate of impact velocity, for example, results in a 44 percent underestimate of the energy. Frequency distributions for winds, currents, tidal elevations, and ice conditions will be required to achieve accurate estimates. Due to the complexity of marine elements, vessel operating data from the Strait should be applied in mechanistic simulations of aberrant drift to determine the impact velocities. Aberrance probabilities can be estimated from the Canadian Coast Guard data and vessel travel statistics.

CONCLUSIONS

For bridges in marine environments, selection of design criteria from probability distributions on the basis of publicly acceptable risks is the preferred method because it avoids evaluation of intangibles, such as the worth of human life.

A methodology has been presented for assessing the probability distribution of impacts from bridge geometry, vessel characteristics, marine site data, and local aberrance statistics. The approach draws on models and methods previously developed by others and by the author. It integrates all factors considered relevant in such risk analysis and can also be applied to shorter bridges and to inland waterways, because it is generic. It can be useful for bridge planning to evaluate alternatives and in design to determine impact load criteria.

The kinetic energy equation is most sensitive to the impact velocity, which is also the most uncertain variable. The complexity of the marine elements and their interaction with vessel behavior pose an analytical challenge in estimating the impact velocity and its probability for bridges in a marine environment. Mechanistic models of vessel behavior can be instrumental in arriving at accurate estimates of the velocity. Site condition statistics must be analyzed in conjunction with vessel operating data to obtain the probability distributions.

Aberrance frequencies should be based on local statistics because foreign data may not be applicable. Long bridges require an aberrance statistic related to vessel-kilometers of travel.

Each variable should be conveniently divided into a number of intervals so that manageable probability mass functions can be analyzed on a microcomputer. In complex risk analyses, breaking the problem into parts and selection of these intervals is an art as much as it is a science, and it is made on the basis of data availability and interactions between various groups of variables. For this reason, a rigid software program encoding all prescribed analytical procedures would not be suitable, but an interactive program might be.

In studies affording collection of all required data in sufficient detail to feed all equations of the present model, Monte-Carlo simulations combined with mechanistic modeling of vessel behavior would be well justified.

ACKNOWLEDGMENT

This paper is based on the author's work for Public Works Canada and for the British Columbia Ministry of Transportation and Highways.

REFERENCES

1. E. Rosenblueth. What Should We Do with Structural Reliabilities. In *Reliability and Risk Analysis in Civil Engineering: Proceedings of the Fifth International Conference on Applications of Statistics and Probability in Soil and Structural Engineering* (N. C. Lind, ed.), Vol. 1, Institute for Risk Research, University of Waterloo, Ontario, Canada, 1987.
2. P. Bein. Probabilistic Model of Barge Impact Energy on the Annacis East Bridge Piers. In *Modelling Under Uncertainty: Proceedings, First International Conference on Modelling Under Uncertainty* (S. B. Jones and D. G. S. Davies, eds.), Institute of Physics Conference Series 80, Institute of Physics, Bristol and Boston, 1986.
3. P. Bein. Risk Modelling of Vessel Impacts on a Multispan Bridge. In *Proceedings, International Conference on Structures Under Shock and Impact (SUSI)*, Wessex Institute of Technology, Southampton, United Kingdom, July 1989.
4. Canadian Coast Guard. *Vulnerability of Bridges in Canadian Waters*. TP3446. Transport Canada, Ottawa, 1982.
5. *Ship Collisions with Bridges: The Nature of the Accidents, Their Prevention and Mitigation*. Marine Board, Commission on Engineering and Technical Systems, National Research Council, Washington D.C., 1983.
6. R. Saul and H. Svensson. Means of Reducing the Consequences of Ship Collisions with Bridges and Offshore Structures. In *Proceedings, International Association for Bridge and Structural Engineering*, Vol. 41, 1982, p. 165.
7. United States Coast Guard. *Statistics of Casualties: Proceedings of the Marine Safety Council*, 1980, 1981, 1982, and 1983 (Microfiche ASI Series 7404–11).

The opinions expressed herein are those of the author.

Publication of this paper sponsored by Committee on General Structures.

Unintended Composite Action in Highway Bridges

SATRIYA SUETOH, EDWIN G. BURDETTE, DAVID W. GOODPASTURE, AND J. HAROLD DEATHERAGE

All available data on unintended composite action in beam-and-slab bridges are reviewed and the factors that may influence the existence of unintended composite action in noncompositely built beam-and-slab bridges are investigated. Test reports summarized in this paper have shown that the existence of a natural or a chemical bond is the single most important factor in determining whether a noncompositely built beam-and-slab system can be counted on to act compositely. There is considerable evidence that indicates the presence of composite action in bridges in which no provisions were made for such action. This composite action may reduce the stress under a given load by a significant amount. However, the uncertainty surrounding the presence of composite behavior and the difficulty associated with verifying the existence of composite behavior make the assumption of composite behavior in a bridge designed noncompositely a questionable one.

An opinion that appears to be widely held by structural engineers involved in the design or the rating of bridges is that composite action will exist in a steel beam–concrete slab bridge whether such action was provided for in the design of the bridge or not. Bridge 4 in the Tennessee bridge tests (*1*) was a steel girder bridge that was designed to act noncompositely but that, in fact, acted compositely up to the load at which yield in the steel girders would have occurred in the noncomposite bridge. This rather widely publicized result has contributed to the widely held opinion just described. Unfortunately, consideration of all available data does not permit the drawing of a general conclusion in this regard.

PURPOSE AND SCOPE

The purpose of this paper is to review all available data on unintended composite action in beam-and-slab highway bridges, to investigate the factors that may influence the existence of unintended composite action, and to make recommendations concerning the consideration of this phenomenon that the writers hope will prove useful to an engineer charged with the task of determining the load capacity of bridges.

Although some discussion of tests performed on other types of bridges is included, this paper is primarily concerned with concrete slab–steel beam bridges designed and built with no provision for composite action.

S. Suetoh, Impell Corporation, Lincolnshire, Ill. 60015. E.G. Burdette, D.W. Goodpasture, and J.H. Deatherage. Department of Civil Engineering, University of Tennessee, Knoxville, Tenn. 37966-2010.

REVIEW OF TESTS ON BEAM-AND-SLAB BRIDGES

This section contains a review of tests done on beam-and-slab bridge systems in which unintended composite action was considered. For each test, the bridge is described briefly, and the significant test results as related to unintended composite action are presented. The names of the authors are given for each case and the date when the test was performed is given in brackets.

Burdette and Goodpasture [1970]

One of the four full-scale bridges that was tested to failure by Burdette and Goodpasture (*1*) was a noncomposite, three-span continuous, concrete slab-and-steel-beam bridge (designated Bridge 4). A 7-in. (17.8–cm) slab was supported by four 27-in. (68.6–cm) steel rolled beams. The ultimate load in the actual test was compared with the ultimate load computed in a manner consistent with the AASHTO specifications and with a theoretical ultimate load considering the entire cross section as a wide beam.

Figure 1 shows the load-deflection curve for Bridge 4. The computed load-deflection curve was first developed assuming no composite action of the girders and bridge deck. Observation of the actual test and resulting strain data indicated that a considerable degree of composite action did exist at load levels approaching the load that would cause yielding of the steel in the noncomposite bridge. The bond between steel and concrete and the friction forces developed at the steel-concrete interface were sufficient to develop forces that resulted in composite action of the girders and deck. The average shearing stress at the steel-concrete interface was approximately 230 psi (1586 kPa) at a load of 500 kips (2225 kN). The load-deflection curve calculated on the basis of composite action in the elastic range matched the measured data almost perfectly up to a load near the capacity of the noncomposite bridge.

Kissane [1985]

Full-scale laboratory and field testing was performed to determine the restraint to elastic buckling of a steel beam supporting a noncomposite concrete deck (*2*). In the laboratory testing, a reinforced concrete slab 6 in. (15.2 cm) thick was placed on top of an American Standard Beam. Before the

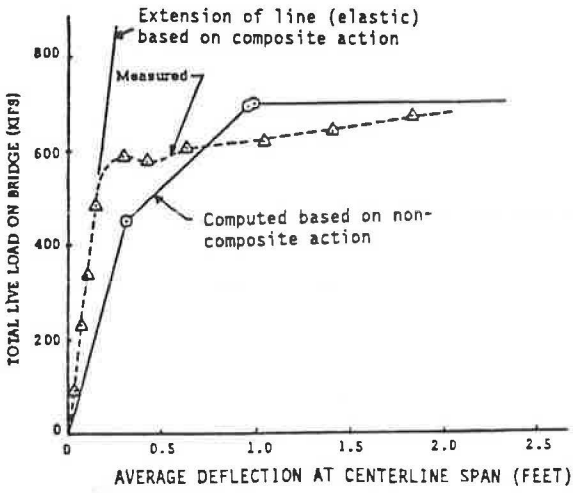

FIGURE 1 Comparison of measured and computed load-deflection curves for Bridge 4 (*1*).

concrete slab was poured, the top flange of the beam was sanded to remove mill scale and irregularities that could offer mechanical restraint at the concrete-steel interface. The bare metal surface of the flange was covered with a light oil to prevent chemical bonding between the concrete and steel.

The ratio of compression to tension flange strain was used as an indicator of composite behavior between the concrete and steel. Experimental data show that there existed some amount of composite behavior, which increased as higher loads were applied. The amount of composite behavior translates to an approximately 10 percent increase in the bottom flange section modulus above that for a noncomposite value.

Because mechanical and chemical bonds were inhibited between the steel and concrete, the partial composite behavior was attributed to friction between these components. As higher loads were applied, there was an increase in friction and pressure developed at the steel-concrete interface, thereby permitting increased composite behavior.

A field test was also performed on a 146-ft (44.5–m) simple span truss bridge built in 1924. Two identically loaded haul trucks were used to load the bridge. Results showed that there was a small change in neutral axis position from that of a noncomposite section. However, the upward shift of 0.82 in. (2.08 cm) in the neutral axis position was considered insignificant because of the low magnitude of the measured stresses and the approximately 300 psi (2068 kPa) experimental error in the measurement. The author concluded that there was no significant evidence of composite behavior between the steel and concrete (*2*).

Bakht and Csagoly [1975]

An extensive diagnostic load test was undertaken (*3*) to detect the sources of distress in the Perley Bridge, where in March 1973 a failure of the connecting angles of the girder-column connection of a trestle span caused the span to drop a few inches. One of the objectives of the diagnostic testing of the trestle span was to determine the degree of composite action that existed between the floor beams and the concrete deck slab in the absence of shear connectors.

Approximately 87 percent of the deck slab area was supported by girders and trusses through the floor beams. The test established that the composite action between the slab and the floor beams varied from beam to beam and could not be relied upon with certainty.

AASHO Road Test [1962]

The AASHO Road Test (*4*) included a study of 18 beam-and-slab bridges. Each bridge was a simple span structure consisting of three beams and a reinforced concrete slab. The beams spanned 50 ft (15.2 m). Ten of these bridges had wide-flange, rolled-steel beams with or without cover plates. Two of the 10 steel bridges were built compositely with shear connectors, whereas the other 8 were noncomposite. The top surfaces of the steel beams in the noncomposite bridges were coated with a 1:4.43 mixture of graphite and linseed oil to inhibit formation of bond. In composite bridges, the interaction between the slab and the steel beams was obtained with 4-in. (10.2-cm), 7.25-lb (3.29-kg) channels 5.5 in. (14.0 cm) long welded to the top flanges.

In the design of the beams, two of the steel bridges were assumed to have complete interaction between the slab and the beams, whereas six of the bridges were assumed to have 10 percent composite action to account for the effects of friction between the slab and the beams. No composite action was assumed for the remaining two bridges in the design.

After the bridges had been tested with repeated stresses, the actual locations of the neutral axes were determined from strains measured on the bottom and top of beams at midspan, assuming straight line strain distribution. In calculating the theoretical location of the neutral axis, the compositely built steel bridges were considered fully composite; for the other steel bridges a complete absence of interaction between the slab and the beams was assumed. Table 1 gives the distance of the experimental location for all 30-mph runs within the 10-month observation period.

The difference between the measured and the theoretical locations of the neutral axis was small, indicating that the bridges with mechanical connectors were fully composite, whereas the others had practically no composite action. The moment-deflection diagrams also showed a much stiffer sec-

TABLE 1 DIFFERENCE BETWEEN EXPERIMENTAL AND THEORETICAL LOCATION OF NEUTRAL AXIS (*4*)

Bridge	Location of * Neutral Axis (inch)
1A, NC	0.0
1B, NC	+0.2
2A, NC	+0.1
2B, C	+0.2
3A, NC	+0.2
3B, C	-0.1
4A, NC	+0.2
4B, NC	-0.1
9A, NC	+0.1
9B, NC	0.0

NC - Non-Composite, C - Composite
*Plus sign indicates position above theoretical

tion for the composite beams; for example, Bridges 1A and 3B had beams of the same depth, but for a midspan moment of 500 kip-ft (678 kN-m), the deflection at midspan for Bridge 1A was 2.2 in. (5.59 cm), whereas Bridge 3B had only 0.6 in. (1.52 cm) of deflection. The report concluded that there was no composite action present for the bridges with no shear connectors.

Thomas [1949]

A 1:3 scale model of a bridge deck system was tested to determine the extent of lateral load distribution of the system and the extent to which the steel joists and the concrete slab acted together in resisting the induced bending moments (*5*). The model consisted of a reinforced-concrete deck 3 in. (7.62 cm) thick supported on six standard 8-in. (20.3-cm) by 4-in. (10.2-cm) longitudinal steel beams spaced at 3-ft (0.914-m) centers. The slab was cast independently of the steel joist system to minimize bond induced by construction methods.

Load was applied to the model by means of a hydraulic jack. The tests were made in three stages: load applied to the slab in its uncracked condition, load applied to the slab after it had been systematically cracked, and final loading to failure.

For the test on the uncracked model, a comparative study of the strains measured in the upper and lower flanges of the beams showed that some partial composite action existed between the beams and the slab. The effect was more pronounced for beams near the load, suggesting that composite action was primarily due to friction between the slab and the flanges of the beams. For the test on the cracked model, a study of strain measurements indicated that there was slightly less composite action between the beams and the slab as a result of cracking. The slab failed by punching shear at a load of 45.1 kips (201 kN). The author concluded that shear connectors should be used if full allowance of composite action is to be made.

Siess and Viest [1945]

Laboratory tests were made on three 1:4 scale models of continuous right I-beam bridges (*6*). Each structure was a two-span right bridge consisting of five steel beams supporting a reinforced-concrete slab. The bridges were labeled N30, C30, and X30. Bridge N30 was a noncomposite bridge, Bridge C30 had shear connectors welded to the top flanges of the I-beams at regular intervals throughout the full length of the bridge, and Bridge X30 had no shear connectors in the negative moment region in the vicinity of the center pier. The top flanges of the beams for Bridge N30 were covered with a coating of wax to prevent a bond between the slab and the beams. For Bridges C30 and X30, the top surfaces of the beams were left in the as-rolled condition. All tests were made with one, two, or four pairs of concentrated loads simulating the rear-axle loads of one or more trucks.

For the test on Bridge N30, it was observed that the bottom and top flange strains were practically equal for applied loads at midspan, an indication that there was no interaction between the slab and the beams. The test data are also in agreement with the calculated values. For the test on Bridges C30 and X30, observation of strain data indicated the presence of composite action for both bridges as expected. Bridges X30 and C30 failed ultimately by punching of the slabs at a load of 10.4 kips (46.3 kN), and Bridge N30 failed by buckling of the beams at a load of 8.49 kips (37.8 kN), even though Bridge N30 had larger beams. On the basis of the test results, it was concluded that the behavior of Bridge N30 was that of a truly noncomposite structure, and Bridges X30 and C30 acted like composite structures.

Tharmabala [1984]

A structural evaluation and load test studies were performed (*7*) on the Flack River Bridge, which consists of pony trusses spanning 70 ft (21.3 m) with a concrete deck cast over stringers and floor beams. Two heavily loaded trucks were used to induce member forces to reach ultimate limit states defined by the Ontario Highway Bridge Design Code (OHBDC). The stringer moments were calculated using measured strains on the bottom flange and both composite and noncomposite section properties. These moments were compared with the theoretical moments using grid analysis. Although the deck is of noncomposite construction, it was observed that the moments obtained with composite section properties were closer to the theoretical moment graphs. Therefore, it was concluded that the deck behaved in a partially composite mode under the applied loads.

Patel [1984]

A structural evaluation and live load test were performed (*8*) on the Irvine Creek Bridge, which is a two-lane steel truss bridge with a sidewalk and two identical steel trusses spanning 104 ft (31.7 m) over Irvine Creek. Two heavily loaded trucks were used for vehicular test loading. The stringer moments were calculated using grillage analysis of the deck under applied loading. Plots were made of corresponding test moments calculated using measured strains with composite and noncomposite section properties of the stringers versus theoretical stringer moments.

It was observed that the graphs for the theoretical moment values lay between the graphs of the moments calculated using the fully composite and noncomposite section properties, indicating that the stringer sections were acting partially composite with the concrete deck. From the strain data on the floor beams, it was observed that for each loading case the floor beam moments obtained from grid analysis compared very well with the measured moments using composite section properties. Even though the steel floor beams were built to be noncomposite with the concrete deck, they were found to act compositely because they carried higher applied loads than the steel beams could have carried by themselves.

REVIEW OF TESTS ON INDIVIDUAL BEAM-AND-SLAB SYSTEMS

This section contains a review of tests done on beam-and-slab systems in which unintended composite action was observed.

These tests are reviewed separately from those in the preceding section because the tests reported here deal with a single beam and slab as opposed to a multi-beam-and-slab bridge system. A brief description of the test and the test results are presented for each case.

Viest et al. [1948]

Four composite steel-and-concrete T-beams with channel shear connectors were tested on simple spans of 37.5 ft (11.4 m) by applying single concentrated loads at the center line and at other points (*9*). In three of the beams tested, provision was made during construction to prevent bonding between the slab and the steel beam to better observe the behavior of the shear connectors. However, one beam was allowed to develop natural bond in order to determine the effectiveness of bond in transmitting horizontal shear. The results of the first test made with this beam revealed the presence of bond. Only after 11 repetitions of a load of 40 kips (178 kN) was the bond broken. The test results showed that as long as bond was present, it proved to be an effective shear connection. Before bond was broken, there was practically no slip between the slab and the beam. The bond withstood a load equal to 1.7 times the design live load, corresponding to a shearing stress of 112 psi (772 kPa). The bond broke after the same load was applied 11 times. However, the researchers believed that if the static load had been increased instead of repeated, at loads approaching ultimate, large deformational bond stresses at the concrete-steel interface would have caused bond failure. Further, they noted that shrinkage and warping of the slab as well as dynamic loading might destroy the bond even at working loads. It was concluded by the researchers that even though bond is a very good shear connection, it may also be an unreliable one.

Viest [1960]

A review of research on composite steel-concrete beams was done by Viest (*10*) on all tests carried out in the period between 1920 and 1958. Tests of specimens with and without mechanical shear connectors were summarized and briefly described. Practically every test that was done led to the conclusion that so long as bond between the concrete and the steel was not definitely broken, complete interaction between the slab and the beam could be assumed. Bond strengths between 400 and 500 psi (2758 and 3448 kPa) were observed in some of the tests. However, it should be noted that most of these tests were pull-out tests on steel beams fully encased in concrete.

One of the first American tests was performed by Caughey. On the basis of his test results and tests published before 1929, he recommended an allowable bond stress of $0.03f'_c$. Viest recommended an allowable bond stress of 60 psi (414 kPa) when the steel beam was fully encased and 50 psi (345 kPa) when the steel beam was only partially encased.

Bryson and Mathey [1962]

An extensive test of bond between concrete and steel beams was performed by the National Bureau of Standards (*11*). Wide-flange structural steel beams with different surface conditions were embedded in concrete and subjected to push-out tests to determine the effect of surface condition on the bond between concrete and steel. Three types of surface conditions were studied: normal rust and mill scale, sandblasted and allowed to rust, and freshly sandblasted. Three push-out specimens for each surface condition were constructed. The specimens were either W 14 × 30 or W 14 × 34 steel sections embedded in 2 ft (61.0 cm) of concrete. The bonded area of the steel beam was limited to the surface of the flanges.

A summary of the test results is shown in Table 2. The results indicated a considerable difference in ultimate strength of the bonds. However, at low values of slip, bond stress was not greatly affected.

SUMMARY

Test reports summarized in this paper have shown that the existence of natural or chemical bond is the single most impor-

TABLE 2 SUMMARY OF TEST RESULTS (*11*)

Specimen	Steel Section	Surface Condition	Maximum bond stress, psi	Free end slip at maximum, inch
SB-1	14 WF 34	freshly sandblasted	420	0.015
SB-2	14 WF 30	"	474	0.008
SB-3	14 WF 34	"	470	0.006
Avg.			455	0.010
R-1	14 WF 30	sandblasted and allowed to rust	508	0.020
R-2	14 WF 34	"	403	0.018
R-3	14 WF 34	"	486	0.007
Avg.			466	0.015
N-1	14 WF 30	Normal rust and mill scale	310	0.003
N-2	14 WF 34	"	355	0.012
N-3	14 WF 30	"	287	0.002
Avg.			317	0.006

tant factor in determining whether a noncompositely built beam-and-slab system can be counted on to act compositely. Every reported test, be it full-scale or model, in which bond between the steel and concrete interface was prevented resulted in noncomposite behavior, with the exception of the laboratory test that was reported by Kissane. Caughey and Viest, Fountain, and Singleton suggested allowable design bond stresses of $0.03f'_c$ and 50 psi (345 kPa), respectively. Though not quantitatively stated, a large factor of safety was implied in all design stresses. In the full-scale tests by Viest et al. (*9*) at Illinois, the beam in which bond was not broken experienced full composite action at the maximum design load of 1.7 times the live load. The bond failed after 11 repetitions of the load. A horizontal shear stress of 112 psi (772 kPa) was resisted by bond at this loading.

Even though bond has been shown to be very effective in transmitting horizontal shear, it is also unreliable, because it is sensitive to fatigue loading, shrinkage, thermal stresses, and impact. There is also the possibility of physical separation of the concrete slab and the steel beam because of uplift forces generated along the beam by certain dispositions of the live load. These uplift forces may also contribute to the rapid deterioration of the natural bond at the steel-concrete interface. It was also stated by Viest et al. that shrinkage and warping of the slab as well as dynamic loading may destroy the bond even at working loads.

Tests have also shown that composite action could be induced by friction. However, the amount of friction that translates into a certain degree of composite action varies from one bridge to another depending on the weight of the deck slab, the magnitude of the load, and the surface roughness of the steel-concrete interface.

From the data obtained in the tests reviewed herein, it appears that even though certain beam-and-slab bridge systems have demonstrated the ability to act compositely without the use of mechanical shear connectors, the degree to which composite action can be counted on is very difficult to quantify because of the variables just discussed.

CONCLUSIONS

The work described in this paper leads to the following conclusions, which are presented in the form of statements that may be useful to a bridge engineer charged with calculating the capacity of a bridge.

First, composite action in a bridge designed to act noncompositely cannot be counted on to increase the load capacity of a bridge significantly if that capacity is defined as the load producing first yield of tensile steel. In Tennessee Bridge 4 the load capacity was simply the sum of the capacities of the four steel girders. The path from zero load to yield, on the other hand, was significantly affected by the presence of composite action. The bridge was effectively much stiffer than that calculated on the basis of noncomposite behavior; thus, at any load level below yield, the deflection was much less than that calculated. This behavior relates also to stresses: it follows that the stress in the steel girders at any load below yield in Tennessee Bridge 4 was less than that calculated on the basis of noncomposite behavior. Therefore, even though unintended composite action does not appreciably enhance load capacity, in the process of altering the behavior of a bridge in the elastic range, it does reduce the stress in the girders at any load level. This reduction in stress for a given load may very well prove to be of significant benefit to a bridge engineer concerned with bridge load capacity.

Second, the discussion just presented was based on the existence of unintended composite action like that found in Tennessee Bridge 4. In fact, the work presented in this paper leads to the conclusion that composite behavior in a bridge designed with no provision for composite action may or may not occur. In some cases the practical and conservative approach is to disregard any potential unintended composite behavior. For the cases in which such an assumption leads to calculated stress levels for certain required loads that are larger than those permitted, further investigation to verify the presence of composite action may be justified. Such an investigation would logically begin with an inspection of the bridge by an experienced bridge engineer—an inspection that would include visual observation of the beam-slab interface as truck traffic goes over the bridge. Details of construction should be observed; for example, encasement of the top flanges of the steel girders would increase the probability of composite action. This investigation may very well prove to be inconclusive. In such a case the next step might be to load the bridge statically with a heavily loaded truck of known dimensions and weight and to measure deflections of the bridge at selected points. Comparison of the measured deflections with deflections calculated on the basis of both noncomposite and composite action should shed considerable light on the question of whether the bridge is behaving compositely or noncompositely. If composite action is found to exist, this behavior can be considered in the calculation of stresses at various load levels below that used in the test. However, the possibility of sudden slippage at loads greater than the test load makes the assumption of composite action at higher load levels questionable.

ACKNOWLEDGMENTS

The research that led to this paper was sponsored by the National Cooperative Highway Research Program (NCHRP) as Project 12–28 (8). The final report for this project has been published as NCHRP Report 306 (*12*).

REFERENCES

1. E. G. Burdette and D. W. Goodpasture. *Full Scale Bridge Testing: An Evaluation of Bridge Design Criteria*. University of Tennessee, Knoxville, Dec. 1971.
2. R. J. Kissane. *Lateral Restraint of Noncomposite Beams*. Research Report 123. Engineering Research and Development Bureau, New York State Department of Transportation, Albany, Aug. 1985.
3. B. Bakht and P. F. Csagoly. Diagnostic Testing of a Bridge. *Journal of the Structural Division*, ASCE, Vol. 106, No. ST7, July 1980, pp. 1515–1529.
4. *Special Report 61D: The AASHO Road Test: Report 4—Bridge Research*. HRB, National Research Council, Washington, D.C., 1962.
5. F. G. Thomas. Investigation on Bridge Deck Systems. *International Association of Bridge and Structural Engineering (IABSE) Publications*, Vol. 9, 1949, pp. 45–59.

6. C. P. Siess and I. M. Viest. *Tests of Continuous Right I-Beam Bridges*. Bulletin 416. University of Illinois Engineering Experiment Station, Urbana, 1953.
7. T. Tharmabala. *Structural Evaluation and Load Testing of Flack Bridge, Mitchell's Creek*. SRR-84–08. Research and Development Branch, Ontario Ministry of Transportation and Communications, Downsview, 1984.
8. N. J. Patel. *Testing and Evaluation of Irvine Creek Bridge*. SRR-84–11. Research and Development Branch, Ontario Ministry of Transportation and Communications, Downsview, 1984.
9. I. M. Viest, C. P. Siess, J. H. Appleton, and N. M. Newmark. *Full-Scale Tests of Channel Shear Connectors and Composite T-Beams*. Bulletin 405. University of Illinois Engineering Experiment Station, Urbana, 1952.
10. I. M. Viest. Review of Research on Composite Steel-Concrete Beams. *Journal of the Structural Division*, ASCE, Vol. 86, No. ST6, June 1960, pp. 1–21.
11. J. O. Bryson and R. G Mathey. Surface Condition Effects on Bond Strength of Steel Beams Embedded in Concrete. *Journal of the American Concrete Institute*, Vol. 59, No. 3, March 1962.
12. E. G. Burdette and D. W. Goodpasture. *NCHRP Report 306: Improving Bridge Load Capacity Estimates by Correlation with Test Data*. TRB, National Research Council, Washington, D.C., Feb. 1988.

Publication of this paper sponsored by Committee on Dynamics and Field Testing of Bridges.

Abridgment

Revitalization of a Suite of Bridge Analysis Codes

PAUL N. ROSCHKE AND SAYED AFTAB

Five bridge analysis codes, which formerly ran only on mainframes and minicomputers, have been enhanced and converted to the microcomputer environment. Refinements include color pre- and postprocessing graphics, panel-oriented input, help and error trapping functions, and an improved user interface. Bridge applications include linear-elastic analysis of beam columns subjected to movable loads, linear and nonlinear frame analyses, and analysis of bent caps and continuous beams. Seamless integration of coded modules is performed so that existing mainframe programs become subroutines to the new microcomputer codes. However, no other modifications are made to the analysis codes to ensure avoidance of new error sources and rapid harmonization.

A large number and variety of mainframe computer programs are in current use by bridge engineers for analysis and design of structures. State highway departments typically have a large library of FORTRAN codes that were each written for a special purpose. Although these codes perform their intended analytical functions, most were written without programming enhancements, such as color graphics, which can simplify data input at the preprocessing stage and graphically summarize output. Engineers currently must sift through large quantities of numerical data in order to interpret results. Other than painstakingly "checking" by hand, no facile means of verifying geometry, materials, and support locations is available to an analyst before execution of the code.

The primary purpose of this effort is to use currently available microcomputer hardware and software to enhance existing mainframe analysis programs toward optimum usefulness for design engineers. Not only are the analysis programs executable at the engineer's own desk, but panel input and graphics capabilities allow error checking before the more time-consuming analysis code is executed. Every effort is made to leave the current analysis program unmodified so that new error sources are not introduced. As a general method of approach, languages and routines that are within the mainstream of engineering and scientific computation are employed. FORTRAN 77 is used as the primary language for new code development.

CODING PHILOSOPHY AND ORGANIZATION

The primary objective of this study is to provide generic pre- and postprocessing codes that can be quickly modified to suit different programs. As a consequence, each program is structured to be modular, with each of six modules operating completely independent of the others. All modules are integrated using a main program that provides the end-user control over the entire process by means of a master menu structure (see Figure 1). The generality and stand-alone nature of these modules make conversions of new codes a relatively simple task. Altogether, five analysis codes have been updated. One code was completed during the first year, and the remaining four codes were converted in the second year of a 2-year effort.

Analysis codes treating a variety of commonly used bridge components, including beam columns, bent caps, continuous beams, and linear and nonlinear frames, were converted to the new environment. BMCOL51 performs finite-element simulation of a linearly elastic beam column whose flexural stiffness may vary along the length and is subjected to fixed and movable loads (*1*). Frame analysis capabilities are provided through FRAME11 and FRAME51 (*2,3*). FRAME51 considers geometric, material, and support nonlinearities of statically loaded plane frames, whereas FRAME11 provides a linear-elastic finite-element solution for the same structure. In both frame codes alphanumeric and graphical results are available for axial, lateral, and rotational displacements as well as for axial, shear, and moment functions. Linear-elastic analysis of a bent cap subjected to fixed and movable loads applied according to AASHTO lane loading requirements is carried out by CAP18 (*4,5*). B30 (*6*) analyzes composite and noncomposite beams with P-loads. In all cases graphical postprocessing similar to that shown in Figure 2 is provided.

The engineer, as user, makes selections from pull-down menu structures according to the task to be accomplished. In

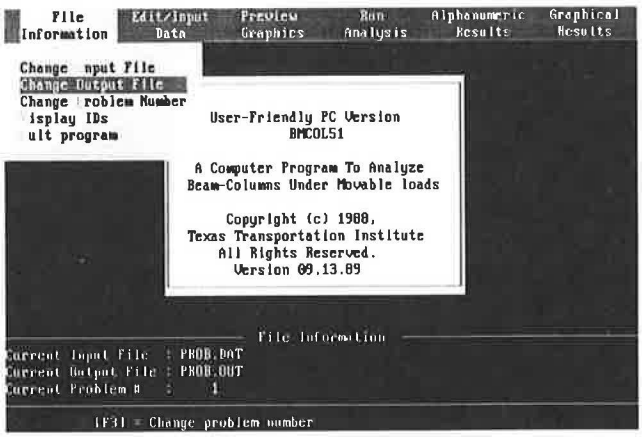

FIGURE 1 Main menu and screen layout.

Texas Transportation Institute, Texas A&M University, College Station, Tex. 77843–3136.

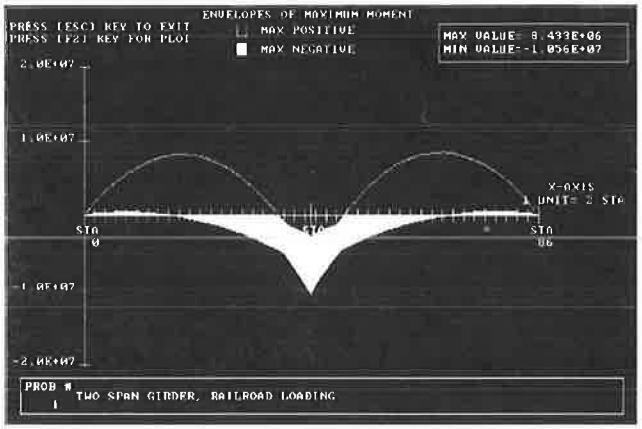

FIGURE 2 Envelope of maximum moment.

the current microcomputer version the input and output files are identical with those of the mainframe version, which allows interchange of ASCII files between microcomputer and mainframe, should that be desirable. Approximately 10,000 to 15,000 lines of new code are added to each of the existing analysis codes. By means of overlays, execution size is always below 600 kilobytes.

CONCLUSION

Five user-oriented analysis packages that are in constant use by the Texas State Department of Highways and Public Transportation have been updated to significantly reduce input preparation time for initial runs as well as to simplify modification procedures to the data file for additional trial runs. Graphics pre- and postprocessors enable the bridge analyst to quickly detect obvious errors or omissions in data files and facilitate understanding of the output. Hard-copy output from a microcomputer conveniently located at the designer's local workstation encourages consideration of alternative structural designs. The modular approach taken for coding organization can be readily applied to other codes in need of enhancement.

A diskette containing executable code and a sample input file as well as documentation for each program can be obtained from the Communications Division, Texas Transportation Institute, Texas A&M University, College Station, Texas.

ACKNOWLEDGMENTS

This study was conducted under a cooperative program between the Texas Transportation Institute, the Texas State Department of Highways and Public Transportation, and the Federal Highway Administration.

REFERENCES

1. H. Matlock and T. P. Taylor. *A Computer Program to Analyze Beam-Columns Under Movable Loads*. Research Report 56-4, Project 3-5-63-56. Center for Highway Research, Austin, Tex., June 1968.
2. H. Matlock and C. O. Hays. *A Nonlinear Analysis of Statically Loaded Plane Frames Using a Discrete Element Model*. Research Report 56-23, Project 3-5-63-56. Center for Highway Research, Austin, Tex., May 1972.
3. H. Matlock and C. O. Hays. *Linearly Elastic Analysis of Plane Frames Subjected to Complex Loading Conditions*. Research Report 56-21, Project 3-5-63-56. Center for Highway Research, Austin, Tex., May 1972.
4. H. Matlock and T. A. Halliburton. *A Computer Program to Analyze Bending of Bent Caps*. Research Report 56-2, Center for Highway Research. The University of Texas, Austin, Oct. 1966.
5. L. K. Willis. *Bent Cap Program: User Manual*. Bridge Division, Texas Department of Highways and Public Transportation, Austin, Jan. 1975.
6. *Continuous Beam Analysis: User Manual*. Texas State Department of Highways and Public Transportation, Austin, Oct. 1978.

Publication of this paper sponsored by Committee on Dynamics and Field Testing of Bridges.